Attenuation of Solitary Waves and Wave Trains by Coastal Forests

Dissertation

submitted to and approved by the
Faculty of Architecture, Civil Engineering and Environmental Sciences
University of Braunschweig – Institute of Technology

and the
Department of Civil and Environmental Engineering
University of Florence

in candidacy for the degree of a
Doktor-Ingenieur (Dr.-Ing.)
in Mitigation of Risk due to Natural Hazards
on Structures & Infrastructures

by
Semeidi Husrin
Born in Bandung, 14 May 1979
From Bandung, West Java, Indonesia

Submitted on	05 March 2013
Oral examination on	22 April 2013
Professorial advisors	Prof. Hocine Oumeraci
	Prof. Lorenzo Cappietti

2013

To my beloved parents and my family

(Kahatur kanggo pun biyang, pun bapa, pun bojo sareng pun anak)

And among His Signs are the ships,
smooth-running through the ocean, (tall) as mountains
(Ash-Shura, 42:32)

Summary

The attenuation of tsunami and storm waves by coastal forests has become increasingly attractive for research. In fact, coastal forests were reported to effectively reduce the impact of tsunami though many of the attenuation processes are still unknown and a reliable process-oriented quantification of this effectiveness based on systematic experimental and numerical studies is still lacking. Based on available knowledge and the field evidence from the latest extreme wave events, the interaction of coastal forests and tsunami as well as storm waves still needs further study directed towards an improved understanding of the attenuation performance of coastal forests and the development of reliable prediction models.

The research objective is to improve the understanding of the physical processes associated with the energy attenuation of tsunami and storm waves through coastal forests by developing a standard methodology for the parameterization of 3-D complex typical coastal forest vegetations. To achieve the objective, systematic laboratory experiments on tsunami and storm wave attenuation by coastal forests have been investigated in the twin wave flume (TWF) of Leichtweiss-Institute, TU Braunschweig. Two typical coastal forest vegetations (mangroves and coastal pines) representing two different coastal habitats were selected. A physically-based parameterization using easily quantifiable parameters of the real tree was carried out with stiff and flexible structure assumptions. Following the parameterization stage, simultaneous large scale model tests in the TWF employing different model setups and wave conditions (solitary waves representing tsunami and regular/irregular waves representing storm waves) were performed to investigate the hydraulic performance (global processes) and the hydraulic resistance characteristics (local processes) of the coastal forest

models. The analyses of the tests with a stiff structure assumption (only roots and trunk) show that wave breaking location, water depth, forest width, wave length and shore topography were found to be significant for the overall hydraulic performance of the forest models. One of the key results is the quantification of the relative contributions of the shore topography and the forest itself to the total attenuation of tsunami / storm waves.

Furthermore, the numerical simulation of tsunami and storm wave attenuation based on Non-Linear Shallow Water Equations (NLSWE) model have been successfully validated by the obtained hydraulic resistance induced by forest models in terms of drag and inertia coefficients (C_D and C_M). The validated model is appropriate to assess the hydraulic performance (wave transmission, energy dissipation and wave reflection) of the existing coastal forests and to "design" new coastal forests given a target wave attenuation performance. Furthermore, an empirical relationship (forest width factor) and a new procedure to assess tsunami attenuation by coastal forests have also been succesfully developed. It can, therefore, be used as a practical tool in coastal zone management to evaluate feasible measures in mitigating and managing risks associated with tsunami and storm waves, particularly in the regions where coastal forests are favourable.

Summary

The attenuation of tsunami and storm waves by coastal forests has become increasingly attractive for research. In fact, coastal forests were reported to effectively reduce the impact of tsunami though many of the attenuation processes are still unknown and a reliable process-oriented quantification of this effectiveness based on systematic experimental and numerical studies is still lacking. Based on available knowledge and the field evidence from the latest extreme wave events, the interaction of coastal forests and tsunami as well as storm waves still needs further study directed towards an improved understanding of the attenuation performance of coastal forests and the development of reliable prediction models.

The research objective is to improve the understanding of the physical processes associated with the energy attenuation of tsunami and storm waves through coastal forests by developing a standard methodology for the parameterization of 3-D complex typical coastal forest vegetations. To achieve the objective, systematic laboratory experiments on tsunami and storm wave attenuation by coastal forests have been investigated in the twin wave flume (TWF) of Leichtweiss-Institute, TU Braunschweig. Two typical coastal forest vegetations (mangroves and coastal pines) representing two different coastal habitats were selected. A physically-based parameterization using easily quantifiable parameters of the real tree was carried out with stiff and flexible structure assumptions. Following the parameterization stage, simultaneous large scale model tests in the TWF employing different model setups and wave conditions (solitary waves representing tsunami and regular/irregular waves representing storm waves) were performed to investigate the hydraulic performance (global processes) and the hydraulic resistance characteristics (local processes) of the coastal forest models. The analyses of the tests with a stiff structure assumption (only

roots and trunk) show that wave breaking location, water depth, forest width, wave length and shore topography were found to be significant for the overall hydraulic performance of the forest models. One of the key results is the quantification of the relative contributions of the shore topography and the forest itself to the total attenuation of tsunami / storm waves.

Furthermore, the numerical simulation of tsunami and storm wave attenuation based on Non-Linear Shallow Water Equations (NLSWE) model have been successfully validated by the obtained hydraulic resistance induced by forest models in terms of drag and inertia coefficients (C_D and C_M). The validated model is appropriate to assess the hydraulic performance (wave transmission, energy dissipation and wave reflection) of the existing coastal forests and to "design" new coastal forests given a target wave attenuation performance. Furthermore, an empirical relationship (forest width factor) and a new procedure to assess tsunami attenuation by coastal forests have also been succesfully developed. It can, therefore, be used as a practical tool in coastal zone management to evaluate feasible measures in mitigating and managing risks associated with tsunami and storm waves, particularly in the regions where coastal forests are favourable.

Zusammenfassung

Die Dämpfung von Tsunami und Windwellen durch Küstenwälder hat sich zu einem zunehmend wichtigen Forschungsschwerpunkt entwickelt. Aus vielen Berichten nach dem Tsunami 2004 wurde die Schutzwirkung der Küstenwälder mehrfach bestätigt, obwohl bislang die Dämpfungsprozesse weitgehend unbekannt waren und hierfür kein verlässlicher Nachweis durch systematische Laborexperimente bzw. prozessbasierte Modelle vorlag. Die Erfahrungen der letzten extremen Tsunamiereignisse haben den Forschungsbedarf hinsichtlich der Interaktion zwischen Tsunami/Windwellen und Küstenwälder besser verdeutlicht.

Vor diesem Hintergrund und den Hintergrund des derzeitigen Wissensstandes bestand das Hauptziel dieser Studie darin, das Verständnis der Prozesse zu verbessern, die für die Dämpfung von Tsunami/Windwellen durch Küstenwälder verantwortlich sind. Den Schwerpunkt der Arbeit bildeten die Entwicklung und systematische experimentelle Verifizierung eines neuen Verfahrens zur Parametrisierung steifer und flexibler Walvegetation hinsichtlich des Strömungswiderstands. Dabei wurden zwei Waldtypen berücksichtigt: Mangrovenwälder und Küstenpinienwälder.

Mit den anhand dieses neuen Verfahrens ermittelten parametrisierten Modellbäumen wurden systematische Untersuchungen über die Dämpfungswirkung der o.g. zwei Waldtypen in den beiden Wellenkanälen des Leichtweiß-Instituts (LWI) durchgeführt. Für diese Studie wurden Tsunami-ähnlichen solitären Wellen sowie regelmäßigem und unregelmäßigem Seegang generiert. Berücksichtigt wurden sowohl globale Prozesse (hydraulische Wirksamkeit) als auch lokale Prozesse (Wellenbrechen, Strömungswiderstand, etc.).

Die Analyse der Experimente mit steifer Vegetation zeigte, dass die Lokation des Wellenbrechens, die Wassertiefe, die Wellenlänge und die Vorlandtopographie die hydraulische Wirksamkeit der Waldvegetation die entscheidenden Einflussparameter darstellen.

Einer der Schlüsselergebnisse der Analyse war die Bestimmung des relativen Beitrages der Vorlandtopographie und des Küstenwaldes zur Dämpfung von Tsunami und Windwellen.

Hinsichtlich der numerischen Modellierung wurde das nichtlinearen Flachwasserwellen-Modell COMCOT mit den aus den Experimenten gewonnenen (i) Strömungswiderstandskoeffizienten C_D und C_M implementiert und (ii) Daten erfolgreich validiert.

Das validierte Modell wurde zur Durchführung einer systematischen Parameterstudie eingesetzt, die in die Entwicklung einer neuen Formel zur praktischen Ermittlung der hydraulischen Wirksamkeit von Küstenwäldern als Funktion eines dimensionslosen Parameters resultierte. Dieser Parameter fasst sinnvollerweise die Einflüsse der Breite und Dichte des Küstenwaldes sowie der Wellenhöhe und Wassertiefe am Vorlandfuß zusammen. Darüber hinaus wurden Empfehlungen für die praktische Bewertung der hydraulischen Wirksamkeit von Küstenwäldern zur Risikoreduzierung bei Tsunami und Sturmfluten ausgearbeitet.

Acknowledgment

The completion of this PhD dissertation would have never beeen possible without the supports of encouerement from many parties during my time as a PhD student in TU Braunschweig. First of all, I would like to thank Prof. Hocine Oumeraci as my supervisor for his continued support and guidance. I am very gratefull for his valuable advice, professional critisms, and best efforts to motivate me in opening my ideas to solve numerous scientific/technical problems and beyond.

My stay in Braunschweig was inevitably unforgettable. A very warm welcome from Mrs. Founier in a gloom 2006 German winter marked the turning point of my thirst on knowledge for years to come. I am very grateful for her great patient and tremendous care during my study in LWI. I am trully indebted to Dr. Kortenhaus for his remarkable support, Dr. Dassanayake and wife for being my great best friend, Dr. Strusińska for her best collaboration in executing the TAPFOR project, Rainer Kvapil for his technical assisstance, Markus Bruehl for his constructive critism, Sina Reimann for her efficient efforts in the beginning of the project, Peter Geisenheiner for his practical helps in the lab, Mathias Kudella for his great l-Davis software, and Silvia Glowania for her patient listening to my poor German. I also would like to thank Gisa Ludwigs, Saskia Pförtner, Andreas Burzel, Tijl Staal, Marie Naulin, Kerstin Hinze, Sven Liebisch, Mike Lieske, Lisham Bonakdar, Marina Zarjow, Hisham el Safti, Muhamed Tayel, Nguyen Quang Thanh, and Ashabul Haque for being so helpful. My special thank also goes to the people in the "Werkstatt", Herr Lehmann, Herr Neumann and Herr Ecklebe, for their great contribution in physical experiments. In short, I would like to thank all colleagus and students in LWI for making my "hardship" in LWI more comfortable.

My PhD study is funded by a three-year fellowship from the international graduate colleauge of TU Braunschweig (GRK-802). My sincere thank goes to Mrs. Wissmann for taking care my administrative matters well organised. My special thank also for Henrich Meyering for his "always ready" to help. Many thanks for all professors from both German and Italian universities for their support. I would like to thank all my German and Italian colleagues for being together in the group in harmony. During my stay in Italy, I would like to thank Prof. Lorenzo Cappietti from Florence University for his best ideas and Professor Stefano Tinti from Bologna University for his advice and guidance in tsunami numerical simulation. I also would like to dedicate my gratitute to Prof. Zhenhua Huang and his group in EOS-NTU and Dr. Widjo Kongko from BPPT for sharing their experience and "the world" of numerical simulation.

My special thank for Yopi and Pak Saptono for sharing happines and difficulties in Rebenring 38. I also would like to acknowledge the members of MuslimBS, especially Pak Amru for keeping my spiritual motivation alive and the Indonesian community for providing me the sense of "feeling-at-home". Last but not least, though we were separated thousands mile away, I would like to dedicate this PhD dissertation to my beloved mother and father for their endless love and my family for their everlasting support.

Semeidi Husrin, Braunschweig - 2013.

Table of Contents

Index of Figures

Index of Tables

Index of Notations and Symbols

$\bar{u}$: averaged velocity [m/s]
$\partial u / \partial t$: flow acceleration = a [m/s^2]
ε : nonlinearity parameter [-]
ν : kinematic viscosity [=1.05 × 10^{-6} m^2 /s for sea water at 20^{o}C]
ϕ : latitude [rad]
λ : longitude [rad]
ξ_{ff} : forest width factor [-]
ρ : water density [kg/m^3]
η : water elevation [m]
θ' : wave making coefficient [-] [Takayama *et al*., 1980]
λ_s : length scale [-]
ε_H : error indicator for wave heights [%]
ε_{time} : error indicator for time arrival of wave [s]
Δh : water depth difference [m]
α : angel of deflection [rad]
β : beach slope [rad]
δ : deflection [m]
δF_D : deviation of measured force [%]
Δx : horizontal distance between H_i and H_t [m]
A_f : frontal area of submerged vegetation [m^2]
A_{fc} : frontal area of canopy [m^2]
A_l : averaged area of leave [m^2]
A_p : projected area of submerged vegetation [m^2]
A_p^i : projected area of ith plant [m^2]
A_v : cross sectional area of the body subjected to flow [m^2]
B : width of the forest model [m]
B/L : relative forest width [-]
C : tsunami/Bore run up velocity [m/s]
C_D : drag coefficient [-]
c_d : turbulent model parameter constant = 0.17 [-]
C_D* : modified drag coefficient [-]
C_{FM} : contribution of forest model to the total wave energy dissipation [%]
C_M : inertia coefficient [-]

C_M* : modified inertia coefficient [-]
C_{SM} : contribution of shore model to the total wave energy dissipation [%]
c_W : turbulent model parameter constant = 0.09 [-]
D_{br} : diameter of branches [m]
D_c : cylinder diameter of mangrove models [m]
D_{dbh} : diameter of the trunk measured at breast height [m]
D_f : drag resistant factor [-]
D_r : diameter of roots [m]
D_s : averaged distance between tree trunk [m]
d_r : distance from platform to the surface elevation [m]
dt : time step [s]
dx : grid size in x-direction [m]
dy : grid size in x-direction [m]
E : modulus elasticity [N/m^2]
E_d : dissipated wave energy [J/m^2]
E_i : incident wave energy [J/m^2]
Ek : kinetic energy [J/m]
$E_{K,t}$: transmitted kinetic energy [J]
$E_{P,t}$: transmitted potential energy [J]
E_r : reflected wave energy [J/m^2]
E_t : transmitted wave energy [J/m^2]
$E_{T,i}$: total incident wave energy [J]
$E_{T,t}$: total transmitted wave energy [J]
E_w : Wave energy of either incident, reflected or transmitted waves [J/m^2]
f : Darcy friction factor [-]
f : Darcy-Weisbach friction factor [-]
F_c : centric force [N]
F_D : drag force [N]
$F_{D(par)}$: measured force of parameterized model [-]
$F_{D(real)}$: measured force of real model [-]
F_I : inertia force [N]
F_{max} : maximum measured force [N]
$F_{max,b}$: maximum measured force at the beginning the forest model [N]
$F_{max,e}$: maximum measured force at the end of the forest model [N]
F_T : total force [N]
f_v : Eddy viscosity coefficient [cm^2/s]

g : gravity acceleration [=9.8 m/s^2]
h : water depth [m]
H : wave height or tsunami height [$H=h+\eta$] [m]
H_f : wave height in front of coastal forest [m]
h/L : relative water depth [-]
h_a : ADV measurement point [m]
h_b : height of buttress of coastal pines [m]
h_c : height of the canopy [m]
H_d : "dissipated" wave height [m]
h_{em} : height of emerged mangrove trees [m]
$H_{gen,max}$: maximum generated wave height [m]
h_h : total height of the tree [m]
H_i : incident wave height [m]
$H_{i,max}$: maximum incident wave height [m]
$H_{i,nom}$: nominal wave height [m]
H_m : mean wave height [m]
$H_{m,i}$: incident mean wave height measured in front of the forest [m]
Hm0 : significant wave height [m]
$H_{m0,i}$: incident significant wave height measured in front of the forest [m]
$H_{m0,t}$: transmitted significant wave height measured behind the forest [m]
H_r : reflected wave height [m]
h_r : the height of root [m]
H_r : total tsunami height in the platform [m]
h_{rt} : total height of roots [m]
h_{sb} : height of submerged roots [m]
h_{sb} : height of submerged roots of mangroves [m]
h_t : height of (branchless) trunk [m]
h_t : height of [branchless] trunk [m]
H_t : transmitted wave height [m]
I : second moment of area [m^4]
KC : Keulegan-Carpenter number [-]
K_d : dissipated wave energy coefficient [-]
K_d(FM): dissipation coefficient due to forest model FM [-]
K_d(SM): dissipation coefficient due to shore model SM [-]
K_d(SM+FM) : dissipation coefficient due to both shore model and forest model SM+FM [-]

K_r : reflected wave coefficient [-]
K_t : transmitted wave coefficient [-]
L : wave length [m]
LAI : leaf area index [-]
l_D : turbulent length scale [m]
L_e : effective length of submerged vegetation [m]
$L_{i,gen}$: wave length of generated wave in front of the slope[m]
l_l : length of leaves [m]
L_v : length of vegetated channel [m]
L_w : length of woodenn beam sample [m]
m : mass or loading mass [kg]
n : Manning's roughness coefficient [$s/m^{1/3}$]
n_b : bottom roughness coefficient [$s/m^{1/3}$]
n_e : equivalent roughness coefficient [$s/m^{1/3}$]
N_s : density of tree model [m^{-2}]
Q : water discharge [m^3/s]
R^2 : correlation of determination [-]
r : radius of wooden beam sample [m]
R^2 : coefficient of determination [-]
R_b : vegetation friction [m]
R_e : Reynolds number [-]
R_F : relatif reduction force [%]
R_h : hyd. radius in open channel or water depth for non-open channel [m]
T : wave period [s]
t_a : age of tree [years]
T_m : mean wave period [s]
$t_{measurement}$: measurement arrival time [s]
t_{model} : model arrival time [s]
T_p : peak wave period [s]
u : current velocity in x direction [m/s]
u_b : horizontal wave orbital velocity at bed [m/s]
u_{max} : maximum horizontal flow velocity [m/s]
u_p : prototype current velocity [m/s]
V : control volume [m^3]
v : current velocity in y direction [m/s]
V_m : submerged vegetation volume [m^3]

V_m/V : submerged root volume ratio [-]
V_v : volume of body subjected to flow [m^3]
w_c : width of canopy [m]
w_r : width of root system [m]
x : horizontal distance [m]

Abreviations

2D	Two dimensional
3D	Three Dimensional
ADRC	Asian Disaster Reduction Centre
ADV	acoustic Doppler velocimetre
ANUGA	Australian National University and Geoscience Australia
Bappenas	Badan Perencanaan dan Pembangunan Nasional of Indonesia
BM	beach model / foreshore model
BTE	Boussinesq-type equation
C1FF	parameterised coastal pine model with flexible trunk nr. 1
C1FS	parameterised coastal pine model with stiff trunk
C2FF	parameterised coastal pine model with flexible trunk nr. 2
C3FF	parameterised coastal pine model with flexible trunk nr. 3
CFD	Computational Fluid Dynamics
CFL	Courant–Friedrichs–Lewy
COBRAS	Cornell Breaking Wave and Structures model
COMCOT	Cornell Multi-grid Coupled Tsunami model
COULWAVE	Cornell University Long and Intermediate Wave Modeling Package
CSD	Computational Structural Dynamics
DANS	Double-Averaged Navier-Stokes
DART	Deep-ocean Assessment and Reporting of Tsunamis
DFG	Deutsche Forschungsgemeinschaft
ECOS	Ecomagazines
EM	Evolution mode
FAO	Food and Agricultural Organisation
FM	Forest model
FT	Force transducer / Dynamometer
FTS	Force transducer attached to single tree models
FUNWAVE	Fully nonlinear wave model, University of Delaware – USA
GEBCO	GEneral Bathymetric Charts of the Oceans
GEJET	Great Eastern Japan Eartquake and Tsunami

GITEWS	German Indonesian Tsunami Ealry Warning System
GTM	Global Tsunami Model- University of Alaska Fairbanks
IfSAR	Interferometric Synthetic Aperture Radar
IOC	Intergovernmental Ocean Committee of UNESCO
IRP	International Recovery Platform
ITTFS	International Teams of Tsunami Field Survey
IUGG	International Union of Geodesy and Geophysics
JONSWAP	Joint North Sea Wave Observation Project
L~DAVIS	LWI~DAta and VISualisation
LAI	Leave Area Index
LES	Large Eddy Simulation model
LiDAR	Light Detection And Ranging
LSWE	Linear shallow water equations
LWI	Leichweiss-Institute TU-Braunschweig
M1FF	Parameterised mangrove model with flexible trunk nr. 1
M1FS	Parameterised mangrove model with stiff trunk nr. 1
M2FF	Parameterised mangrove model with flexible trunk nr. 2
M2FS	Parameterised mangrove model with stiff trunk nr. 2
M3FF	Parameterised mangrove model with flexible trunk nr. 3
M3FS	Parameterised mangrove model with stiff trunk nr. 3
M4FS	Parameterised mangrove model with stiff trunk nr. 4
M5FS	Parameterised mangrove model with stiff trunk nr. 5
MOAC	Ministry of Agriculture and Initiatives of Thailand
MOST	Method of Splitting Tsunami
MSL	Mean sea level
NLSWE	Nonlinear shallow water equations
NOOA	National Oceanic and Atmospheric Administration
NSE	Navier-Stokes Equation
PNG	Papua New Guinea
PT	Pressure transducer
PTFE	Polytetrafluoroethylene
RANS	Reynolds Averaged Navier Stokes
ReCS	Real coastal pine model with stiff trunk

ReMS	Real mangrove model with stiff trunk
RT	Root and trunk model
SB3	Wood sample of mangrove
SC1,SC2,SC3	Wood samples of coastal pine
SDS	Sub-depth Scale
SM+FM	Combination of both forest model and shore model platform
SPM	Shore Protection Manual
SRTM	Shuttle Radar Topography Mission
SWAN	Simulating WAves Nearshore
SWE	Shallow Water Equation
TAPFOR	Tsunami Attenuation Performance of Coastal Forests
TIME	Tsunami Inundation Modeling Exchange
TOPICS	Tsunami Open and Initial Condition System
TRIAS	Tracing tsunami impacts on- and offshore in the Andaman sea region
TSUNAMOS	Tsunami Open Source model
TsunAWI	Tsunami modelling at AWI (Alfred-Wegener Institute, Germany)
TU	Technical University
TUNAMI	Tohoku University's Numerical Analysis Model for Investigation of Near-field tsunamis
TWF	Twin Wave Flume
UNEP	United Nation Environment Programme
UNESCO	United Nations Educational, Scientific and Cultural Organisation
USACE	United State of America Corp of Engineers
VOF	Volume of Fluid
WG	Wave gauge
WP	Work Phase

1 Introduction

1.1 Motivation

Tsunami[1] has long been associated with typical natural disaster events in Japan and the Pacific regions. Based on tsunami historical records, these regions, particularly along the so-called "Pacific Ring of Fire", have experienced the highest tsunami occurrences where some of them generated major deadly and damaging tsunamis (e.g. 1960 Chilean tsunami and 2011 GEJET[2]). Tsunamis can occur anywhere in a vast ocean of the world. Despite the fact that tsunami frequently occurred in active fault lines, the world deadliest tsunamis were also recorded in geologically less active sea bottom oceans, e.g. the Atlantic Ocean (e.g. 1755 Portugal Tsunami) and the Indian Ocean (e.g. 2004 Asian Tsunami). Though tsunamis are mostly triggered by earthquakes in the ocean, other disturbances that may generate massive tsunamis are sea-bottom volcano eruptions like Krakatau Eruption in 1883 (De Lange *et al.*, 2001), submarine landslides like Lituya Bay Tsunami in 1958 (Lockridge, 1998), and meteorites impacts (Hills and Goda, 1998).

Another common threat is storm surges. Storm surges occurred much more often than tsunami and claimed significant casualties in term of human lives and economic losses. Unlike tsunami, storm surges are generated by disturbance to the water body due to extreme wind (weather systems) pushing a considerable amount of water to the shore (surges). Though, storm surges are more predictable than tsunamis, underestimating their impact might lead to deadly disaster as tsunamis. For instance, Hurricane Katrina in 2005 devastated the US's coastlines around the Gulf of Mexico (Jordan II, 2008) and Cyclone Nargis in 2008 swept out hundreds of thousands of people along Myanmar coastlines (Lin *et al.*, 2009).

[1] Tsunami is a combination of two Japanese words: "Tsu" means harbour and "Nami" means waves

[2] GEJET stands for Great Eastern Japan Eartquake and Tsunami (Mimura *et al.*, 2011)

a) Trees in Thailand were firmly standing after 2004 tsunami (FAO/MOAC, 2005)

b) Forest in Takata Matsubaa left only 1 tree after hit by tsunami (Yomiuri[@])

c) The 2011 Great Eastern Japan tsunami engulfed the area behind the forest (Reuters[@])

Fig. 1.1: The effectiveness of coastal forest against tsunami (FAO/MOAC (2005), Yomiori (2011) and Reuters (2011))

Besides the dramatic damages and losses, the disasters also provide opportunities to learn more on natural processes (earthquakes, tsunamis, storms, etc) and how to mitigate such destructive forces in the future. Immediate measures based on the available knowledge, modelling tools and methods are urgently required. Several efforts have been made to reduce the impact of tsunamis or storm waves. Traditionally, tsunami/storm wave mitigation measures are limited to structural measures, such as: massive barriers along the coastlines (e.g. tsunami breakwaters and seawalls in Japan, dike rings in the Netherlands).

As tsunami travel time can now be better predicted than in the past, non-structural measures are more widely implemented. Educations and social awareness are also increasingly considered as one of the effective measures to avoid human casualties. When tsunami is generated far enough off the ocean (i.e. tsunami travel time is in hours), tsunami early warning system in some countries like Japan and USA has been proved to be effective and efficient measures to reduce tsunami impacts, at least reducing loss of human lives. However, when tsunami is generated nearby (i.e. tsunami travel time in the order of minutes), the role of other mitigation measures, such as: structural measures become much more important in reducing the impacts of tsunami.

In the last two decades, coastal forests have been considered by many parties as one of mitigation measures against both tsunamis and storm waves. Coastal forest vegetation is generally appropriate to withstand extreme winds, storms, and salt sprays. But, the ability to withstand large tsunami impacts has controversially been discussed among scientists. These discussions are still on going on the role of coastal forests (e.g. mangroves and other coastal vegetation, such as: coastal pines) as an effective natural tsunami barrier. Many reports and surveys based on field observations, experienced damage, and satellite images (mostly after the 2004 Asian Tsunami) have apparently shown that coastal forests have played an important role as natural protection against tsunami (Shuto (1987), Dahdouh-Guebas *et al*. (2005), Danielsen *et al*. (2005), UNEP (2005), Kathiresan & Rajendran (2005)) (Fig. 1.1a). Those findings are also supported by semi-analytical and empirical approaches based on series of experiments in both physical and numerical models (Harada and Imamura (2000), Istiyanto *et al*. (2003), Imai and Matsutomi (2005), Latief and Hadi (2006), Tanaka *et al*. (2007), and Yanagisawa *et al.* (2011)). However, another opinion is that there are still many unknown aspects, so that no final conclusions can be drawn on the effectiveness of coastal vegetations as a protective green-shield (ECOS, 2010; Kerr, *et. al*, 2006; Wolansky, 2006). The large uncertainties associated with tsunami onshore propagation, the effect of complex bathymetry and topography, and vegetation behaviours against tsunami force are examples which illustrate some of the poorly understood aspects. Field evidence (damage observations) also showed that not all coastal forests effectively protected coastal area from destruction. Even in some areas with dense and healthy mangrove and vegetation, forests did not provide any protection against tsunami (FAO/MOAC

(2005), Bappenas (2005), Latief and Hadi (2006), EJF (2006), Forbes & Broadhead (2007)).

The latest three tsunami events (Chilean tsunami 2009, Mentawai tsunami 2010 and GEJET 2011) events remarkably revealed evidence of considerable damages on the coastal forest itself and the surrounding areas (Fig. 1.1b and Fig. 1.1c). Morton *et al*. (2010) reported that many trees were found to be uprooted, broken or bent down during the 2010 Chilean tsunami. The causes of the damage vary and depend on many environmental aspects, such as: direction of incoming waves, beach characteristics and tree species. Similar damages were also found in the South Pagai Islands, in Mentawai Indonesia where most trees in the front lines suffered heavy damages against tsunami (ITTFS, 2010). The 2011 tsunami event in Japan provided for the first time a live event tsunami showing how tsunami destroyed many infrastructures after passing coastal forest barriers as shown in Fig. 1.1c. Moreover, as reported by medias, the 2 km wide forest along the coastline of Iwate prefecture with 70000 red and black pines was swept away leaving only one tree standing and dying[3]. Early investigations from ADRC (2011) also mentioned that the coastal forest along the coastline of Sendai was mostly flattened and did not provide any noticeable protection.

Learning from the past tsunami and storm wave events, practical tools (e.g. a numerical model) are urgently needed to assess many possible mitigation efforts. Models describing the interaction of tsunami with coastal forest vegetation have been developed based on diverse assumptions and methodologies. Consequently, different models have resulted from these development efforts in order to better describe tsunami attenuation by coastal forest vegetation. For the characteristics of coastal forest vegetation, the concept of submerged volume ratio (ratio of submerged biomass to the control volume), tree geometry, and forest characteristics have been converted into a wide range of hydraulic resistance parameters such as drag and inertia force coefficients or global Manning roughness coefficients (Hiraishi & Harada (2003), Harada & Kawata (2004), Istiyanto *et al*. (2003), and Kongko (2004)). Furthermore, numerical models (mostly based on Shallow Water Equations models) have been developed to describe the effectiveness of coastal forest barriers by introducing the derived hydraulic resistance

[3] http://www.yomiuri.co.jp/dy/national/T110523003977.htm, access date Tuesday, July 26, 2011

coefficients into the 1-D momentum equation (Harada and Imamura (2000), Latief and Hadi (2006), Yanagisawa *et al.*(2009)). For storm waves, Massel *et al*. (1999) and Hadi *et al*. (2003) developed analytical wave attenuation models based on potential flow in which the dissipation is introduced by applying linearized drag losses induced by vegetation. The model has successfully contributed to understand the role of forest and vegetation dimensions, changing water depth, and dissipation due to breaking waves. However, linearization of the model and the lack of information on the range of the prevailing flow regimes (i.e. Reynolds numbers) have led to limited applications of the model. Moreover, research methodologies on how coastal forests had been treated are too simple and far from representing real conditions, particularly, vegetation parameters that related to hydraulic losses (Oumeraci, 2006). Therefore, the interaction of coastal forests and tsunami / storm waves still needs further study directed towards an improved understanding of the attenuation performance of coastal forests and the development of more reliable prediction models, including a proper physically based parameterisation of coastal forest vegetations.

1.2 Objectives

The main objectives of this study are summarised as follows:

- Develop and test experimentally a physically based methodology for forest parameterisation. The main result should be a generic parameterisation of typical coastal forest vegetation (i.e. mangroves and coastal pine)
- Use this parameterisation for investigating wave attenuation by forests made of parameterised tree models. The results should be an improved understanding of the physical processes associated with the interaction of tsunami/storm waves and coastal forests as well as physically based formulae for the drag and inertia coefficient describing the energy dissipation
- Based on this improved understanding and the derived drag and inertia coefficients, select the most appropriate numerical model among the existing models and improve/extend and validate it to better predict the attenuation performance of coastal forest to tsunami/storm waves.

1.3 Scope of work and reporting

In order to achieve the objectives, the PhD study is sub-divided into 5 main work phases as depicted in Fig.1.2. First, the available knowledge related to the interaction of tsunamis/storm waves and coastal forest vegetation is reviewed and

analysed by focusing on the diverse physical aspects and models as well as on the different approaches available for forest parameterisation and the implementation of the flow resistance induced by forests. Second, field studies and laboratory works related to the processes of tree parameterisation and have been conducted and analysed based on typical characteristic of vegetation (including stiff and flexible structure behaviours) for mangroves and coastal pines which represent the most commonly found vegetation in estuaries and sandy beaches, respectively. After that, large scale laboratory experiments have been carried out to investigate the attenuation of tsunami/storm wave by the parameterised forest models. Afterwards, the obtained hydraulic resistance is adopted into available numerical model to predict the damping performance of coastal forest vegetation against tsunamis/storm waves which is validated and verified by the available data from large scale laboratory experiments.

Based on the scope of the work, this PhD report is organised in the following five chapters:

- Chapter 1: The introduction.
  The introduction contains brief information on general background, research objectives and scope of work.
- Chapter 2: Literature review (state of the art).
  Literature review focuses on previous works related to many aspects (i.e. model parameterisation, damping performance, and tsunami/storm wave modelling) on the damping performance coastal forest vegetation against the impact of tsunami and storm waves. Specification of objective and methodology implemented in the current study are the goal of this chapter.
- Chapter 3: Parameterisation of coastal forest vegetation.
  Parameterisation processes for typical coastal forest vegetation (i.e. mangrove and coastal pine) based on physically-based assumptions (stiff and flexible assumptions). Hydraulic tests and analyses are performed to produce representative parameterised models and their hydraulic resistance.
- Chapter 4: Wave flume experiments.
  Wave flume experiments are performed in the Twin Wave Flume (TWF) of LWI, TU-Braunschweig to investigate the damping performance of parameterised forest model subjected by storm waves and tsunami.
- Chapter 5: Numerical simulation.

Numerical simulation employing Shallow Water Equation model are discussed in details to simulate wave attenuation by coastal forest based on the derived hydraulic resistance from model scale tests in Chapter 4.

- Chapter 6: Conclusions and remarks.
  The last chapter provides the conclusion of current studies on the damping performance of coastal forest vegetation against the impact of tsunami/storm waves. Remarks and recommendations for the implementation of new findings from this study and upcoming researches are discussed in brief.

Accompanying this thesis report, thirteen technical reports are also provided for more detailed information concerning many aspects discussed in this report. Those reports are compilations of internal reports (Reports Nr. 1 - 13) during the entire period of the PhD work (Husrin and Oumeraci, 2012a-k, Husrin *et al.* 2010 and Husrin *et al.* 2011).

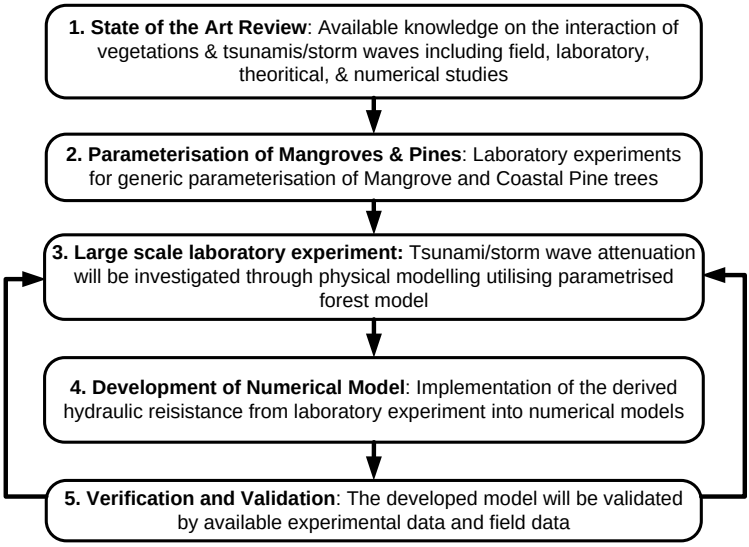

Fig.1.2: Scope of work of modelling tsunami and storm wave attenuation by coastal forest including parameterisation of coastal forest vegetation

2 Current knowledge and models (state of the art)[4]

2.1 Types of coastal forest vegetations

Coastal forests are located in a narrow region along the coastline which is characterized by the ecosystem of well-adapted vegetations that may extend up to hundreds of kilometres inland. The trees and other plants that make up coastal forests are morphologically and biologically 'designed' to their habitat in a semi-marine environment. Coastal forests can be found on almost all kinds of coastal landforms, such as mud flats, sandy beach, dunes, deltas, river bank, estuaries, and on even steep cliffs above the shore. Among the many coastal forest types, mangroves and beach forests (i.e. coastal pine forests) are the most commonly considered coastal forests as natural protections against tsunamis and storm waves (Forbes and Broadhead, 2007).

Mangroves are often classified based on their general appearances (e.g. colours, shapes and sizes), reproduction mechanisms (propagules, seeds, or spores) and their habitat characteristics (intermittently submerged, periodically submerged and always submerged soils). Their habitats are mostly around sheltered areas such as estuaries and lagoons. But, some of mangrove species are also well adapted to open sea environments (e.g. fringe mangrove forest). Mangroves commonly grow in most tropical regions, but can also be found in more than 120 countries and territories around the world (FAO, 2005). The largest mangrove species diversity exists in South East Asia where the main species consist of *Avicenna* sp., *Rhizophora* sp., *Bruguiera* sp. and *Sonneratia* sp. (Duke, 1992). A typical mangrove forest and types of roots for typical mangrove species are shown in Fig. 2.1.

[4] More detailed information on this chapter is in Reports Nr. 1 and 2 (Husrin and Oumeraci, 2012a and 2012b)

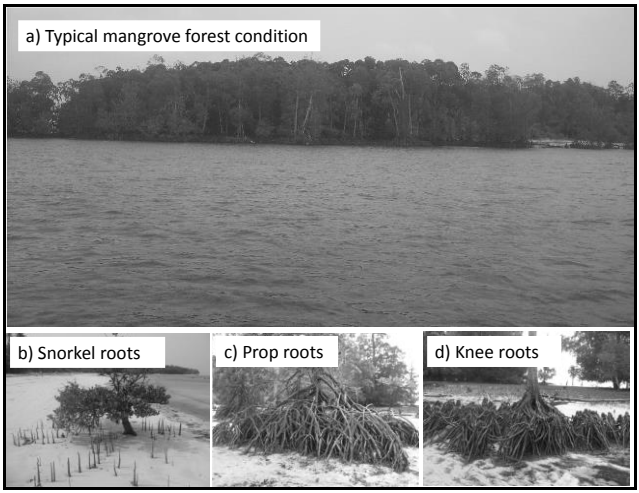

Fig. 2.1: Typical mangrove forest found in Mentawai Island, (a) Mangrove in a low energy environment and (b, c & d) Examples of mangrove roots

Considering their widespread distributions and their ability to survive in a highly saline environment, the role of mangroves as a natural shoreline protection has long been investigated. Earlier investigations were limited to the interaction between mangrove and wind-generated waves. Wolansky *et al.* (1992), Mazda *et al.* (1997), Massel *et al.* (1999), have extensively studied on how mangroves influence the hydrodynamics of estuaries and lagoons. As tsunami threats became more apparent, especially in the regions where mangroves grow naturally, more research efforts were directed towards the effectiveness of mangroves against extreme tsunami waves as reported by Latief and Hadi (2006), Harada and Kawata (2004), and Tanaka *et al*. (2007).

Beside mangroves, another type of coastal forest considered for natural protection against extreme events is beach forest. Examples of beach forest vegetations that are commonly found in dry sandy beach are coastal pines or Australian pines (*Casuarina equisetifolia*), Coconut palm (*Cocos nucifera*), Waru-laut (*Thespesia populnea*) and Screwpines (*Pandanus odoratissimus*) (see Fig. 2.2). Those vegetations have served as sources of various human livelihoods, forestry

products, and also as coastal erosion controls (Prasetya, 2007). Beach forests may play an important role in reducing the impact of tsunamis as reported by Shuto (1987) for pine trees (*Pinus* sp.), Imai and Matsutomi (2005) for coastal pines (*Casuarina equisetifolia.)*, and Hiraishi and Harada (2003) for Waru trees (*Thespecia* sp.). The 2004 Indian ocean tsunami and the 2006 South of Java tsunami have also shown the importance of those typical beach vegetations in reducing the impact of tsunami (Tanaka *et al*., 2007 and Latief and Hadi, 2006).

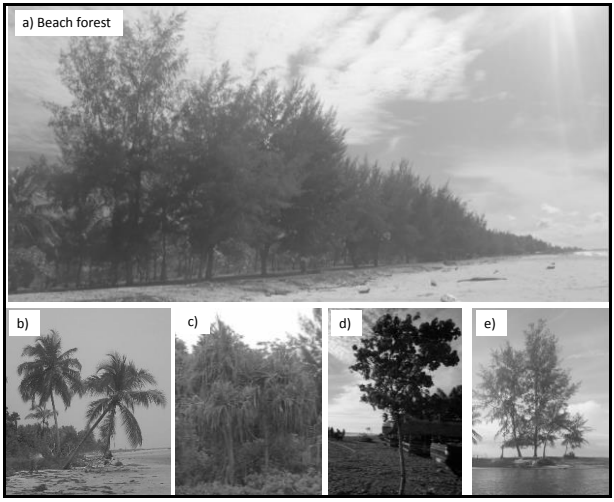

Fig. 2.2: Typical beach forest conditions found in West Sumatera: (a) Coastal pine forest, (b) Coconuts (*Cocos nucifera*), (c) Screwpines (*Pandanus odoratissimus*), (d) Waru-laut (*Thespesia populnea*), (e) Coastal pines (*Casuarina equisetifolia*)

The utilisation of those beach forest vegetations as natural tsunami/storm wave barriers has become the subject of many studies. Among many types of coastal forest vegetations, only red mangroves or *Rhizophora apiculata* and coastal pines or *Casuarina equisetifolia* have long been considered. Therefore, the following aspects may justify the selection of mangroves and coastal pine as one of natural mitigation measures implemented in current study:

- Both species are widely spread, particularly in tropical countries and representing two different coastal habitats, i.e. mangroves represent estuaries and coastal pines for sandy beaches,
- Both species have been implemented by many authorities in many countries as natural barrier against extreme events e.g. storm waves and tsunami,
- The hydraulic resistance coefficients either in term of drag, inertia or *Manning* roughness coefficients for both species have been available for a wide range of applications and implementations in the field of hydraulic/coastal engineering. For the purpose of tsunami mitigation, however, the implementations are still controversially discussed,
- In the processes of deriving the hydraulic resistance coefficients, both species have been parameterised using different methodologies and assumptions leading to unclear conclusion for the selection of proper coefficients,
- The damping performance of both species in reducing the impact of storm waves and tsunami has long been studied based on different assumptions and methodologies either by means of physical or numerical approaches,
- Finally, the effectiveness of both species as a natural barrier of extreme events is still questionable. New evidence of heavy damages experienced by thousands of pine trees due to the 2011 Great Eastern Japan Earthquake and Tsunami along Tohoku coastline shows the needs for more comprehensive investigations on this topic.

2.2 Parameterisation of coastal forest vegetation

Parameterisation is a simplification process of a complex 3D structure of a real tree into a much simpler tree model with a condition that the hydraulic losses of both real tree and the parameterised tree model should be similar. This is a very important step in the modelling of tsunami/storm wave's attenuation by coastal forests because without a proper parameterization, the resulted hydraulic resistance of coastal forest vegetation resulted from the interaction with tsunami/storm waves may lead to incorrect results and interpretations.

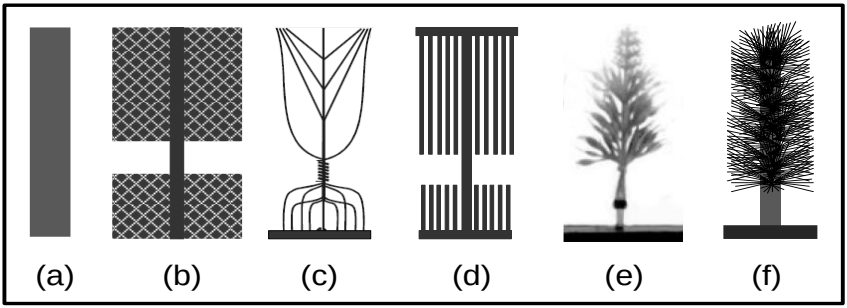

Fig. 2.3: Parameterised tree models (a) Uniform group of cylinders (Petryk & Bosmaijan, 1975) (b) A model consists of artificial porous media (Harada and Immamura, 2000) (c) A model built by forming mangrove tree structures made of wires (Istiyanto *et al.*, 2003) (d) A model consists of cylinders (Kongko, 2004) (e) Artificial tree model of coastal pine tree (Imai & Matsutomi, 2005), (f) Artificial plastic tree model (Irtem *et al.*, 2009)

Coastal forest vegetation has been parameterised using different materials and assumptions to derive the hydraulic resistance either in terms of drag, inertia or *Manning* roughness coefficients (C_D, C_M and n, respectively) (Fig. 2.3). Earlier, the hydraulic resistance of vegetation in term of drag coefficient (C_D) based on scale model tests using a simple group of cylinders (Petryk & Bosmaijan (1975) and USACE (1984)) have been directly adopted for coastal vegetation species, i.e. mangroves (e.g. by Massel *et al.*, 1999). More specific empirical formulations of the hydraulic resistance of mangrove were proposed by Harada and Imamura (2000) based on laboratory experiments utilising artificial porous media for the stiff tree canopy and a stiff cylinder for the trunk. The porous media were designed with certain porosity to meet the assumption of real mangrove root and canopy densities in term of submerged volume ratio. A mangrove model made of wires, shaped in such ways forming a stiff mangrove-like model was then proposed by Istiyanto *et al.*, (2003). Here, the occupied volume concept similar to the concept of submerged volume ratio was also adopted as an important parameter affecting the hydraulic resistance. Kongko (2004) used group of stiff cylinders to form entire root systems, trunks, and canopy of mangroves in different density and forest configuration. Meanwhile, for coastal pines, Imai and Matsutomi (2005) used an artificial flexible plastic tree model to represent coastal pine trees. Irtem *et al.* (2009) also used artificial stiff tree models and

group of stiff cylinders with equivalent submerged volume to investigate the damping performance of the forest models.

Among those parameterised models, models consisting of simple stiff cylinders were likely preferred because of their simplicity. Moreover, the derived hydraulic resistance can be easily implemented into numerical models to investigate tsunami and storm wave attenuation. The derived resistance based on these parameterised models has been adopted in many available numerical models, such as: SWAN model (Burger, 2005), TUNAMI model (Yanagisawa *et al.*, 2010) and COULWAVE model (Huang *et al*., 2011).

Basically, each part of the tree has its specific role in providing hydraulic resistance induced by tsunami/storm waves. *A mangrove tree* has, for example, at least three zones (roots, trunk and canopy) which play an important role in mitigating the impact of tsunamis (see Fig. 2.4). The root system with its complex and dense structures (Zone I) behaves generally as a stiff structure and is always involved in the dissipation processes, even for smaller inundation depth. The trunk with its strength properties (Zone II) may behave as a stiff or flexible structure depending on the inundation depth which also governs its relative contribution to the total energy dissipation. The canopy with its density characteristics (Zone III) behaves as a flexible structure and its contribution to the total wave attenuation strongly depends on the inundation depth. Those three main components have been parameterized in many ways in both physical and numerical approaches, varying from using a simple group of cylinder to building complex shapes representing a real tree structure (Istiyanto *et al*., 2003).

For a *coastal pine tree*, a similar zonation (except for zone I) can also be distinguished with respect to their importance or tsunami attenuation (Fig. 2.4). Zone I for coastal pine tree does not provide any resistance because the root system is covered by top soil. Similar to mangroves, the resistance of single coastal pines against the impact of tsunamis varies in vertical direction and therefore depends on vegetation characteristics, soil characteristics, and tsunami heights.

When tsunami height reaches the top of the trees, all resistances provided in those 3 zones are linked together interdependently. The canopy will not provide any resistance if the trunk is broken or if the roots are uprooted, as in most cases

of young trees. For mature trees of coastal pine, where branchless trunks can reach up to 10 meters high, the individual trees (trunks and roots) are strong enough to withstand tsunami height up to 10 meter (Tanaka *et al*., 2007), but '*fail'* to provide any protections.

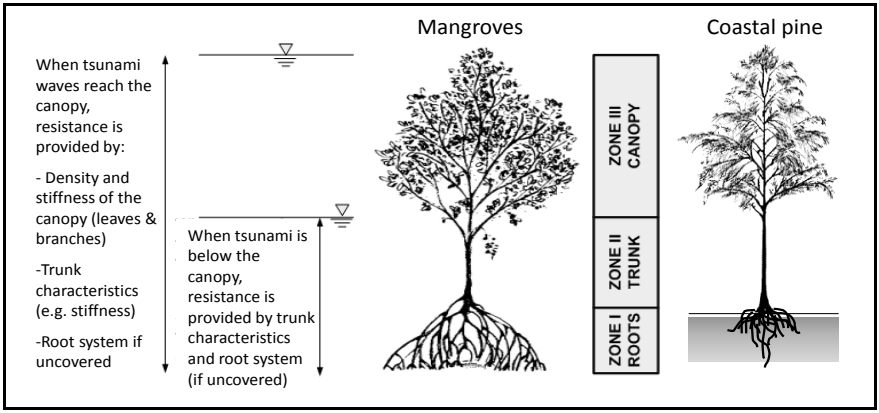

Fig. 2.4: Role of roots, trunk, and canopy in attenuating tsunami for both mangrove (*Rhizophora apiculata)* and coastal pine *(Casuarina equisetifolia)*

From the discussion above, the hydraulic resistance of mangrove and coastal pine trees against storm waves and tsunamis is mainly given by the following aspects:

- Geometry
- Density of mangrove roots and the canopy (leaves and branches) for both mangroves and coastal pines
- Strength of the trunks and branches which depends on age, geometry, and wood stiffness

2.2.1 Geometry

The geometry is a general parameter of tree structures that cover all aspects related to length, width, diameter and area. The geometry can be easily observed and measured and has a very strong relationship with the age of the tree. Therefore, the age of the tree should also be considered in the determination of the tree

geometry as shown exemplary in Fig. 2.5 for both mangrove and coastal pine trees.

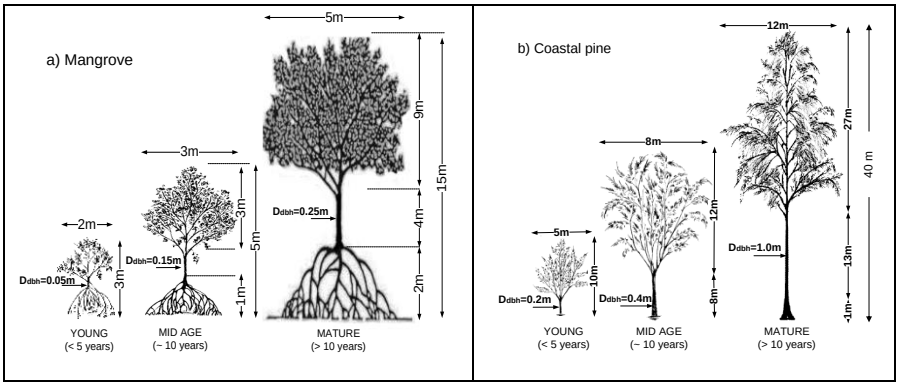

Fig. 2.5: Typical geometry of mangrove and coastal pine trees for different ages (from various sources)

The most common damage to coastal forest vegetations induced by tsunami is broken trunks. Broken trunks of coastal vegetations have been widely reported as early as the investigations on the effectiveness of coastal forests in mitigating tsunami. The characteristics of broken trunk of Japanese pines as a function of tsunami wave heights and trunk diameter during the last five major tsunamis in Japan (1896, 1933, 1944, 1960, and 1983) were identified by Shuto (1987) showing the importance of trunk geometry (

Fig. 2.6). Following the 2004 Indian Ocean tsunami, numerous reports describing the damage of coastal forests have been investigated. Tanaka *et al.* (2007) collected eight different vegetation species in coastal area of Sri Lanka and Thailand. It was found that many aspects contribute to the damage of coastal vegetations. Broken trunks are commonly found in a forest dominated by smaller diameter trees or by young age vegetations or in the area where tsunami heights were extremely large. The importance of the lateral distribution of trees to the direction of tsunami propagations has also been outlined.

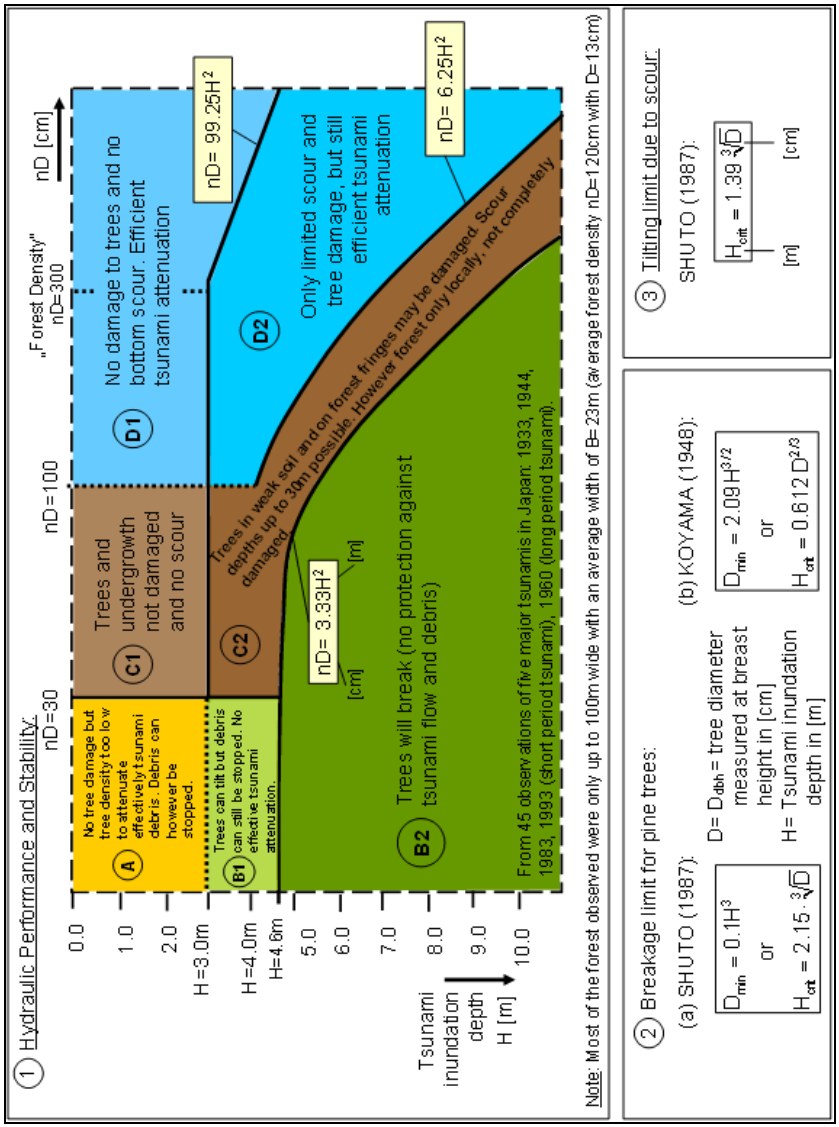

Fig. 2.6: Observed damages of coastal pine trees related to tsunami height according to Shuto (1987) (Synthesis of results by Oumeraci, 2006)

2.2.2 Density of roots

From the stability point of view, the complex root system of mangroves is considered as an appropriate adaptation form to the soft and muddy soils. In order to have a stable and standing structure, the roots develop complex foundation arrangement to support the upper structures of the tree. The dense roots also play role in trapping sediments and reducing the impact of incoming wave loads. The density of mangrove roots was measured as one of the important parameters in reducing the impact of storm waves by Mazda *et al*. (1997b). They measured the density variation of mangrove roots for different species and locations in Japan (Nakama Gawa) and in Australia (Coral Creek). Based on the results, a parameter called "submerged root volume ratio" (V_m/V) was proposed which is the ratio of the total volume of submerged roots (V_m) and the submerged control volume for a single tree (V). This ratio (V_m/V) is a function of the root density and the water depth. The submerged volume ratio concept and the field data curves from Mazda *et al*. (1997a) are depicted in Fig. 2.7. This concept was partially implemented by Latief *et al*. (1998), Harada and Imamura (2000), Istiyanto *et al*. (2003), and Kongko (2004) in their physical model experiments for the interaction of tsunami and mangrove forest models. However, the root volume ratio used in their models do not followed the pattern as described by the field measurements in Mazda *et al.* (1997a) because the effect of the water depth on the root density was neglected.

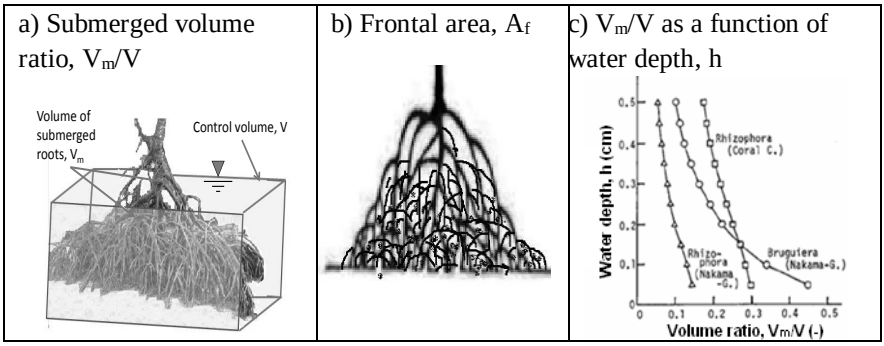

Fig. 2.7: Root density in terms of submerged root density and frontal area (after Mazda *et al*., 1997a)

The frontal area (A_f) is also often considered as an indicator for root density. The frontal area is defined as the area of an object (e.g. root system of mangrove) as seen perpendicular to the direction of the flow (Fig. 2.7b). The frontal area and the submerged volume ratio provide significant contribution to the hydraulic resistance (The Morisson equation) and determination of effective length (L_e) in which smaller L_e means denser root systems as defined by Mazda *et al.* (1997a).

Fig. 2.8: Spreading and shallow roots of coastal pines exposed by soil erosion

The habitats of pine trees in a dry sandy beach naturally determine the root system characteristics. In order to reach moisture beneath the soil, the roots have to spread in all direction with fibrous root system (Fig. 2.8). In general, the roots of coastal pines are always beneath the soils but can also form large surface roots. They have long main root system and distinctive short, lateral roots with equal branches (*dichotomous*). As long as the top soil layers are not eroded by wave or tsunami induced currents, the root system of pines is strong enough to withstand such forces. In many cases, the top soil layers are severely eroded and the trees were uprooted and collapsed by tsunami though some well grown species remained unbroken and safe (Tanaka *et al.*, 2007). The stability of root system has been found to be very important as reported by Imai and Matsutomi (2005) and

Tanaka *et al*. (2007). However, so far, this aspect is still 'a black box' due to the scarcity of the data and the high complexity of the underlying processes and interactions.

2.2.3 Density of canopy

Leaves and branches form the canopy of the tree. The canopy of the tree is a complex 3D biosphere structure and uniquely belongs to any species and environment. Mangroves and coastal pines do not have a consistent canopy shape and highly dependent on the species, age and environmental conditions. Simplification of canopy shapes becomes more difficult since there are hardly any publications or field measurements available for these two species. Therefore, the concepts as suggested by Tahvanainen and Forss (2007), Asano (2008) and Matsutomi *et al.* (2006) to form a constant shape of canopy in vertical direction is conceivable.

For engineering purposes, the density of the canopy should always be considered. There are at least three definitions determining the density of the canopy. i.e. based on canopy volume, canopy closure, and frontal area (Ellis and Bell, 2004). The first definition, the canopy density based on mass volume (3D) is the only definition that may also include the other two density definitions. The density of canopy in a 3-D sense is defined as the ratio of mass volume of the tree to the defined control volume which is similar to the definition of submerged volume ratio of mangrove roots system (see Fig. 2.7).

Leave Area Index (LAI) is often considered as the parameter for canopy density (Clough *et al*., 1997 and Clough, 2000). Generally, LAI is defined as the ratio of total one-sided leave area to the downward projected area of the canopy (Fig. 2.9). LAI has also been used widely for the general assessment of sustainable forest management, particularly by ecologists and biologists as a basic parameter for the estimation of the forest biomass. Therefore, field data for different forest types and the survey techniques to obtain further data are available (Clough *et al*, 2000 and Parrotta, 1995). Surprisingly, for engineering purposes, LAI has however not yet been implemented as a parameter to describe the hydraulic re-

sistance of forest vegetation. Efforts to investigate the relationship of canopy density characterised by LAI to the flow attenuation in open channel had been initiated by Fathi-Moghadam & Kouwen (1997) and Järvelä (2004) for riparian vegetations. However, the implementation to a much larger scale (i.e. coastal forest vegetation) in which the mass volume is much more important than the surface area of leaves has never been investigated. Since the relationship of LAI to the mass volume of tree canopy is not yet available, an estimation of the canopy mass volume based on the value of LAI is necessary.

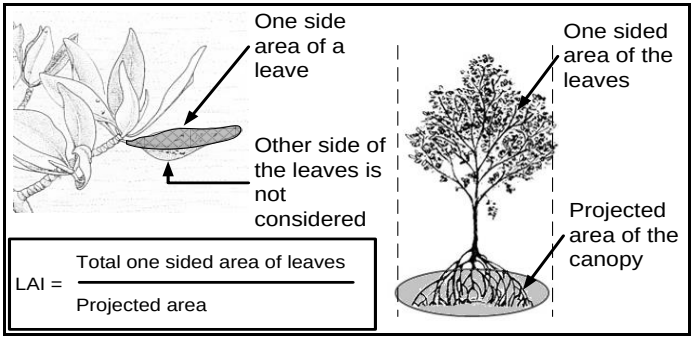

Fig. 2.9: Leave Area Index (LAI) concept of canopy for mangroves

The canopy of mangroves is considered as dense based on the measured Leaf Area Index (LAI) parameter. The LAI of mangroves can reach values up to 7 (Green and Clark, 2000). The LAI for mangrove below 5 years old is larger than 5 (Clough *et al*., 2000) while for coastal pine with similar age is ranging from 2.5 - 3.1 (Parrotta, 1995). However, as the age also controls the density of the canopy, the LAI decreases as the age of tree increases. The LAI of mangrove decreases up to 1.8 (for a 36-year old tree) and even smaller for coastal pine (Clough *et al.*, 2000).

Hirasihi and Harada (2003) and Harada *et al*. (2000) used artificial porous media to represent mangrove canopy density and derive drag coefficients based on porosity variations of the porous materials. Similarly, Istiyanto *et al*. (2003) and Kongko (2004) apply density variations for the canopy. Unfortunately, the bases

for the determination of canopy density are not clearly defined. All authors concluded that the canopy play a major role in reducing the impact of tsunamis. Instead of using LAI, the canopies of the mangroves are quite often parameterized as a function of the density and frontal area due to higher densities compared to trunk and roots. Therefore, considering 3D aspect of the problem, the concept of LAI might provide a better approximation to parameterize the mangrove canopy density.

2.2.4 Stiffness of woods

The stiffness of tree trunk represents one of the parameters controlling the attenuation performance of coastal forest vegetations. Shuto (1987) was one of the first authors to identify the role of trunk diameter in attenuating tsunami based on historical records of five major tsunami events in Japan. Later, numerous studies attempted to describe in more details not only the dimension of the trunk but also the age of the trees (Asano, 2008), forest density (Harada and Kawata, 2004), different species of trees (Imai and Matsutomi, 2004) and trunk strength and flexibility (Yanagisawa *et al.*, 2009). The strength of trunk characterized by wood stiffness is found to be considerably important since this characteristic is closely related to both the geometry and the age of trees. Broken trunks do not provide any damping and the debris carried by the flow may be very hazardous (Latief and Hadi, 2006). However, most of the available models as well as the derived resistance vegetation still have not fully considered this important aspect.

Traditionally, the strength indicator of wood for both mangroves and coastal pines is provided by the wood density and the moisture content[5]. A relationship between wood density and stiffness (represented by Young modulus, E) exists for certain tree species (Ayarkwa *et al*., 1999). However, due to the composite structure, the relationship between wood density and its Young modulus is not always the same for all species. Elasticity tests have to be performed for each sample species by considering environmental aspects such as water content and temperature. A simple three-point bend test can be used to estimate the Young modulus

[5] www.worldagroforestry.org

of a tree trunk. It is a simple deflection tests by pointing series of loads in the middle of wood sample and the deflections created by the processes of loading and unloading are recorded. From the obtained data, the Young modulus is calculated by applying the equation of deflection (Liu *et al*., 2002).

$$E = \left(\frac{gL_w^3}{48I} \right) \left(\frac{m}{\delta} \right) \qquad (2.1)$$

Where:

E : Young modulus [N/m^2]
g : gravity acceleration [m/ m^2]
L_w : length of wooden beam sample [m]
I : second moment of area [m^4]
m : loading mass [kg]
δ : deflection [m]

The previously measured E-modulus value of *Rhizophora* sp. is E = 8.27x10^{9}N/m^2 with moisture content 17% (Hawa, 2005) while Vallam *et al.* (2011) mentioned that the E for mangrove may reach up to 20.03x10^{9}N/m^2. Since the hydraulic resistance is derived from model scale experiments, scaling methodology of the E-modulus - and thus the stiffness- becomes another challenge. Matsutomi *et al.* (2006) proposed the concept of parameterisation for a trunk based on the Froude similitude, i.e. the scale of the trunk stiffness (characterised by E-modulus) is the same as the length scale λ_s. This scaling approach has also been implemented to scale down the elasticity of mooring line (Hughes, 1993) and to scale down the stiffness of ship's propeller (Steen, 2009). A similar approach by comparing the E of the prototype fender and its model based on Froude similitude was also applied to select a representative elastic fender model (Pathirana *et al.*, 2008).

2.2.5 General and specific tree parameters

Mangroves (*Rhizophora apiculata*) and coastal pines (*Casuarina equisetifolia*) have different abilities to attenuate tsunami. Considering all aspects that have been discussed, all tree parameters for both mangrove and coastal pine trees can be sorted as shown in Table 2.1 and Fig. 2.10.

Table 2.1: Parameters applied for both mangroves and coastal pines (see Fig. 2.10)

Parameters	**Geome-try**	**Densi-ty**	**Stiff-ness**	**Applicable for*):**
Total height of the tree (h_h)	x			Mg. & CP
Height of (branchless) trunk (h_t)	x			Mg. & CP
Height of canopy (h_c)	x			Mg. & CP
Trunk diameter (D_{dbh})	x			Mg. & CP
Diameter of the branches (D_{br})	x			Mg. & CP
Width of canopy (w_c)	x			Mg. & CP
Frontal area of canopy (A_{fc})	x			Mg. & CP
Frontal area of tree (A_f)	x			Mg. & CP
Leaf Area Index (LAI)		x		Mg. & CP
Modulus elasticity for trunk (E)			x	Mg. & CP
Total height of the roots (h_{rt})	x			Mg.
Height of submerged roots (h_{sb})	x			Mg
Height of emerged trees (h_{em})	x			Mg. & CP
Width of roots (w_r)	x			Mg. & CP
Root volume ratio (V_m/V)		x		Mg.
Canopy volume ratio $(V_m/V)_c$		x		Mg. & CP
Height of root buttress (h_b)	x			CP

*)Notes: Mg. = Mangroves, CP = Coastal pines

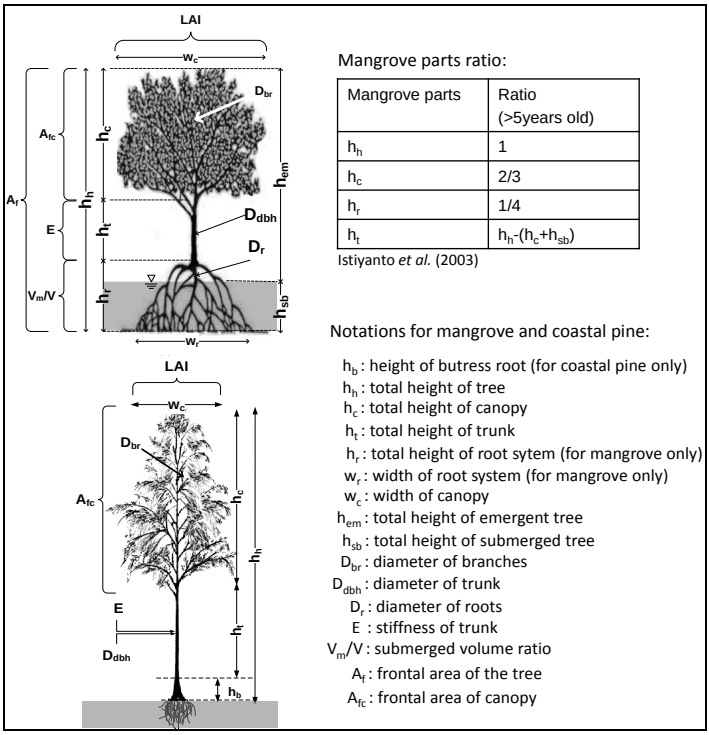

Fig. 2.10: Parameters for mangrove and coastal pines

The most difficult parameter to be included in the parameterised model is trunk stiffness characterised by the modulus elasticity E. Wood is a composite material primarily depending on the considered species. Estimation does exist for the stiffness of specific woods. Therefore, material selections and range of stiffness applicability have to be broadened in order to avoid missed-information on the parameterisation results. Moreover, considering the height of the incident wave relative to the height of the tree, studies on the parameterisation of mangroves and coastal pines should be divided into two assumptions based on vegetation structures and material characteristics:

– Stiff structure assumption considering only bottom part of the tree (root system) and the trunk. This assumption is implemented for mangroves

without the canopy due to the fact that mangroves have complex root system, so that the analyses should start with stiff structure assumption.

– Flexible structure assumption considering the whole part of tree structures (root system – trunk - canopy). This assumption is implemented for both mangroves and coastal pines. For this purpose, as already discussed above, the scaled trunk stiffness (represented by Young's modulus E) and flexibility of the canopy based on Froude similitude (length scale) for the trunk should be implemented. The assumption of "unbroken" trunk should also be adopted in orther to simplify the complexity of the problem. This assumption implies that the damping performance of the tree subject to extreme flow conditions which cause a breaking or/and uprooting of the trees is not considered in this study. Trunk structural integrity and uprooting of trees will not be discussed because it requires specific knowledge on geotechnics and root-system science which are beyond the scope of this study.

2.3 General characteristics of tsunami and storm waves

Tsunami and storm waves principally differ by their wave length and duration. Tsunami has very long waves (L > 500 km) with wave period ranging from 2 minutes to 2 hours while storm waves have wave length, L = 100 – 200 m with wave period from 5 - 20 seconds (Tomczak, 1996). Storm waves may last for hours causing gradual rise of water level and inundation depending on the strength and duration of storms while tsunami may last for less than 30 minutes with destructive forces. Tsunami and storm waves also cause different sedimentation behaviour along the coastline. Tsunami transports more sediment further inland as a result of fast transient flow while storm waves tend to accumulate sediment close to the zone of breaking waves (Morton *et al*., 2007).

Fig. 2.11 shows wave classifications based on different wave lengths and periods including the position of tsunami and storm waves. Tsunami and storm waves are two different phenomena that can cause as much as damages to the coastal area. The 2004 Sumatran Tsunami claimed 230000 human lives in more than 13 countries around Indian Ocean (Forbes & Broadhead, 2007) while the 1970 Bhola Cyclone killed at least 300000 people only in Bangladesh (Kabir *et al*.,

2005). Inundation and high velocity of flows are the most damaging forces when the waves reach the inhabited lands. Several measures have been taken to mitigate the impacts by reducing inundations and subsequent flows. Coastal forest vegetations are considered to provide such reducing effects from both tsunami and storm waves although their damping effectiveness is still uncertain.

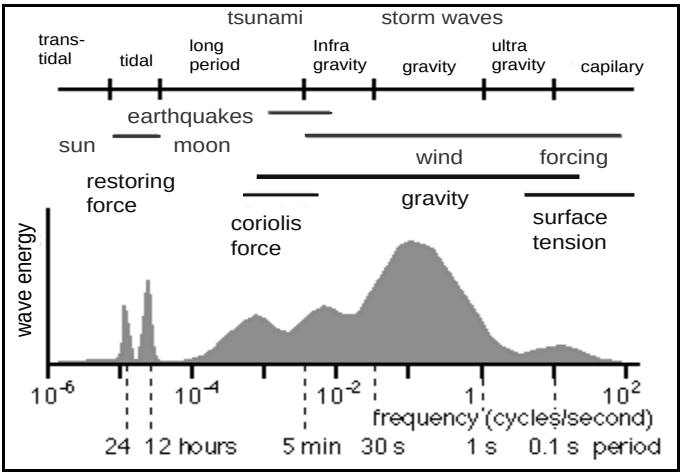

Fig. 2.11: Wave classifications (Tomczak, 1996)

Tsunami is a series of long waves generated by massive disturbances to the water body in the ocean. Earthquakes are by far the most frequent tsunami generator comprising 72% of all recorded noticeable tsunami events (Mc. Creery, 2007). Other causes of tsunami generation are landslides, volcanic eruptions, and meteorite impacts. The sudden movement of sea-bottom causing the entire water column to shake and transfer the energy in the form of water surface motions in all directions in the ocean. In the deeper ocean, the tsunami amplitude is small and hardly recognizable by naked eyes, carrying huge amount of energy and propagating fast with wave periods ranging from 10 minutes to 2 hours. The propagation of tsunami in deep sea can be well represented by linear shallow water wave theory, so that the velocity of tsunami is dependent only on the water depth:

$$C = \sqrt{gh} \tag{2.2}$$

Where,

C : tsunami velocity [m/s]
g : gravity acceleration [=9.81 m/s^2]
h : water depth [m]

For the 2004 Sumatera tsunami where the water depth of the fault line is h = 4000 m, the tsunami speed according to Eq. 2.2 can reach up to 700 km/hour (~200 m/s) and slows down up to ~10 m/s (at water depth h ≈ 10 m) as it propagates into shallower waters. This was the reason why Sri Lanka was hit by the 2004 tsunami almost at the same time as Thailand (~2 hours after the rupture) though Sri Lanka is located three times further from the fault line than Thailand (Rossetto *et al*., 2007). When tsunami waves travel over shallower waters, shoaling and refraction may amplify the waves. In the near shore, the waves start to feel the bottom frictions causing the wave length (L) to shorten, the wave height (H) to rise and the wave velocity (C) to decrease.

Incident tsunami may result in different type of waves and flow regimes as it propagates nearshore and over the dry land. Fig. 2.12 shows common observed characteristics of tsunami propagation and run-up in coastal areas. The term "solitary waves" for tsunami has long been used mostly in laboratory scale (Synolakis *et al*, 2007) though based on its physical characteristics (nonlinearity and horizontal length scale), this term is not completely true (Madsen *et al*., 2008). In practice, the term "N-waves" for tsunami generated by sea bottom disturbances is the most common one (Carrier *et al*., 2003, Synolakis *et al*., 2007). Moreover, the term "tsunami bore" has also been used to describe tsunami characteristics particularly during its propagation over shallow waters and dry lands (Yeh, 1991, Madsen *et al*., 2008). From the latest tsunami events (Indian Ocean Tsunami 2004, South Java 2006, and GEJET 2011), the appearance of tsunami bore was clearly observed as shown by numerous video recordings and tide gauges records on the time history of water levels.

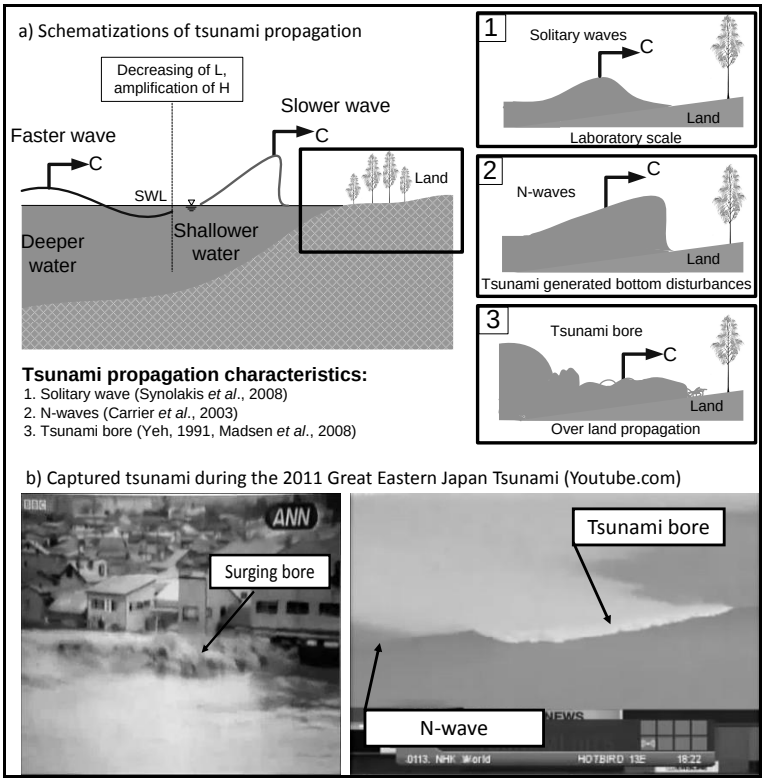

Fig. 2.12: Nearshore and onshore tsunami propagation characteristics

Unlike tsunami, storm waves are generated by offshore extreme winds from tropical storms, hurricanes, typhoons, or monsoons. The extreme winds may exceed 200 km/hour over large area in the ocean blowing towards the coastline and rising up the water level by several meters above mean sea level (MSL) and generating larger wind waves. The rise of water level (storm surge) accompanied by relatively shorter waves (with wave set-up nearshore) and their long duration are the main aspects that cause damages and widespread inundation particularly in the low lying coastal areas (Walton and Dean, 2009). The magnitude and duration of storm waves in coastal area depend on several factors such as off-

shore storm intensity, speed of storms, location of eye landfall, coastal bathymetry, coastal topography including the existence of natural and artificial barriers, and tidal elevation. Storm waves that are generated by only offshore extreme winds are commonly called storm surges while the combination of storm surge and high tides is called storm tides (Fig. 2.13).

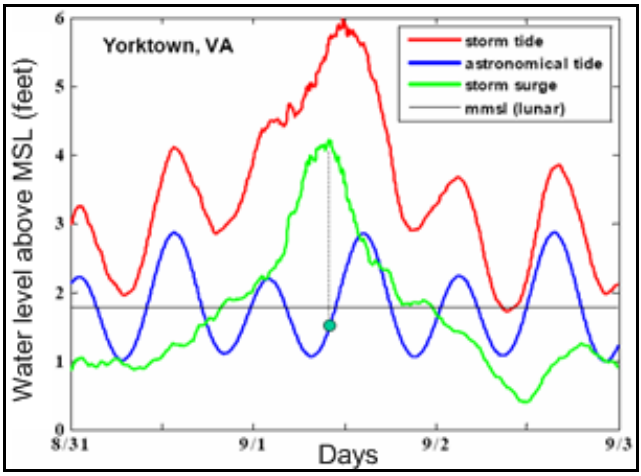

Fig. 2.13: Example of measured rising elevations due to storm surge and storm tide at the coastline of Virginia, USA (Boon, 2009)

Another component of storm waves that has damaging impacts to the shores is wave set-up and wave run-up. During the storm, certain duration of waves that breaks in the shore causing the elevation to rise conveying both energy and momentum of broken waves and hardly set-back to the sea as fast as their incoming behaviours. Large waves commonly occur around beachfront causing serious damage to the infrastructures, coastal forest and beach erosion. However, most of large waves are not transmitted further inland as they are already broken resulting in turbulent bores, wave set-up and wave run up. The magnitude of wave set-up depends on several factors such as beach profile, wave conditions (nonlinearity and directionality), and obstacles (e.g. vegetations). Wave set-up contribution can be 30%-60% of the rising water level due to storm surge (Dean and Bender, 2006). Numerous studies on wave set-up from laboratory and field survey are

available in Stive and Wind (1982), Goda (2000), USACE (1984) and Stockdon, *et al*. (2006).

From the discussion above, it is clear that the wave length is a key parameter for the effectiveness of damping performance of coastal forests. The fact that tsunami has much longer wavelength compared to the wind generated waves and that the forest geometry (length and width) is spatially limited, the damping efficiency of coastal forest is less prominent for the case of extreme tsunami. Since other environmental aspects also provide certain reduction effects to the extreme waves, damping performance contribution of the coastal forest and other enviromental aspects (e.g. bathymetry and topography) should be clearly distinguished.

2.4 Damping of Tsunami and Storm Waves by Coastal Forests

2.4.1 Types of damage to coastal forest vegetations

Observations from recent tsunami events (e.g. 2004 Indian Ocean Tsunami and 2006 South Java Tsunami) have demonstrated the significant role of coastal forest vegetations in damping the impacts of tsunami, resulting in reduced tsunami inundation distance, flow velocity and depth, and providing 'life saving fence' from tsunami backwash flow.

On the other hand, considerable damages of coastal forests due to tsunami have also been observed. The 2010 Mentawai tsunami and the 2011 Great Eastern Japan Tsunami showed that coastal forests were completely destroyed by the tsunami (Fig. 2.14). The scale of tsunami magnitude might contribute to the damage of most coastal forests along the coastline. However, other aspects that have not been investigated in more details such as foreshore topography, bathymetry, and characteristics of coastal forest vegetation may also play important role. Coastal forest vegetation becomes completely ineffective in mitigating tsunami if the structural stability of the trees constituting the forest is not sufficient. Moreover, the destroyed trees may also be carried landward by tsunami flow as deadly debris (Latief and Hadi, 2006).

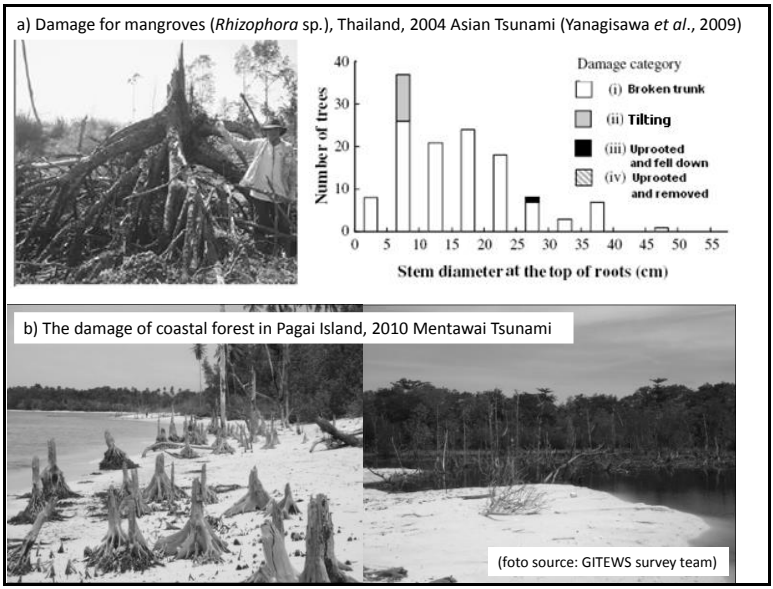

Fig. 2.14: Typical damage of mangrove forest hit by tsunami (Yanagisawa *et al.* (2009) and GITEWS Survey Team, private communications)

Shuto (1987) was among the first reporting tree damage conditions hit by tsunami (see Fig. 2.6). Following the 2004 Indian Ocean tsunami, numerous reports describing the damage of coastal forests have been investigated such as: broken trunk, uprooted, tilted and removed (Tanaka *et al*. (2007), Latief and Hadi, (2006), and Yanagisawa *et al.* (2009)). Broken trunk were found to be the most common damage of coastal forest hit by tsunami (Bappenas, (2005) and Yanagisawa *et al.*, (2009)). Uprooted trees are also commonly found in the front lines of the forest for most of tsunami cases. The resistance of trees against uprooting depends on the age of the tree, species, soil characteristics, and stand density of the forest. Therefore, all vegetation species and particularly those characterised by shallow roots system are most vulnerable to uprooting (Latief & Hadi, 2006; Tanaka *et al*., 2007). Mangroves at younger age (e.g. *Rhizophora* sp.) are also vulnerable to uprooting.

Table 2.2: Most relevant failure modes of mangroves and coastal pines

No.	Failure modes	Vegetations	Related influencing aspects
1	Broken trunk/branches	Mangroves (*Rhizophora* sp.)	Complex root system, thick canopy, trunk diameter and stiffness related to the age of tree
		Coastal pines (*C. equisetifolia*)	Trunk diameter and stiffness related to the age of tree
2	Uprooting	Coastal pines (*C. equisetifolia*)	Soil characteristics, shallow root system, young age, stand density of the forest, and location (most cases found in the front line)
		Mangroves (*Rhizophora* sp.)	Young age, soil characteristics, and stand density of the forest
3	Tilting	Both Mangroves and Coastal pines	Trunk diameter and stiffness related to the age of tree

A further failure mode that may contribute to the effectiveness of coastal forest vegetations against tsunami and storm waves is tilting. Laid-down trees are also considered as a failure mode in this category. These cases were found for almost all type of forest vegetations and are related to the strength of tsunami/storm waves, soil characteristics, species, trunk stiffness and age (Yanagisawa *et al*., 2009). Fig. 2.15 shows an example of damaged coastal forest vegetation where most trees were tilted and laid down due to storm waves in the East coast of Thailand.

In summary, the damage of coastal forest as related to their effectiveness to damp tsunami and storm waves can be categorised into three different failure modes based on their structural integrity and morphological characteristics. Table 2.2 shows the summary of failure modes for mangroves (*Rhizophora* sp.) and coastal pines (*Casuarina equisetifolia*).

Fig. 2.15: Examples of broken trunk (young age trees), uprooted trees, and tilting/inclined trees for *Casuarina equisetifoila* due to storm waves in the East Coast of Thailand (courtesy of Dr. P. Rattanamanee, private communication)

2.4.2 Hydraulic resistance of coastal forest vegetations

Field measurements, laboratory experiments as well as theoretical and numerical approaches have been carried out to derive the resistances of coastal forest against tsunami and storm waves. Generally the hydraulic resistance of coastal forest includes:

- Drag and inertia losses which may be described by drag and inertia coefficients (C_D and C_M) as a function of water depth, flow regimes (R_e), and forest density.

- Bottom frictions which may be described in terms of *Manning* roughness (n) as a function of the beach landscape types of coastal beds (i.e. sands or mud), and the undergrowth

- Eddy viscosity and vortex loses due to turbulent flow through the forests

So far, drag coefficient C_D, inertia coefficient C_M and *Manning* roughness coefficient '*n*' have been widely used in both theoretical and numerical models to investigate the role of coastal forest in mitigating the impact of tsunami and storm waves. Besides different approaches and methodologies, the existing coefficients describing the hydraulic resistance of forest vegetation have been derived mainly from laboratory experiments by modifying general *Manning* roughness coefficient (*n*) as a function of drag and inertia coefficients (C_D and C_M). The drag and inertia coefficients are highly influenced by the geometrical characteristics of the tree, the vegetation stiffness, and the flow regime characterised by the Reynolds number (R_e). C_D and C_M have been derived indirectly from the measured velocities and surface elevations of laboratory experiments (or field measurements) using the Morison equation (Morison *et al*., 1950):

$$F_T = \underbrace{\frac{1}{2} C_D \rho A_f u^2}_{\textit{Drag force}} + \underbrace{C_M \rho V_v \frac{\partial u}{\partial t}}_{\textit{Inertia force}} \qquad (2.3)$$

Where:

F_T : total force [N]
ρ : water density [kg/m^3]
A_f : cross sectional area of the body subjected to flow [m^2]
V_v : submerged volume of body subject to flow [m^3]
u : flow velocity [m/s]
$\partial u / \partial t$: local flow acceleration [m/s^2]
C_D : drag coefficient [-]
C_M : inertia coefficient [-]

Previous studies show that parameters affecting the attenuation performance of coastal forests were treated differently. Moreover, damping performance of mangrove forests for practical applications is still largely unknown. Laboratory experiments were widely used for the derivation of hydraulic resistance (*Manning* roughness, drag and inertia coefficients) based on different parameterized models.

Extensive field investigations on the role of mangroves (*Kandelia candel*) in reducing the impact of frequent storm waves were investigated in the coastlines of Vietnam (Mazda *et al.*, 1997b). The relative reduction of the incident waves travelling through a certain distance of forest width (ratio of incident and transmitted waves) was adopted as a main indicator for the attenuation performance of mangroves. They analysed the effect of both age and density of the mangrove forest (slope 5/10000) and found that the relative wave reduction is up to 20% (forest width, B = 300 m) for 6-year old mangroves and less for younger ones. The reduction rate was 10% - 15% (B = 250 m) and 1% - 3% (B = 500 m) for 3-year-old mangroves and 0.5-year-old mangroves, respectively. This study also showed that the increase of water level generally reduces the relative wave reduction. For the case of 6 year old mangrove forest, however, the increase of water level did not significantly reduce the relative wave reduction, because the short mangrove canopy may also have contributed to the relative wave reduction. Another investigation with different mangrove species (*Sonneratia* sp.) showed that the relative wave reduction was found up to 45% (slope 1/1000, B = 100m, tree density, N_s= 0.08 m^2) as compared to the shore without the presence of mangroves (Mazda *et al.*, 2006).

Wave attenuation by coastal forests has also been studied using laboratory experiments. The work of Petryk and Bosmajian (1975) on vegetation resistance in terms of Manning roughness coefficient (*n*) induced by drag has been adopted for mangroves by using a vegetation density (roots and trunks) for a pre-defined cross-sectional area of the channel (Wolanski *et al*., 1980). Most of the parameterised tree models used stiff structure assumption. Recent flume tests considering both stiff and flexible parameterised tree models of wetland vegetation (*Spartina alterniflora*) were carried out by Augustin *et al*. (2008). The stiff models were made from cylindrical wooden dowels while the flexible models were made from cylindrical polyethylene foam with a deflecting angle up to 20^o. Wave attenuation was investigated under breaking and non-breaking conditions for different water levels (emergent and submerged conditions). Wave transmission coefficient K_t was found to be significantly larger by 15 - 20% under emergent conditions than submerged conditions. Surprisingly, the flexible vegetation model was found to dissipate more energy by only 1-4 % higher as compared to the rigid vegetation model.

An analytical approach to investigate the attenuation performance of mangrove forests under storm waves was carried out by Massel *et al.* (1999). They proposed a concept of energy dissipation by mangrove forests in the frequency domain by considering linearized drag losses. Additionally, based on field data, Massel *et al.* (1999) also outlined that the attenuation performance of mangrove forests is influenced not only by tree dimensions and density but also by the spectral characteristics of the incident waves.

For the case of tsunami, several laboratory studies with different parameterised mangrove tree models and different experimental set-ups were performed, resulting in different hydraulic resistance and consequently different attenuation performance. Different definitions/values of drag/inertia coefficients C_D and C_M as well as general *Manning* roughness coefficients *n* are in fact due to the different methods used to parameterise coastal forest vegetations and the simplifying assumptions behind them. Coastal forest vegetations have been represented and scaled down by different shapes and materials based on different parameters, e.g. porosity/density of canopy represented by porous media (Harada *et al.*, 2000) or by number of cylinders with different arrangement (Kongko, 2004). Other influencing aspects are the generated tsunami/waves at laboratory scale with different wave generation mechanisms and different wave conditions to represent tsunami, and using different beach topography models. Harada *et al*. (2000) used solitary waves to represent tsunami waves while Istiyanto *et al*. (2003), Hiraishi and Harada (2003), Kongko (2004), and Imai & Matsutomi (2004) used bore generators with different generating mechanisms. The role of beach topography for the attenuation performance of forests from the findings of the field surveys was found to be significant (Chatenoux and Peduzzi, 2005). However, none of the previous model experiments implemented similar beach topographies or made any attempt to distinguish between the energy dissipation due to forest and that due to beach topography. Harada *et al*. (2000) used beach models with 1/5, 0, and 1/100 slopes, Hiraishi and Harada (2003) with 1/3, 0, and 1/50 slopes, Istiyanto *et al*. (2003) with 5^o, 10^o, 15^o slopes or 1/11, 1/5.8, and 1/3.9 slopes, Kongko (2004) with ½ slope, while Imai and Matsutomi (2004) constructed a beach model with 1/26 slopes. None of these studies provided any indication on the effect of these foreshore slopes on the incident and transmitted waves behind

the forest model. The resistance of vegetations for both tsunami and storm waves can be summarised as shown in Table 2.3.

Table 2.3**:** Available coefficients for the flow resistance of forest vegetation

Hydraulic resistance	**Formulation**	**Notes & Remarks**	**References**
Manning roughness coefficient, n	$n^2 = \frac{R_h^{4/3}}{2g}\left(\frac{C_D \sum A_p^i}{A_f L_v}\right)$, C_D~1	Based on model test in a channel flow with cylinders	Petryk and Bosmajian (1975)
Drag coefficient, C_D	$C_D = \begin{cases} 1.2 & for\ R_e \le 2\times10^5 \\ 1.2-0.5\left(\frac{R_e}{3\times10^5}-\frac{2}{3}\right) & for\ 2\times10^5 \le R_e \le 5\times10^5 \\ 0.7 & for\ R_e \ge 5\times10^5 \end{cases}$	Based on model test in a channel flow with cylinders	SPM (1984), Yanagishawa *et al*. (2009)
Drag coefficient, C_D, inertia coefficient, C_M	$C_D = -2g\frac{\partial \eta}{\partial y}\frac{L_e}{u^2}$, C_D = 0.4 - 15 C_M~0	Based on tidal scale measurements	Mazda *et al*. (1997a)
Drag coefficient, C_D, inertia coefficient, C_M	$C_D = \frac{8.4V_m}{V_w} + 0.66$ C_D = 0.5 – 1.75, C_M=1.7	Based on models made of porous media (canopy and roots) and cylinders (trunk)	Harada and Imamura (2000), Hiraishi & Harada (2003)
Equivalent *Manning* roughness coefficient, n_e	$n_e = \sqrt{\frac{H^{4/3}}{2gV}(C_D A_f) + n_b^2}$	Generalising resistance of vegetation including bottom friction	Harada & Kawata (2004)
Drag coefficient, C_D, Inertia coefficient, C_M	$C_D = 0.5818e^{-0.00034\,\mathrm{Re}}$, C_D = 0.2 – 0.4, C_M=0	Based on models made of group of cylinders for canopy, trunk, and roots	Kongko (2004)
Drag coefficient, C_D, Eddy viscosity, f_v	$f_e = \frac{C_D u\lvert u\rvert}{2L_e}\left(\frac{\partial^2 u}{\partial y^2}\right)^{-1}$, C_D (see Mazda et al., 1997b)	Derived from field measurements, tidal scale	Kobashi and Mazda, 2005

Drag coefficient, C_D, inertia coefficient, C_M wave making resistance θ’	C_D = 0.9 - 1.5, C_M = 1.5 – 3.25, θ’= 0.02 – 0.07	Based on artificial tree model with simplifications into group of equivalent cylinders	Imai & Matsutomi (2005)
Manning roughness coefficient, n and Inertia coefficient, C_M	$n = \begin{cases} 0.16 + 0.17\frac{V_m}{V} & if\ \frac{V_m}{V} \geq 0.07 \\ 0.03 & if\ \frac{V_m}{V} < 0.07 \end{cases}$ $C_M\ \frac{V_m}{V} = \begin{cases} 0.67 + 6.65\frac{V_m}{V} & if\ \frac{V_m}{V} \geq 0.06 \\ 1 & if\ \frac{V_m}{V} < 0.06 \end{cases}$	Based on experiment similar to Harada *et al.* (2000)	Latief and Hadi (2006)
Vegetation friction R_b Drag coefficient, $C_{D,}$	$R_b = f\frac{u_b\lvert u_b\rvert}{h+\eta}$, C_D = 0.1 – 1.0	Generalising vegetation as a friction (f) into numerical model (Boussinesq model-COULWAVE)	Augustin *et al.* (2008)
Drag resistance factor, D_f	$D_f = \frac{4}{3\pi}C_D D_{dbh} N\bar{u}$ $C_D = 1.0$, $D_{dbh} = trunk\ diameter$ $N : number\ of\ trees$ $\bar{u} : tsunami\ averaged\ velocity$	The drag resistance factor is used along side tree growth model assuming that only trees satisfy critical moment will provide protection.	Asano (2008)
Drag coefficient, $C_{D,}$ Eddy viscosity coefficient bottom roughness	C_D ~ 0.17 $f_v = c_W\frac{E_k^2}{\varepsilon_D}; where\ \varepsilon_D = c_D\frac{E_k^{1.5}}{l_D};$	Based on Sub-depth Scale (SDS) turbulence model by Nadaoka and Yagi (1998); E_k: kinetic energy; l_D: length scale; c_D & c_w: constants	Thuy *et al.* (2009)

Like the methodologies on the parameterisation of coastal forest vegetation, the derived hydraulic resistance which are mostly derived from laboratory experiment also vary. Other aspects related to the experimental setup are also determinant to the derived hydraulic resistance induced by a coastal forest model, such as: model scale, inclusion of shore topography (e.g. different slopes), type of generated waves (e.g. bore and solitary waves), and measurement devices.

Drag and inertia coefficients C_D and C_M are the most commonly used hydraulic resistance coefficients for tsunami and storm waves. Inertia coefficients can be as important as the drag coefficient during the first wave impact. Other types of hydraulic resistance such as wave making resistance and eddy viscosity were found less significant as the drag and inertia resistance. The derived drag and inertia coefficients vary widely from C_D =0.1 to C_D =15. Besides the flow regime, the specific underlying physical processes behind this large variation on the drag coefficients are still not fully understood. For the practical implementation of the given values of drag coefficient would require more information, including the range of flow regimes for which they are valid. This problem may be solved by implementing an appropriate parameterisation of coastal forest vegetations. Moreover, during laboratory experiments direct and simultaneous force measurements in the model as well as surface elevation and current velocity are absolutely needed in order to avoid any unnecessary simplifications that may lead to large deviations in the analysis.

Unlike the drag coefficient, the derived inertia coefficients from previous studies vary within a narrower range from C_M =1.5 to C_M=3.25. However, the inertial component is also often neglected as compared to the drag component. This indicates that the inertia coefficient which is a function of the submerged volume of the body and the flow acceleration is less influenced by the different shapes of the parameterised tree models. The drag coefficients, however, is very sensitive to different shapes (frontal area and submerged volume ratio). Proper parameterisation methodology should therefore ensure a consistent representation of both frontal area and submerged volume ratio of the tree models.

Particularly after the 2004 tsunami field surveys, the effectiveness of coastal forests in reducing the impact of tsunami has been the subject of controversies. This often occurs because there are many important effects which were not properly considered in the analysis of the field surveys. Shore topography and the natural habitats of coastal forests (sheltered areas for mangroves and dry beach for coastal pine) are only two of these important effects that have led to such controversies. Those who are against the use of coastal forest for tsunami protection mention that sheltered areas and high ground elevations (shore topography) are the most determining aspects protecting the area behind the forest. For many areas which withstood tsunami without significant damage, very often tsunami energy was already largely dissipated by the shore topography. The role of shore topography in attenuating the energy of tsunami has been thoroughly discussed after the 2004 Indian Ocean Tsunami by Chatenoux and Peduzzi (2005). Moreover, recent forest damage from recent tsunami events (the 2010 Mentawai Tsunami and the 2011 Great Eastern Japan Tsunami) shows that the effectiveness of forest in damping tsunami energy is still controversially discussed. Consequently, there are no conclusive approaches on the conditions for which the derived coefficients describing the hydraulic resistance induced by coastal forest are applicable. Therefore, it is very clear that wave attenuation by coastal forest should always consider the contribution of the bathymetry/topography in order to estimate and validate the actual wave/tsunami damping solely induced by coastal forests.

2.5 Modelling of tsunami and storm wave attenuation by coastal forests

Long wave models (tsunami and storm wave models) have been developed mainly for the purpose of tsunami hazard mapping area based on estimated deep sea disturbances (earthquakes, landslides, or volcanic eruptions), arrival time, run-up distances, and inundation depths. The available operational models that sufficiently describe the interactions of tsunami flows and vegetations are mainly limited to the applications of depth-integrated Boussinesq-type equations (BTE) models and Shallow Water Equations (SWE) models (Table 2.4). Both BTE and SWE are depth-averaged models which have their strengths and limitations in terms of the relative importance of the wave propagation properties such as non-

linearity and dispersion, computational performance and other operational aspects.

Models based on Navier-Stokes Equations (NSE) were used for laboratory scales but still impractical as operational tools for prototype scales due to expensive computational times (Dao & Tkalich, 2007). Recent development showed that NSE based models are also capable to simulate more complicated structures (e.g. vegetation structures) by averaging NSE twice in time (phase) and space. This approach is called Double-Averaged Navier-Stokes (DANS model). The flow field through submerged canopy was investigated by Lowe *et al.* (2005) using a DANS model by decomposing and averaging fluid velocities in time and space. A single term is used which consists of a depth-averaged form of the phase, spatially averaged for the momentum conservations with associated losses such as drag and inertia, and all fluid stresses. They found that oscillatory flow inside the canopy generates larger velocities as compared to canopy subject to unidirectional flow. Further investigations using a DANS model can also be found in Righetti (2008) for channel flow applications and Finnigan & Shaw (2008) for wind atmospheric applications.

Table 2.4**:** Available models for tsunami and storm waves

Model names	Abbreviation	Model type	Availability
Tohoku University's Numerical Analysis Model for Investigation of Near-field tsunamis	TUNAMI	SWE	Free www.tsunami.tohoku-u.ac.id
COrnell Multigrid COupled *Tsunami model*	COMCOT	SWE	Free www.ceeserver.cee.cornell.edu/pll-group/comcot.htm
Australian National University and Geoscience Australia Model	ANUGA	SWE	Free http://www.ga.gov.au/hazards/tsunami/tools.jsp
Method of Splitting Tsunami model (NOAA-USA)	MOST	SWE	Free by request http://nctr.pmel.noaa.gov/model.html

TsunamiClaw model is part of a larger Calwpact model from Washington University-USA	Tsunam-iClaw	SWE	Free http://www.amath.washington.edu/~dgeorge/tsunamiclaw.html
Tsunami modelling at AWI (Alfred-Wegener Institute, Germany)	TsunAWI	SWE	Free by request http://www.awi.de/
Global Tsunami Model-University of Alaska Fairbanks	GTM	SWE	Free by request http://www.sfos.uaf.edu/tsunami/global/index.html
Tsunami module from DELFT3D model of Deltares – the Netherlands	DELFT3D	SWE	Commercial http://delftsoftware.wldelft.nl
Tsunami module from MIKE21 model of DHI - Denmark	MIKE21	SWE	Commercial *www.dhigroup.com/*
Fully nonlinear wave model, University of Delaware - USA	FUNWAVE	BTE	Free http://chinacat.coastal.udel.edu/programs/funwave/funwave.html
Cornell University Long and Intermediate Wave Modeling Package	COUL-WAVE	BTE	Free https://ceprofs.civil.tamu.edu/plynett/COULWAVE/
Combination of TOPICS (Tsunami Open and Initial Condition System) model and FUNWAVE	GEOWAVE	Hybrid (SWE and BTE)	Free www.tsunamicommunity.org
Tsunami Open Source, Texas A&M, Cornell University, University of Puerto Rico, University of Hawaii, and University of Puerto Rico	TSUNA-MOS	Hybrid (SWE, BTE and NSE models)	Free https://www.nees.org/

Selecting appropriate model for given applications depends on different aspects which need to be considered. In this study, the attenuation of tsunami and storm waves due to coastal forest is the main objective. The interactions of tsunami as

well as storm waves should be sufficiently described in the model. The available models, e.g. MOST from NOAA are practically robust to model tsunami generation, propagation, and inundation. However, since it has been mainly designed to simulate maximum possible run-up in coastal area, bottom roughness due to forests and other large obstacles has been ignored (Gonzalez *et al*., 2007). Other models, e.g. TUNAMI-N2 and COMCOT do consider roughness due to forest vegetation and other obstacles. These are very important since the reduced run-up height and distance of inundations are determinant in the decision-making process of designing optimum protection by using green-belts along the coast-lines (or other possible measures). Type of vegetations, width of forest, density and age of trees are some of the main aspects that have to be considered in determining the values of the flow resistance coefficients.

From the numerical point of view, finite difference schemes were widely implemented in tsunami propagation from deeper water to intermediate water. The schemes have shown excellent performance in accuracy and efficiency throughout the simulations (TUNAMI, COMCOT, and TUNA-M2). Another scheme that has been used to simulate tsunami and storm waves is finite-element method allowing adaptive non-structured numerical grids into the domains (TsunaClaw and TsunAWI). However, this method is computationally more demanding than finite difference methods and very sensitive in changing model parameters (Myers and Baptista, 1995). Recently, finite volume methods offer additional features to the model such as describing hydraulic jump when dealing with sudden obstacles (e.g. ANUGA) (Roberts *et al*., 2009).

Horrillo and Kowalik (2006) simulated the 2004 Indian Ocean tsunami and compared three models (NLSWE, BTE, and RANS) to examine the importance of nonlinearity and dispersion effects for the main characteristics of tsunami propagation (arrival time and wave height). The three models are generally in agreement to simulate the main characteristics of tsunami. Dispersion effects (by BTE and RANS models) were observed to produce higher harmonics in leading waves as time advances. However, NLSWE is computationally much faster compared to the BTE models and RANS models which are even much slower (Table 2.5).

Table 2.5: Model performance based on CPU time Horrillo and Kowalik (2006)

Model	Grid size			Nr. of cells	CPU time
	dx (m)	dz (m)	dt (s)		
NLSW	100 m	-	0.2	157059	30 minutes
BTE	100 m	-	0.2	157059	5 hours
RANS-VOF	5 - 875	0.2 - 40	0.08-0.8	800000	72 hours

Other aspects that may lead to some discrepancies in modelling of tsunami propagation, run-up, and inundations are frictions, generating sources, Coriolis forces, and numerical aspects (e.g. grid sizes). Tsunami source constraints were investigated by Grilli *et al.* (2007) by using NLSWE and BTE models to model the 2004 Indian Ocean tsunami. They found very large errors in surface elevations (~20%) in deeper sea that consequently lead to wrong boundary in shallower waters. Coriolis force is also very important for the propagation of tsunami in the ocean, because it can influence tsunami propagation speed and run-up (Dao & Tkalich, 2007). Using NLSWE model, Myers and Baptista (2001) implemented different frictions values to the model to analyse sensitivity of different friction values to tsunami heights and they found larger differences observed for shallow waters (h = 0 - 10 m) and run-ups varied from -6 to +6 m. These indicate that choosing the correct values of frictions, particularly when dealing with vegetations are very important aspects for the simulation of tsunami run-up and inundation over land. Moreover, Kongko (2012) found significant differences for the estimation of tsunami run-up and inundation for the city of Padang based on different bathymetry/topography details.

Considering the robustness of the model, the flexibility of numerical techniques and for the practical aspects, SWE models represent a more practical and operational tool to simulate the interactions of tsunami and vegetations. Their sufficient accuracies and computational efficiency have brought the SWE models being implemented in most countries. For instance, the UNESCO/IOC has been using and distributing the Tohoku University's Numerical Analysis Model for Investigation of Near-field tsunamis (TUNAMI) model to more than nineteen institutions in fifteen countries as a part a programme for tsunami mitigation measures programme (Imamura *et al*., 2006).

Table 2.6: Freely available SWE models

Model	Main Features	Numerical schemes	Vegetation treatment	Main users
TUNAMI[1]	Solve LSWE and NLSWE, varying grids, weakly nonlinear and weakly dispersive,	2nd order explicit staggered leaf-frog	Equivalent *Manning* roughness (*n*), and loses as function of C_D and C_M	Tohoku Univ. (Japan), UNESCO/IOC country members
COMCOT[2]	Solve LSWE and NLSWE, nested grid system, weakly nonlinear and weakly dispersive, breaking dissipation included	2nd order explicit staggered leaf-frog	Equivalent *Manning* roughness (*n*), can be extended to hydraulic losses as function of drag coefficient C_D and inertia coefficient C_M	Cornell Univ. (USA), Countries in Pacific regions
MOST[3]	Solve LSWE and NLSWE, weakly nonlinear and weakly dispersive, nested grid system,	Finite element, adaptive grid	Not included	NOAA and countries in DART group
ANUGA[4]	Solve LSWE and NLSWE, nested grid system, hydraulic jump.	Finite volume	*Manning* roughness (*n*) (not fully validated)	AG Australia

Notes: 1) Imamura *et al.* (2006), 2) Liu *et al* (1998), Wang (2009), 3) Titov & Synolakis (1995), (1998), (4) Robert *et al*. (2009)

TUNAMI model solves LSWE divided into modules that can be run simultaneously. Further development to solve both linear and nonlinear aspects leads to the development of Cornell Multi-grid Coupled Tsunami model (COMCOT). COMCOT model was developed in Cornell University based on theoretical and numerical works of Shuto (1991) and Imamura *et al*., (1988). Additional important features such as moving boundary schemes (Liu *et al*., 1995), grid matching algorithm, nonlinear equations solver and grid nesting algorithm, and

dispersion algorithm have been introduced making COMCOT model able to simulate linear/weakly nonlinear dispersive waves with high efficiency (Wang, 2009). Other SWE model that has been used for the application of Tsunami Warning system is MOST models. Method of Splitting Tsunami (MOST) model has been widely used in Pacific regions and operated by the *National Oceanic and Atmospheric Administration* of United States (NOAA) through Deep-ocean Assessment and Reporting of Tsunamis (DART), a tsunami real time early warning system (Mc. Creery, 2007). Different numerical approaches have been developed in Australian National University and Geoscience Australia (ANUGA) model by employing finite volume method. However, the model has not yet been fully validated for bottom friction problems (Robert *et al*., 2009).

TUNAMI model has been adopted by IOC/UNESCO as one of the operational models for the generation, propagation, and inundation tsunami model in the pacific region (Imamura et al., 2006). Since its establishment, COMCOT model has also widely been used for the simulation and tsunami mitigation assessment from its source until run up and inundation in several regions such as the Indian Ocean (Wijetunge, 2009 and Wang & Liu, 2006), South China sea (Huang *et al*., 2008), East Atlantic regions (Olabarrieta *et al.,* 2010 and Omira *et al.,* 2009) and West Pacific regions (Gale & Power, 2010 and Wang & Liu, 2005). Due to the fact that both models are originated from similar old model developed by Shuto (Wang, 2009), both models still have several similarity aspects including model structures, the numerical schemes (explicit staggered leaf-frog), the language programming (FORTRAN), and implementation of *Manning* roughness.

TUNAMI model features roughness coefficient in the form of *Manning* coefficient, *n*. Though *Manning* roughness coefficient is originally applied for the sea bottom conditions, in TUNAMI, coastal forest vegetation has also been treated similarly with certain value of *Manning* roughness coefficients *n* as a function of submerged volume ratio (Latief and Hadi, 2006). Moreover, Harada & Imamura (2003) derived a comparable relationship of Manning roughness as a function of drag and inertia coefficients for forest vegetation based on laboratory experiments. Though, the derived roughness coefficients are different and sometime contradict each other, TUNAMI model is by far the most widely implemented model dealing with coastal forest vegetations. COMCOT model also implement

Manning roughness coefficient for the sea bottom roughness similar as in TUNAMI model (Wijetunge, 2009). Up to now, the use of *Manning* roughness *n* for typical coastal vegetation trees in COMCOT model is still not implemented yet. However, similar *Manning* roughness modification as in TUNAMI model (Harada and Imamura, 2000) can be also adopted in COMCOT model.

As time passes, TUNAMI model has been further developed by many groups of researchers such as the one developed by the group of Prof. Yalciner from the Middle East University, Ankara Turkey. The TUNAMI model has been developed into a more user friendly model in which all required inputs and the outputs can be viewed via window interface. The name of the user-friendly TUNAMI model becomes NAMIDANCE[6]. Unfortunately, this model version is not freely available. Similarly, COMCOT model has also been developed and maintained by the group of Prof. Liu from Cornell University[7]. The latest version of COMCOT model is version 1.7 in which all numerical codes as well as the documentation are downloadable in the website. The records of model development and modifications are well documented. In the latest version, the input parameters can be easily stored in a single input file and the outputs can be analysed (plotted) by the help of available MATLAB codes. Besides that both model are reliable for tsunami modelling, COMCOT model has some advantage compared to TUNAMI model as follows:

1. The codes of the latest version from COMCOT model (version 1.7) are freely available while only the codes from the old version of TUNAMI model are available.
2. The latest version of COMCOT model has been migrated from FORTRAN 77 to FORTRAN 90. This makes COMCOT is more compact, convenient and can be easily adapted to the current computer programs and operating systems. The available old version of TUNAMI model is still based on FORTRAN 77.
3. The format of bathymetry file in COMCOT is more flexible allowing three different bathymetry formats files.

---

[6] http://namidance.ce.metu.edu.tr/

[7] http://ceeserver.cee.cornell.edu/pll-group/comcot.htm

4. Automatic adjustment of grid size based on the Courant condition
5. Forcing parameters can be selected from the control input file. Four choices are available: fault, land slide, water surface displacement or incident wave maker. For the incident wave maker, both regular and solitary wave parameters (i.e. wave height H and period T) can be directly adopted. For irregular waves, a time series format is applicable.

Another important aspect of numerical simulation is benchmarking problems (Synolakis *et al.*, 2007). Ideally, a numerical model should be validated by three benchmarking problems: analytical solutions, laboratory experiment and field measurements. During the 3rd International Workshop on Long Wave Run-up Models in Wrigley Marine Science Centre of the University of Southern California in 2004, COMCOT model has been well tested with the three benchmarking problems as described in Zhou *et al*. (2009) for analytical benchmarking, Wang *et al*., (2008) for experimental benchmarking and Liu and Wang (2005) for field data benchmarking. In summary, COMCOT as one of NLSWE-based models satisfies all the required benchmarking problems, simply to use, well maintained (up to date) and widely implemented in many tsunami events.

The use of the COMCOT model for this study should provide a reliable analysis on the interaction of tsunami / storm wave and coastal forests in the wave flume. The model can also be further implemented under field conditions for either model calibration/validation or prediction based on the hydraulic parameters found from laboratory experiments. Moreover, open access to the model source code allowing ones to make necessary modifications or improvements for specific purposes or to enhance model performance.

2.6 Specification of objective and methodology of PhD study

From the above discussion, the current study should consider the following aspects:

1. Proper physically-based parameterised tree models to derive the hydraulic resistance in terms of drag and inertia coefficient. Besides different approaches and methodology, the existing coefficients describing the hy-

draulic resistance of forest vegetation, the drag and inertia coefficients C_D and C_M are also highly influenced by the geometrical characteristics of the tree, structural elasticity, and the flow regime characterised by the Reynolds number (R_e). C_D and C_M have yet been derived indirectly from the measured velocities and surface elevations mostly in laboratory experiments using the Morison equation. Therefore, direct measurements of wave forces acting directly on the vegetation models will be required.

2. Experimental setup should be designed to measure directly the hydraulic force, current velocity and water surface elevation. Moreover, a wide variation on wave conditions as a function of different water depths will provide a wide range of applicability of the derived C_D and C_M values, depending on the prevailing flow regime (R_e).
3. Wave attenuation due to shore topography should be carefully analysed and its relative contribution to the wave attenuation should be distinguished from the attenuation induced by the forest itself.
4. The model scale should be properly determined and large enough so that scale effects particularly due to the incorrect reproduction of the energy dissipation are significantly reduced. Moreover, the scale should be large enough to avoid any disturbances by the necessary measuring devices to be deployed, such as: force and flow velocity transducers
5. The generated waves should include regular, irregular, tsunami-like solitary waves and tsunami bores in order to have broader applications for both tsunami and storm waves.
6. Numerical simulation employing SWE based model is necessary to provide a practical tool in assessing tsunami attenuation by coastal forest based on the derived hydraulic resistance in laboratory tests.

Those six aspects are in line with the priority of tsunami research recommendations formulated by Oumeraci (2009a) and Oumeraci (2009b) to fulfil the research gaps particularly on the damping performance of coastal forest vegetation except for a more detailed numerical simulation such as the use of a DANS model and a 3D CFD-model coupled with a CSD-model for the simulation of tsunami propagation through the forest. The tentative objectives and methodologies of the PhD thesis are already described in chapter 1. Based on previous discussion

in chapters 2 and considering available resources in the frame of the PhD research (duration, laboratory equipments, etc), the objectives and methodology are specified below more precisely.

2.6.1 Specification of objectives

The objectives of the PhD thesis may be specified as follows:

i) Development of a generic parameterisation of coastal forest vegetations based on physically-based parameterisation of two basically different types coastal forest vegetations (mangroves and coastal pines). The parameterised models should consider sufficiently both physical and morphological parameters such as: stiff structure assumption for the bottom part of mangrove (roots and trunk) and flexible structure assumption for the entire tree structure for both mangrove and coastal pine trees.
ii) Description of global wave attenuation in terms of transmission, reflection and dissipation and derivation of forest resistance coefficients based on the parameterised model in the form of modified drag and inertia coefficients (C_D* and C_M*respectively) as a function of geometry, volume ratio (V_m/V), frontal area (A_f), and flow regimes (Reynolds numbers, R_e).
iii) Selection, improvement and validation of a numerical model based on NLSWE for tsunami / storm waves attenuation performance of forest vegetation using available open-source models such as COMCOT with the proposed new developed resistance coefficients for coastal forest vegetations obtained from model test results.

2.6.2 Specification of methodology

In order to achieve the aforementioned research objectives and based on the results of Chapter 2 (state of the art review), the general methodology of the thesis covers the following four work phases (Fig. 2.16):

i) ***Work phase 1 (WP1)***: Comprehensive review and analysis of available knowledge on the characteristics of coastal forest vegetations, tsunami and storm wave characteristics, and existing numerical models to describe the interaction of coastal forest vegetations and tsunami / storm waves. A detailed discussion and the results can be found in chapter 2.

ii) ***Work phase 2 (WP2***): Field investigations of the most important parameters of coastal forest vegetations (mangroves and coastal pines), namely: the geometry, root/canopy density (represented by V_m/V and A_f), and the stiffness of the trunk (represented by Young's modulus E). This step, which is also very important for validating the information obtained from WP1, is described in Chapter 3.

iii) Work phase 3 (WP3): Performance and analysis of two types of laboratory experiments. The small-scale experiments on the parameterisation of coastal forest vegetations in a current flume will build the basis for larger scale model experiments in a wave flume. A more generic parameterisation methodology for a single tree and parameterised tree models for coastal forest vegetations will constitute the main results of the parameterisation processes. Following the parameterisation stage, larger scale model tests with a forest of parameterised tree models will be carried out to investigate the global and local processes involved in the wave-forest interaction. The global processes such as wave reflection, wave transmission and wave energy dissipation generally describe the hydraulic performance of the entire forest for various wave types and conditions. The local processes are those which contribute to the generation of the global processes such as wave breaking in and outside the forest, energy dissipation of each single tree within the forest in different configurations resulting in modified hydraulic vegetation resistance coefficients (C_D* and C_M*), etc.

iv) ***Work phase** 4 (WP4)*: Selection, improvement and validation of a numerical model for the damping performance of coastal forest vegetations subject to tsunami and storm waves. The numerical model COMCOT based on NLSWE, is implemented for the simulation of tsunami/storm wave interactions with coastal forest vegetations. Resistance terms in the model will be modified by introducing the vegetation resistance coefficients developed in WP3 to the governing equations. The NLSWE based model will be validated by the experimental data from the tests in the wave flume. The validated model will be used for a more detailed parameter study, thus extending the range of the testing conditions in the laboratory and allowing the develop-

ment of simpler semi-analytical models for the prediction of the attenuation performance of coastal forest vegetation subject to tsunami and storm waves.

Aside from the aspects mentioned above, the following aspects related to the hydraulic performance of coastal forests are excluded from this study due to complexity of the problems, time restriction and limited resources:

1. *Scouring and uprooting of trees.* Structural stability of the tree subject to extreme waves is obviously influenced by the stability of the roots attached to the soils. Toppled-down trees are commonly found after the floods and scouring is the main cause. In this study, *scouring and uprooting of trees* are excluded as the analysis is primarily focused in the understanding of the distinct contributions of individual tree components (roots, trunk and canopy) to the wave attenuation under the assumption of the integrity of the trees subject to wave or tsunami induced flow. Inclusion of the effect of uprooted trees on wave attenuation by coastal forests may represent the next logical challenging task for further studies when considering extreme flow conditions.

2. *Structural integrity of trees*. The effect of broken trunks and branches on storm wave/ tsunami attenuation is not considered in this study. This is particularly not true for extreme flow conditions since this type of damage is quite common under field conditions. The effect of broken trunk/branches (floating debris) on the wave attenuation needs specific modelling tools and methodologies that were not available during this study und therefore need to be addressed in future research.

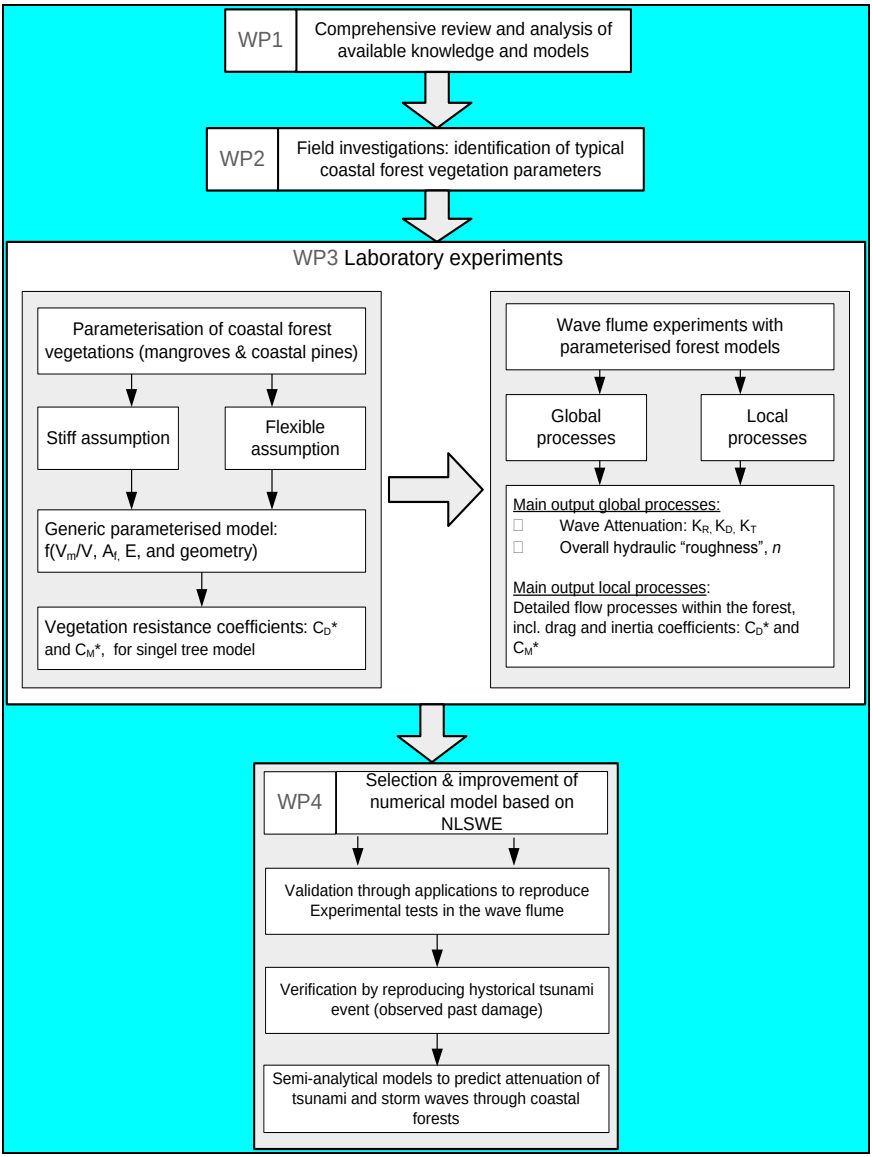

Fig. 2.16: General methodology and work phases (WP) of PhD study

3 Parameterisation of coastal forest vegetation

The primary objective of the parameterisation is to obtain a parameterised model which has a similar hydraulic resistance to its prototype counterpart. From the general parameters of vegetations that have been discussed in chapter 2 and the information from field investigations, the parameterisation of mangroves and coastal pines is based on two assumptions:

- *stiff structure assumption* considering only the bottom part of the tree (root system) and the trunk, adopted only for mangrove forests,
- *flexible structure assumption* considering the whole part of tree structures (root system - trunk - canopy), adopted for both mangrove and pine forests.

In order to precede with the parameterisation processes, detailed data on the characteristics of coastal forest vegetation (i.e. mangroves and coastal pine) are required. Therefore, field investigations to obtain information about the geometry, root/canopy density (submerged volume ratio and LAI), frontal area and other supporting information (e.g. age and surrounding environmental conditions) were carried out first.

3.1 Field investigations on mangroves and coastal pines

The field investigations in this study are focused on young, mid-age and mature mangroves. According to the field measurements reported by Mazda *et al.* (1997a), the maximum measured root height is up to 0.5 m, but no information is provided on the age of mangrove trees. Moreover, data related to submerged volume ratios higher than 0.5 m are also not provided, because the field measurements were intended to study tidal flow characteristics. As the roots of mangrove may be higher than 0.5 m and tsunami heights are often larger than 0.5 m, investigations on the characteristics of submerged volume ratio higher than 0.5m are also required. Moreover, since the growth of mangrove depends on many aspects and since it is not clear which mangrove age in Mazda *et al*. (1997a) belongs to, field measurements for mangrove with different ages are also needed to verify the assumption made in the recent studies (Istiyanto *et al.*, 2003 and Harada and Kawata, 2005) .

On the other hands, the current knowledge on the canopy of mangrove and coastal pines (two typical coastal forest vegetations) is still limited, particularly their structural properties (i.e. stiffness and density) as a function of the age and the prevailing environmental conditions. LAI as well as the Young modulus E of the trunk are the two important parameters that should be considered in the modelling of tsunami attenuation by coastal forest vegetation. Therefore, detailed information on the characteristics of tree components (roots, trunk and canopy) for different ages is required from field surveys.

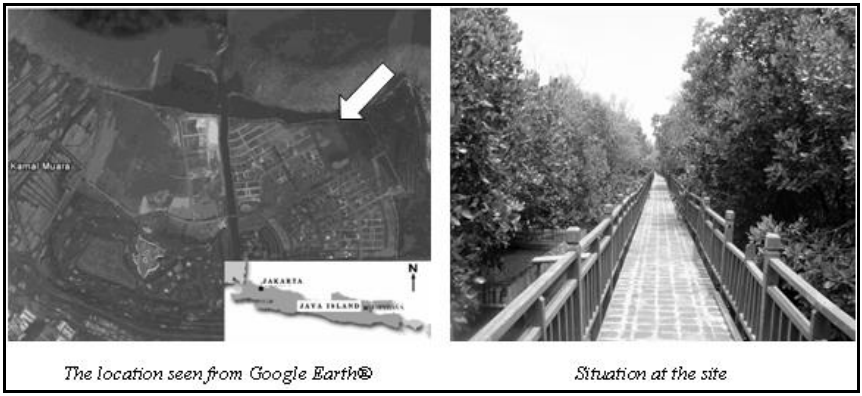

Fig. 3.1: Protected Forest Region in Angke Kapuk , Northern Jakarta

A field survey in the frame of this study was carried on Friday, 3 April 2009 and Tuesday, 30 March 2010 or during the end of the rainy season for Java Island (Indonesia) and surrounding. The site is a small wildlife conservation area (44.76 Ha) containing 15 types of mangroves with 8 indigenous species including *Rhizophora apiculata* and 7 types of other coastal forest vegetations including *Casuarina equisetifolia* (coastal pines) (Onrizal *et al.*, 2004). This protected forest (Angke Kapuk Protected Forest Region) is one of other two surviving protected wildlife regions in North Jakarta around 12 km North East of Jakarta's Soekarno-Hatta International Airport ($6^{o}06'15"S$, $106^{o}45'40"E$) (Fig. 3.1). More detailed descriptions on this topic can be found in Husrin and Oumeraci (2012f).

3.1.1 Objective and methodology

The objectives of these field investigations are as follows:

- To investigate the patterns of submerged root volume ratio (V_m/V) based on the work of Mazda *et al.* (1997a) for mangrove with different age.
- To validate the assumption of generalising structural dimensions of mangrove with variation of age that has been implemented during the study of mangrove parameterisation.
- To investigate the variation of leaf area index (LAI) and other canopy properties for different age of mangroves and coastal pines
- To measure the stiffness of mangrove's trunk and branches

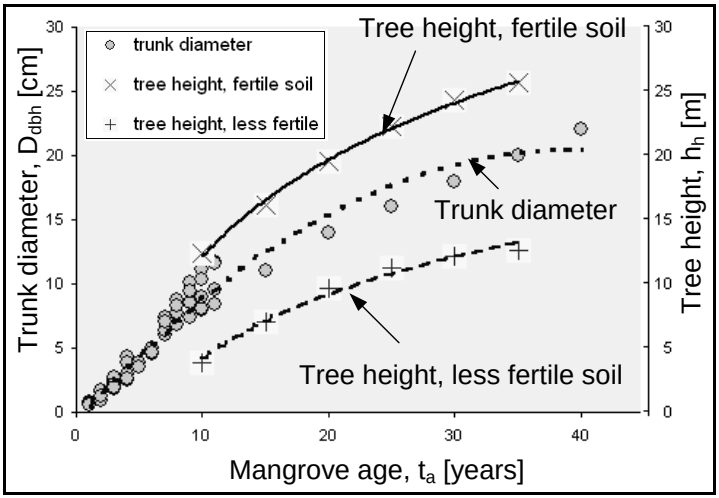

Fig. 3.2: The trunk diameter and tree height of mangrove versus age (after Mulia, 2001)

For mangroves, submerged roots volume ratio measurement methodology were carried out similar to the one implemented by Mazda *et al.* (1997a) by counting the number of roots based on root classifications for different water levels. Throughout the field survey, up to a maximum of three water levels over the entire root height were considered. The geometry of the tree was measured by using a simple measurement tape while the measurement of LAI was carried out by using destructive method (trimming the branches and measure the area of

leaves). Three red mangrove trees with different ages (young, mid age and mature) and one coastal pine tree were considered.

Table 3.1: Measurement results for mangroves

Geometry parameters	Mature	Mid-age	Young
Age of tree, t_a [year]	>25	< 8	0.8
Total height of the tree, h_h [m]	10.34	7	1.38
Height of the roots, h_r [m]	1.54	1.2	0.9
Height of the trunk, h_t [m[	1.8	1.5	-
Height of canopy, h_c [m]	4.2	4.2	0.48
Diameter of trunk, D_{dbh} [m]	0.2	0.09	0.03
Diameter of roots, D_r [cm]	1.0 - 9.0	1.0 - 3.5	0.02
Diameter of branches, D_{br} [cm]	1.5 - 15	0.5 - 1.5	0.5
Width of the canopy, w_r [m]	5.6	3	0.98
Width of the canopy, w_c [m]	7	3	0.6
Number branches [-]	24	24	8
Number of leaves/branches [-]	1680	346	134
Averaged area of leaves, A_l [m^2]	0.0028	0.0028	0.0028
Estimated LAI [-]	2.9	3.3	1.3

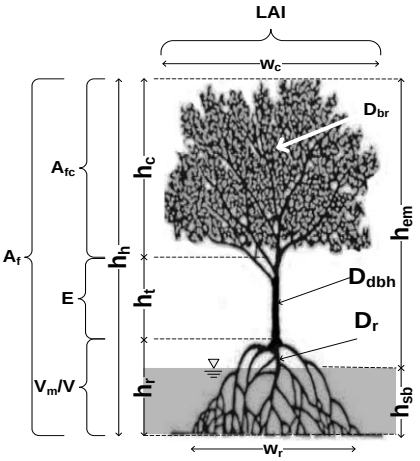

The presented analysis in this report mostly deals with the analysis of geometry, density of roots and canopy and wood strength of mangroves. For wood testing, samples from both mangroves and coastal pines are measured and analised to obtain the Young modulus of the trunk, E. In total, there are only three man-

grove trees (*Rhizophora apiculata*) and one coastal pine tree (*Casuarina equisetifolia*) were measured. The age of mangrove trees were estimated based on the available distribution data from Mulia (2001) as shown in Fig. 3.2. Based on the diameter of the tree, they belong to young, mid-age, and mature tree (Table 3.1). The site characteristics have to be taken into consideration in determining the age of tree because according to Mulia (2001), the soil in Java Island is considered as 'less fertile' for this type of mangrove species (Fig. 3.2).

3.1.2 Submerged root volume ratio

The following calculation concept has been implemented throughout the analysis in this report. The submerged roots are calculated based on the measurement of root geometry and the water level classifications. The calculation of control volume V is based on the maximum dimension of the width of the roots w_r. A square shape has been adopted for the calculation of the control volume, V. Therefore, the control volume for any water depth h is determined as follows:

$$V = h\, w_r^2 \qquad (3.1)$$

Where:

V : control volume [m^3]
h : water depth [m]
w_r : width of the root system [m]

The results of submerged volume ratio calculation are shown in Fig. 3.3a. As shown in Fig. 3.3a, due to short and small dimension of young mangrove tree, the root system was not vertically divided and the V_m/V was found to be far smaller than the mid-age and mature trees ($V_m/V = 0.0047$). The trunk of young mangrove is also not observed because the roots are well distributed just right below the canopy (see also Fig. 2.5). For mid-age and mature trees, the root system was able to be vertically divided into three levels. The root components were classified based on their geometry (length and diameter) and the volume of the roots can be calculated directly for different water levels. The submerged volume ratio can be determined afterwards by dividing the volume of roots for each level V_m by the control volume V.

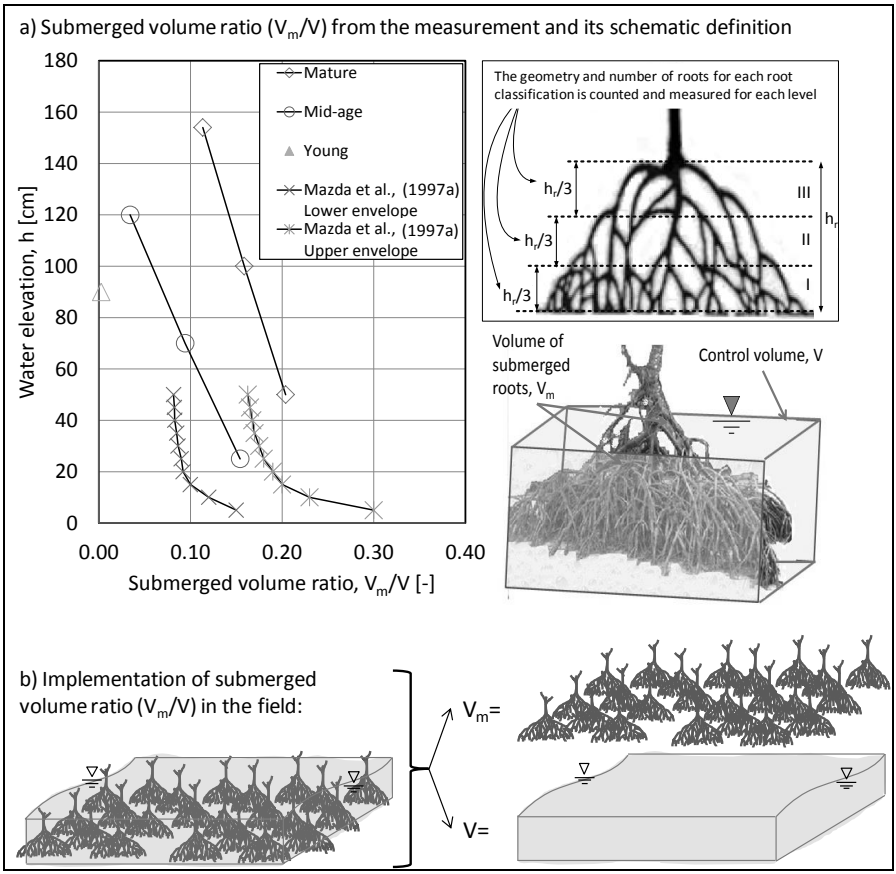

Fig. 3.3: Submerged root volume ratio for mangroves V_m//V

The submerged volume ratio measurements in this study are compared to the same measurement presented by Mazda *et al.* (1997a) (Fig. 3.3). It should be noted that the measurements of V_m/V from Mazda *et al.* (1997a) are until the water depth h = 0.5 m due to limitation on the analysis of tidal range up to 0.5 m. In the current study, the tidal range is not considered. Thus, it was assumed that the water level reaches the top of the root system and the measurement was carried out for the whole root system.

The obtained submerged volume ratio V_m/V variation over the water depth h from this study is qualitatively and quantitatively comparable to the data from Mazda *et al.* (1997a). The similarity on the patterns of V_m/V curves between the measurement and the data from Mazda *et al.* (1997a) shows consistent results. Moreover, it was concluded also that the desired V_m/V curve of either mid-age or mature tree based on Mazda *et al.* (1997a) is confirmed for the bases of root model construction and further investigation. The V_m/V for young mangrove tree will not be considered for the construction of root model because of its insignificant values.

3.1.3 Leave Area Index (LAI) of mangroves

For the measurement of LAI, a conventional method (destructive method) has been implemented (Ishi & Tateda, 2004). The measurement of LAI was carried out by cutting one of the main branches, measuring the dimension of the branches, counting number of leaves, and measuring the average area of the leaves. Knowing the number of leaves, the area of each leaves, and number of main branches, LAI of the tree can be estimated directly.

The averaged dimension of leaves from current study shows that the width of a fully grown leave is generally w_l = 4 cm and the length of the leave l_l = 14 cm. This measured averaged dimension is slightly different to the measurement found by Farnsworth and Ellison (1996). Larger dimension as found in the current study probably due to the fact that the species measured by Farnsworth and Ellison (1996) is strictly for *Rhizophora mangle*, while in the current field study, the spesies is *Rhizophora apiculata*. Moreover, Satriono (2007) found that the length of the leave for *Rhizophora apiculata* varies from 10 - 15 cm which is within the finding of the current study.

The LAI of mangrove for different age is shown in Table 3.1 and Fig. 3.4. It is found that the LAI for young mangrove is very small (LAI=1.33). This small value of LAI may have resulted from very few number leaves it has. The LAI for young mangrove with age less than a year is beyond the curve provided by Clough *et al.* (2000) (Fig. 3.4a). Meanwhile, the LAI of mature tree is smaller compared to the mid-age tree. This also confirms the finding of Clough *et al.* (2000) that the LAI of a mangrove tree decreases as the age of the tree increases.

This occurs due to the fact that the canopy of mature tree is more spreading and self-pruning is more prominent compared to mid-age tree. Thus, the projected area become much larger compare to the total area of the leaves. Smaller values of LAI for mature and mid-age tree in the current study may have resulted from the fact of poor soil fertility in the investigated area as already discussed above.

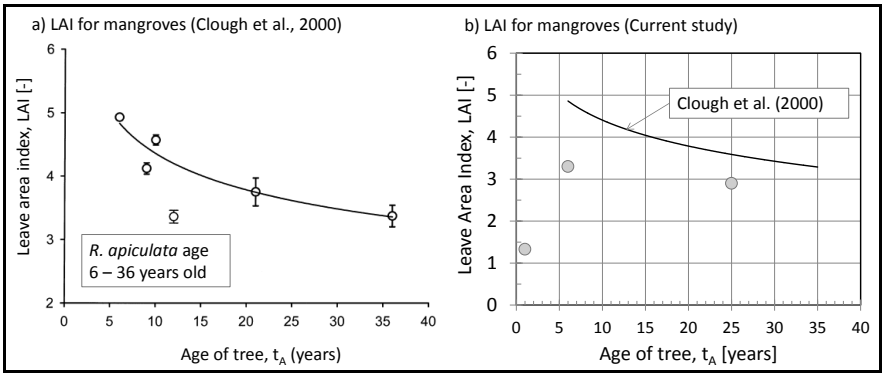

Fig. 3.4: LAI for mangroves

3.1.4 Wood strength

Wood samples were collected from both mangrove and coastal pine trees. The collected samples were selected from different parts of the tree (trunk and branches). The wood sample diameters were ranging from 0.86 cm – 1.05 cm with 25 cm long. Samples from coastal pines are named SC1, SC2 and SC3 while a sample from mangrove is SB3 with moisture content around 15%. After the samples have been put on centric load tests, the following equations are used to calculate the Young modulus E as an indicator of wood strength:

$$E = \left(\frac{L_w^3}{48I}\right)\left(\frac{F_c}{\delta}\right) \tag{3.2}$$

$$I = \frac{\pi r^4}{4}, \quad F_c = mg \tag{3.3}$$

Where,

E : Young modulus [N/m^2]
g : gravity acceleration [m/s^2]
L_w : length of wood sample [m]
I : second moment of area [m^4]
F_c : centric force [N]
m : loading mass [kg]
δ : deflection [m]
r : radius of wood sample [m]

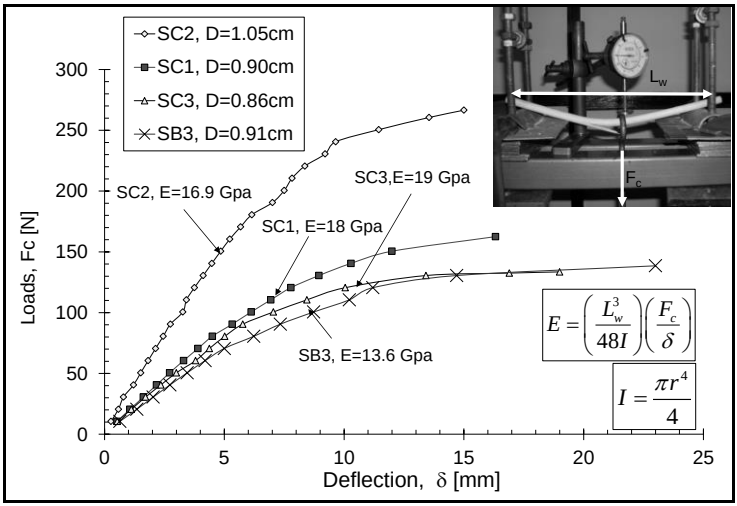

Fig. 3.5: Load-deflection curves of four tested samples

The force (F_c) and the deflection (δ) in equation 3.2 are used when curve of force-deflection is still linear. The results from the tests are shown in Fig. 3.5. It is found that for mangrove (B3) the Young modulus E = 13.6 $x10^9 N/m^2$. The previously measured E value of *Rhizophora* sp. is E = 8.27 $x10^9 N/m^2$ with moisture content 17% (Hawa, 2005) while Vallam *et al.* (2011) mentioned that the E for mangrove may reach up to 20.03 $x10^9 N/m^2$. Therefore, the finding from current study is still within the range of previous reported E. The E values for the woods of coastal pine are found between 16.9 – 19 $x10^9 N/m^2$ (averaged E = 18 $x10^9 N/m^2$). Higher values of E for coastal pines may have resulted in wood characteristic of vulnerable to breakage, heavy, brittle, and difficult to work.

Woods of coastal pines are widely used as fences, firewood, and other light-load purposes. In general, those values of E for both mangrove and coastal pines are found to be within general wood E values between 3.2 – 21 $x10^9 N/m^2$[8].

Information about E of wood is very important to determine the material of trunk model. With scale of model 1:25 and the range of mangrove and coastal pine E is between 8.27 – 19 $x10^9 N/m^2$, the expected scaled E for mangrove and coastal pine is ranging from 0.33 $x10^9 N/m^2$ – 0.76 $x10^9 N/m^2$. The only feasible material for this range of E values is *Polytetrafluoroethylene* (PTFE) which has E = 0.5 $x10^9 N/m^2$ (Table 3.2). However, this material also has a drawback. The density of PTFE is double the density of woods. Therefore, breakage is not expected when this material is used for the model of trunk.

Table 3.2: Characteristics of PTFE rods (www.gruenberg-kunstsoffe.de)

Modulus elasticity, E	:	0.5 $x10^9 N/m^2$
Hardness	:	22 – 32 $x10^6 N/m^2$
Density, ρ	:	2140 – 2180 kg/m^3
Moisture absorption	:	0.0005%
Maximum service temperature	:	260 ^oC

3.1.5 Remarks on the results of the field investigations

The field investigations allowed one to obtain the missing data which are required for the construction of real tree model for both mangroves and coastal pines. The following are the benefits obtained from field investigations already discussed above.

- Determination of V_m/V for mid-age and mature mangrove trees. This information was previously not available. Moreover, the pattern of V_m/V over water depth as described by Mazda *et al.* (1997a) is also confirmed

[8] DoITPoMS: Teaching and Learning Packages, University of Cambridge (www.doitpoms.ac.uk)

to be scaled down to other deeper water depths. With these information, the construction of real mangrove models become feasible.

- The field surveys enabled to get the density of mangrove canopy and its characteristics as an important input for the construction of the canopy model. LAI is used as a controlling parameter in determining the density of canopy model for both mangroves and coastal pines. This is a complement to the concept of the submerged volume ratio V_m/V for the canopy based on LAI.
- The determination of the Young modulus E of the collected wood samples enabled to select a suitable trunk model material (i.e. PTFE).

3.2 Parameterisation with stiff structure assumption

3.2.1 Testing programme and setup

The parameterisation methodology for the stiff structure assumption is depicted in Fig. 3.6. Three mangrove models of complex roots with different density, analogue to the prototype, were constructed at a scale of 1:20. These are called hereafter *'real tree models'* or models A1, B1, and C1 (see Fig. 3.7). The dimensions of the roots refer to the work of Istiyanto *et al*. (2003) and are based on the field measurements of the mangrove forest in Jakarta Bay, Indonesia. The height of a mature *Rhizophora* sp. is typically 15 m from the bottom and the height of the root system for a 15 m high tree is 2.50 m.

For each real tree model, three parameterised models made of a group of cylinders with different diameters were constructed. The different diameters indicate the influence of different frontal area A_f, submerged root volume ratio V_m/V, and cylinder dimensions on the hydraulic performance of the parameterised tree models. The frontal area A_f is defined as the area perpendicular to the flow direction of the submerged tree model. Hence, the A_f is determined by taking the picture of the intended side of the model subject to the flow (Fig. 3.7b). Both A_f and V_m/V vary as the water level changes. Fig. 3.7 also shows real mangrove models and their counterpart parameterised models with the nomenclature used.

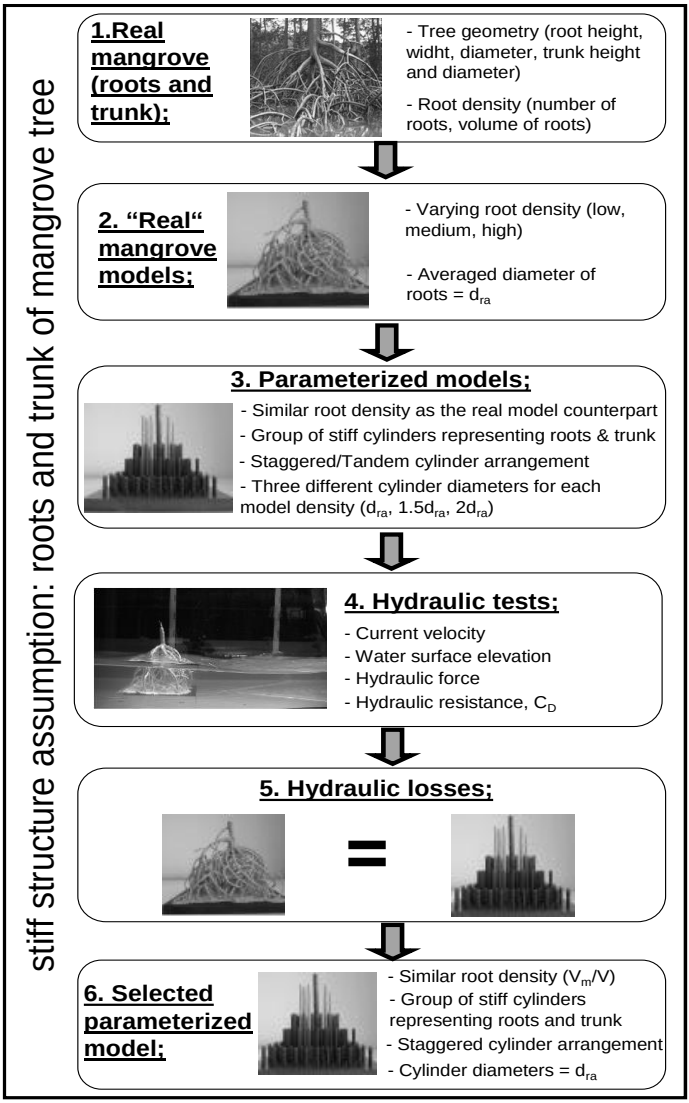

Fig. 3.6: General methodology of parameterization with stiff structure assumption

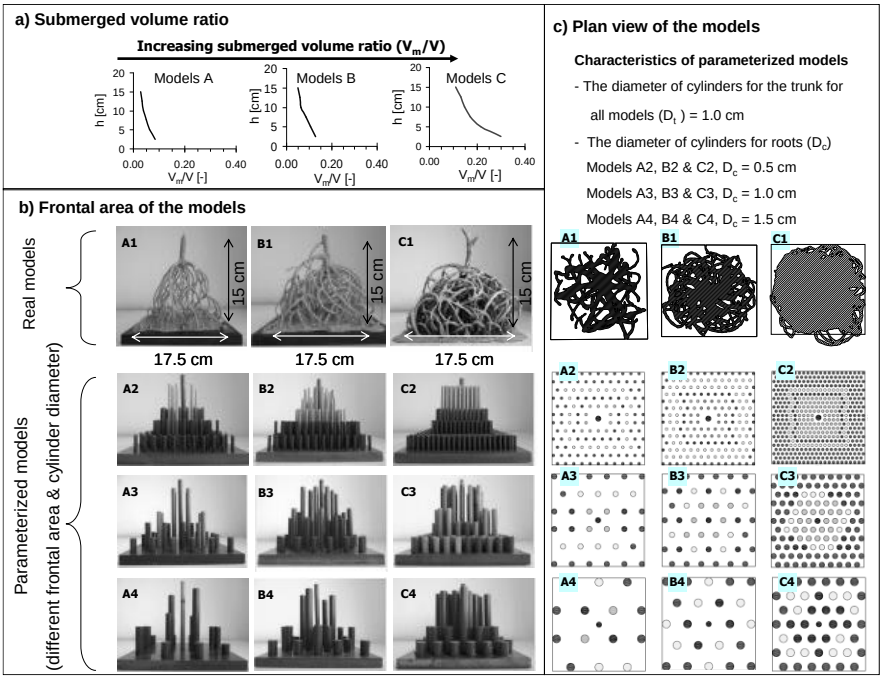

Fig. 3.7: Three types of real mangrove root models with different submerged volume ratio V_m/V and corresponding parameterized models of varying frontal area and cylinder diameters assumption

A flume with steady flow was used to measure the hydraulic properties of the models. The models and the measuring devices (current meters, surface elevation gauges, and a force transducer) were installed in the middle of the flume (see Fig. 3.8). With a scale of 1:20, Froude's similitude law was applied to obtain the required flow velocities (discharges) for the whole series of the experiments. Maximum measured tsunami onshore velocities range from 2 - 5 m/s (Fritz *et al.*, 2006), so that the required current velocities in the model should be at least within the range of 0.4 - 1.0 m/s. Flow velocities were measured using Acoustic Doppler Velocimeter (ADV) in front of and behind the model. Surface elevation was measured at three locations: in front of, at and behind the mangrove model. Hydraulic forces were measured by means of a force transducer mounted to the bottom of the tree model.

Table 3.3: Testing programme for all models

Model	No. of tests	Velocity, u [m/s]	Prototype velocity, u_p [m/s]	Discharge, Q [m^3/s]	Water depth, h [m]
(Same conditions for all models)	1	0.20	0.89	0.0060	0.050
	2			0.0120	0.100
	3			0.0150	0.125
	4			0.0180	0.150
	5	0.50	2.24	0.0150	0.050
	6			0.0300	0.100
	7			0.0375	0.125
	8			0.0450	0.150
	9	0.75	3.35	0.0225	0.050
	10			0.0450	0.100
	11			0.0563	0.125
	12			0.0675	0.150
	13	1.00	4.47	0.0300	0.050
	14			0.0600	0.100
	15			0.0750	0.125
	16			0.0900	0.150
	17	1.42	6.40	0.1200	0.180

All models were tested in the flume according to the experimental set-up shown in Table 3.3. Different flow velocities ranging from u = 0.2 - 1.4 m/s (or relative flow discharges q = 0.2 - 1.4 $m^3/s/m^2$) for four water depths (h = 0.05, 0.10, 0.125 and 0.15 m) were employed in the testing programme to investigate the effect of varying frontal area A_f and submerged root volume ratio V_m/V on the measured hydraulic forces. The flow velocity is measured at the level of at least 0.4h above the platform which can be considered as the depth-averaged flow velocity. Each model was subjected to a combination of different current velocities and water depths in 17 tests. Therefore, the total number of tests is 204 (17 tests × 12 mangrove models).

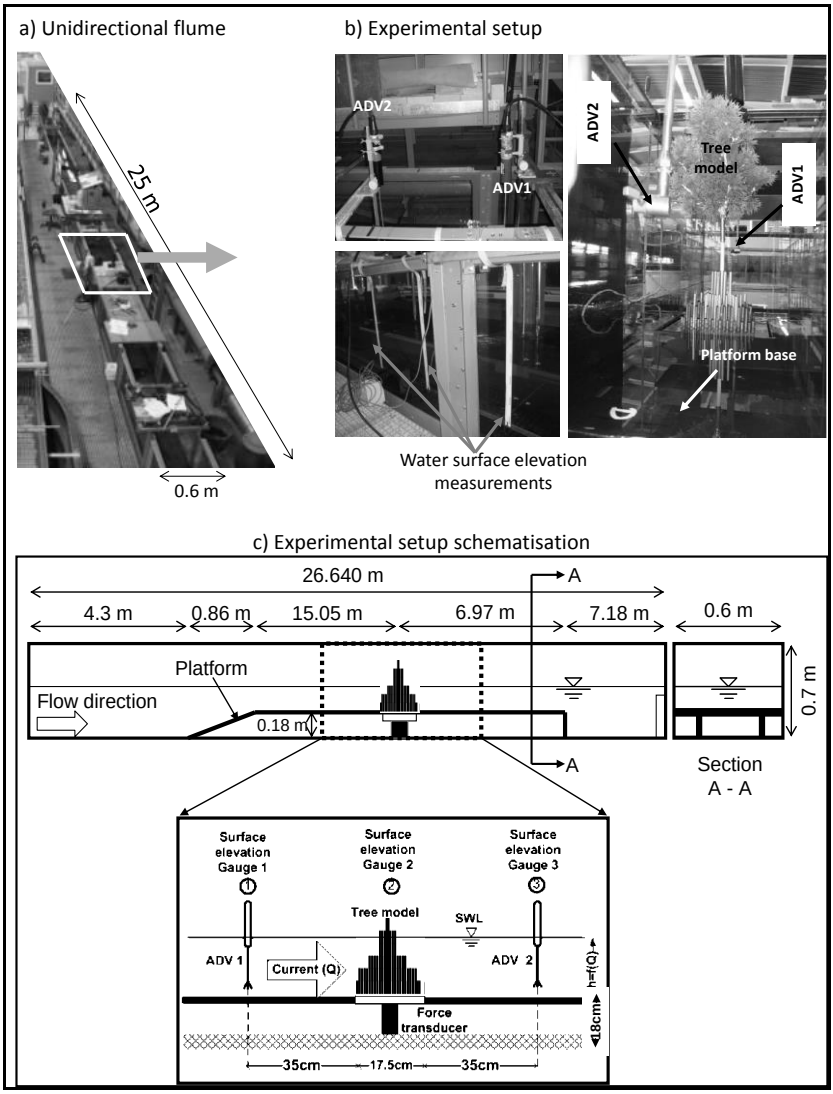

Fig. 3.8: Experimental set-up in the current flume

3.2.2 Flow induced force (F_D)

Prior the analysis of flow induced force, hydraulic gradient and current velocity reduction were first analysed. However, it was found that these two parameters are difficult to compare as the bases for determination of representative parameterised models due to highly turbulent flow behind the tree models and measurement device sensitivity (Report nr. 4, Husrin and Oumeraci, 2012d). The hydraulic force is measured by means of a force transducer located below the tree model. Different flow discharges (and thus different flow velocities) were employed to study the effect of the variation of root density V_m/V on the flow induced force F_D. Moreover, as the water depth changes, the frontal area of the model also varies. In a preliminary analysis, the comparison of the measured forces for all models (real and parameterised models) is necessary to identify which parameterised model is most appropriate to represent its counterpart real model. Fig. 3.9 shows the comparison of the real models to the corresponding parameterised models.

The effect of root density is clearly visible. The force increases as the root density increases. The measured force increases by about 65% from 8.5 N for the lowest root density to 14 N for the highest root density. The relationship in term of flow induced forces of the parameterised models to their real model counterparts is better represented compared to those in terms of hydraulic gradient or current velocity reduction (Husrin and Oumeraci, 2012d). It is also clear that, the size of cylinder diameter influences significantly the measured forces. As the root density increases, the effect of the cylinder diameter used to represent the root system decreases. The cylinder diameter, D_c = 0.5 cm, which is close to the averaged root diameter of the real model shows consistent results for all different root densities.

The deviation of the measured forces of the parameterized models from those of the real models is calculated similarly as for the deviation of the hydraulic gradient and current velocity:

$$\delta F_D = \frac{F_{D(par)} - F_{D(real)}}{F_{D(real)}} * 100\% \qquad (3.4)$$

Where:

δF_D : deviation of measured force [%]

$F_{D(par)}$: measured force of parameterized model [-]

$F_{D(real)}$: measured force of real model [-]

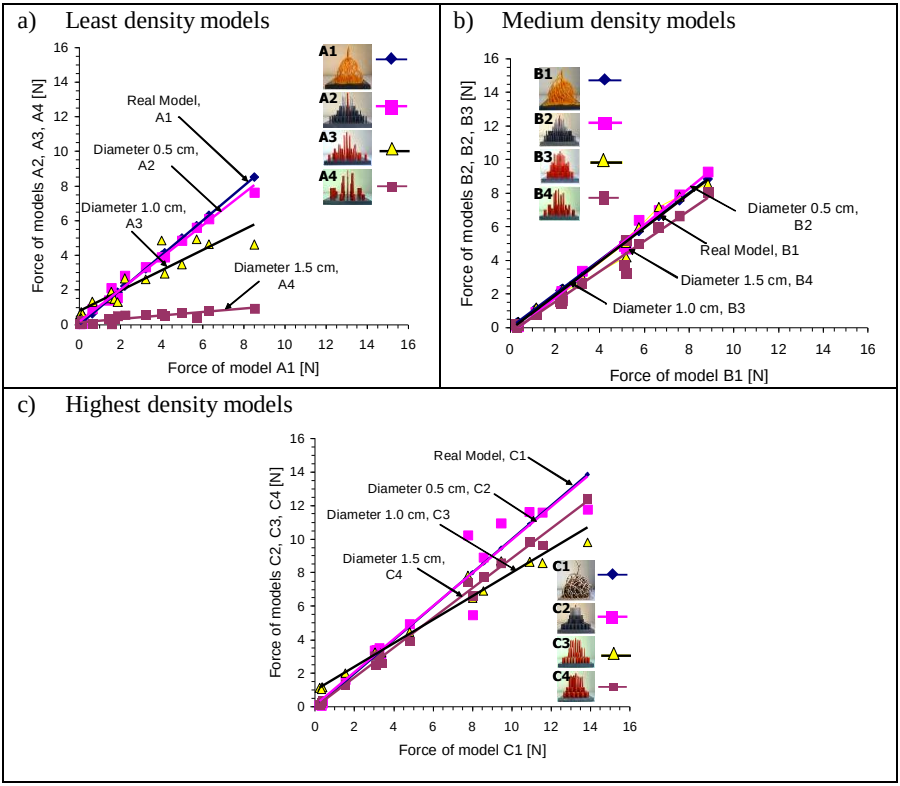

Fig. 3.9: Flow-induced force for a) the least density models, b) the medium density models and c) the highest density models

Table 3.4: Deviation of force measurement from the parameterized models

Cylinder diameter	Parameterised models	Deviation of F from the real model			Averaged deviation
		A1	B1	C1	
0.50	A2	-9%	-	-	-13%
	B2	-	-23%	-	
	C2	-	-	-8%	
1.00	A3	74%	-	-	42%
	B3	-	-6%	-	
	C3	-	-	58%	
1.50	A4	-66%	-	-	-35%
	B4	-	-27%	-	
	C4	-	-	-12%	

The performance of hydraulic force measurements showed much more conclusive results. The measured forces for both real and parameterised models are comparable and consistent with the physical characteristics of models (i.e. density and frontal area). In term of the force measurement, the parameterised models with cylinder diameter 0.5 cm provide a better representation of the real model with a deviation of about -13% (Table 3.4).

Root density, characterised by the submerged volume ratio V_m/V, greatly influences the measured hydraulic forces. Fig. 3.10 shows the comparison of measured forces as a function of measured velocity for both real models (Fig. 3.10a) and parameterised models (Fig. 3.10b-d). The forces are function of quadratic velocity u^2 which is consistent with the Morison equation particularly for the real models and the parameterized models with cylinder diameter D_c = 0.5 cm. As the root density increases, the measured force will increase as well. For example, from Fig. 3.10a, the averaged increase of measured force from the least to the highest root density is ranging from 60 % to 260 % (Table 3.5). The increase of the measured forces are tabulated and compared between the real and the parameterised models (Table 3.5). It shows that the parameterised models with cylinder diameter D_c = 0.5 cm give closer averaged value compared to the other parameterised models with larger cylinder diameters (142 % and 113%, respectively).

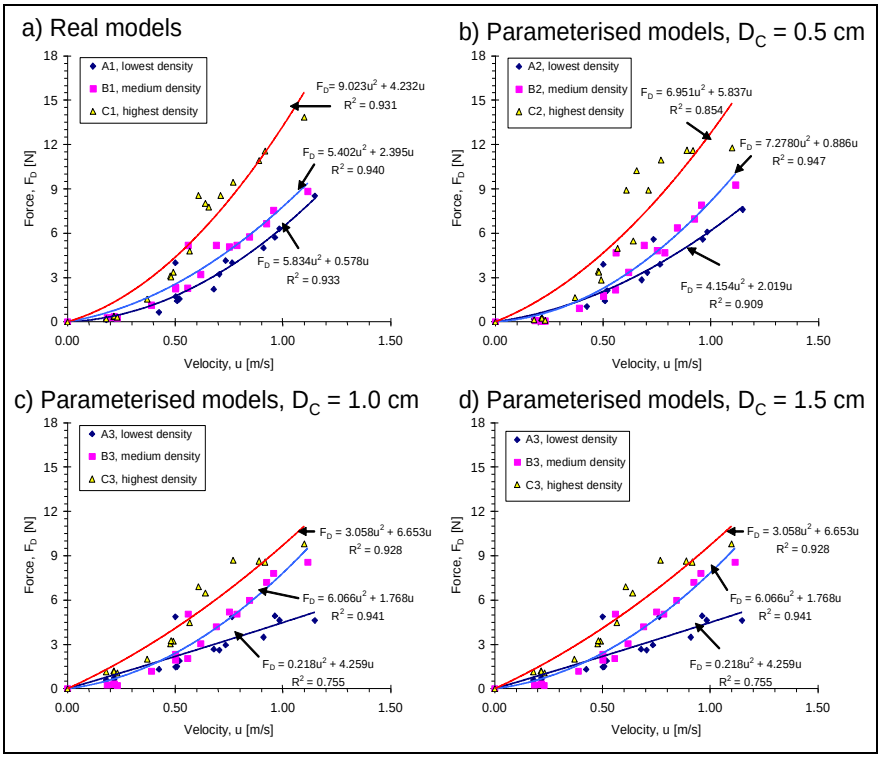

Fig. 3.10: Hydraulic force as a function of averaged velocity for all models

Table 3.5: Increase of measured forces from the lowest to the highest root density (see Fig. 3.10)

No	Measured hydraulic force, F_D [N]								Increase of measured force, [%]			
	A1	C1	A2	C2	A3	C3	A4	C4	A1 to C1	A2 to C2	A3 to C3	A4 to C4
1	0.29	1.05	0.50	1.28	0.77	1.30	0.10	-0.48	259%	156%	67%	-598%
2	0.40	1.33	0.63	1.57	0.93	1.57	0.12	0.01	231%	149%	68%	-92%
3	1.30	2.80	1.61	3.11	1.85	2.88	0.25	2.22	116%	94%	56%	773%
4	0.40	1.33	0.63	1.58	0.93	1.58	0.12	0.03	235%	151%	69%	-78%
5	0.38	1.46	0.61	1.72	0.91	1.70	0.12	0.23	282%	181%	87%	102%
6	1.87	4.08	2.16	4.37	2.27	3.87	0.32	3.76	118%	102%	71%	1065%
7	3.08	5.30	3.29	5.54	2.99	4.76	0.45	5.06	72%	69%	59%	1023%
8	1.80	4.26	2.10	4.55	2.22	4.01	0.32	3.97	136%	116%	80%	1156%
9	1.75	4.12	2.05	4.41	2.19	3.90	0.31	3.81	135%	115%	78%	1127%
10	3.30	6.41	3.48	6.58	3.11	5.51	0.47	6.12	94%	89%	77%	1199%
11	1.75	5.91	2.05	6.12	2.19	5.17	0.31	5.65	237%	198%	137%	1724%
12	3.57	6.65	3.72	6.81	3.24	5.67	0.50	6.34	86%	83%	75%	1177%
13	5.35	8.59	5.27	8.60	4.05	6.92	0.65	8.00	60%	63%	71%	1122%
14	3.85	7.56	3.97	7.65	3.38	6.27	0.52	7.14	96%	93%	85%	1267%
15	5.95	10.88	5.78	10.67	4.30	8.32	0.70	9.76	83%	84%	94%	1285%
16	6.21	11.47	6.01	11.20	4.40	8.67	0.73	10.19	85%	86%	97%	1303%
17	8.34	15.53	7.79	14.79	5.17	10.99	0.89	12.88	86%	90%	112%	1342%
Averaged									142%	113%	81%	876%

3.2.3 Selection of appropriate parameterised model

Based on the comparison of the measured force deviation, parameterised models with cylinder diameter D_c = 0.5 cm showed a better representation of the real model counterparts with averaged deviation of -13% (Table 3.4). There are two advantages of selecting parameterised models with cylinder diameter D_c = 0.5 cm in term of the measured hydraulic force, F_D.

- Measured forces include the effect of flow velocity and water depth. They are consistent and easily comparable.
- The hydraulic force is a function of both flow regime and characteristics of the body in the flow.
- The averaged deviation of parameterised models with cylinder diameter D_c = 0.5 cm is the smallest, -13% compared to the other models (42% and -35%), see Table 3.4.
- Minus deviation values mean that the measured force of the parameterised model is 13% less compared to the real model. For design purposes, this condition is on the safe side.

Therefore, considering the discussion above, the parameterised model with cylinder diameter D_c = 0.5 cm is selected as the most representative one.

3.2.4 Hydraulic resistance (Drag coefficient)

According to the Morison equation, the total hydraulic force (F_T) consists of the drag force F_D and the inertia force F_I (Eq. 2.3). Since the employed flow in the flow flume is quasi-uniform and quasi-steady, the velocity is almost constant and the flow acceleration is negligible ($\partial u / \partial t \sim 0$) in a narrow space where the measurement is taking place. Thus, only the drag force is dominant and the inertia force can be neglected. Therefore, Eq. 2.3 only contains drag component and the drag coefficient C_D can be derived directly:

$$F_T = F_D = \frac{1}{2}\rho C_D A_f u^2 \tag{3.5}$$

$$C_D = \frac{2F_D}{\rho A_f u^2} \tag{3.6}$$

Where:

F_T : total force [N]
F_D : drag force [N]
ρ : water density [kg/m^3]
A_f : cross sectional area of the body subjected to flow [m^2]
u : flow velocity [m/s]
C_D : drag coefficient [-]

The drag force is a function of the frontal area (A_f) of the body subject to flow. Fig. 3.11 shows the relationship between drag coefficient C_D and the frontal area of the model. The C_D values seem to be larger for smaller frontal area as predicted by Eq. 3.6. However, other aspects (shapes, velocity, etc) may contribute to the higher values of C_D for smaller A_f. A closer examination of the figure shows that for similar frontal area, an increase of C_D is also observed. The increase of C_D for similar frontal area might be associated to different flow velocities and different configurations of the models

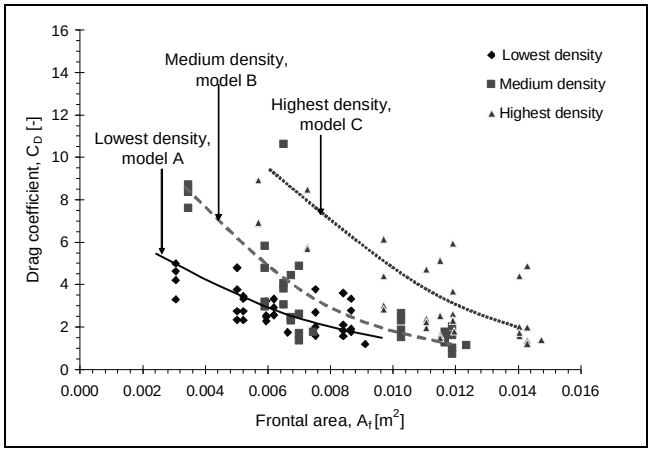

Fig. 3.11: Drag coefficient, C_D as a function of frontal area, A_f

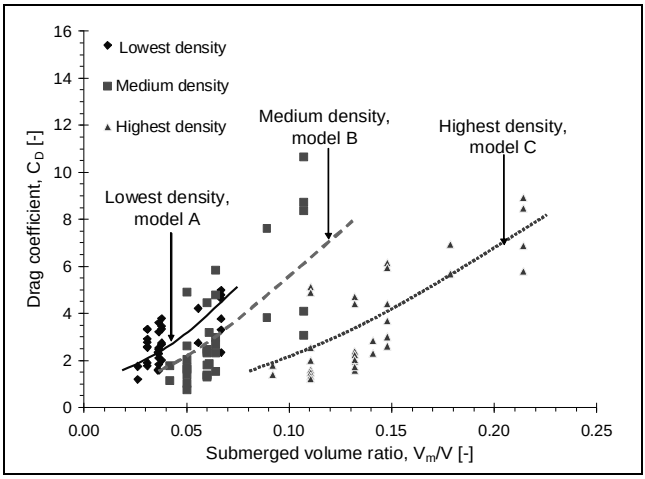

Fig. 3.12: Drag coefficient, C_D as a function of submerged volume ratio, V_m/V

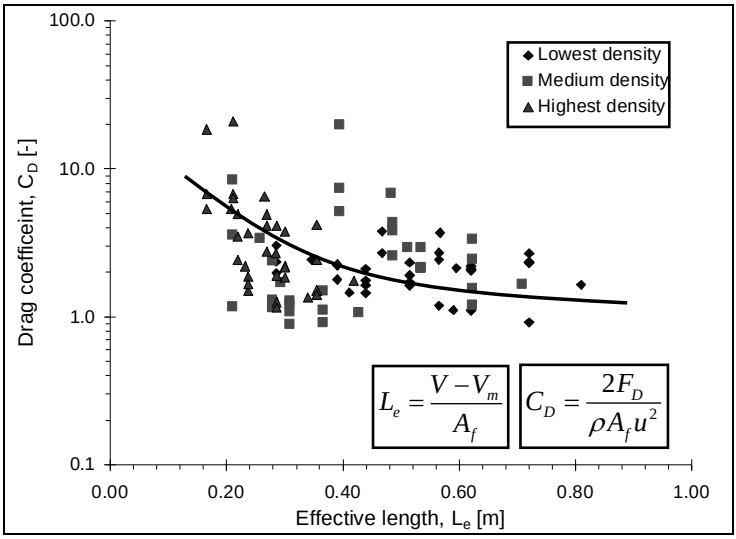

Fig. 3.13: Drag coefficient C_D as a function of effective length, L_e

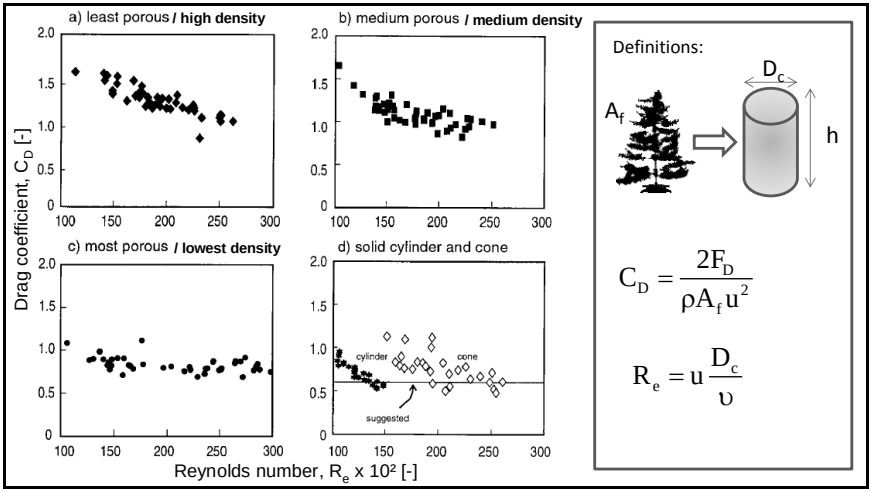

Fig. 3.14: C_D variation as a function of R_e for shrubs subjected to wind flow (After Grant and Nickling, 1998)

Another important parameter of the model has also been considered, the submerged volume ratio, V_m/V. Fig. 3.12 shows the relationship between drag coefficient C_D and submerged volume ratio, V_m/V. The C_D values increase as the V_m/V values increase. However, this relationship cannot explain thoroughly the effect of three different root densities on drag coefficient C_D. It is clear that a parameter that can explain both the physical object properties and flow characteristics is needed to describe more properly the hydraulic resistance of the mangrove root models.

First, The C_D values, plotted against effective length L_e in Fig. 3.13, clearly show the influence of both the submerged root volume ratio and the frontal area. The C_D increases for smaller L_e (higher root density) for all mangrove models and it decreases towards 1.0 as the effective length increases. This means the higher L_e values lead to sparser root system. Thus, at this condition, the root system may act as a single cylinder because the associated C_D is equivalent to the C_D for a single cylinder (C_D = 1.0 for $R_e = 10^2 - 10^5$). The results shown in Fig. 3.13 are comparable with other measurements such as those presented by Grant and Nickling (1998) for the case shrubs with various densities subjected to wind (Fig. 3.14). Higher root density (smaller L_e) is associated with higher drag coefficients due to the fact that the flow may skim around the object instead of penetrating through the root system. At some points, the flow interaction within the roots (or a group of cylinders) may experience pressure losses in the wake, thus resulting in higher C_D values. In contrast, lower root density (higher L_e) allows the flow to penetrate freely into the root system without losing much of the momentum and low wake interference.

Mazda *et al.* (1997a) proposed a relationship between C_D and Reynolds number R_e, in which the Reynolds number has been redefined for the mangrove root system. Therefore, the characteristic length scale in the original definition of the Reynolds number should be replaced by an effective length L_e which can be interpreted as a measure of porosity expressed in a length scale. Larger L_e values mean smaller root density and smaller L_e values mean larger root density. The effective length of a mangrove root system is defined according to the concept of submerged root volume ratio V_m/V and frontal area A_f:

$$L_e = \frac{V - V_m}{A_f} \tag{3.7}$$

and the Reynolds number is defined as follows:

$$R_e = \frac{uL_e}{\upsilon} \tag{3.8}$$

Where:

V : control volume [m^3]

V_m : submerged root volume [m^3]

L_e : effective length [m]

u : averaged flow velocity [m/s]

ν : kinematic viscosity of water (ν = 1.004 x 10^{-6} m^2/s for water temperature = 20 ^oC)

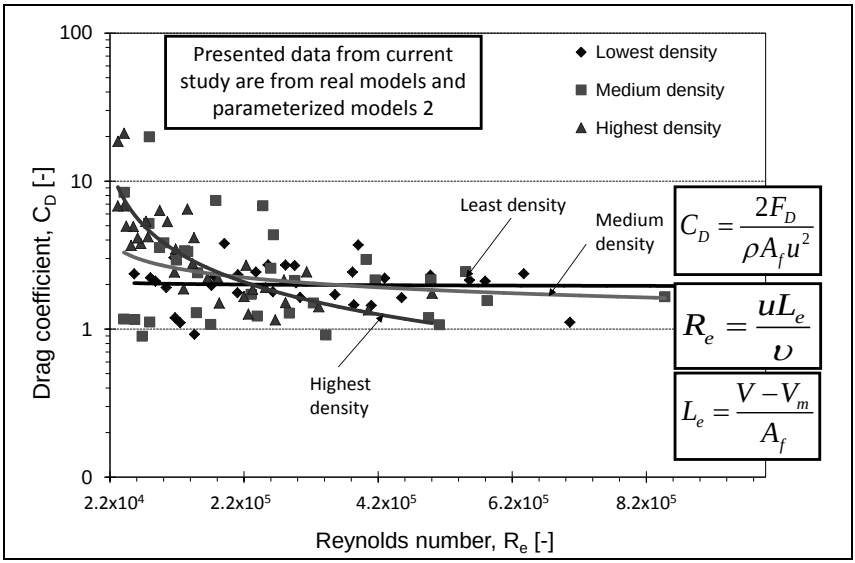

Fig. 3.15: Drag coefficient C_D as a function of Reynolds number R_e

Based on Eqs. 3.6, 3.7 and 3.8, the relationship of C_D ad R_e can be derived for all models as shown in Fig. 3.15. The clouds of data from all three models with different root density are mixed. However, there is a clear tendency that the C_D values decrease towards 1 as the Reynolds number increases.

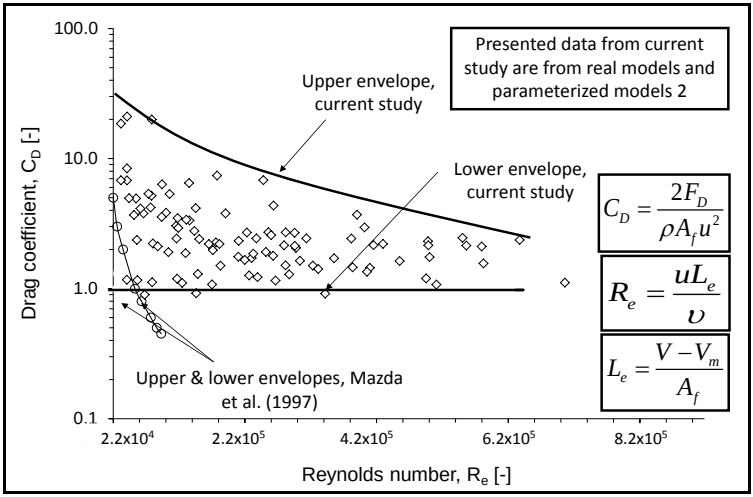

Fig. 3.16: Drag coefficient C_D comparison to the work of Mazda *et al.* (1997a)

The results of the current study are compared to the results presented by Mazda *et al*. (1997a). In the current study, a wider range of flow conditions was considered as compared to the work of Mazda *et al.* (1997a) which is applicable only for tidal flow conditions (smaller R_e number compared to the present study). Thus, the current study has wider Reynolds number range which is suitable for storm waves and tsunami applications. The field study from Mazda *et al.* (1997) considered not only the density of roots but also the density of mangrove forest, including the space between individual trees. Therefore, when the measurement took place in the area where the mangrove trees are highly sparse (this means (V-V_m) is very large), they found very large L_e values and smaller C_D values leading to C_D = 0.4 which is different to the present study (C_D leads to 1). Moreover, in the field, there are more aspects that may influence the measurements such as bed roughness and the presence of undergrowth. In the current study, the

control volume V was kept constant and the root density varied. The total force was measured directly on each model so that the derivation of the flow resistance is more straightforward. This controlled environment allows higher C_D values compared to the work of Mazda *et al.* (1997a). For smaller Reynolds number, results from current study intersect the work of Mazda *et al.* (1997a) though for higher R_e, C_D from Mazda are much smaller (Fig. 3.16).

Larger values of drag coefficient C_D is also discussed by Struve *et al.* (2003) through their laboratory experiments employing a group of cylinders in a flume. They concluded that larger value of C_D is expected for higher density of vegetations defined as the projected surface area as well as for the increase of flow velocity. However, for the numerical model, Struve *et al.* (2003) recommended the C_D value around $C_D = 1$, which corresponds to the lower envelope of the current study.

Harada and Imamura (2000) conducted laboratory experiments using artificial porous media for mangrove model. They found a relationship explaining the influence of submerged volume ratio V_m/V on the drag coefficient C_D as follows:

$$C_D = 8.4\frac{V_m}{V} + 0.66 \tag{3.9}$$

However, it should be noted that Eq. 3.9 is physically unclear because when V_m/V is zero (without trees), the C_D cannot be 0.66 due to bottom roughness. Eq. 3.9 is plotted and compared to the current study (Fig. 3.17). The C_D curve from Harada and Imamura (2000) almost represent the lower envelope for the data of the current study. This result is very important since the equation developed by Harada and Imamura (2000) has never been extrapolated for $V_m/V > 0.08$. The work of Imai and Matsutomi (2005) for coastal pine model showed C_D fluctuation in the range of 0.9 – 1.5. However, the study did not revealed any conclusive dependency of C_D on the physical characteristics of coastal forest. The benefit of the current study is a wider range of drag coefficient C_D and the inclusion of frontal area A_f together with submerged volume ratio V_m/V as the most influencing aspects.

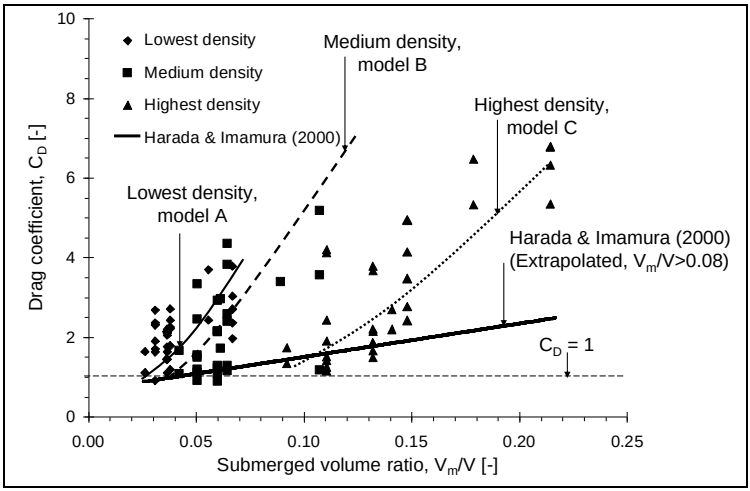

Fig. 3.17: Drag coefficient as a function of submerged volume ratio V_m/V compared to the work of Harada and Imamura (2000)

Moreover, a new relationship for the flow resistance in terms of drag coefficient C_D can be derived as a function of Reynolds number (see Fig. 3.18):

for the upper envelope:

$$C_D = \frac{2.126x10^4}{R_e^{0.869}} \tag{3.10}$$

and for the lower envelope:

$$C_D = 1.0 \tag{3.11}$$

Combining all of the obtained data from the experiments with the real models (models A1, B1 and C1) and the parameterized mangrove models (models A2, B2 and C2), the optimum relationship of C_D as a function of the Reynolds number can be derived as follows:

$$C_D = \frac{1.686x10^3}{R_e^{0.542}} \qquad (3.12)$$

where:

$$R_e = \frac{uL_e}{\upsilon} \text{ and } L_e = \frac{V - V_m}{A_f}$$

V : control volume [m^3]
V_m : root volume [m^3]
L_e : effective length [m]
u : averaged flow velocity [m/s]
ν : kinematic viscosity of water (ν = 1.004 x 10^{-6} m^2/s for water temperature = 20 ^oC)
A_f : frontal area [m^2]

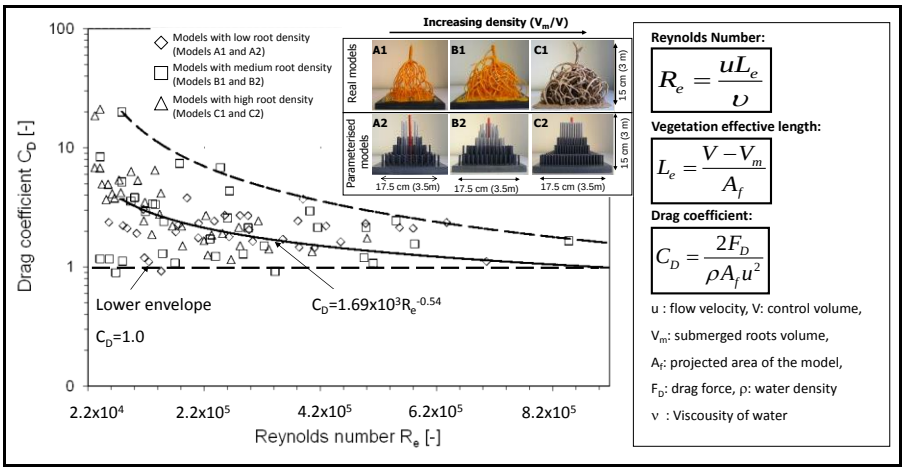

Fig. 3.18: Drag coefficient C_D as a function of Reynolds number R_e

The relationships shown in Eqs. 3.10 – 3.12 and in Fig. 3.18 explain thoroughly the effect of both physical properties of the body subject to flow (root density

V_m/V, frontal area A_f,) and of the flow regime (Reynolds number R_e) on drag coefficient C_D. Therefore, the parameterized model, which has been selected in the current study, is physically based and sufficiently verified under steady flow conditions to be further implemented for a larger scale of model experiments on tsunami attenuation by a mangrove forest under a stiff structure assumption in a wave flume.

3.2.5 Remarks on the parameterisation with stiff structure assumption

Important key findings from the parameterisation of mangrove with stiff structure assumption are summarized as follows:

- The use of a "real" model as a reference model and its generic parameterisation methodology has enabled us to successfully determine the most representative parameterised model. Among other tested models, the later was selected because the induced hydraulic losses are closest to the hydraulic losses induced by its real model counterpart. The selected parameterised model consists of group of cylinders with similar submerged volume root density (V_m/V) and frontal area (A_f) as the "real" model. The dimensions of the constitutive individual cylinders of the root model system are also similar to the averaged dimensions of roots in the "real" model.

- The drag losses is dominant over the inertia losses due to the relatively low flow acceleration in the experiments so that inertia losses can be neglected. Moreover, the exclusion of inertia losses is justified as the structural integrity of the trees is not considered. If structural integrity of the trees is taken into account, the inertial losses may reach half of the drag losses.

- The derived hydraulic resistance in term of drag coefficient (C_D) from the parameterised models is comparable to the previous findings, fills the gaps of some missing information (related to physical characteristics of tree) and extends its possible application for a wider range of flow regimes (Reynolds number) that has never been described in previous studies.

3.3 Parameterisation with flexible structure assumption

3.3.1 Testing programme and setup

Parameterization with flexible structure assumption includes also stiff structure assumption for the bottom part of the mangrove tree (roots) (Fig. 3.6). Additionally, within the flexible structure assumption, stiff trunk is also used for checking the reliability of the proposed canopy model. Therefore, two types of parameterized model are prepared; stiff-trunk parameterized models and flexible-trunk parameterized models. Stiff-trunk parameterized models are needed to investigate the hydraulic properties of the parameterized canopy which is going to be implemented for both mangrove and coastal pine tree models. Moreover, a stiff trunk will also provide more controllable environment without any disturbance from any tree structure changes due to deflections. First, laboratory experiments using stiff-structure parameterized models are only conducted for mangrove tree models (Test series I). Once the hydraulic resistance of the canopy is confirmed from the comparison of measured hydraulic forces, the parameterized models with flexible trunk are also tested (Test series II) to study the hydraulic resistance with deflection in more details.

The step by step methodology for the parameterization as shown in Fig. 3.21 can be described as follows:

- Parameters from the prototype trees are known from literatures or field survey such as geometry, density of canopy/roots, trunk stiffness, etc.
- Real canopy models made of plastic (for leaves) and hardened-clay (for branches) are constructed using the obtained parameters from the prototype trees (the geometry and LAI) (Fig. 3.19).

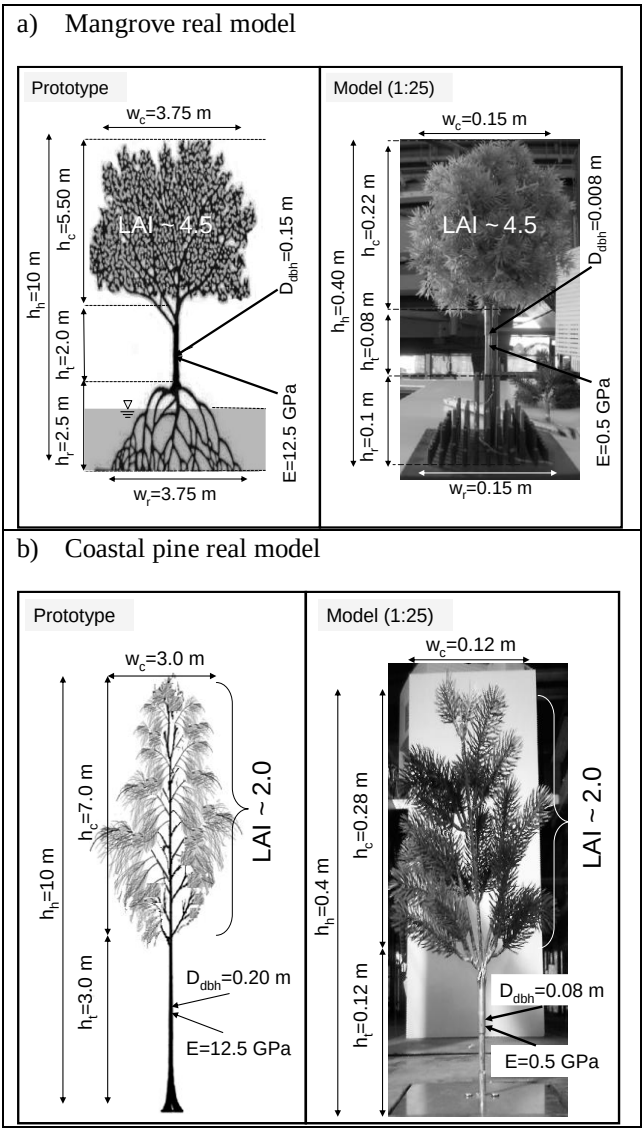

Fig. 3.19: Parameters of mangrove and coastal pine trees for both prototype and scaled "tree model"

– For the trunk, since the length scale is 1 : 25 and by taking the averaged values of E for mangrove and coastal pine trees are 18 GPa and 11 GPa respectively (Husrin and Oumeraci, 2012h), the expected scaled E values for mangrove and coastal pine is ranging from 440 MPa – 720 MPa (Averaged = 580 MPa). A feasible material for this range of E values is *polytetrafluoroethylene* or PTFE. However, this material also has a drawback because its density is double of wood density ($\rho_{t,m} = 2\rho_{t,p}$). This means rupture stress of PTFE is much higher compared to the real wood or in another word the trunk is hardly breakable. The effects of "unbreakable" trunk influence the analysis of hydraulic forces because the deflection angles in the tree models will be "unlimited". Therefore, maximum allowable deflection angles for typical trees represent a threshold for the analysis of measured hydraulic forces in the experiments.

$$\frac{E_p}{E_m} = \lambda_s \quad \text{and} \quad \frac{\rho_{t,p}}{\rho_{t,m}} \neq 1 \tag{3.13}$$

– Two materials are prepared for the parameterised canopy; sponge and fibrous materials. Both proposed parameterised canopy models are then tested hydraulically in the current flume using stiff trunk (Test series I). The measured hydraulic losses for both proposed models are in agreement. However, sponge canopy did not perform well when dealing with permeability and skin friction of the canopy[9]. Therefore, the use of sponge was rejected and fibrous material is selected to be used further for the parameterised canopy model.
– The parameterised models for mangrove and coastal pine with different density characteristics are then constructed by combining the parameterised canopy, flexible trunk and the root (for mangrove). For coastal pine tree, there are only canopy and the flexible trunk (Fig. 3.20).
– Test series II is then conducted to investigate the hydraulic properties of the parameterised model including flexibility behaviours of the tree subject to currents. Parameterised model with similar hydraulic losses as the real model is selected. The force induced by the flow on the middle tree is measured

[9] More detailed information in Report Nr. 8 (Husrin and Oumeraci, 2012h)

together with the flow velocity and the water surface elevation, so that the flow resistance in terms of drag coefficient can be derived.

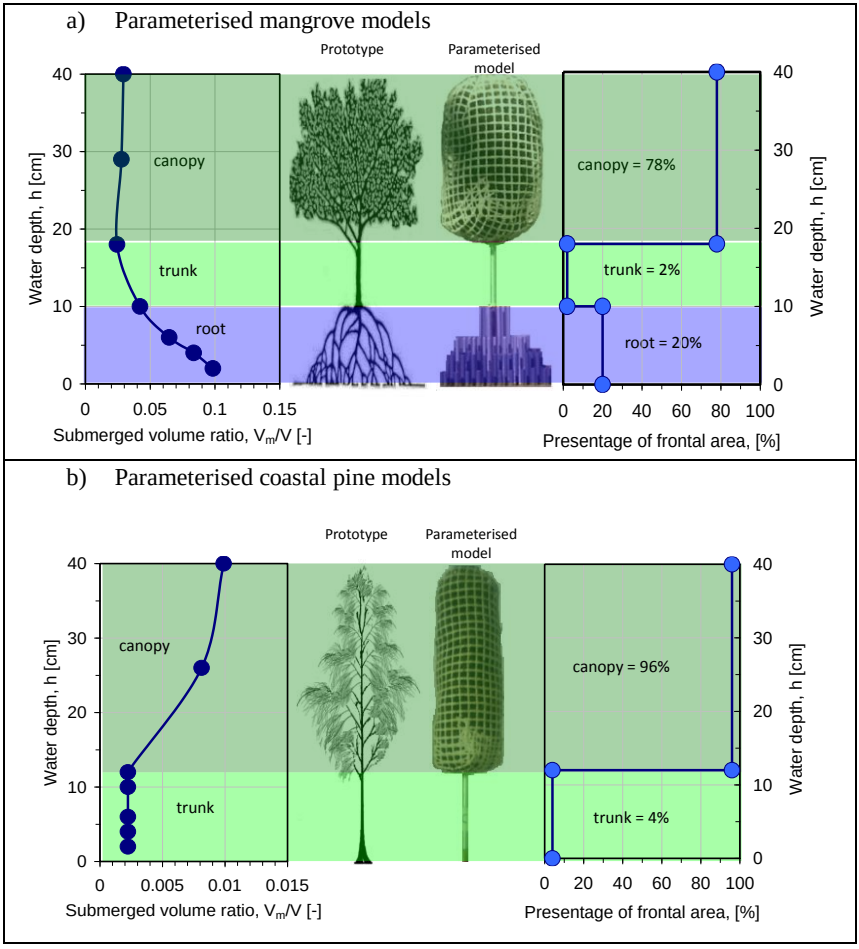

Fig. 3.20: Characteristics of parameterised model of mangrove and coastal pine

Similar facilities and types of experimental setup used for the experiments with stiff structure assumption were implemented (Fig. 3.8). The hydraulic resistance of the mangrove and coastal pine models are measured in a current flume. The procedure used for the experiments in a current flume including the measured parameters (current velocity, head difference and flow-induced force), measurements devices, and experimental setup are also similar as for the parameterisation experiment with stiff structure assumption except for the measurement of the deflection (Table 3.6). A video camera is installed in such away so that the deflection of the tree model can be observed from the side of the flume.

Table 3.6: Testing programme for all models

Model	Prototype velocity, u_p [m/s]	Velocity in flume, u [m/s] (scale 1:25)	Water level. h [m]	Discharge, Q [m^3/s]	Relative discharge, q [$m^3/s/m^2$]
The same program for all models	1	0.2	0.20	0.026	0.20
			0.30	0.037	0.20
			0.40	0.048	0.20
	1.5	0.3	0.20	0.038	0.30
			0.30	0.055	0.30
			0.40	0.096	0.40
	2	0.4	0.20	0.051	0.40
			0.30	0.074	0.40
			0.40	0.096	0.40
	2.5	0.5	0.20	0.064	0.50
			0.30	0.092	0.50
			0.40	0.120	0.50
	3.75	0.75	0.20	0.096	0.75
			0.30	0.138	0.75
			0.40	0.180	0.75
	4	0.8	0.20	0.102	0.80
			0.30	0.147	0.80
			0.40	0.192	0.80
	5	1	0.20	0.128	1.00
			0.30	0.184	1.00
			0.40	0.240	1.00

Table 3.7: Characteristics of parameterised mangrove models with stiff trunk

Description	symbol	total sub-merged volume, V_m [cm³]	width of cano-py, w_c [m]	width of roots, w_r [m]	height of cano-py, h_c [m]	Fron tal area, A_f [m²]	Total height, h_h [m]	Trunk diam-eter, D_c [m]	Height of trunk, h_t [m]
Real model, stiff trunk	**ReMS**	165.20	0.15	0.15	0.22	0.02 91	0.4	0.008	0.08
same density and frontal area as the real model ReMS	**M1FS**	174.20	0.135	0.15	0.22	0.02 97	0.4	0.008	0.08
30% less dense than M1FS, same frontal area as M1FS	**M2FS**	116.16	0.135	0.15	0.22	0.02 97	0.4	0.008	0.08
50% less dense than M1FS, same frontal area as M1FS	**M3FS**	87.10	0.135	0.15	0.22	0.02 97	0.4	0.008	0.08
30% less dense than M1FS, 30% less frontal area than M1FS	**M4FS**	116.16	0.095	0.15	0.22	0.02 08	0.4	0.008	0.08
50% less dense than M1FS, 50% less frontal area than M1FS	**M5FS**	87.10	0.068	0.15	0.22	0.01 49	0.4	0.008	0.08

Table 3.8: Characteristics of parameterised mangrove models with flexible trunk

Description	symbol	total submerged volume, V_m [cm³]	width of canopy, w_c [m]	width of roots, w_r [m]	height of canopy, h_c [m]	Frontal area, A_f [m²]	Total height, h_h [m]	Trunk diameter, D_c [m]	Height of trunk, h_t [m]
same density as ReMS model but reduced frontal area	**M1FF**	174.20	0.124	0.15	0.22	0.02728	0.4	0.008	0.08
30% less density than M1FF, same frontal area as M1FF	**M2FF**	116.16	0.124	0.15	0.22	0.02728	0.4	0.008	0.08
50% less density than M1FF, same frontal area as M1FF	**M3FF**	87.10	0.124	0.15	0.22	0.02728	0.4	0.008	0.08

Table 3.7, table 3.8 and table 3.9 show the characteristics of the parameterized model for both mangrove and coastal pine trees. Parameterized models with stiff cylindrical trunk are intended for checking the reliability of the proposed canopy model made of artificial fibrous material (Fig. 3.21). For the root of mangrove tree model, group of cylinders with staggered arrangement is used based on the stiff structure assumption.In table 3.8, the frontal areas of the models with flexible trunk are 8% smaller compared to the real model (ReMS) by reducing the width of the canopy. This reduction is intended for practical reasons when large scale experiment should be performed in the wave flume. By having 8% less area, the gap between individual tree models in the wave flume will be wider (3.2 cm), allowing the tree model to be freely deflected for certain degrees when hit by incoming waves.

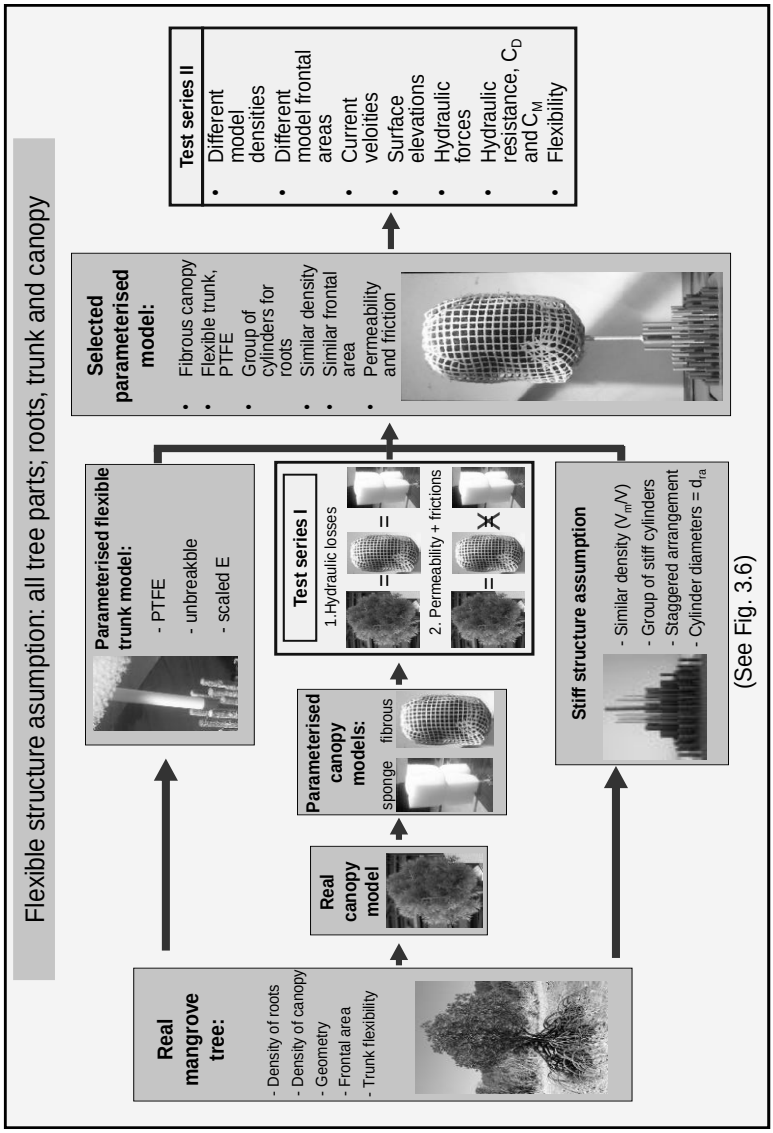

Fig. 3.21: General methodology for flexible structure assumption

In Table 3.9, the width of the canopy between the real model and the parameterized models is different. This occurs due to the fact that the real pine tree has spreading canopy characteristics though the density is less. Therefore, to compensate that, the width of the canopy has to be reduced to accommodate the most important parameters such as the frontal area and the submerged volume ratio.

Table 3.9: Characteristics of parameterised coastal pine models with stiff and flexible trunk

Description	symbol	total submerged volume, V_m [cm^3]	width of canopy, w_c [m]	height of canopy, h_c [m]	Frontal area, A_f [m^2]	Total height, h_h [m]	Trunk diameter, D_c [m]	Height of trunk, h_t [m]
Real model, stiff trunk	**ReCS**	82.86	0.15	0.28	0.0233	0.4	0.008	0.12
stiff trunk, same density and frontal area as the real model	**C1FS**	89.90	0.08	0.28	0.0224	0.4	0.008	0.12
flexible trunk, same density & frontal area as ReCS	**C1FF**	89.90	0.08	0.28	0.0224	0.4	0.008	0.12
flexible trunk, 16% less density than ReCS, same frontal area as C1FF	**C2FF**	75.20	0.08	0.28	0.0224	0.4	0.008	0.12
flexible trunk, 50% more density than ReCS, same frontal area as C1FF	**C3FF**	134.40	0.08	0.28	0.0224	0.4	0.008	0.12

3.3.2 Measurement results

There are 240 tests for 15 models where each model is subjected to 16 test programs. Three water depths are considered here (h = 0.2 m, 0.3 m and 0.4 m) for mangrove models. However, since h = 0.2 m considers only for the roots and the trunk which is all similar for all models, the experiment for h = 0.2 was only conducted once. The test for h = 0.2 m is represented by model RT for all mangrove models (Table 3.10 and Table 3.11). For coastal pine models (C1FF, C2FF and C3FF), two water depths (h = 0.3 m and h = 0.4 m) as for mangrove models are considered in order to investigate the hydraulic performance comparison between the two tree models.

Table 3.10: Force measurement results for test series I (stiff trunk)

No.	Water depth, h [m]	Current velocity, u [m/s]	Hydraulic force, F_D [N]								
			RT	ReMS	M1FS	M2FS	M3FS	M4FS	M5FS	ReCS	C1FS
1	0.3	0.20	0.1209	0.598	0.517	0.452	0.538	0.354	0.311	0.692	0.379
2	0.4	0.20	0.1998	1.036	0.932	0.891	0.831	0.656	0.528	0.899	0.583
3	0.3	0.30	0.4120	1.422	1.309	1.313	1.356	0.965	0.807	1.470	0.879
4	0.4	0.30	0.4722	2.280	2.237	2.119	2.031	1.674	1.273	1.893	1.455
5	0.3	0.40	0.7787	2.524	2.457	2.478	2.485	1.844	1.521	2.521	1.723
6	0.4	0.40	0.8723	4.506	4.375	4.004	3.899	2.998	2.333	2.911	2.708
7	0.3	0.50	1.1360	3.964	3.800	3.967	3.850	2.744	2.327	3.462	2.642
8	0.4	0.50	1.3050	6.482	6.399	6.041	5.950	4.479	3.506	3.893	3.871
9	0.3	0.60	1.6900	5.973	5.846	5.989	5.542	4.345	3.575	4.632	4.115
10	0.4	0.60	1.9040	8.840	9.310	9.012	8.420	6.664	5.181	4.645	5.924
11	0.3	0.75	2.6540	9.876	9.567	9.765	9.420	6.870	5.794	5.817	6.327
12	0.4	0.75	3.0510	15.653	14.475	12.953	12.721	10.500	7.820	5.764	8.870
13	0.3	0.80	3.0255	11.807	11.049	11.281	10.879	8.063	6.601	6.426	7.388
14	0.4	0.80	3.2011	17.074	15.404	13.796	13.283	11.225	8.444	5.979	9.851
15	0.3	1.00	4.4270	18.2749	16.568	16.539	15.339	11.693	9.849	8.049	10.708
16	0.4	1.00	4.8330	23.244	22.091	19.761	19.297	16.016	12.127	7.719	13.603

As already discussed in the previous sections, test series I or the preliminary experiment should be first conducted to confirm the use of the proposed canopy model made of the artificial fibrous materials. Later on, test series II is carried out to study the influence of tree deflection to the measured hydraulic force. Complete test series I is conducted for mangrove tree models where 5 models with different densities and frontal areas are constructed. For coastal pine tree models, test series I is only conducted to check whether similar parameterised material can also be applicable for different type of real tree model because the

characteristic of coastal pine canopy is different to the mangrove one. Therefore, in the test series I for coastal pine tree, there is only 1 parameterised model (C1FS) which has similar a canopy density and frontal area as the real model (ReCS). Table 3.10 shows the measurement results for test series I (preliminary experiment) while Table 3.11 shows the results from test series II.

Table 3.11: Force measurement with flexible trunk for mangrove & coastal pine models (test series II)

No.	Water depth, h [m]	Current velocity, u [m/s]	Hydraulic force, F_D [N]						
			RT	M1FF	M2FF	M3FF	C1FF	C2FF	C3FF
1	0.3	0.20	0.1209	0.507	0.476	0.504	0.422	0.421	0.354
2	0.4	0.20	0.1998	0.908	0.817	0.859	0.680	0.654	0.645
3	0.3	0.30	0.4120	1.409	1.318	1.315	0.977	0.982	0.913
4	0.4	0.30	0.4722	2.170	2.116	1.938	1.420	1.344	1.387
5	0.3	0.40	0.7787	2.606	2.450	2.367	1.772	1.761	1.840
6	0.4	0.40	0.8723	3.666	3.581	3.370	2.350	2.161	2.317
7	0.3	0.50	1.1360	4.036	3.816	3.683	2.763	2.489	2.849
8	0.4	0.50	1.3050	5.030	4.746	4.685	2.842	2.409	2.576
9	0.3	0.60	1.6900	6.127	5.792	5.377	3.176	2.528	3.306
10	0.4	0.60	1.9040	6.356	6.315	6.050	2.983	3.047	3.018
11	0.3	0.75	2.6540	8.304	8.066	7.931	4.375	3.801	3.785
12	0.4	0.75	3.0510	7.991	7.974	7.644	3.565	3.637	3.617
13	0.3	0.80	3.0255	9.481	9.278	9.033	4.543	3.961	4.088
14	0.4	0.80	3.2011	8.959	8.507	8.336	4.333	3.730	3.779
15	0.3	1.00	4.4270	12.873	12.723	11.613	5.599	4.859	5.201
16	0.4	1.00	4.8330	11.511	11.198	10.661	5.123	4.481	4.625

3.3.3 Analysis of test series I (Mangrove models)

For the roots and the trunk (h = 0.2 m), the measured hydraulic force has quadratic function to the flow velocity. Similar pattern is also observed for water depth h = 0.3 m (emergent condition), the force F_D seems to have quadratic relationship to the flow velocity u. This occurs due to the fact that the structure is still relatively stiff at this water depth (Fig. 3.22).

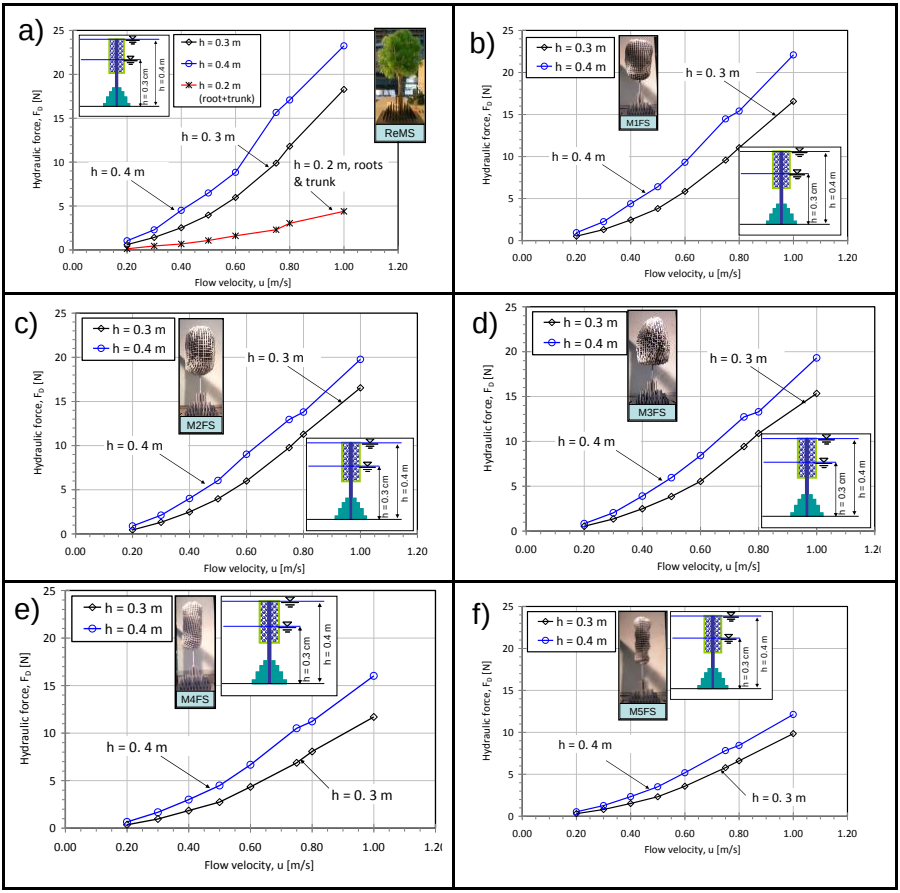

Fig. 3.22: Force measurement of mangrove real model with stiff trunk (ReMS) and the five parameterised models (M1FS, M2FS, M3FS, M4FS and M5FS)

For a fully submerged condition h = 0.4 m, similar behaviour as for emergent condition (h = 0.3) is also observed until u = 0.75 m/s. For u > 0.75 m/s, the curve of F_D Vs. u tends to be more linear. This shows that at higher flow velocities, deflection of the plastic leaves in the canopy has started to take effect. Therefore, F_D as a function of u is no longer quadratic. This behaviour confirms the finding of previous laboratory experiment conducted by Wilson *et al.* (2010).

Moreover, the measured forces for h = 0.4 m are always larger than those for h = 0.3 m for all flow velocities (Fig. 3.22).

For the parameterised models with similar frontal area and different canopy density (models M1FS, M2FS, and M3FS), the measured hydraulic forces for all conditions show a similar pattern. The force as a function of flow velocity has quadratic relationship. This occurs due to the fact that all parameterised model have relatively homogenous structures. The tree models have different canopy densities where M1FS has the highest canopy density. Therefore, M1FS clearly has larger forces compared to M2FS and M3FS.

Fig. 3.23 shows the plots of the measured hydraulic forces for all models for emergent (h = 0.3 m) and fully submerged conditions (h = 0.4 m) as a function of flow velocity. These figures show clearly quadratic patterns of the measured hydraulic force as a function of flow velocity for all models including the 'real' model (ReMS) and also the root and trunk model (RT). The measured forces for ReMS are always bigger for all conditions than the parameterized models. M1FS which has similar submerged volume ratio and frontal area has the closest measured hydraulic forces compared to the other models. From the figure, it is also noticed that for the velocity up to u = 0.75 m/s, the measured hydraulic force of ReMS and M1FS seem to be similar. However, when the flow velocity is larger than u = 0.75 m, the measured hydraulic forces of ReMS are larger than M1FS. Smaller forces in M1FS for faster flow velocities may be attributed to the fact the flow around model M1FS which has a regular shape is more streamlined compared to the real model ReMS which has an irregular shape. All parameterized model has more or less a circular shape as seen from the top.

The plot of relative difference between the parameterized models and the real model is shown in Fig. 3.24 for both emergent and fully submerged conditions. The x-axis belongs to the real model while the y-axis is for the parameterized models. From this figure, it is clear that the difference between real model and the parameterized model. The difference hydraulic force (δ_F) as shown in Fig. 3.24 and also Table 3.12 is calculated as follows:

$$\delta_F = \frac{F_{D,(ReMS)} - F_{D,(par models)}}{F_{D,(ReMS)}} x100\% \qquad (3.14)$$

Therefore, minus sign of δ_F means that the measured hydraulic force is smaller compared to the real model force (Table 3.12). Model M1FS has the averaged smaller of δ_F compared to the other model.

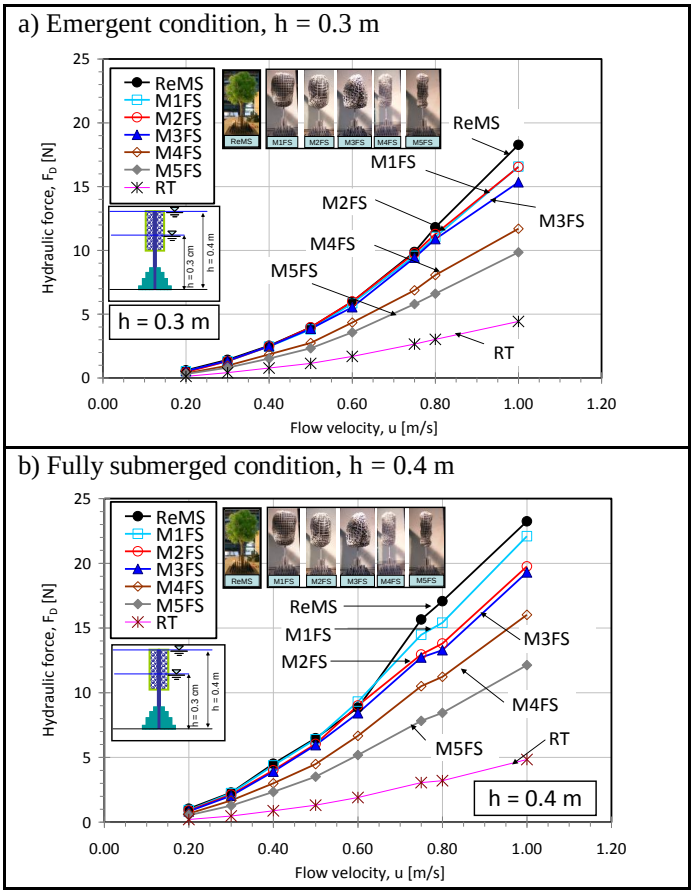

Fig. 3.23: The measured hydraulic forces for emergent and fully submerged conditions

Table 3.12: Comparison of parameterised models to the real model of mangrove (test series I)

Water depth, h [m]	Current velocity, u [m/s]	Relative force difference to the real model ReMS				
		M1FS	M2FS	M3FS	M4FS	M5FS
0.3	0.20	-14%	-24%	-10%	-41%	-48%
0.4	0.20	-10%	-14%	-20%	-37%	-49%
0.3	0.30	-8%	-8%	-5%	-32%	-43%
0.4	0.30	-2%	-7%	-11%	-27%	-44%
0.3	0.40	-3%	-2%	-2%	-27%	-40%
0.4	0.40	-3%	-11%	-13%	-33%	-48%
0.3	0.50	-4%	0%	-3%	-31%	-41%
0.4	0.50	-1%	-7%	-8%	-31%	-46%
0.3	0.60	-2%	0%	-7%	-27%	-40%
0.4	0.60	5%	2%	-5%	-25%	-41%
0.3	0.75	-3%	-1%	-5%	-30%	-41%
0.4	0.75	-8%	-17%	-19%	-33%	-50%
0.3	0.80	-6%	-4%	-8%	-32%	-44%
0.4	0.80	-10%	-19%	-22%	-34%	-51%
0.3	1.00	-9%	-10%	-16%	-36%	-46%
0.4	1.00	-5%	-15%	-17%	-31%	-48%
Averaged		**-5%**	**-9%**	**-11%**	**-32%**	**-45%**

M1FS has a similar density as the real model (ReMS) while M2FS is 30% less dense compared to M1FS and M3FS is 50% less dense compared to M1FS. The averaged different of measured forces between M1FS, M2FS and M3FS to the real model ReMS is around 5%, 9% and 11% smaller, respectively (Table 3.12). This means by changing a half of the canopy density, the hydraulic force is reduced by 10%.

Model M4FS has similar density as M2FS (30% less dense as the real model ReMS) but the frontal area is also reduced by 30%. The measured force is far much smaller up to 32%. When the frontal area is also reduced for up to 50% (Model M5FS), the reduction force reaches 45% smaller compared to the real model ReMS. This means by reducing of the frontal area, the measured force is far much smaller compared to reducing the canopy density.

Contribution of the root system to the total measured forces is shown in Table 3.13. Table 3.13 shows that with similar frontal area (Models ReMS, M1FS, M2FS, M3FS), the relative contribution of roots to the measured hydraulic force increases slightly as the canopy density increases. For emergent condition h =

0.3 m, the contribution of roots increases only 2% (from 27% to 29%) as the canopy density reduce by 50%. Similarly, for h = 0.4 m (fully submerged condition), the root contribution increases by only 2% (from 20% to 23%) as the canopy density reduces by 50%. With smaller frontal area (Models M4FS and M5FS), the relative contribution of roots to the total measured force increases significantly. Model M4FS has similar density to M2FS by the frontal area reduce by 30%. By keeping similar density and reducing the frontal area by 30%, the contribution of roots increases by 10 % (from 28 to 29%) for emergent condition and by 6% (from 23% to 29%) for a fully submerged condition. Similarly, for model M5FS which has similar canopy density as M3FS but reduce frontal area by 50%, the contribution of root increases by 18% (from 29% to 47%) for emergent condition and by 15% (from 23% to 38%) for fully submerged condition. This again shows that the variation of the frontal area has more effect to the hydraulic force compared to the changing of canopy density. All the calculation data from the hydraulic test I with coastal pine model can be found in Report Nr. 10 (Husrin and Oumeraci, 2012i).

Table 3.13: Relative root contribution to the measured hydraulic force (test series I)

Water depth, h [m]	Current velocity, u [m/s]	Root contribution					
		ReMS	M1FS	M2FS	M3FS	M4FS	M5FS
0.3	0.20	20%	23%	27%	22%	34%	39%
0.3	0.30	29%	31%	31%	30%	43%	51%
0.3	0.40	31%	32%	31%	31%	42%	51%
0.3	0.50	29%	30%	29%	30%	41%	49%
0.3	0.60	28%	29%	28%	30%	39%	47%
0.3	0.75	27%	28%	27%	28%	39%	46%
0.3	0.80	26%	27%	27%	28%	38%	46%
0.3	1.00	24%	27%	27%	29%	38%	45%
Averaged		**27%**	**28%**	**28%**	**29%**	**39%**	**47%**
Water depth, h [m]	Current velocity, u [m/s]	Root contribution					
		ReMS	M1FS	M2FS	M3FS	M4FS	M5FS
0.4	0.20	19%	21%	22%	24%	30%	38%
0.4	0.30	21%	21%	22%	23%	28%	37%
0.4	0.40	19%	20%	22%	22%	29%	37%
0.4	0.50	20%	20%	22%	22%	29%	37%
0.4	0.60	22%	20%	21%	23%	29%	37%
0.4	0.75	19%	21%	24%	24%	29%	39%
0.4	0.80	19%	21%	23%	24%	29%	38%
0.4	1.00	21%	22%	24%	25%	30%	40%
Averaged		**20%**	**21%**	**23%**	**23%**	**29%**	**38%**

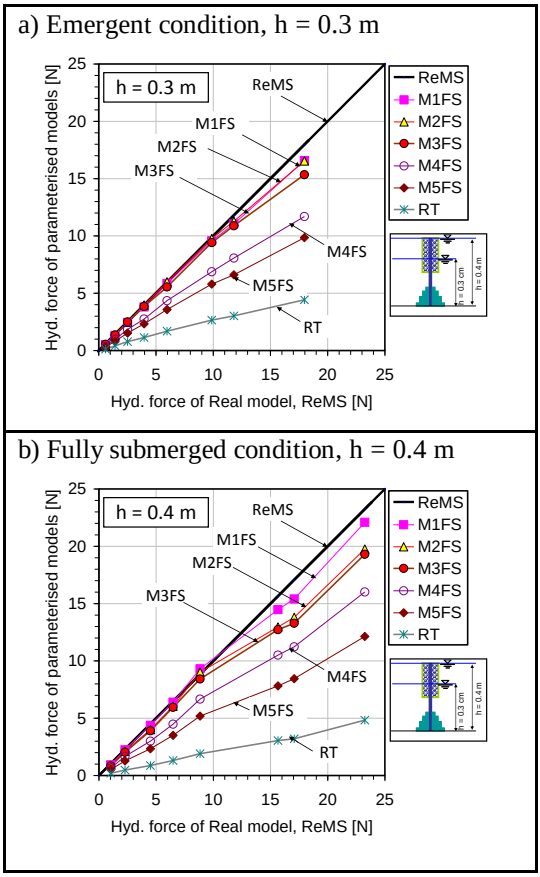

Fig. 3.24: Relative difference of the measured force of parameterised models to the real model

3.3.4 Analysis of test series I (Coastal pine models)

The canopy density of coastal pine is much smaller compared to mangrove. Moreover, it is also more open and spreading. The needle-like leaves make the coastal pine canopy can be easier to deform as it is subjected to fluid flow (e.g wind or water) compared to broad-leaves canopy of mangroves (Fig. 2.15). This

behaviour was observed during the hydraulic test in the current flume. The canopy of real model from coastal pine tree was easily flipped over as subjected wind flow. Fig. 3.25 shows how the canopy is flipped over significantly as subjected to different flow velocities in the current flume.

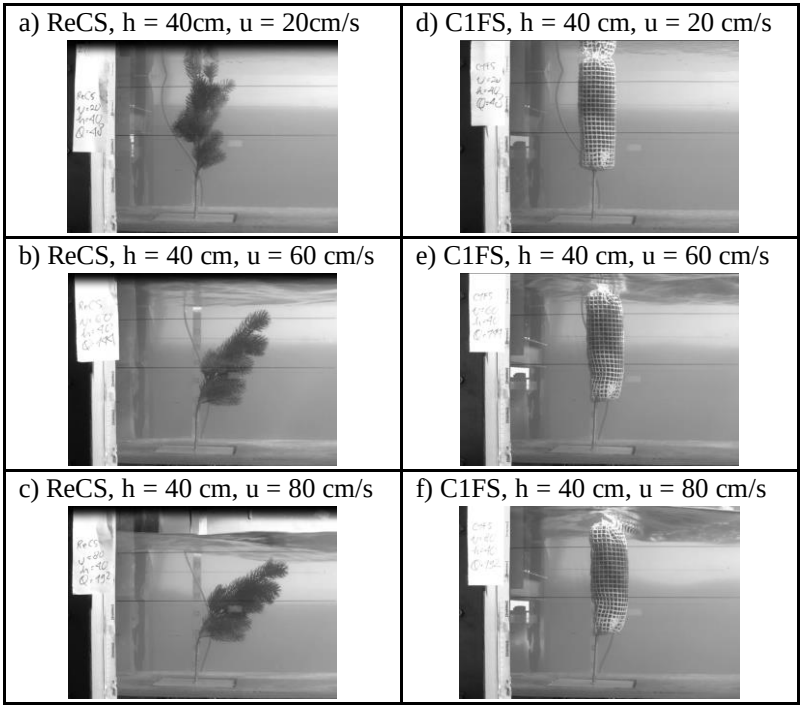

Fig. 3.25: The difference between the canopy of the real model (ReCS) and C1FS

Fig. 3.26 shows the plot of the measurement results from real coastal pine model (ReCS) and the parameterized model with stiff trunk (C1FS). The relationship of the measured hydraulic force as a function of flow velocity for ReCS is clearly not quadratic as observed in the case of mangrove model (see Fig. 3.22a) because the individual canopy branches of real coastal pine tree is rather flexible not as stiff as for the case of mangrove real model. However, this condition makes the analysis rather difficult because the difference between the canopy characteristics of real coastal pine model and the parameterized model becomes too large. This

difference leads to different measured forces between the real model and the parameterized model for both emergent and fully submerged conditions (Fig. 3.27).

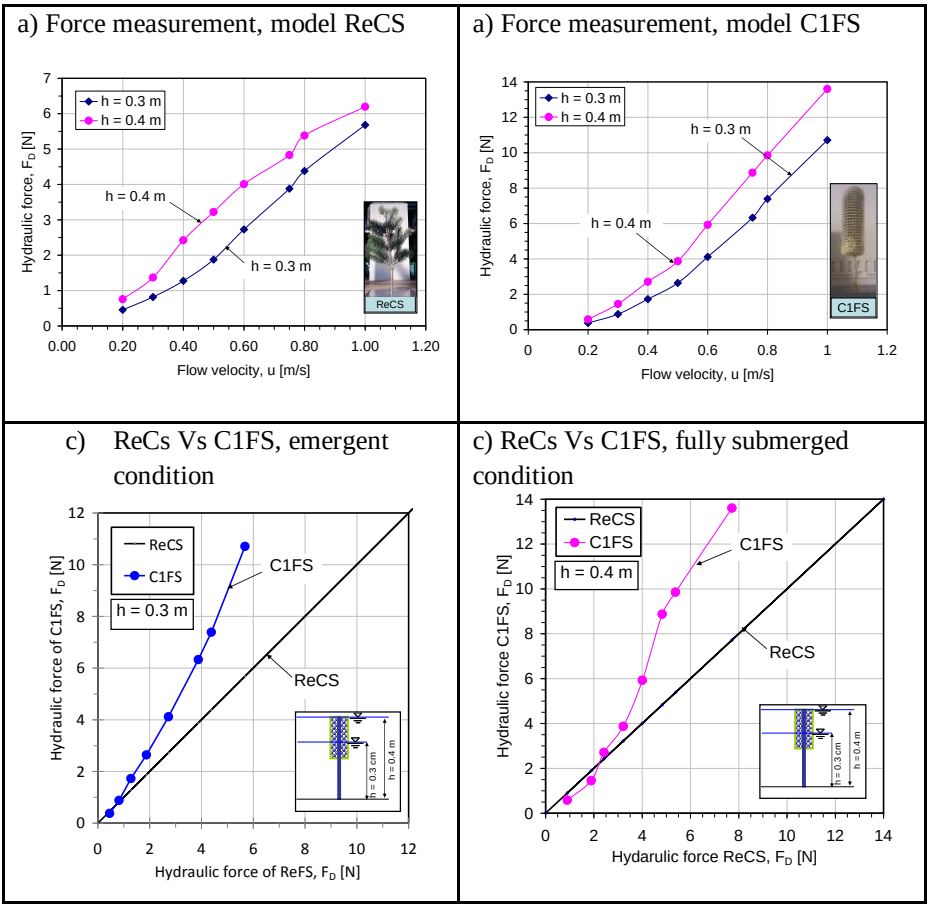

Fig. 3.26: Comparison of ReCS and C1FS models

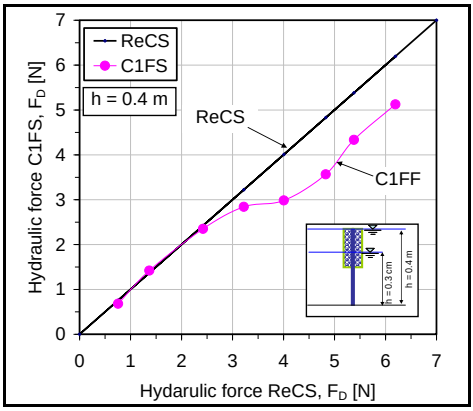

Fig. 3.27: Comparison of ReCS and C1FF models

In the beginning, for smaller flow velocities, the hydraulic force for real model is larger as we observed also for the case of mangrove models. As the flow velocity increases, the measured force of model C1FS increases and even larger than ReCS for u > 0.75 m/s. This may occur due to flipped over of the canopy as already explained leading to smaller measured forces for ReCS. It is clear that due to this elastic behaviour the comparison of the measured forces between ReCS and C1FS cannot be made. These two models are completely different. Therefore, because ReCS is actually become a flexible model, C1FF model which has similar submerged volume ratio and frontal area to ReCS is compared and analysed further.

The comparison of the measured forces from models ReCS and C1FF is shown in Fig. 3.27. Fully submerged condition is selected for the analysis because it includes the entire canopy system. It is clear that for smaller flow velocities (u < 0.6 m/s), the measured forces are almost identical while for larger flow velocity, C1FF is smaller than ReCS. The difference in higher flow velocities is due to highly deflected behaviour of model C1FF. Moreover, with higher flow velocities, the flow around model C1FF is more streamlined resulting smaller measured forces. This behaviour is also observed for the cases of parameterised models for mangroves. All the calculation data from test series I with coastal pine models can be found in (Husrin and Oumeraci, 2012i).

3.3.5 Remarks on test series I

The following aspects are drawn based on the analysis from the hydraulic test I:

- The use of fibrous materials as the parameterized canopy model based on hydraulic force measurement is highly encouraging for mangrove model. The averaged different on the measured hydraulic force between the 'real' model and the parameterized model with similar submerged volume ratio and frontal area is 5%.
- The effect of changing of frontal area is larger compared to the effect of changing canopy volume. However, frontal area is also influenced by the volume of the canopy. Unfortunately, the relationship of these important parameters does not exist yet. Field investigation on the relationship of frontal area and canopy density for typical coastal forest vegetation such as mangrove and coastal pine trees is absolutely needed.
- For the coastal pine tree, a problem was observed for the real model (ReCS) because the canopy of the real model was not controllable and turned to be 'a flexible model', particularly for high flow velocities where deflected canopy cannot be avoided. However, for smaller velocities, ReCS was found to be identical to C1FF which is a flexible model with similar submerged volume ratio and frontal area. Moreover, other factors may contribute to these differences such as spreading characteristics of the real canopy model which is reduced significantly in the parameterized model to compromise much simpler geometry considering similar the submerged volume ratio and the frontal area.

3.3.6 Analysis of test series II (Mangrove models)

Flexible trunk is implemented for all tested models (M1FF, M2FF and M3FF). All models have similar frontal area but different canopy densities. M2FF has 30% less density compared to the model M1FF while model M3FF has 50% less density to the model M1FF. The measurement setup and methodology are similar as for test series I. Detailed measurement results of the deflection angle from all mangrove models can be found in Husrin and Oumeraci (2012i).

Table 3.14: Deflection angles for emergent and fully submerged conditions

M1FF							
Emergent (h = 0.3 m)				Fully submerged (h = 0.4 m)			
u [m/s]	α (°) for h=0.3m	Force, F_D [N]	Elastic/ plastic	u [m/s]	α (°) for h=0.4m	Force, F_D [N]	Elastic/ plastic
0.20	2.74	0.507	Elastic	0.20	6.27	0.908	Elastic
0.30	5.52	1.409	Elastic	0.30	14.35	2.170	Elastic
0.40	14.44	2.606	Elastic	0.40	27.29	3.666	Plastic
0.50	29.95	4.036	Plastic	0.50	33.74	5.030	Plastic
0.60	62.51	6.127	Plastic	0.60	45	6.356	Plastic
0.75	66.02	8.304	Plastic	0.75	60.78	7.991	Plastic
0.80	67.16	9.481	Plastic	0.80	64.5	8.959	Plastic
1.00	77.38	12.873	Plastic	1.00	73.01	11.511	Plastic

M2FF							
Emergent (h = 0.3 m)				Fully submerged (h = 0.4 m)			
u [m/s]	α (°) for h=0.3m	Force, F_D [N]	Elastic/ plastic	u [m/s]	α (°) for h=0.4m	Force, F_D [N]	Elastic/ plastic
0.20	2.12	0.476	Elastic	0.20	4.13	0.817	Elastic
0.30	5.49	1.318	Elastic	0.30	13.46	2.116	Elastic
0.40	13.19	2.450	Elastic	0.40	31.29	3.581	Plastic
0.50	29.78	3.816	Plastic	0.50	41.62	4.746	Plastic
0.60	65.94	5.792	Plastic	0.60	65.32	6.315	Plastic
0.75	74	8.066	Plastic	0.75	69	7.974	Plastic
0.80	75.05	9.278	Plastic	0.80	70.78	8.507	Plastic
1.00	79.2	12.723	Plastic	1.00	75.81	11.198	Plastic

M3FF							
Emergent (h = 0.3 m)				Fully submerged (h = 0.4 m)			
u [m/s]	α (°) for h=0.3m	Force, F_D [N]	Elastic/ plastic	u [m/s]	α (°) for h=0.4m	Force, F_D [N]	Elastic/ plastic
0.20	1.57	0.504	Elastic	0.20	2.81	0.859	Elastic
0.30	4.46	1.315	Elastic	0.30	10.86	1.938	Elastic
0.40	5.74	2.367	Elastic	0.40	23.18	3.370	Elastic
0.50	15.31	3.683	Elastic	0.50	33.34	4.685	Plastic
0.60	32.64	5.377	Plastic	0.60	47.27	6.050	Plastic
0.75	64	7.931	Plastic	0.75	61.53	7.644	Plastic
0.80	66.49	9.033	Plastic	0.80	62.98	8.336	Plastic
1.00	72.33	11.613	Plastic	1.00	70.18	10.661	Plastic

One of the key features from test series II is the different behaviour of measured force in emergent and fully submerged conditions (h = 0.3 m and h = 0.4 m, respectively). As shown in Fig. 3.28 and Fig. 3.29, the measured hydraulic force for emergent condition overtakes those from fully submerged conditions after certain flow velocity. For emergent conditions, the relationship of forces and flow velocity is quadratic up to certain limits. As the flow is getting faster, the

relationship turns to be more linear as observed for all the cases with fully submerged conditions.

This occurs because for emergent conditions, when the tree is deflected or almost fully deflected, the frontal area as a function of water depth is larger compared to fully submerged conditions. In other words, for emergent conditions, the more tree model gets deflected the larger the hydraulic forces are, while for a fully submerged conditions are other way around. This can be schematically described as shown in Fig. 3.30 for emergent and fully submerged conditions, respectively. Moreover, the deflection angles for emergent conditions are larger compared to those with fully submerged conditions (Table 3.14). It is obvious that buoyancy play an important role in maintaining the tree models with smaller deflection angels in fully submerged conditions.

Fig. 3.28 and Table 3.14 are also very important in determining the limit of trunk flexibility. From the observations after each test, it was found that for the deflection larger than 23°, (see Table 3.14 for M3FF) the trunk is no longer elastic. This means the trunk does not return to its original position after being hit by the steady current. Fig. 3.29 shows examples of this behaviour for model M2FF. It is also found that submerged condition leads to earlier plastic conditions compared to emergent conditions with similar flow velocity. Moreover, this elastic condition can be assumed as a guarantee that the trunk will not break up to this limit. According to the results of pulled-test for scots pine, Norway spruce and birch trees, the deflection angles for a broken trunk may ranges from 23° – 42° (Peltola *et al.*, 2000). If we take the assumption that the breakage limit of the mangrove model is similar to the breakage limit of the tree according to Peltola *et al.* (2010), the obtained plots for emergent conditions may provide information that within the quadratic curves, the tree may still survive and provide hydraulic damping as shown in Fig. 3.31a for all mangrove models. According to the obtained data and the assumption, the limiting flow velocity that the tree may survive from the attack of flow is u = 0.6 m/s for emergent condition and u = 0.4 m/s for fully submerged conditions. This velocity is equivalent to the velocity in prototype u = 3 m/s.

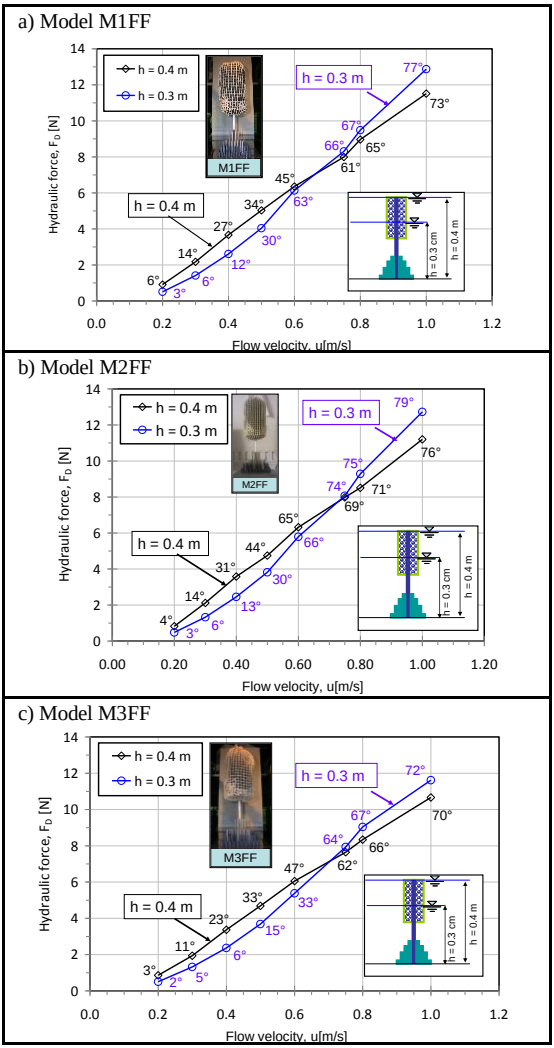

Fig. 3.28: Force measurement of parameterised mangrove model with flexible trunk

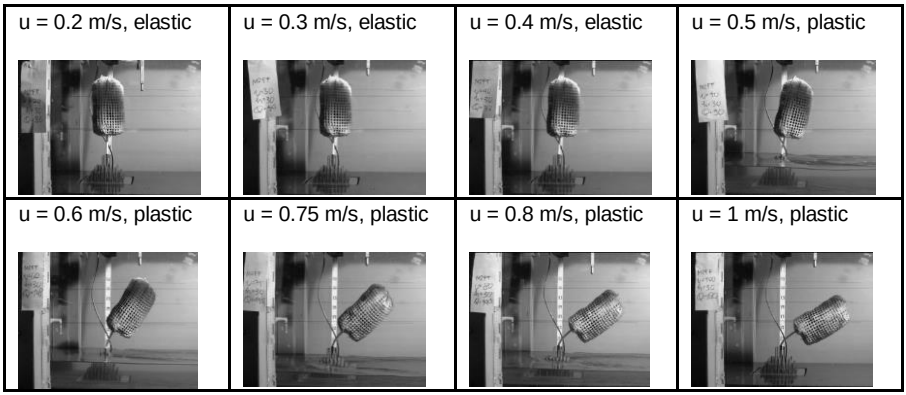

Fig. 3.29: Limit of elastic behaviour for model M2FF observed after the test for emergent conditions

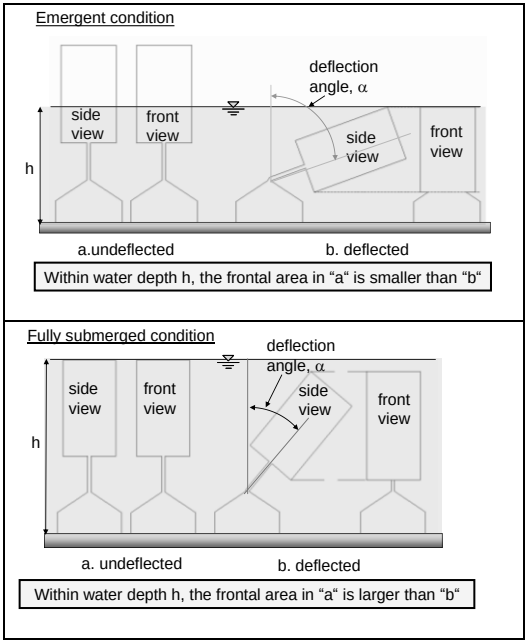

Fig. 3.30: Effect of deflection to the change of frontal area and submerged volume ratio for emergent and fully submerged condition

For fully submerged conditions (h = 0.4 m or h = 10 m in prototype), the deflection of tree reach more than 30° for velocity u = 0.4 m/s or u = 2 m/s. This may lead to the indication that it is very unlikely that trees may survive from such high water depth. Even with a very low flow velocity, the deflection is already high (Fig. 3.31b).

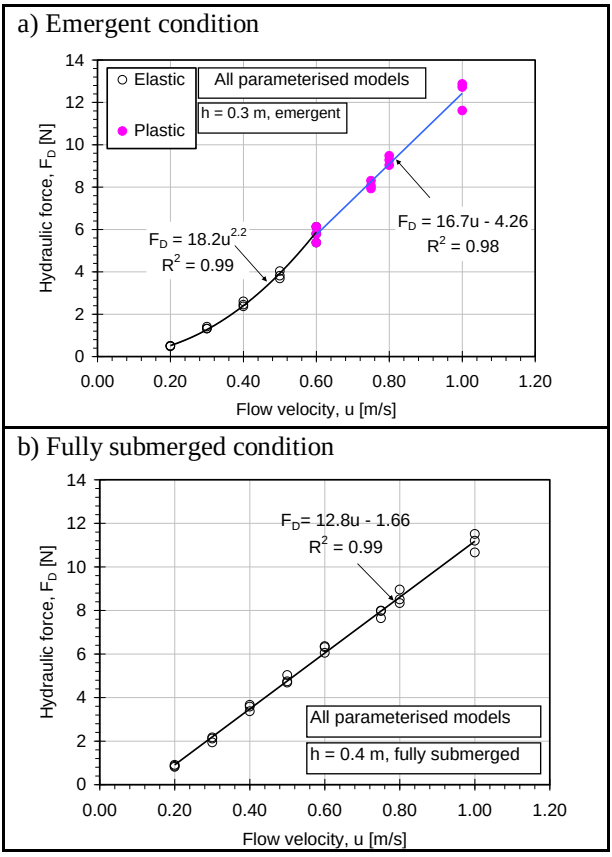

Fig. 3.31: Hydraulic force as a function of flow velocity for all mangrove models

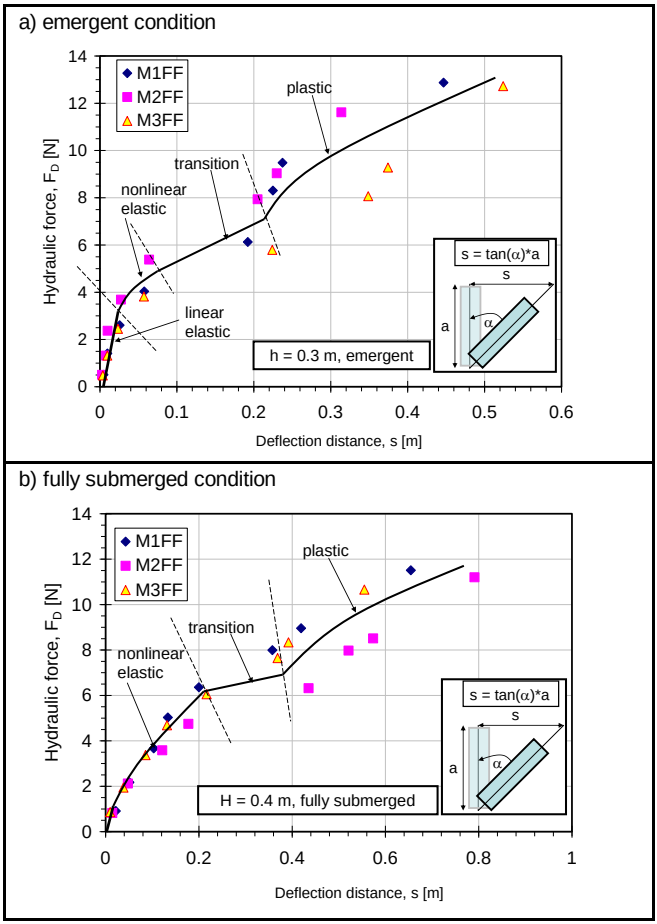

Fig. 3.32: Relationship of the three parameterised models (M1FF, M2FF and M3FF)

However, it has to be noted that the velocity limitation is only valid for the water levels as defined in the experimental set up. Shallower water depth and larger velocities may also be possible to deflect the trunk by 23° or more until it breaks. Along the west coast of Thailand after the 2004 Indian ocean tsunami, Yanagisawa *et al.* (2009) found that most mangrove trees did not survive with tsunami higher than 6 m with maximum predicted velocity is around u = 5 m/s. They

also found that some trees may still provide reduction up to 30% when the tsunami height is still below 3 m with predicted tsunami velocity up to u = 4.3 m/s.

Moreover, the age and diameter of the trunk should also be considered (Shuto, 1987 and Asano, 2010). In the current study, mid age tree is assumed with trunk diameter is around D_{dbh} = 0.2 m. As the trunk diameter is getting larger, the ability to withstand the hydraulic force increases (Harada and Kawata, 2005). For young mangrove trees, structural stability is a major problem because most of them were uprooted and washed away by tsunami (Forbes and Broadhead, 2007).

The "elastic" and "plastic" behaviours as shown in Fig. 3.31 are highly related to the characteristics of PTFE material which is used for the trunk. By plotting the horizontal distance of the deflected canopy, these elastic/plastic behaviours are clearly visible. Fig. 3.32 shows how the deflected distance (s) behaves to the measured hydraulic force. It is found that for both emergent and fully submerged conditions, the behaviour can always be divided into 3 regions; "elastic", "transitions" and "plastic" regions. The definition of elastic, transition and plastic behaviours are based on the observation of the ability of the trunk to return to its original position after loaded by steady current within short period of time (in this case less than 5 minutes) because PTFE is actually a highly elastic material though its elasticity behaviour tends to be nonlinear (Rae and Dattelbaum, 2004). Therefore, the definition of "plastic" in this report should be carefully distinguished because of the implemented time limitation.

Linear elastic behaviour is observed for emergent conditions with smaller flow velocity. This pattern is in agreement with the plot of hydraulic force versus flow velocity as shown in Fig. 3.31. For fully submerged conditions, it is difficult to distinguished linear elasticity because there are only 2 or 3 points (Table 3.14). Therefore, for fully submerged conditions all points are grouped as nonlinear elastic conditions because there are mostly not fully return back to its original positions (observation on this was rather difficult because time restriction in the adopted definition). The transition region is the region where the trunk starts to be plastic. The jump as shown in Fig. 3.32 is due to high deflection angle at that

point. Afterwards, the plastic region is consistently observed for all flow velocities.

As previously has been discussed in test series I with stiff trunk, changing canopy density does not affect significantly to the measured hydraulic force. M2FF is 30 % less dense while M3FF is 50% less dense compared to model M1FF. However, the measured hydraulic force only reduces slightly. For example, the measured hydraulic force of M2FF and M3FF are only 4% and 7% smaller compared to M1FF, respectively (Fig. 3.33).

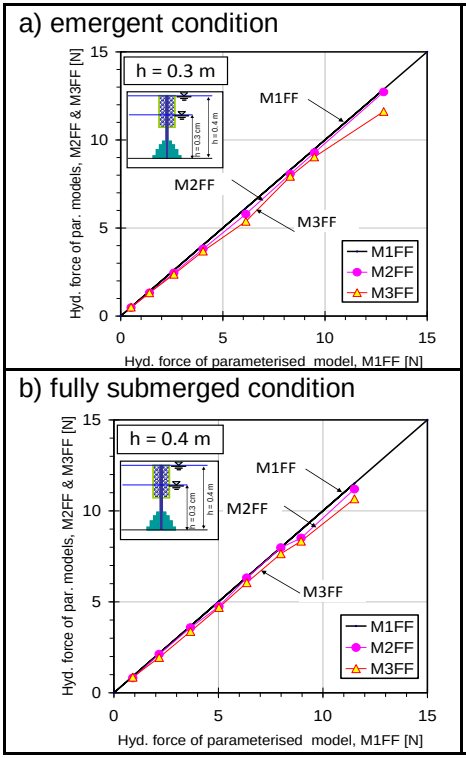

Relative force difference to M1FF			
Water depth, h [m]	Current velocity, u [m/s]	M2FF	M3FF
0.3	0.20	-6%	-1%
0.4	0.20	-10%	-5%
0.3	0.30	-6%	-7%
0.4	0.30	-2%	-11%
0.3	0.40	-6%	-9%
0.4	0.40	-2%	-8%
0.3	0.50	-5%	-9%
0.4	0.50	-6%	-7%
0.3	0.60	-5%	-12%
0.4	0.60	-1%	-5%
0.3	0.75	-3%	-4%
0.4	0.75	0%	-4%
0.3	0.80	-2%	-5%
0.4	0.80	-5%	-7%
0.3	1.00	-1%	-10%
0.4	1.00	-3%	-7%
Averaged		-4%	-7%

Fig. 3.33: Relationship of the three parameterised models (M1FF, M2FF and M3FF)

3.3.7 Analysis of test series II (coastal pine models)

Coastal pine models have much smaller submerged volume ratio compared to mangrove models. This difference can be observed from the measured hydraulic forces which are much smaller as well (

Table 3.15). The maximum measured hydraulic force in mangrove models is around 15N while for coastal pine model is only 6N or almost 60% smaller as shown in Fig. 3.34 where the measured hydraulic force is plotted as function of flow velocity. Similar pattern as found in mangrove models is also observed for coastal pine models.

Table 3.15: Deflection angles for emergent and fully submerged conditions

C1FF							
Emergent (h = 0.3 m)				Fully submerged (h = 0.4 m)			
u [m/s]	α (°) for h=0.3m	Force, F_D [N]	Elastic/plastic	u [m/s]	α (°) for h=0.4m	Force, F_D [N]	Elastic/plastic
0.20	2.94	0.422	Elastic	0.20	7.44	0.680	Elastic
0.30	13.09	0.977	Elastic	0.30	18.36	1.420	Elastic
0.40	26.48	1.772	Plastic	0.40	30.6	2.350	Plastic
0.50	51.11	2.763	Plastic	0.50	45.98	2.842	Plastic
0.60	62	3.176	Plastic	0.60	59.93	2.983	Plastic
0.75	67.1	4.375	Plastic	0.75	66.35	3.565	Plastic
0.80	71.99	4.543	Plastic	0.80	67.98	4.333	Plastic
1.00	73.31	5.599	Plastic	1.00	72.38	5.123	Plastic

C2FF							
Emergent (h = 0.3 m)				Fully submerged (h = 0.4 m)			
u [m/s]	α (°) for h=0.3m	Force, F_D [N]	Elastic/plastic	u [m/s]	α (°) for h=0.4m	Force, F_D [N]	Elastic/plastic
0.20	3.43	0.421	Elastic	0.20	9.73	0.654	Elastic
0.30	14.36	0.982	Elastic	0.30	23.04	1.344	Elastic
0.40	33.4	1.761	Plastic	0.40	35.25	2.161	Plastic
0.50	46.6	2.489	Plastic	0.50	55.48	2.409	Plastic
0.60	67.74	2.528	Plastic	0.60	60.41	3.047	Plastic
0.75	72.04	3.801	Plastic	0.75	67.28	3.637	Plastic
0.80	73.77	3.961	Plastic	0.80	68.94	3.730	Plastic
1.00	79.1	4.859	Plastic	1.00	74.38	4.481	Plastic

C3FF							
Emergent (h = 0.3 m)				Fully submerged (h = 0.4 m)			
u [m/s]	α (°) for h=0.3m	Force, F_D [N]	Elastic/plastic	u [m/s]	α (°) for h=0.4m	Force, F_D [N]	Elastic/plastic
0.20	4.27	0.354	Elastic	0.20	10.59	0.645	Elastic
0.30	13	0.913	Elastic	0.30	20.66	1.387	Plastic
0.40	26.49	1.840	Plastic	0.40	30.17	2.317	Plastic
0.50	43.94	2.849	Plastic	0.50	48.09	2.576	Plastic
0.60	59.78	3.306	Plastic	0.60	58.53	3.018	Plastic
0.75	66.62	3.785	Plastic	0.75	68.13	3.617	Plastic
0.80	71.37	4.088	Plastic	0.80	69.96	3.779	Plastic
1.00	75.31	5.201	Plastic	1.00	73.73	4.625	Plastic

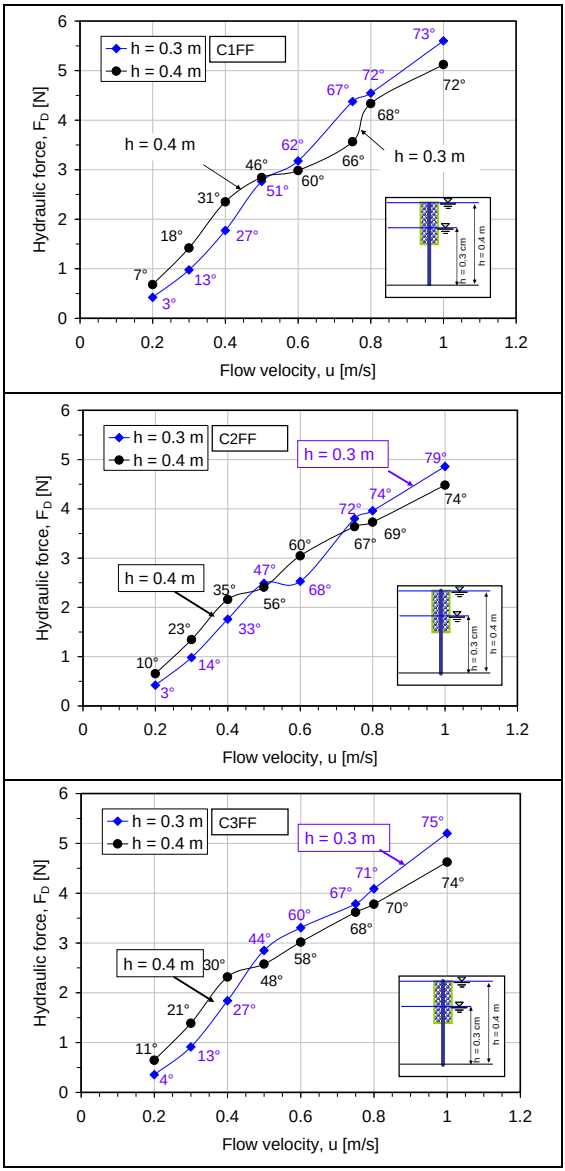

Fig. 3.34: Hydraulic force as a function of flow velocity and deflection angel of parameterised coastal pine models with flexible trunk

The relationship of hydraulic force and flow velocity is quadratic for flow velocity less than 0.5 m/s. Beyond that, the relationship is somewhat arbitrary but not quadratic anymore. Role of deflected angles to the measured forces are also observed though it is not completely as clear as for mangrove models such as the case of model C2FF. This inconsistency may result from too small measured forces that lead to sensitivity problems of the instrument because the force transducer is less precise for such small forces (below 5 N).

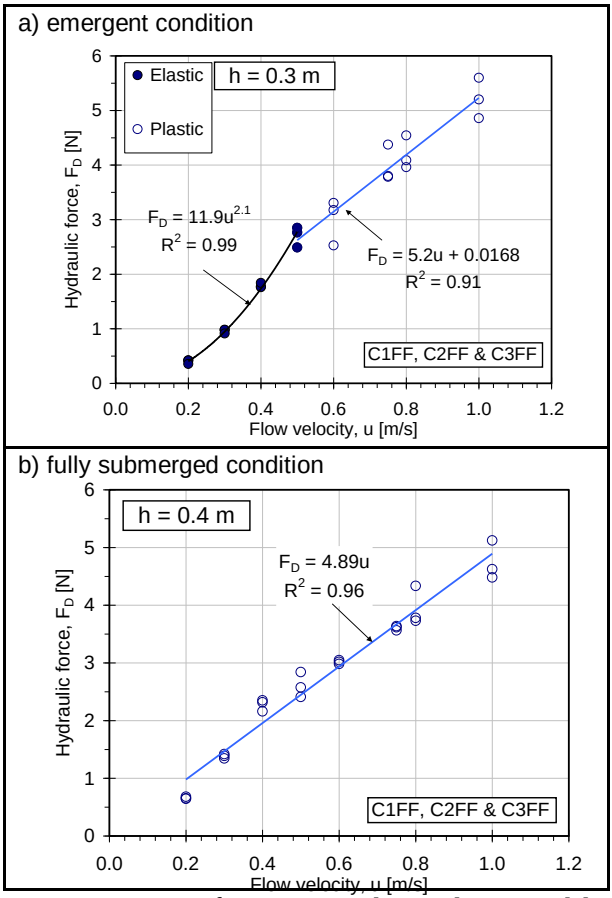

Fig. 3.35: Force measurement of parameterised coastal pine models with flexible trunk

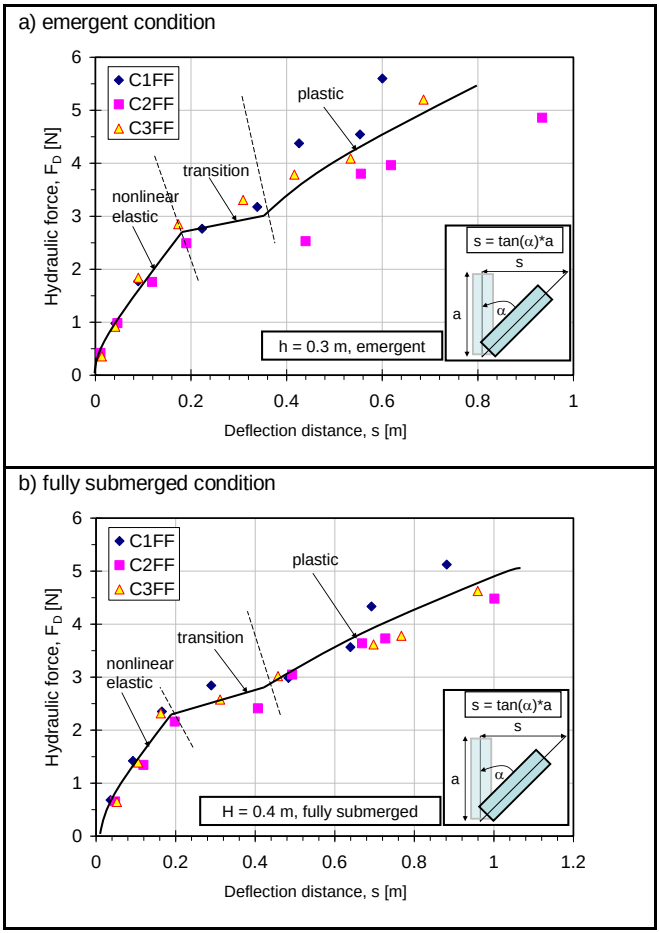

Fig. 3.36: Hydraulic force comparison between mangrove and coastal pine models

Fig. 3.34 shows the combined plot of hydraulic force as a function of flow velocity for all coastal pine models (C1FF, C2FF and C3FF). For emergent conditions, similar pattern as in mangrove models is also observed for coastal pine models where elastic behaviour of the trunk belongs to the quadratic part in the curves. Arbitrary behaviour is observed beyond the quadratic curve where flow velocity is beyond u = 0.5 m/s. For fully submerged conditions, linear pattern is observed

for all models (Fig. 3.34b). The effect of canopy density variation cannot be observed for coastal pine models. This problem may occur due to inability of the instrument to measure precise measurement for such small forces as already discussed previously. Moreover, similar frontal area for the canopy that has been adopted for all coastal pine models makes the observation of the measured forces even more difficult as already found in the test series I.

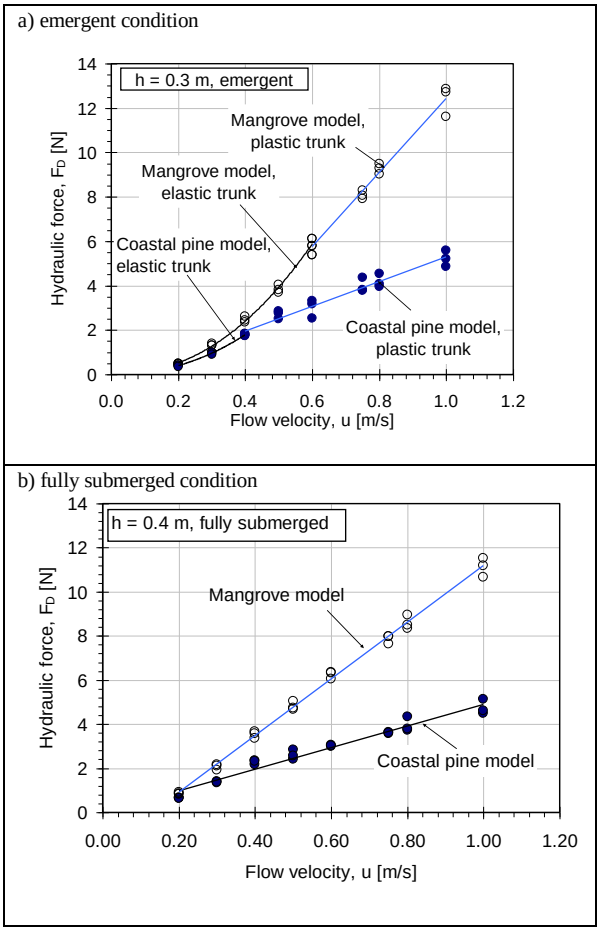

Fig. 3.37: Hydraulic force comparison between mangrove and coastal pine models

Coastal pine models have longer trunk and longer canopy compared to mangrove models. Therefore, coastal pine models are more flexible as subjected by similar flow velocity compared to mangrove models. Fig. 3.36 shows the division non-linear elastic, transition and plastic regions for coastal pine models based on the measurement of deflection angles. Nonlinear elastic behaviours are generally observed for both emergent and fully submerged conditions. The curves in Fig. 3.36 confirm the curve characteristics of hydraulic force as a function of flow velocity as shown in Fig. 3.35. Linear elastic is not observed because of the resulted larger strains for both emergent and fully submerged conditions.

The effect of changing canopy density cannot be observed for coastal pine models due to much smaller measured hydraulic forces for coastal pine compared to mangrove models. Fig. 3.37 shows clearly the hydraulic force comparison between the mangrove and the coastal pine models. The hydraulic force for mangrove models are far much larger compared to coastal pine models. Due to limitation capability on the instrument, the observation to distinguished hydraulic force variation for different canopy densities in coastal pine models becomes difficult.

3.3.8 Drag coefficient

Calculation tables for the derivation of the drag coefficients for both mangrove and coastal pine models using equations 3.6, 3.7 and 3.8 are shown in more details in Husrin and Oumeraci (2012i). Fig. 3.38a shows the plot of C_D as a function of R_e. For mangrove models, it clearly shows the variation of canopy density affects the derived C_D values. Model M1FF which has the highest canopy density shows higher C_D compared M2FF and M3FF which have smaller canopy density respectively. The effect of canopy variation however cannot be observed for coastal pine models (Fig. 3.38b). Model C3FF which has the highest canopy density in fact lies below C1FF which has smaller canopy density. This is a recurrence problem for coastal pine models because of much smaller measured hydraulic forces for all models.

The range of C_D for both mangrove and coastal pine models are almost identical from $C_D \sim 1.5$ until $C_D \sim 0.8$. However, R_e number for coastal pine models are much larger for coastal pine models. For mangrove models, C_D ranges from 1.6

– 0.8 with Reynolds number ranging from $5.3x10^4$ – $3.5x10^5$ while for coastal pine model, C_D ranges from 1.46 – 0.75 with Reynolds number ranging from $6.8x10^4$ – $7.7x10^5$. Both mangrove and coastal pine models have similar C_D-R_e pattern where C_D decreases as R_e increases. This pattern is in line with the previous laboratory experiment with stiff structure assumption (only roots and trunk).

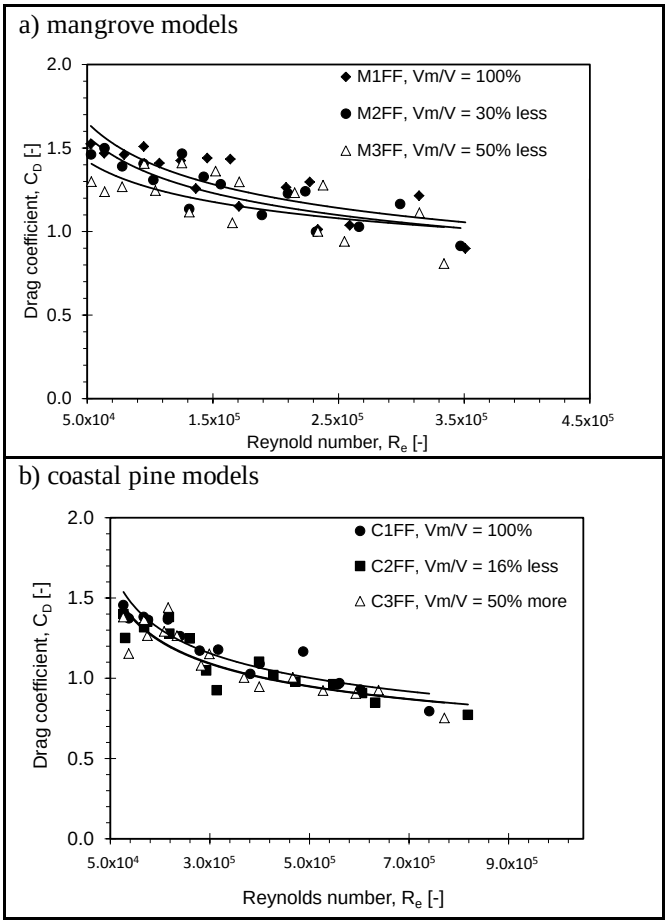

Fig. 3.38: Drag coefficients for mangrove and coastal pine models with flexible structure assumptions

In general, C_D values for mangrove models are larger than C_D values for coastal pine models (Fig. 3.39) due to the fact that mangrove models have larger submerged volume ratios as well as frontal areas. However, the C_D values from flexible structure assumption are much smaller compared to the C_D values from stiff structure assumption (only roots and trunk). The effect of submerged volume ratio obviously play important role to the derivation of C_D values. Fig. 3.40 shows the combine plot of C_D for both stiff and flexible structure assumptions. It shows that C_D from flexible structure assumption lie in the lower envelop of C_D from the stiff structure assumption.

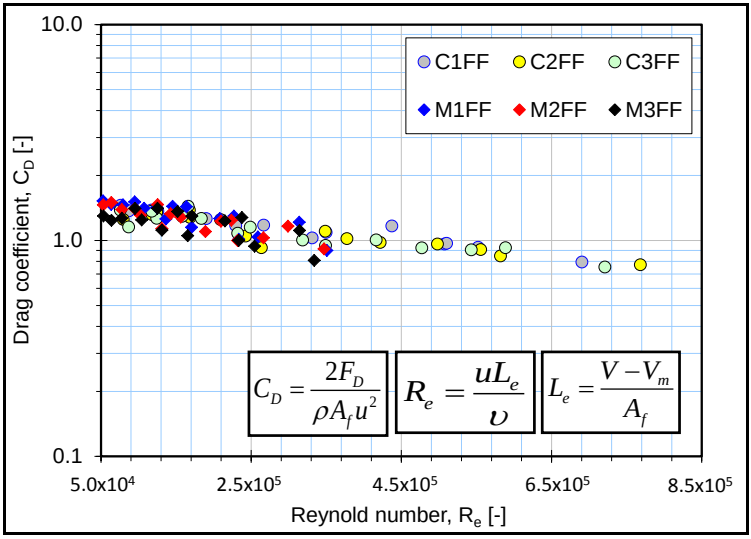

Fig. 3.39: Comparison of C_D between mangrove and coastal pine models

In stiff structure assumption, submerged volume ratio V_m/V ranges from 0.22 – 0.03 (Fig. 3.18) while V_m/V for both mangrove and costal pine with flexible structure assumption ranges from 0.029 until 0.009 (see Fig. 3.20). These figures shows that when water level reaches the canopy, the control volume (V) is much larger compared to the combined submerged volume of roots, trunk and canopy. Large differences on the submerged volume ratio between the stiff and flexible structure assumption is the sole aspect that causing big difference on the derived C_D.

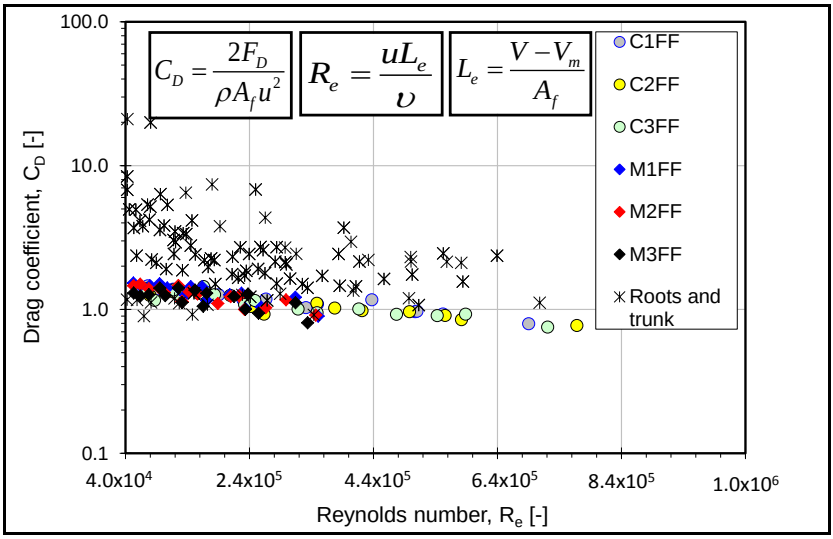

Fig. 3.40: Comparison of C_D between stiff structure assumption (roots and trunk only) and flexible structure assumption (entire tree)

Though, C_D values between stiff and flexible structure assumption are different as shown in Fig. 3.40. Both values are closely related if we plot them as a function of submerged volume ratio V_m/V as shown in Fig. 3.41. The derived C_D in flexible structure assumption is just a continuation from the stiff structure assumption towards smaller C_D values as well as smaller V_m/V. This pattern seems to be consistent as well with the previously reported C_D values by Harada and Imamura (2000) which lies in the lower envelope of the current study (Eq. 3.9).

Eq. 3.9 is plotted and compared to the current study (Fig. 3.41). The C_D curve from Harada and Imamura (2000) almost represent the lower envelope for the data of the current study for both stiff and flexible structure assumptions. This result is very important since the equation developed by Harada and Imamura (2000) has never been extrapolated for $V_m/V > 0.08$ and unable to explain the possibility of having larger C_D as reported by many previous studies (e.g. Struve *et al.*, (2003) and Mazda *et al.* (1997a)). The work of Imai and Matsutomi (2005) for coastal pine model showed C_D fluctuation in the range of 0.9 – 1.5.

However, the study did not revealed any conclusive dependency of C_D to any flow regimes. The benefit of the current study is a wider range of drag coefficient C_D to the flow regime and the inclusion of frontal area A_f together with submerged volume ratio V_m/V as the most influencing aspects.

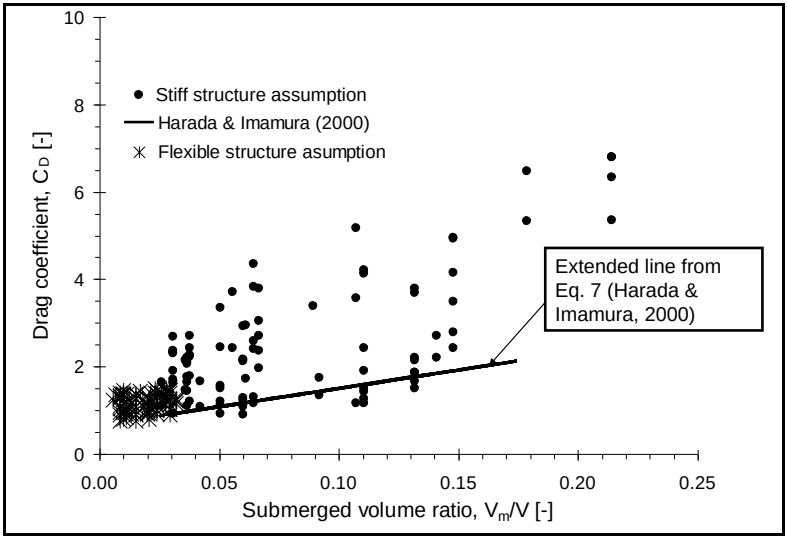

Fig. 3.41: C_D as a function of submerged volume ratio for both stiff and flexible structure assumptions

The field of forestry has conducted lots of laboratory and field measurement for forest management, i.e. shelterbelts purposes for large trees which are appropriate for the current study. The obtained C_D in the current study is also in agreement with the C_D obtained from this field. Most of the derived C_D values from big tree are reported based on the measurement either in the wind tunnel or directly in the field. Ishikawa *et al*. (2006) reported C_D values for real living trees of conifer range from 0.6 – 1.3 (Fig. 3.42). Lower value of C_D belong to conifer#1 which is 30% taller compared to conifer#2 which has C_D almost constant C_D = 1. This happens because taller trees experiences much larger deflections compared a shorter one after certain flow velocity. Consequently, the drag force from the taller tree will decrease as also observed in the current study between mangrove and coastal pine models.

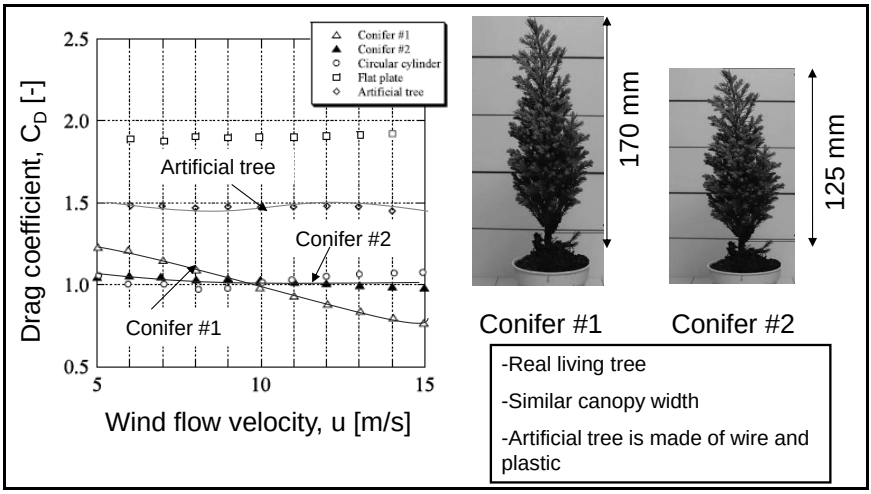

Fig. 3.42: C_D from living trees of conifers (Ishikawa *et al.*, 2006)

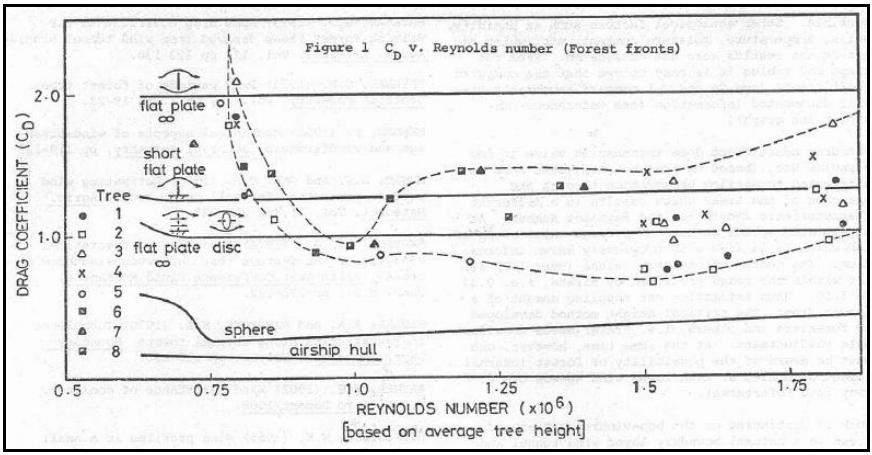

Fig. 3.43: C_D for the trees at the front forest (Papesch, 1977)

Comparable results as in the current study are also found in field measurement of C_D for the trees at the front of the forest (Fig. 3.43). Papesch (1977) measured directly the forces acting on individual trees, frontal area and averaged wind speed for the trees located at the front of the forest. The analysis shows that C_D

ranges from 0.8 – 2.2 with averaged C_D = 1.28. Different definition on R_e in Papesch (1977) resulted on different range of R_e from the current study.

Latest field measurement for conifer trees presented by Grant and Nickling (1998) provide range of C_D as a function of R_e and canopy density/porosity (Fig. 3.14). The range of C_D is almost identical and the effect of canopy density is also equivalent as for the case of mangrove models where the lowest density model provides smaller C_D (Fig. 3.14a).

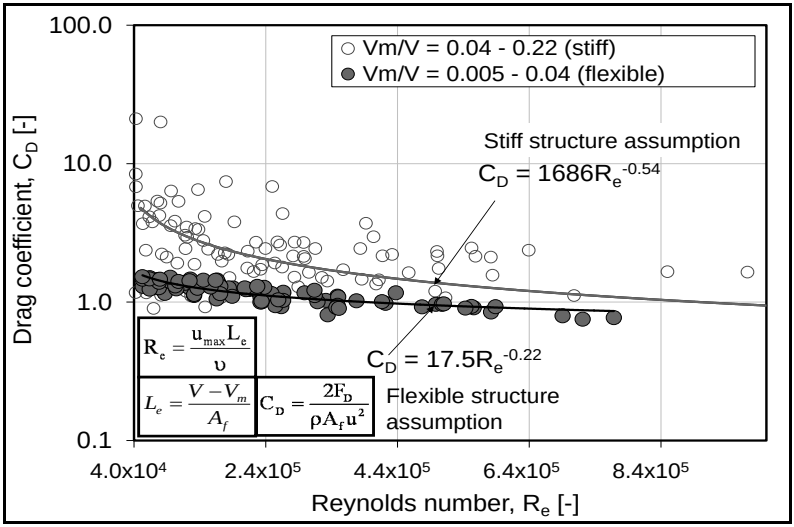

Fig. 3.44: C_D variation with both stiff and flexible structure assumptions

To be concluded, based on the analysis of both stiff and flexible structure assumptions, the relationship of C_D as a function of R_e can be drawn as a function of both Reynolds number and submerged volume ratio is shown in Fig. 3.44.

For flexible structure assumption where the submerged volume ratio is much smaller (V_m/V = 0.005-0.04), relationship of C_D to R_e is:

$$C_D = \frac{17.5}{R_e^{0.22}} \qquad (3.15)$$

where:

$$R_e = \frac{uL_e}{\upsilon} \text{ and } L_e = \frac{V - V_m}{A_f}$$

V : control volume [m^3]
V_m : root volume [m^3]
L_e : effective length [m]
u : averaged flow velocity [m/s]
ν : kinematic viscosity of water ($\nu = 1.004 \times 10^{-6}$ m^2/s for water temperature = 20 ^oC)
A_f : frontal area [m^2]

The C_D as a function of R_e as shown in Fig. 3.44 explain thoroughly the confusion on how and when should these C_D values be implemented for the assessment of tsunami / storm wave attenuation by coastal forests. Wide range of C_D values has been previously reported without assessing accurately the physical bases behind them, particularly on how to parameterize the tree (see for example Mazda *et al*., 1997a, Imai and Matsutomi, 2006; Kongko, 2004; Harada and Imamura, 2000; Struve *et al*., 2003; Latief and Hadi, 2006). The C_D values obtained in the current study can describe why the use of cylinders is suitable to model mangrove forests to describe the attenuation of tsunami because it is found that C_D may reach 1 for certain conditions (small V_m/V values) which is equivalent to the value of C_D for a cylinder. However, C_D also may have much larger values due to much larger V_m/V, which is mostly belong to the condition where the water elevation or tsunami height is within the root system. Therefore, ones should carefully check the selection of C_D values for the estimation of tsunami attenuation by coastal forest, for example to be used in numerical simulation which is normally conducted by trial and error process. With the results from the current study, the selection of C_D values for coastal forest now has clearer guidance based on reliable physical bases.

3.3.9 Remarks on the parameterisation with flexible structure assumption

Parameterisation with flexible structure assumption is an ultimate process of parameterisation because the entire tree components (roots, trunk and canopy) as

well as stiff structure assumption are involved. Remarks and conclusion for the parameterisation of coastal forest vegetation with flexible structure assumption are as follows:

- The use of materials such as PTFE for flexible trunk and fibrous material for the canopy has allowed us to successfully determine the parameterised models for mangrove and coastal pine trees based on similar hydraulic characteristics as the "real" tree model through series of model tests. The limitation of this parameterised model is its inability to break due to high density of PTFE. However, the measured hydraulic forces still show indications of breakage limits through the characteristics of elastic, transition, and plastic behaviours of the trunk. The results from the elastic behaviour of the trunk mostly represent the prototype conditions while for the transitions and plastic behaviours, the trunk mostly will break.

- The frontal area (A_f) has been found to be much more influential than the submerged volume ratio (V_m/V) to the hydraulic force. This phenomenon can be physically described by the fact that as the water level rising (reaching the canopy or beyond), the frontal area increases whereas the submerged volume ratio decreases.

- The derived hydraulic resistance in term of drag coefficient (C_D) regardless the variation of canopy density and water level changes, converges towards C_D=1.0. This indicates that smaller submerged volume ratio (due to the increase of water levels) lead to the decrease of hydraulic resistance. The frontal area variation contributes significantly to the measured hydraulic forces as well as the hydraulic resistance though the variation is relatively small. This finding may explain why many numerical simulations prefer to put C_D = 1 (or even smaller) to describe tsunami attenuation by coastal forest vegetation (e.g. Imai and Matsutomi (2005), Dekker (2006), Teo (2008), Thuy *et al.* (2009) and Huang *et al.* (2011)).

4 Wave flume experiments with mangrove forests

4.1 Testing programme and experimental setup

The experiments conducted in the Twin Wave Flume (TWF) of Leichtweiss Institute (LWI), TU Braunschweig are intended to study both global and local processes. The TWF (2-m and 1-m wide, 90 m long, and 1.20 m deep) is equipped with two wave paddles that can be operated simultaneously or independently to generate regular/irregular waves and solitary waves (Fig. 4.1). These experiments were performed in the framework of the DFG-TAPFOR project in close collaboration with other co-workers. The contributions of co-workers are related to the analyses of solitary wave attenuation and thus the references are provided. Regular/irregular waves, solitary waves and tsunami bores were included in the DFG-TAPFOR project. Tsunami bores are exluded from the PhD topic and the details on this topic can be found in Oumearci *et al*. (2011).

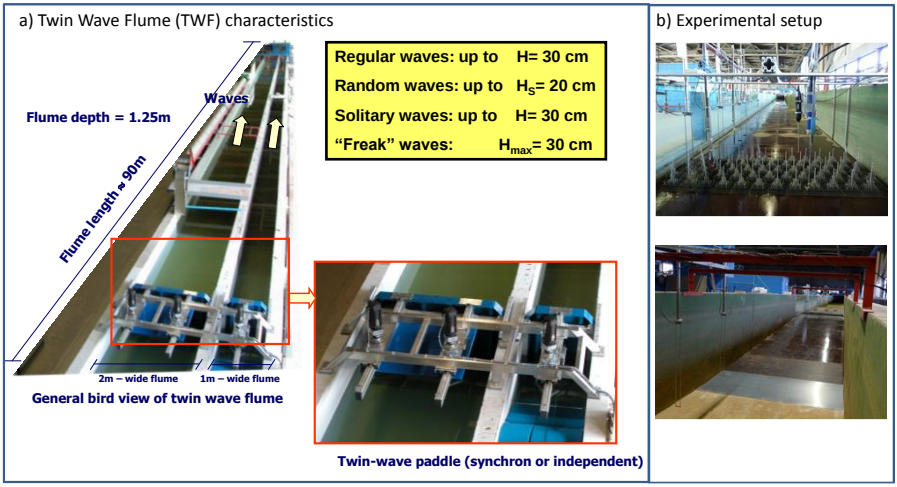

Fig. 4.1: The Twin Wave Flume and overview of the experimental setup

Table 4.1: Testing programme for regular/irregular and solitary waves in the TWF (model scale, 1:25)

Wave types	Model values				Prototype values				Wave steepness, H/L(-)
	Water depth in front of the slope, h (m)	Forest width, B (m)	Incident wave height, H_m or H_{m0} (m)	Wave period, T or T_p(s)	Water depth in front of the slope, h (m)	Forest width, B (m)	Incident wave height, H_m or H_{m0} (m)	Wave period, T or T_p(s)	
Regular & Irregular Waves	0.465 0.515 0.565 0.615	0.75 1.50 2.25 3.00	0.04	0.7	11.625 12.875 14.125 15.375	18.75 37.50 56.25 75.00	1	3.5	0.052
				0.9				4.5	0.032
				1.1				5.5	0.021
			0.08	1			2	5.0	0.051
				1.2				6.0	0.036
				1.4				7.0	0.026
				1.6				8.0	0.020
			0.12	1.2			3	6.0	0.053
				1.4				7.0	0.039
				1.6				8.0	0.030
				1.8				9.0	0.024
			0.16	1.4			4	7.0	0.052
				1.6				8.0	0.040
				1.8				9.0	0.032
				2.0				10.0	0.026
				2.2				11.0	0.021
			0.20	1.5			5	7.5	0.057
				1.7				8.5	0.044
				1.9				9.5	0.035
				2.1				10.5	0.029
				2.3				11.5	0.024
				2.5				12.5	0.020
Soitary waves			0.04 0.08 0.12 0.16 0.20	-			1 2 3 4 5	-	-

The main objective of these tests is to improve the knowledge of both global and local processes associated with the wave-forest interaction. The investigations of the global processes are focused on the derivation of functional relationships between the hydraulic performance (wave reflection, wave transmission and energy dissipation) and the main forest parameter (i.e. forest width). For the local processes the focus is put on the determination of the hydraulic losses induced by single trees and the entire forest based on the measurement of the flow together with the measurement of the flow-induced forces on a single tree and the entire forest. For this purpose, force transducers for the entire forest model (FT) and for a single tree in different group configurations (FTS) were installed. The details on the development of this new measuring technique using force transducer for singel tree model (FT) and for entire forest model (FTS) can be found in Oumeraci *et al.* (2011).

For wave flume experiments, only mangrove models with stiff structure assumption were tested in the frame of this PhD study (Fig. 4.2). Regular and irregular waves were implemented to reproduce storm wave conditions, while solitary waves were generated for tsunami-like waves. The forest models consist of individual mangrove forest models in staggered configuration with four forest widths, B (B = 0.75, 1.5, 2.25 and 3.0 m). The water depth was varied in such way that the effect of the submerged volume ratio V_m/V on the wave attenuation can also be obtained. Since the attenuation performance is very sensitive to the wave periods, the full range of possible periods of regular and irregular waves, including a variation of the wave height, has been considered.

All wave conditions including wave decay and propagation through the forest were measured by wave gauges installed in front, along and behind the forest model. Current meters (ADV) and pressure transducers (PT) were also deployed along the forest model to capture the detailed processes associated with fluid-tree interaction. Table 4.1 shows the testing programme for both regular/irregular waves and solitary waves.

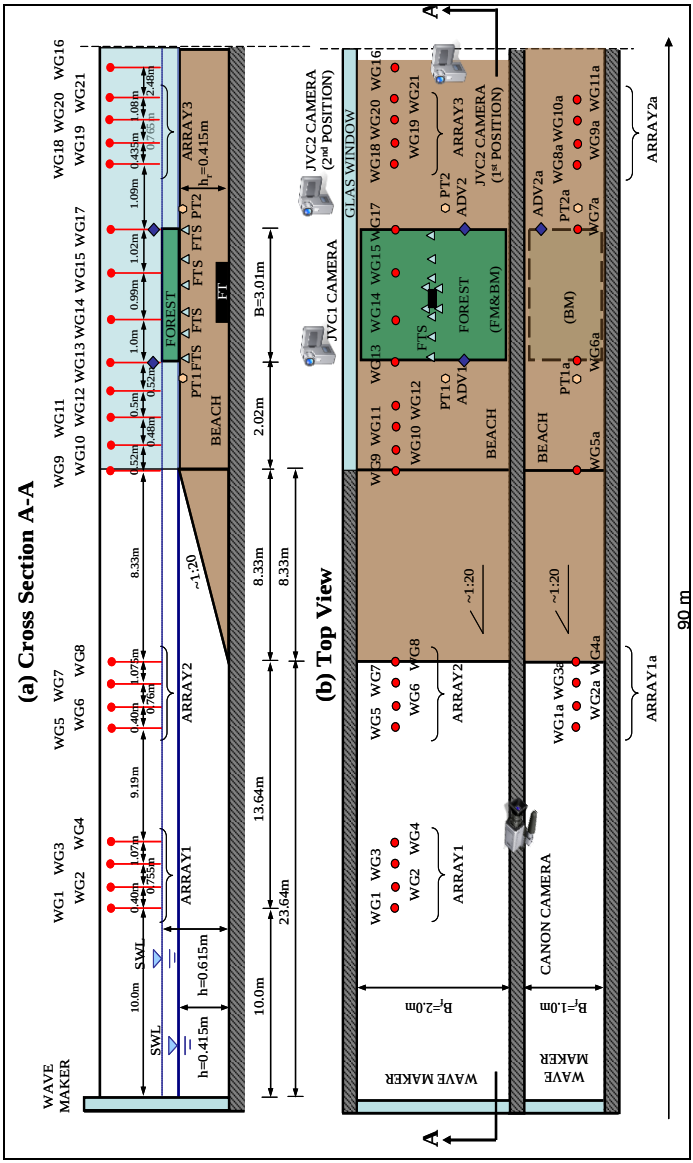

Fig. 4.2: Experimental set-up in the Twin Wave Flume of Leichtweiss Institute (LWI), exemplarily for forest width B = 3.0 m

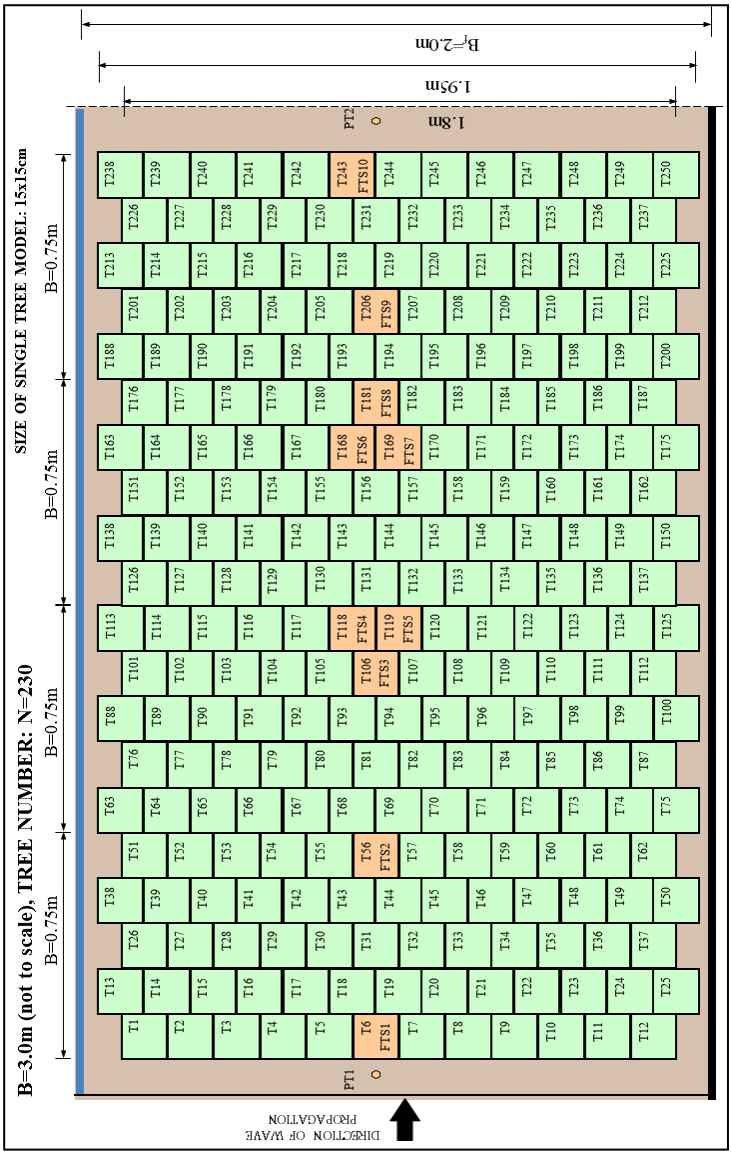

Fig. 4.3: Arrangement of force transducers for individual tree model, exemplarily for forest width B = 3.0 m

The force transducers for single tree model (FTS) were arranged for selected individual tree models within the forest model as shown exemplarily in Fig. 4.3, for forest width B = 3 m. The force transducers are located below the base of mangrove tree model with sufficient spaces around it allowing the transducer to measure fluid-induced forces on the model.

4.2 Analysis of regular and irregular wave tests

4.2.1 Characteristics of regular and irregular waves

Regular and irregular waves were generated in the flume to cover the common range of wave steepness H/L= 0.02 -0.06. The characteristics of wave propagation along the shore platform and through the forest model are the main concern in the analyses. Therefore, the following four regions are considered throughout the analyses (Fig. 4.4 and Fig. 4.5):

- *Region 1 (foreshore slope):* region where most of incident waves break. Therefore, this region is divided into 5 different sections.
- *Region 2 (flat shore):* flat region in front of the forest model
- *Region 3 (forest):* region of forest model varies for four different forest widths.
- *Region 4 (behind the forest*): region of wave transmission due to the presence of the forest model.

The characteristics of the generated regular waves (wave height H and wave length L) in the wave flume are as follows: $H_{i,nom}$ = 0.04 – 0.2 m and wave period T = 0.7 - 2.5 s corresponding to H = 1 – 5 m and T = 3.5 – 12.5 s in the prototype. Based on the measured signals by the individual wave gauge and wave gauge arrays, the regular waves in deeper water were sinusoidal (measured by wave gauge arrays 1 and 2, see Fig. 4.2 and Fig. 4.4). When the waves reach the shore platform, they were amplified by shoaling processes and the shape of the waves slightly changes. The trough becomes flatter and the crest is steeper. Some of the waves broke along the slopes (Region 1) and some of them broke along the flat shore just in front of the forest model (Region 2). In few cases, non-breaking waves were observed mainly for the conditions where the water level was at the highest one (h = 0.615 m).

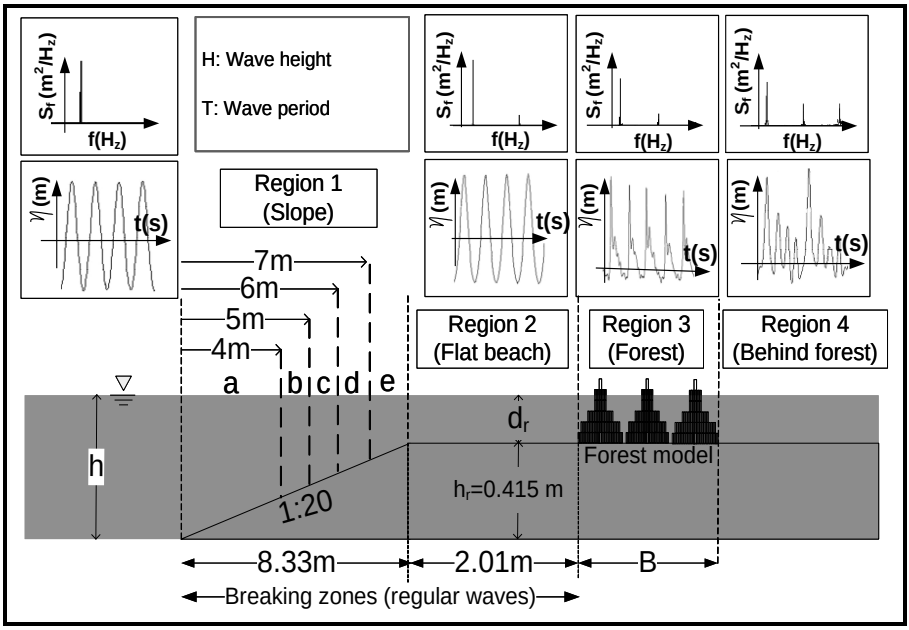

Fig. 4.4: Characteristics of regular waves for different regions in the time domain and frequency domain.

Inside the forest, regular patterns of the measured waves were still observed. However, higher frequency signals were also observed due to wave-forest interaction and turbulent flow. Similarly, the measured waves behind the forest become more irregular, including higher frequency waves (Fig. 4.4). The irregular waves (significant wave height H_{m0} and peak wave period T_p) in the wave flume were generated based on JONSWAP wave spectrum (Holthuijsen, 2007). The variation of wave period T_p and water depth h were similar as for the regular waves. Breaking wave locations varied over a wider range than for regular wave cases. For irregular waves, the waves started to break from the shore slope until behind the forest model (from region 1 until region 4). For each single test, the breaking locations were more or less covering these four regions with different occurrence frequency for each region depending on the given water depth h. However, dominant breaking waves occurred along the foreshore slope.

Similar to the case of regular waves, the propagated waves through the forest model experienced turbulent flows and wave components with higher frequencies (higher harmonics). These processes were observed throughout the experiments as clearly shown from the measured signal with frequency domain. The wave energy decreases as the frequency bands are wider for the measured waves inside the forest and behind the forest model (regions 3 and 4) (Fig. 4.5).

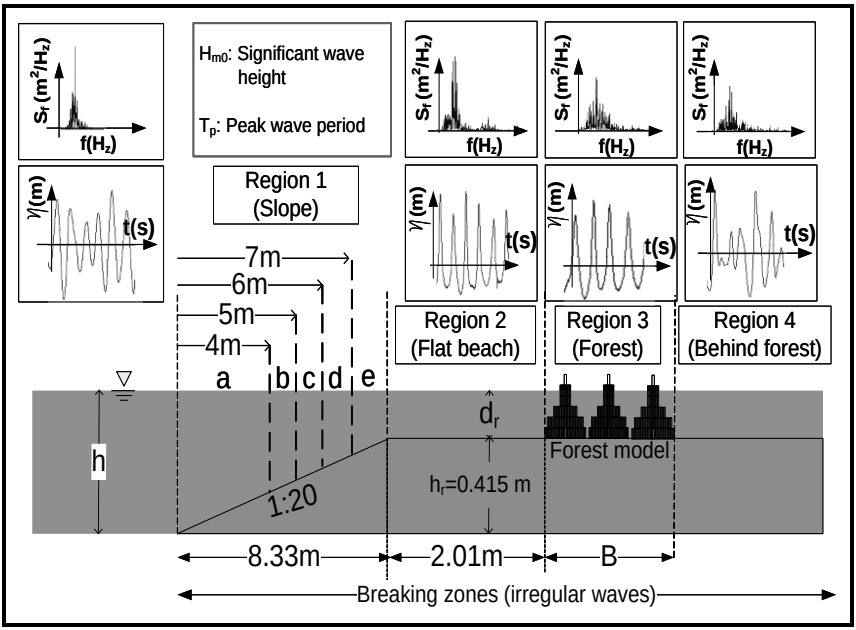

Fig. 4.5: Characteristics of irregular waves for different regions in the time domain and frequency domain.

4.2.2 Wave analysis and hydraulic performance of tested mangrove forests

The wave reflection (as well as wave transmission) occurs when there is an abrupt change in depths or channel widths. Reflection analysis is mostly performed in order to determine the incident wave conditions in front of the structure. The reflection coefficient is not further used for the interpretation of the hydraulic

processes at the structure or behind it. The analysis of the reflection coefficient (K_r), transmission coefficient (K_t), dissipation coefficient (K_d) and the effects of different variables (dimensional and non-dimensional) is required to develop an efficient model for the hydraulic performance.

Although the processes in the far field and the associated hydraulic performance are clearly the results of the local processes occurring directly at the constitutive obstacles, a global approach (far field) based on the energy conservation relationship has first been adopted before analyzing the local processes (near field):

$$E_d = E_i - E_t - E_r \tag{4.1}$$

$$\text{with } E_W = \frac{1}{8}\rho g H^2 \tag{4.2}$$

where:

E_i : incident wave energy [J/m^2]
E_r : reflected wave energy [J/m^2]
E_t : transmitted wave energy [J/m^2]
E_d : dissipated wave energy [J/m^2]
ρ : water density [kg/m^3]
g : gravity acceleration [m/s^2]
H : wave height of either incident, reflected or transmitted waves [m]
E_w : wave energy of either incident, reflected or transmitted waves [J/m^2]

The incident, the reflected and the transmitted wave energy (E_i, E_r, E_t) components are determined from the analysis of the associated wave height by using Eq. (4.2). The dissipated wave energy (E_d) is then calculated according to Eq. (4.1). By defining the reflection, transmission and dissipation coefficient as:

$$K_t = \sqrt{\frac{E_t}{Ei}},\ K_R = \sqrt{\frac{E_r}{E_i}},\ K_d = \sqrt{\frac{E_d}{E_i}} \tag{4.3}$$

The energy conservation relationship (Eq. (4.1)) can be rewritten in terms of energy coefficient as:

$$K_r^2 + K_t^2 + K_d^2 = 1 \tag{4.4}$$

The unknown dissipation coefficient (K_d) follows from Eqs. (4.1) - (4.4) as

$$K_d = \sqrt{1-(K_t^2 + K_r^2)} \tag{4.5}$$

where:

K_d : dissipated wave energy coefficient [-]
K_r : reflected wave coefficient [-]
K_t : transmitted wave coefficient [-]

By inserting equation Eq. (4.2) into Eq. (4.3), the energy terms for wave transformation coefficient calculations can be simply replaced by the wave height (H). Therefore, Eq. (4.3) can be rewritten:

$$K_t = \frac{H_t}{H_i},\ K_r = \frac{H_r}{H_i},\ K_d = \frac{H_d}{H_i} \tag{4.6}$$

where:

H_t : transmitted wave height [m]
H_r : reflected wave height [m]
H_d : "dissipated" wave height [m]
H_i : incident wave height [m]

The measured waves (regular and irregular waves) inside the flume are the result of the superposition of both incident and reflected waves due to the presence of shore platform and the forest model. In order to distinguish between the incident and the reflected waves, the methodology proposed by Mansard and Funke (1980) has been implemented. Wave gauge arrays 2 and 3 in the two-meter wide flume and wave gauge arrays 2a and 3a in the one-meter wide flume were analysed for the reflection analyses (see Fig. 4.2). The calculation processes were carried out using L-Davis data analysis tools (Kudella, 2009).

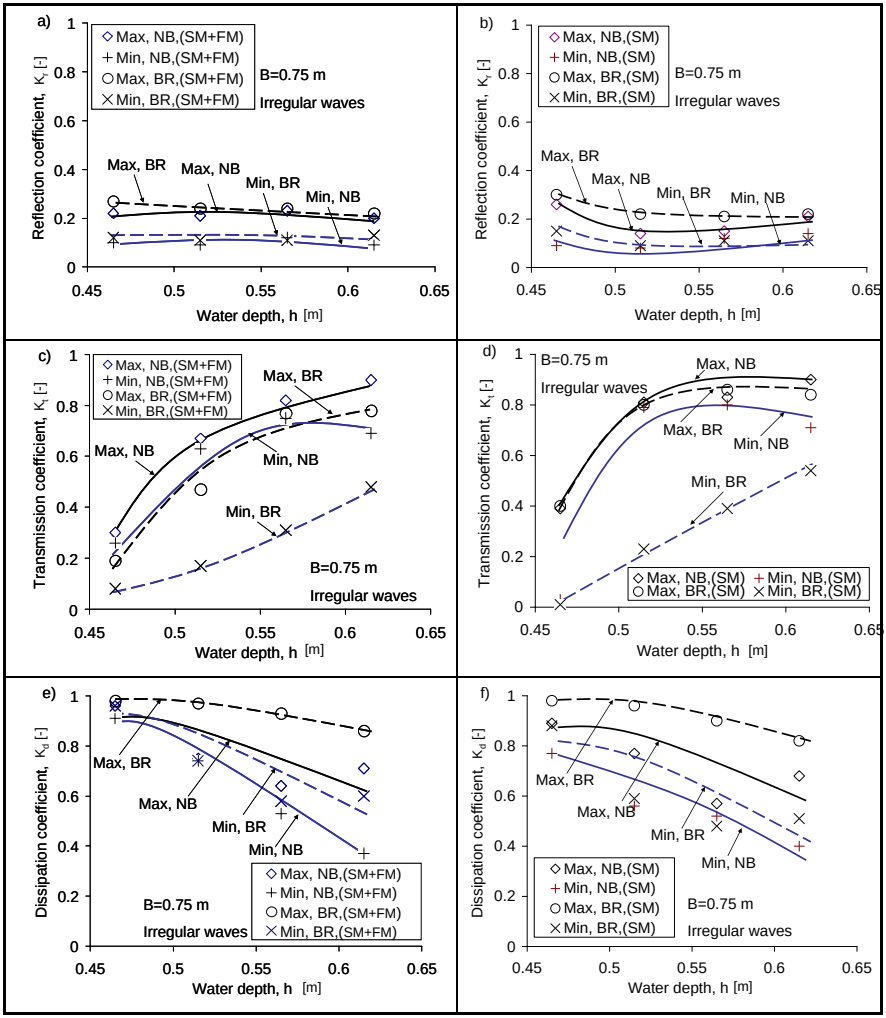

Fig. 4.6: Results of statistical analysis for K_r, K_t, and K_d for irregular waves and forest width B = 0.75 m. (FM: forest model only, SM: shore model only and SM+FM: shore and forest model, BR: breaking wave conditions, NB: non-breaking wave conditions)

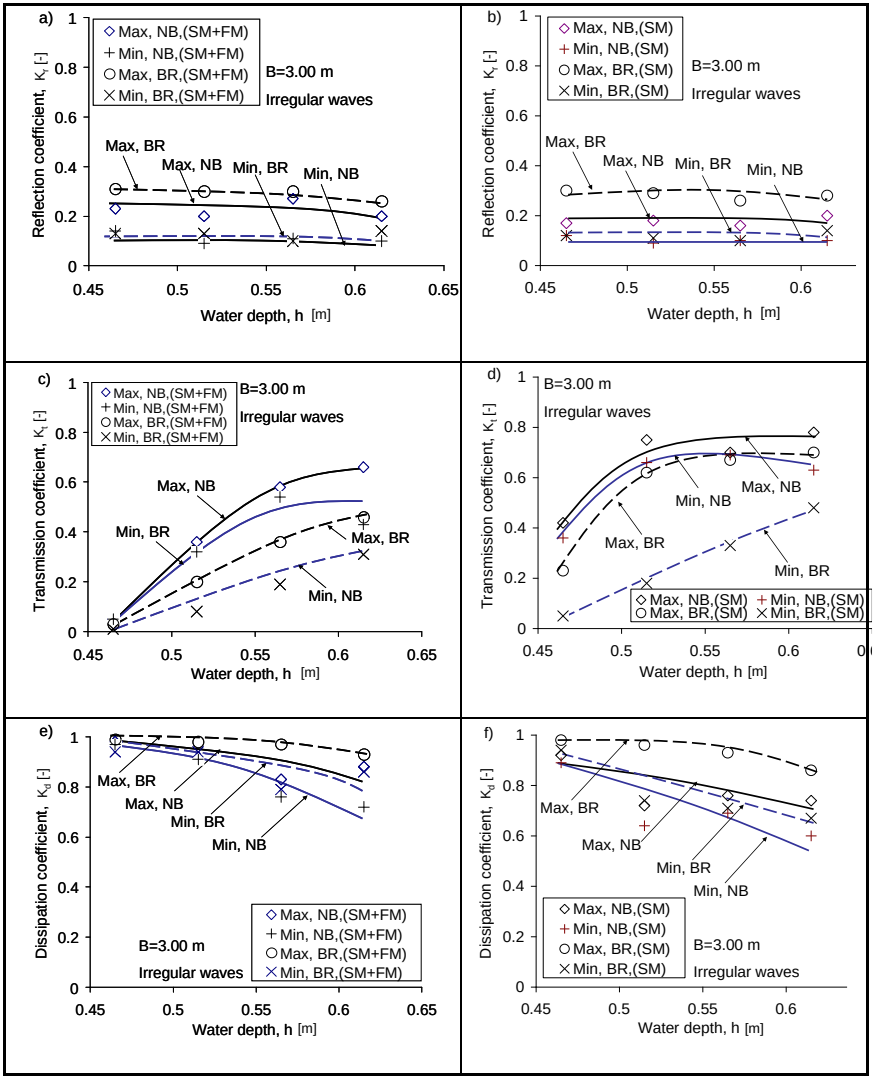

Fig. 4.7: Results of statistical analysis for Kr, K_t, and K_d (irregular waves, B = 3.00 m). (FM: forest model only, SM: shore model only and SM+FM: shore and forest model, BR: breaking wave conditions, NB: non-breaking wave conditions)

The following figures (Fig. 4.6 and Fig. 4.7) present the statistical results of reflection, transmission and dissipation coefficients for the minimum and the maximum forest widths B = 0.75 m and B = 3.0 m (figures for other forest widths can be found in Husrin *et al.*, (2010)). The figures are divided into breaking and non-breaking wave conditions (irregular waves) and for different water depths h. The influence of forest model (FM), shore model platform (SM) and combination of both (SM+FM) are also described. The quantitative analysis is based on maximum (Max) and minimum (Min) calculated values.

The reflection coefficients, K_r are generally almost constant for all cases (different forest widths, water depths, breaking and non-breaking conditions, regular and irregular waves) for both shore models with forest (SM+FM) and without forest (SM). Non-breaking wave conditions (NB) give slightly smaller reflection as compared to the breaking wave conditions (BR). For instance, in the case of wave reflection due to both forest model and shore model (SM+FM) the reflection coefficients are 13% higher for breaking wave conditions as compared to non-breaking waves (Fig. 4.7a). This occurs because non-breaking waves belong to larger water depths allowing more wave energy to be transmitted over the shore platform. For shallower water depths, the fore slope reflects a relatively larger portion of the incident waves. Nearly-constant values of K_r in all cases are due to the fact that the frontal areas of different forest width B from the forest model are always similar. Forest widths (B) and water depths (h) largely affect on transmission coefficient, K_t. The values of K_t vary greatly from the shallower water depths h = 0.465 m to the larger depths h = 0.615 m. The K_t values for non-breaking conditions are always higher than breaking conditions. For example, for the case of irregular waves (shore model with forest, non-breaking condition, h = 0.465 m), K_t = 0.30 for B = 0.75 m (Fig. 4.6c) and K_t = 0.07 for B = 3.0 m (Fig. 4.7c), K_t reduces by 76%. Similarly, the increase of water depth can increase the transmission coefficient by 88% (Irregular waves, Non-breaking, B = 3.0 m) (Fig. 4.7c).

The role of the shore topography and the forest can clearly observed from the dissipation coefficients (K_d). K_d as a function of K_t and K_r (see Eq. 4.5) shows higher values for smaller water depth due to the fact that in these conditions K_r and K_t are small. As reflection coefficients remain nearly constant for different

water depth, the transmission coefficients and breaking wave conditions become the main factors affecting the dissipation coefficients, K_d. K_d values decrease as K_t values increase. It is also clear from Fig. 4.7e and Fig. 4.7f that the contribution of the shore topography to energy dissipation is substantial as compared to that of the forest.

4.2 3 Wave reflection

The analysis of the reflection coefficient (K_r), is examined both graphically and statistically. The analysis of the reflection coefficient for four different forest widths (B) and water depths (h) is treated first in the following. The effects of water depth are shown in Fig. 4.8 (regular case and irregular cases). K_r is plotted versus B/L (B: forest width, L: generated wave length measured in front of the slope) for different water depths. The figures show that for a given value of forest width, the measured reflection coefficient slightly increases with decreasing water depth. This is in agreement with the results found by Rathbun *et al*. (1998), Melito and Melby (2002) and Muttray *et al*. (2006) for the cases of breakwaters. However, the effect of forest width (B) on wave reflection is almost negligible for relative forest widths (B/L > 1.0) as shown exemplarily in Fig. 4.8 for regular wave tests. This is due to the fact that the forest models have a similar frontal area which seems to govern the reflection performance and that the effect of wave-wave interaction inside the forest is negligibly small for larger B/L values. This is in line with the results of wave absorbers (Oumeraci & Koether, 2009).

Furthermore, though it can be seen from Fig. 4.8 that the waves are slightly reflected from shore, but from statistical analysis, the effect of forest on wave reflection is found to be almost negligible. It should be noted that in these cases, the forest that consist of only the bottom part of the tree does not contribute noticeably to wave reflection. So far, studies on wave reflection only due to forest are not available in the literatures. The available references (e.g. Harada *et al.*, (2000) and Istiyanto *et al.,* (2003)) do not explicitly mention reflections due to the forest. Instead, they showed reflections as a combination of both forest and shore platform.

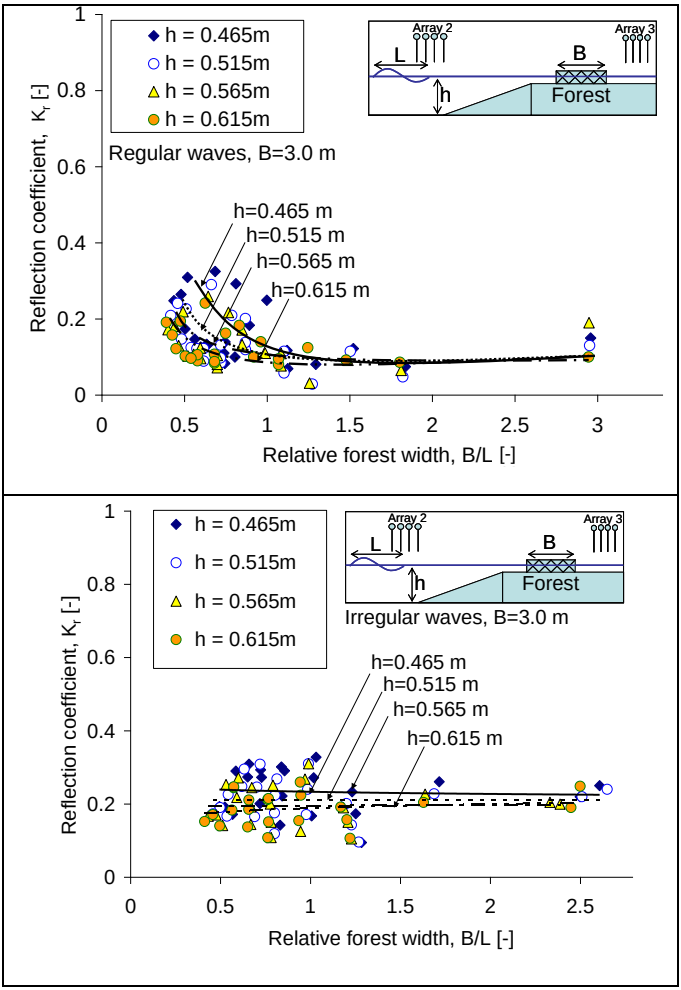

Fig. 4.8: Reflection coefficients (K_r) for B = 3 m and different water depths (h) as a function of relative forest width (B/L) for regular and irregular waves

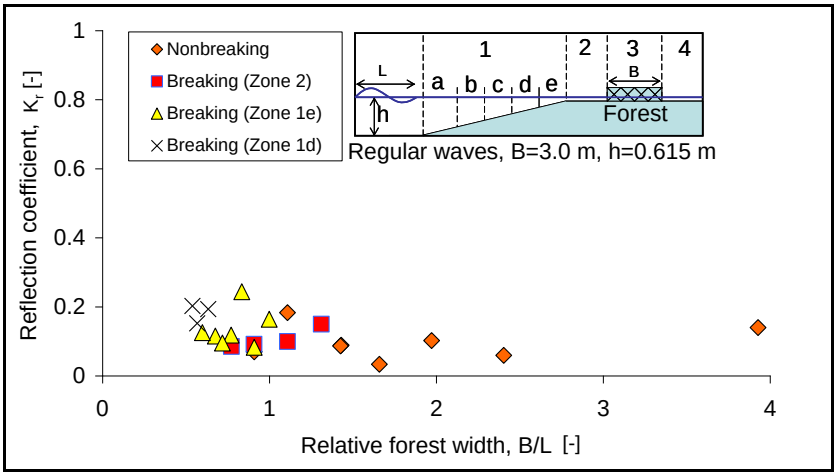

Fig. 4.9**:** Reflection coefficients (K_r) for B = 3.0 m and h = 0.615 m as a function of relative forest width (B/L) for regular waves

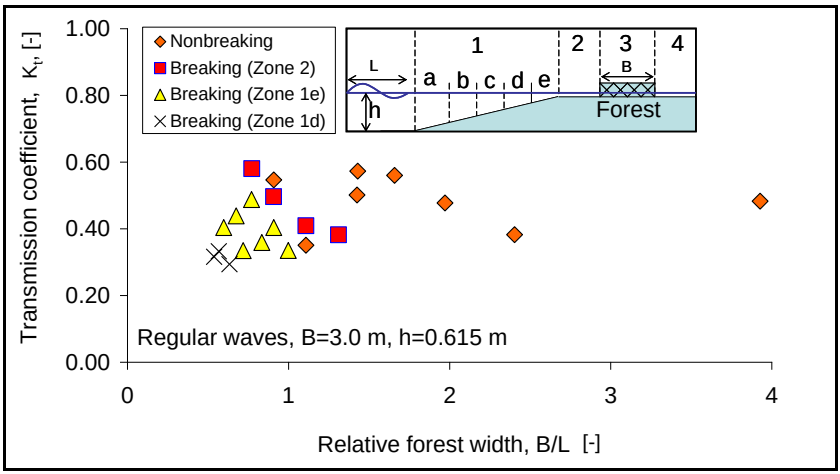

Fig. 4.10: Transmission coefficients (K_t) for B = 3.0 m and h = 0.615 m as a function of relative forest width (B/L) for regular waves

Wave reflection is also affected by the location of breaking wave along the shore platform (Fig. 4.9). The K_r values increases with the increasing distances between forest and breaking location. That is, wave reflection decreases with the increasing of horizontal distance from the shore initiating position. For non-breaking wave conditions, K_r generally tends to be smaller compared to breaking wave conditions. This is rather surprising result due to the fact that most wave energy for non-breaking conditions is transmitted (Fig. 4.10).

4.2.3 Wave transmission

The transmission coefficient is calculated as the ratio of the transmitted wave height to the incident wave height (see Eq. 4.6). The analysis of wave transmission was performed in the frequency domain for not only irregular waves, but also for regular waves behind the forest. In regular waves, the shallow water depth and the effect from forest obstruction cause a change in wave characteristics within and behind the forest model as shown clearly by the shape of wave energy spectra compared to those in deep water and in front of the forest (Fig. 4.4). In this situation, the transmitted wave height behind the forest was measured based on frequency domain (H_{m0}) for different forest widths (B). Therefore, the transmission coefficient (K_t) is calculated using the following equations:

- For regular waves

$$K_t = \frac{H_{m0,t}}{H_{m,i}} \tag{4.7}$$

- For irregular waves

$$K_t = \frac{H_{m0,t}}{H_{m0,i}} \tag{4.8}$$

Where:

$H_{m0,t}$: transmitted significant wave height measured behind the forest [m]
$H_{m0,i}$: incident significant wave height measured in front of the forest [m]
$H_{m,i}$: incident mean wave height measured in front of the forest [m]

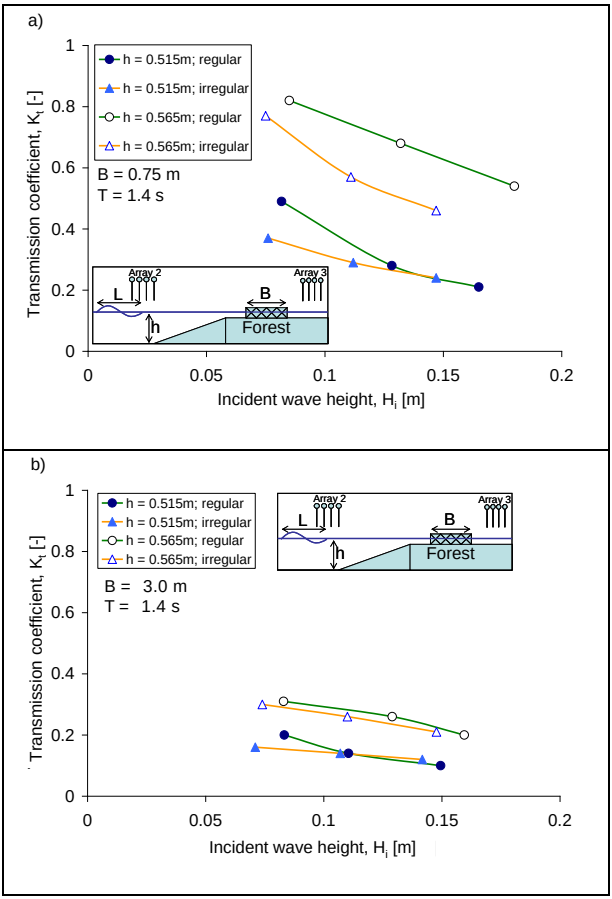

Fig. 4.11: Transmission coefficients (K_t) against incident wave height (H_i) for different water depth h: (a) B = 0.75 m and (b) B = 3.00 m.

We compared the wave transmission coefficients (K_t) for two kinds of flume arrangements (two meter flume with forest and one meter flume without forest) with that of 100 regular waves and about 200 - 400 irregular waves. The variation of the transmission coefficient is plotted in Fig. 4.11 as a function of incident wave height and wave period. Graphical representation demonstrates that the transmission coefficients decrease with increasing incident wave height. That

is, the increasing incident wave causes the transmission coefficient to decrease due to stronger wave breaking. The effect of forest width on the transmission coefficient is clearly shown in Fig. 4.11 where wider forest width provide smaller transmission coefficient. It can also be seen that the transmission coefficients increase with water depth for both regular and irregular waves.

Indeed, non-dimensional parameters can provide a more effective correlation for the above-dependent dimensional variables. Based on the single parameters above, the following dimensionless parameters are considered to be most relevant for further analysis:

$$K_t = f\left(\frac{B}{L}, \frac{h}{L}\right) \tag{4.9}$$

where:

B/L : relative forest width [-]
h/L : relative water depth [-]
B : forest width [m]
L : wave length [m]
h : water depth [m]

The wave length (L) used in both parameters h/L and B/L are the wave length measured in front of the slope. Therefore, the L for irregular waves is calculated based on the measured peak period (T_p) in front of the slope and for regular waves, L is based on the measured wave period (T) or mean wave period (T_m).

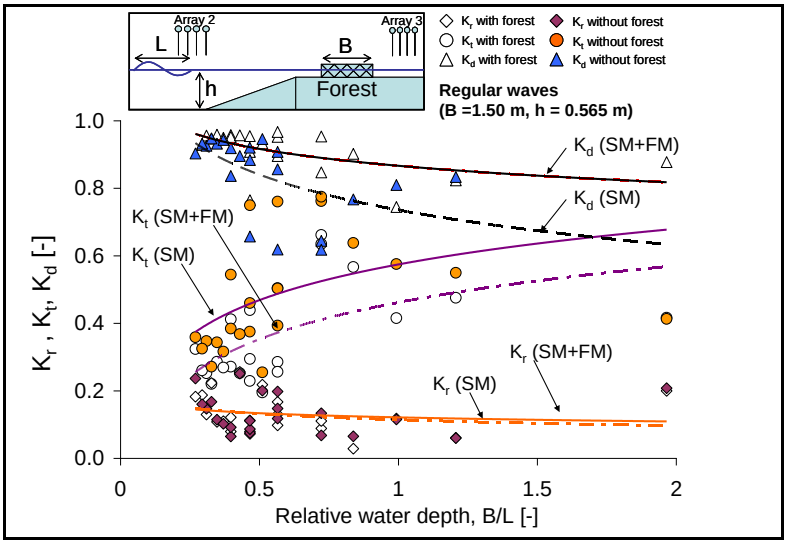

Fig. 4.12: Transmission coefficient (K_t) as compared to the reflection and dissipation coefficients (K_r and K_d) against relative forest width (B/L) for regular waves (B = 1.50 m, h = 0.565 m).

The transmission coefficient is plotted as a function of non-dimensional parameters B/L and h/L in Fig. 4.12 and Fig. 4.13 respectively. The waves are effectively reduced, and the transmission coefficients of the two arrangements in both flumes (with forest and without forest) exhibit a significant difference. Fig. 4.12 illustrates the influence of the forest width on transmission coefficient with B/L. In this figure the influence of forest width on wave transmission is clearly observed. The effect of relative water depth (h/L) on wave transmission is shown in Fig. 4.13. In general, a larger water depth allows more transmission comparatively to lower water depth. Moreover, comparing the effects of various forest widths on wave transmission results presented in Fig. 4.13, we can see that the width of the forest reduces the transmitted wave significantly.

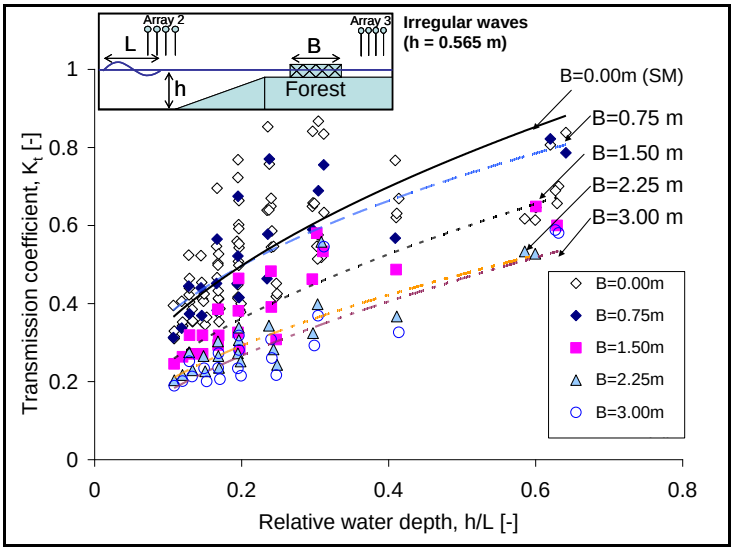

Fig. 4.13: Transmission coefficient (K_t) for different forest widths against relative water depth (h/L) for irregular waves (h = 0.565 m).

4.2.4 Wave energy dissipation

Wave parameters are subject to changes due to wave transformation, including wave breaking and energy dissipation. The amount of wave energy dissipation depends on the incident wave height and the cross-shore topography. In addition, the instantaneous water level affecting the actual water depth is also very important.

Fig. 4.14 shows the wave reflection, transmission and dissipation coefficients (K_r, K_t, K_d) with the effect of forest (SM+FM) and without forest (SM). It is seen that the reflection coefficient is only slightly affected by the forest width and the dissipation coefficient is found to be in the same order as the transmission coefficient. We can observe from Fig. 4.14a, that when h = 0.515 m, the effect of forest model on K_r, K_t and K_d tend to be zero for smaller relative forest width around B/L < 0.5. However, for higher water depth (h = 0.615 m), the effect of

forest model increases because the effect of shore model decreases as water level increases. The shore topography (shore model) remains almost constant over the entire range of tested B/L-values.

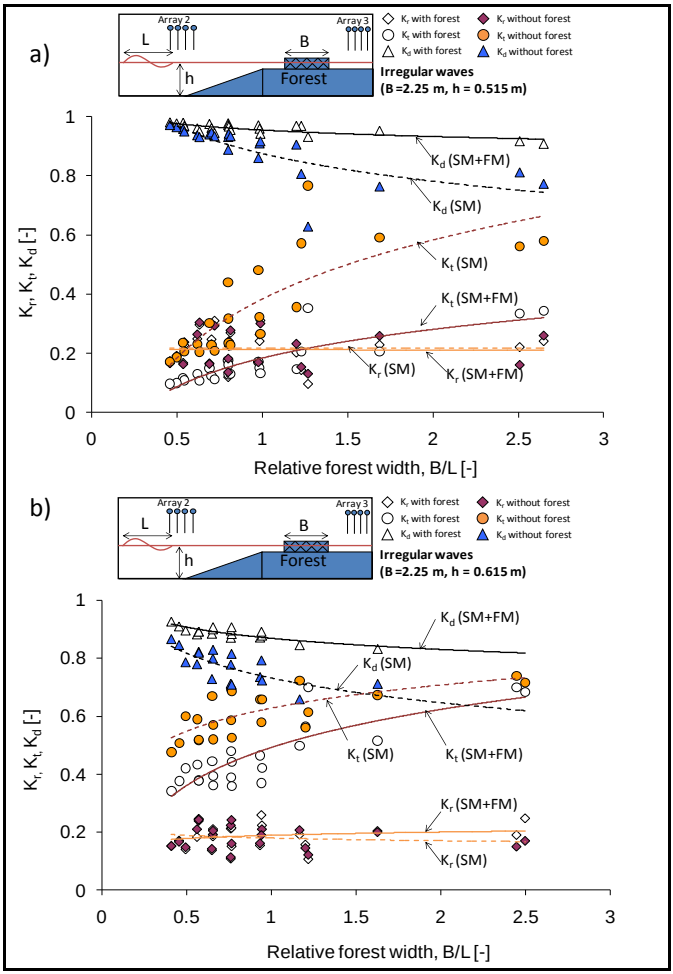

Fig. 4.14: K_r, K_t, and K_d as a function of relative forest width for B = 2.25 m: (a) regular (h = 0.515 m) and (b) irregular (h = 0.615 m)

Dissipation coefficient (K_d) is plotted in Fig. 4.15 as a function of relative water depth (h/L) for all non-breaking and breaking wave conditions. In all cases, dissipation coefficient decays with increasing relative water depth (h/L). Since forest width B has a direct influence on the transmission coefficient and insignificant effect on the reflection coefficient, so the dissipation coefficient is directly related to the transmission coefficient. It is also important to notice that for smaller relative depths (h/L <0.1) dissipation coefficient reaches a maximum value for K_d = 0.98 all tested forest widths. However, as h/L increases, the effect of forest width B on wave energy dissipation becomes increasingly larger.

The results shown in Fig. 4.16a-d describe the total energy dissipated due to both shore topography (platform with slope in the flume) and mangrove forest. In order to discriminate between the part dissipated by shore topography and that dissipated by the forest, it is also necessary to analyse the result of the simultaneously performed tests in the one meter wave flume. While this analysis provides only the contribution of the shore topography to the total energy losses, the analysis of the tests in the two meter flume provides both contributions together (forest and shore topography).

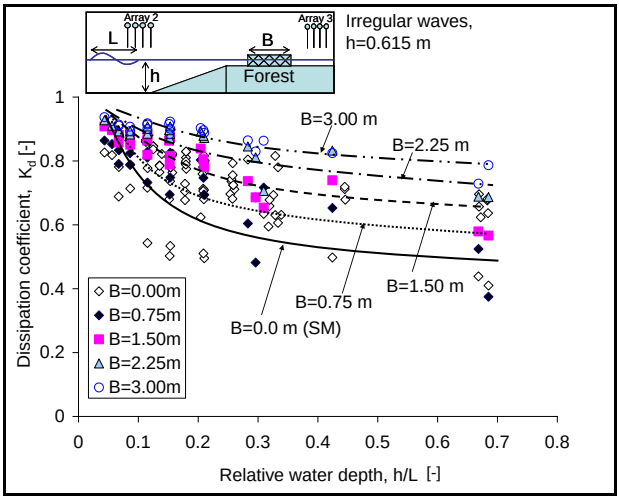

Fig. 4.15: Variation of dissipation coefficient (K_d) against relative water depth (h/L) for irregular waves, h = 0.615 m

.

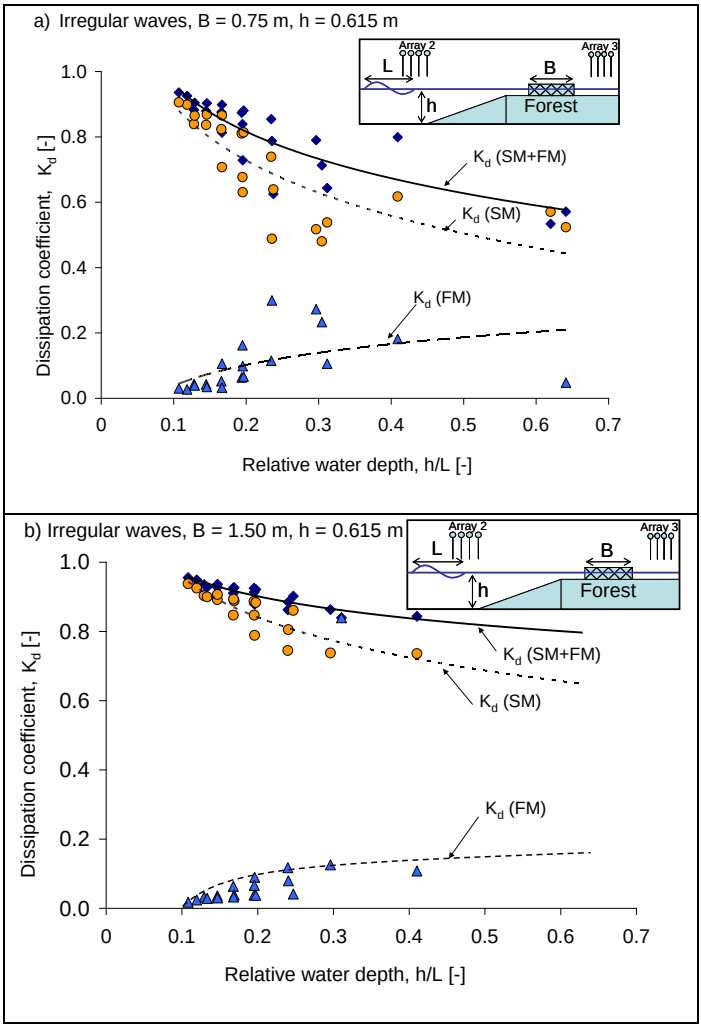
a) Irregular waves, B = 0.75 m, h = 0.615 m
Array 2
Array 3
L
B
h
Forest
Dissipation coefficient, K_d [-]
K_d (SM+FM)
K_d (SM)
K_d (FM)
Relative water depth, h/L [-]
b) Irregular waves, B = 1.50 m, h = 0.615 m
Array 2
Array 3
L
B
h
Forest
Dissipation coefficient, K_d [-]
K_d (SM+FM)
K_d (SM)
K_d (FM)
Relative water depth, h/L [-]

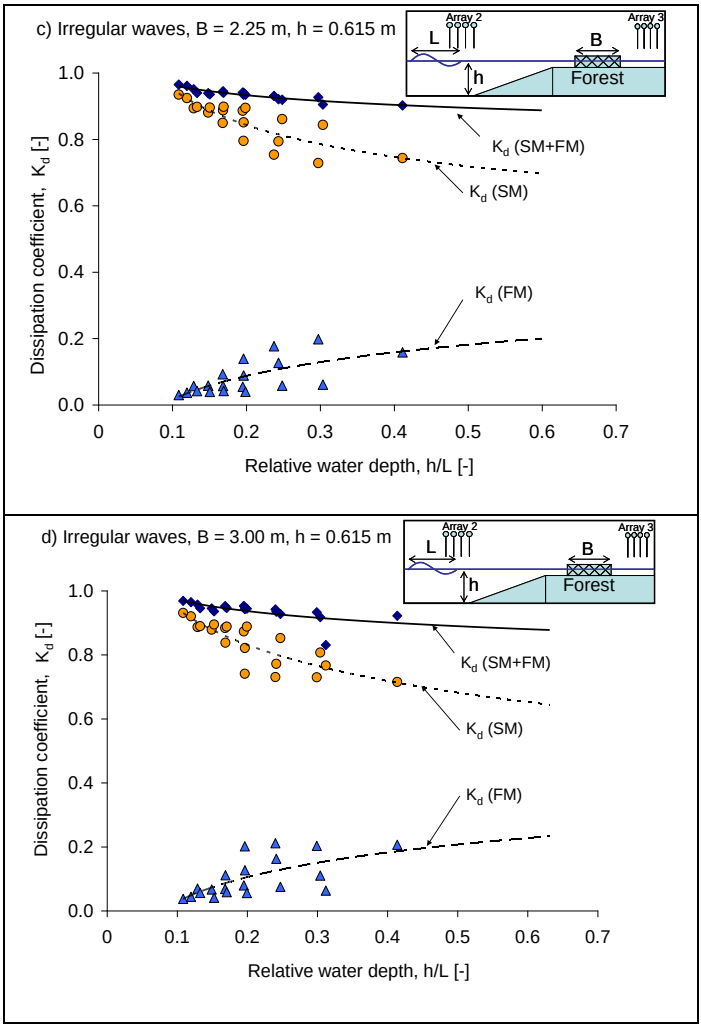

Fig. 4.16: Variation of dissipation coefficients (K_d) against relative forest width (B/L) for irregular waves: (a) B = 0.75 m, (b) B = 1.50 m, (c) B = 2.25 m and (d) B = 3.0 m.

Exemplarily results for the tests with water depth h = 0.565 m and forest width B = 0.75 - 3.0 m are given in Fig. 4.16 for different relative water depth (h/L) under both breaking and non-breaking wave conditions. For smaller relative water depth (h/L < 0.2), the contribution of forest width is found not so significant, because all incident waves have already been dissipated by the slope (shore topography). However, for higher relative water depth (h/L > 0.2), the influence of forest width on dissipation coefficients due to both forest and shore topography (SM+FM) considerably increases with increasing forest width B. As shown for example in Fig. 4.16a and Fig. 4.16d, the minimum dissipation coefficient for B = 0.75 m is only 0.55 (h/L = 0.65) while for B = 3.0 m, it becomes 0.90 (h/L = 0.65) or increases by about 64%. Meanwhile, the minimum dissipation coefficient due to shore topography (SM) only increases by 44% (from K_d = 0.45 (B = 0.75 m) to K_d = 0.65 (B = 3.0 m)). A similar behaviour was also observed for other water depth conditions and forest widths B (Fig. 4.16a-c) as well as for regular waves (Husrin *et al*., 2010)

The contribution of shore model (SM) and forest model (FM) to the total wave energy dissipation has been averaged for all forest widths for different water depths. The results are summarized in Table 4.2, showing that the forest model increasingly dissipates more energy as the water depth increases. The following definitions are for C_{SM} and C_{FM} in Table 4.2:

$$C_{SM} = \frac{K_d(SM)}{K_d(SM+FM)} * 100\% \tag{4.10}$$

$$C_{FM} = \frac{K_d(FM)}{K_d(SM+FM)} * 100\% \tag{4.11}$$

$$\text{with:} \quad K_d(FM) = K_d(SM+FM) - K_d(SM) \tag{4.12}$$

where :

C_{SM} : contribution of shore model to the total wave energy dissipation [%]

C_{FM} : contribution of forest model to the total wave energy dissipation [%]
K_d(FM) : dissipation coefficient due to forest model FM [-]
K_d(SM) : dissipation coefficient due to shore model SM [-]
K_d(SM+FM) : dissipation coefficient due to both shore model and forest model SM+FM [-]

Table 4.2: Contribution of shore model (C_{SM}) and forest model (C_{FM}) to the total wave energy dissipation averaged for all forest widths with different water depths

Water depth, h [m]	Regular waves		Irregular waves	
	C_{SM} [%]	C_{FM} [%]	C_{SM} [%]	C_{FM} [%]
0.465	96.77	3.28	96.14	3.86
0.515	94.58	5.42	93.33	6.67
0.565	90.12	9.88	90.41	9.59
0.615	84.72	15.28	86.52	13.48

It is obvious that these unique results will have vital implications for practice, and it is worth to mention again the necessity of using the Twin Wave Flume (TWF) for simultaneous measurements with the same shore topography with and without the forest model.

4.2.5 Drag coefficient of mangrove under regular/irregular waves

Morison's approach is implemented for the analysis of the hydraulic resistance induced by mangrove forest subject to regular and irregular waves (Morison *et al.*, 1950). The Morison's method (or wave-by-wave's method) is very simple and straightforward because only the peak waves are considered. The current study provides horizontal total force F_T and horizontal flow velocity u. Once the current velocity and total force data are available, C_D and C_M can be derived directly with the following assumptions (Fig. 4.17):

- Drag and inertia forces have 90° phase difference
- Maximum drag force is for the maximum current velocity or when flow acceleration is minimum ($du/dt = a \sim 0$)

– Maximum inertia force is for the maximum acceleration or when flow velocity is minimum (u ~ 0)

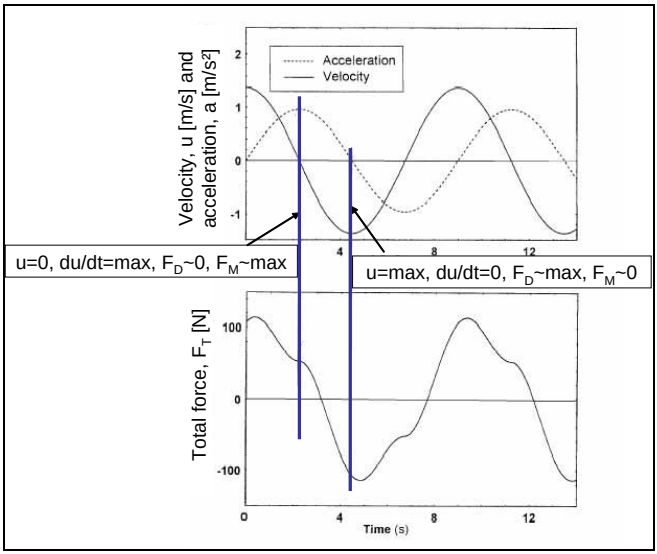

Fig. 4.17: Relationship of total force and velocity/acceleration (Journee and Massie, 2001)

Fig. 4.17 shows descriptive relationship of current velocity, acceleration and the total force. Afterwards, C_D and C_M can be directly calculated based on the Morison' equation (Eq. 2.3):

$$C_D = \frac{2F_T}{\rho A_f u^2} \tag{4.14}$$

$$C_M = \frac{F_T}{\rho V_v \frac{\partial u}{\partial t}} \tag{4.15}$$

Where:

F_T : total force [N]

C_D : drag coefficient [-]
C_M : inertia coefficient [-]
ρ : water density [m^3/s]
A_f : frontal area of the object [m^2]
V_v : submerged volume of body subject to flow [m^3]
$\partial u / \partial t$: flow acceleration [m/s]

Since this method utilizes only maximum values of velocity/acceleration and its associated total force, a large number of data is required to obtain statistically meaningful results. The final C_D and C_M values are then the result of averaging these calculated data.

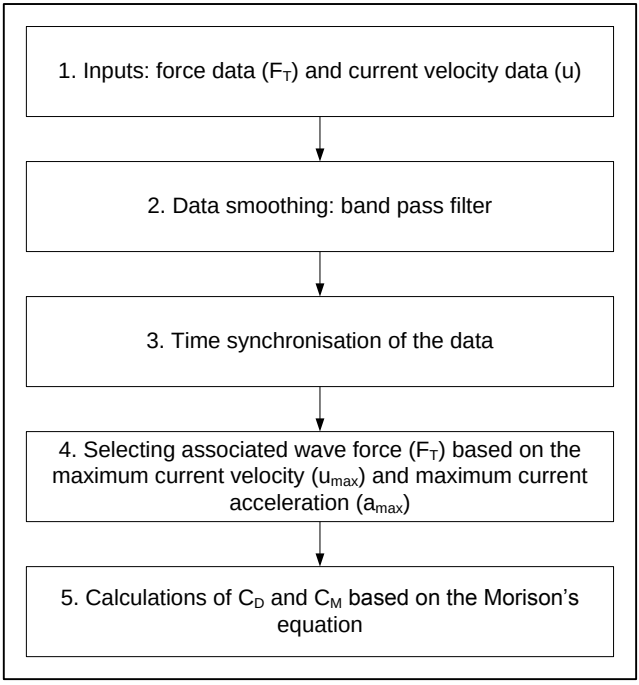

Fig. 4.18: Flow chart for the determination of drag and inertia coefficients using the Morison approach.

Fig. 4.18 shows the steps of the methodology which is applied to determine the hydraulic resistance of mangrove forest subject to regular and irregular wave based on the Morison's method. The aspects that have to be carefully considered to use this method are data smoothing and signal synchronization between current velocity and total force data. Misalignment between measurements devices is a common problem encountered in laboratory experiments (Yuan & Huang, 2010). As a result, the signals from the measurements devices should be first synchronized. The details on how to deal with data smoothing and signal synchronisation can be found in Husrin *et al*. (2011).

The analysed data of each regular waves and irregular waves consist of 176 data sets (different wave heights, wave periods, water depths and forest widths) for four different forest widths, B = 0.75 m, 1.5 m, 2.25 m and 3.0 m. Each forest width has two different water depths, h = 0.565 m and h = 0.615 m and for each water depth there are 22 wave conditions (different wave heights and periods). This means for each forest width B there are 44 data sets (22 wave conditions x 2 water depths) that should be analysed.

The drag coefficient C_D and the inertia coefficient are plotted against the Reynolds number R_e and Keulegan-Carpenter number KC. The Reynolds number R_e and the KC numbers are defined as follows:

$$R_e = \frac{u_{max} L_e}{\upsilon} \tag{4.16}$$

$$KC = u_{max} \frac{T}{L_e} \tag{4.17}$$

$$L_e = \frac{V - V_m}{A_f} \tag{4.18}$$

Where:

u_{max} : maximum horizontal flow velocity [m/s]

T : wave period [s], mean wave period for regular wave T_m and peak wave period

V : control volume [m^3]

V_m : submerged root volume [m^3]

L_e : effective length of the tree model [m]

ν : kinematic viscosity of water (= 1.004 x 10^{-6} m^2/s for water temperature = 20 ^oC)

A_f : frontal area of the tree model [m^2]

Table 4.3: Calculated parameters for the analysis

Parameters	h = 0.615 m or h_r = 0.20 m	h = 0.565 m or h_r = 0.15 m	Notes
A_f [m^2]	0.007624	0.007384	For both regular and irregular waves and for all forest widths B = 0.75 m, 1.5 m, 2.25 m and 3.0 m
V [m^3]	0.0045	0.003375	
V_m [m^3]	$9.88x10^{-05}$	$9.73x10^{-05}$	
T [s]	WG-13	WG-13	
u and u_{max}	ADV1	ADV1	
L_e [m]	0.577279	0.44389	
V_m/V [-]	0.0220	0.0288	

Water depths considered for the data analysis

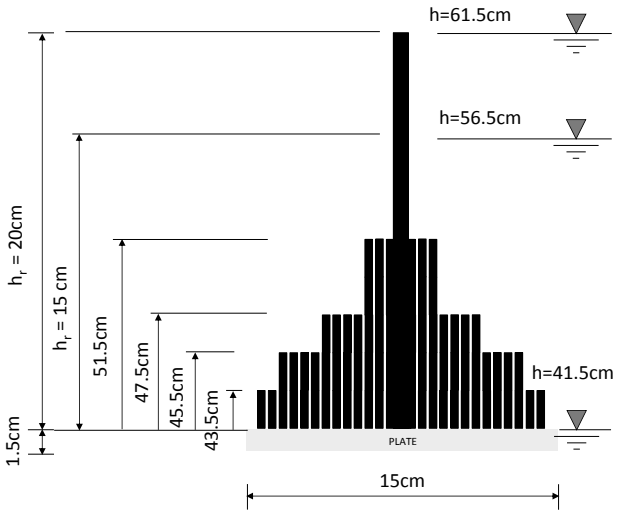

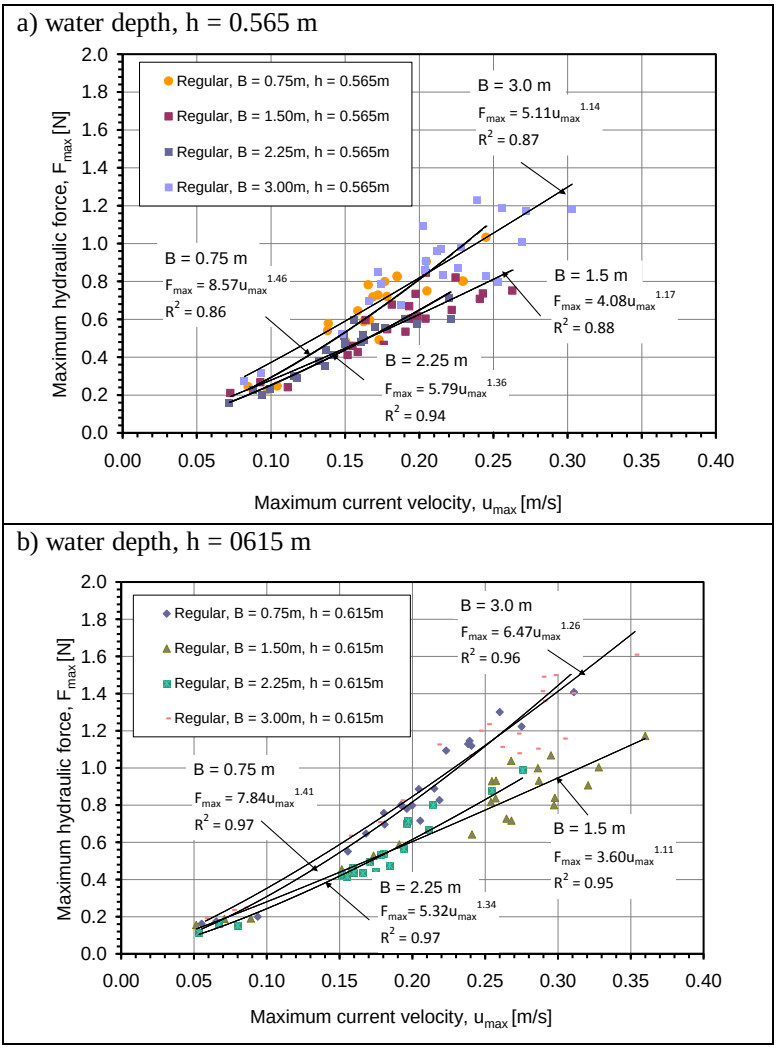

Fig. 4.19: Relationship of hydraulic force and current velocity for different forest widths

a) forest width, B = 0.75 m

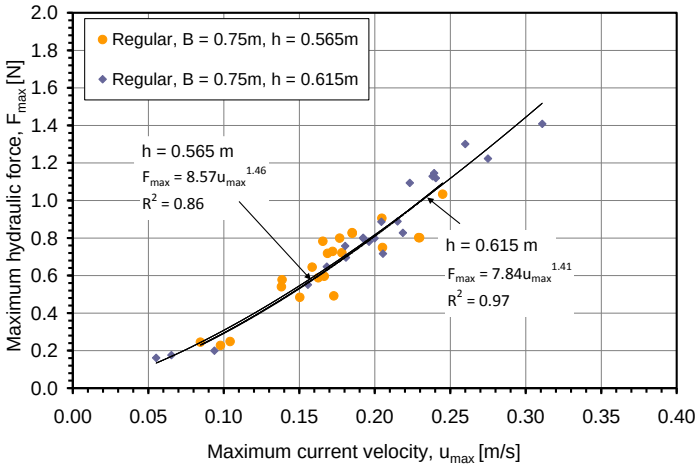

b) forest width, B = 1.50 m

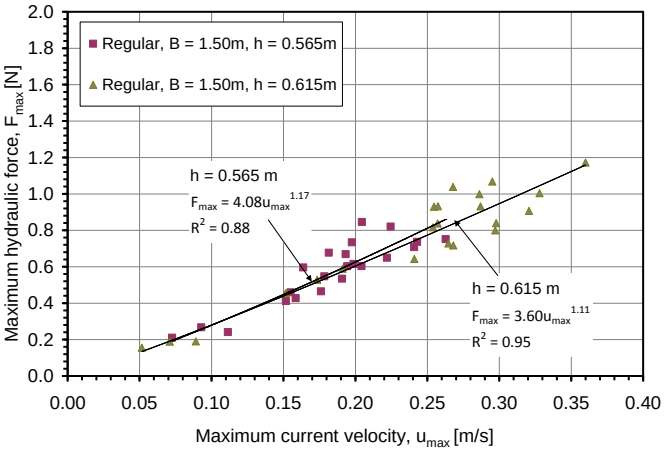

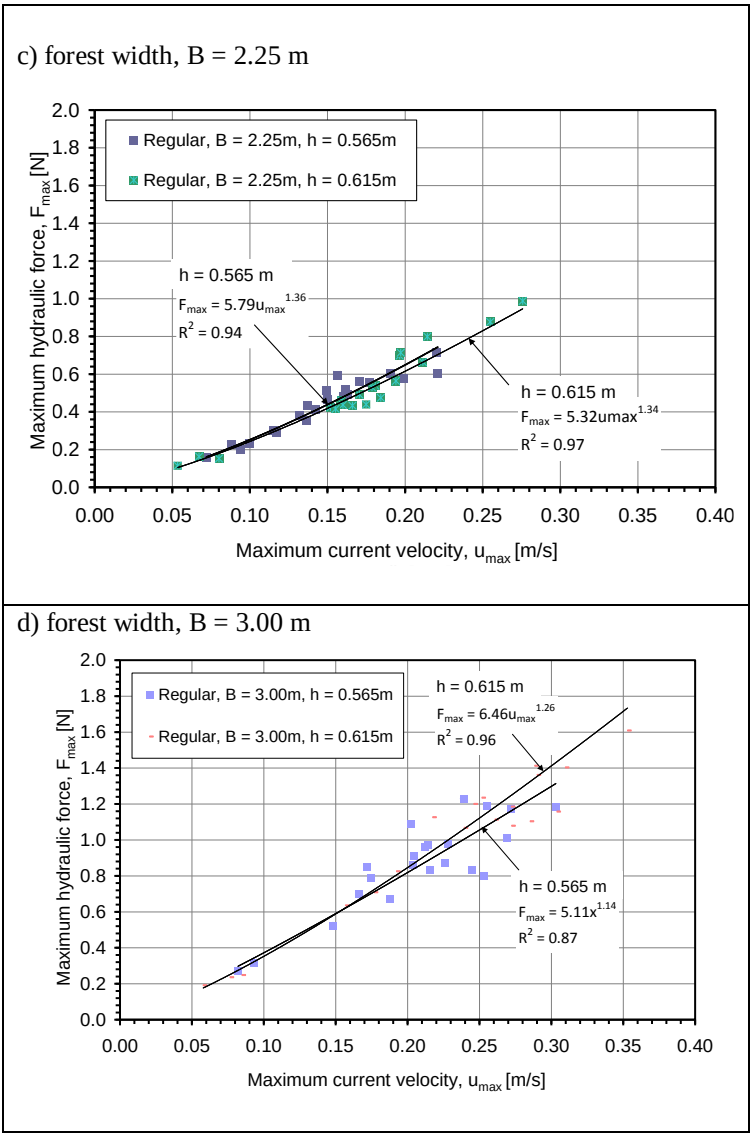

Fig. 4.20: Relationship of hydraulic force and current velocity for each forest widths B

The wave period is determined from wave gauge 13 which is located parallel to the ADV. The frontal area A_f , the control volume V and the submerged volume of roots V_m are determined according to the variation of water depth on top of the shore platforms (h_r). The shore platform has 0.415 m height. Therefore, for h = 0.565, h_r = 0.15 m and for h = 0.615, h_r = 0.20 m (Fig. 4.19). Complete values for those parameters are tabulated in Table 4.3

First, we look at the relationship of maximum hydraulic force and current velocity to the variation of forest widths for each water depth (h = 0.565 m and 0.615 m) as shown in Fig. 4.19. Exponential trend lines with correlation of determination (R^2) larger than 80% are drawn to have general pattern of the curves. For stiff structures, the current velocity is theoretically supposed to be quadratic ($F_{max} \sim u_{max}^2$). However, the relationship as shown in the figures indicates there are other parameters other than current velocity influencing the measured hydraulic force. The influencing parameters could be either from the model characteristics (e.g. frontal area) or aspects related to the measurement devices and the set-up. In general, the measured forces range from 0.1 N – 1.6 N while the current velocity ranges from u = 0.05 m/s – 0.36 m/s.

Generally, the measured hydraulic force as well as the current velocity for larger water depth (h = 0.615 m) are higher compared to shallower water depth (h = 0.565 m). However, forest width variation does not have any clear influences on the measured forces. As shown in Fig. 4.19, the measured forces for B = 3.0 m and B = 0.75 m are almost similar and consistently larger than for B = 1.5 m and B = 2.25 m. Similarly, the effect of water depths on the measured force for each forest width is also difficult to identify (Fig. 4.20). For B = 0.75 m, the measured forces for both water depths are almost identical while for B = 3.0 m, the measured forces for h = 0.615 m are larger than for h = 0.565 m. Forest widths B = 1.5 m and B = 2.25 m, however, have completely different patterns where for water depth h = 0.565 m, the hydraulic forces are larger compared to h = 0.615 m. The following aspects related to the experimental set up and tested conditions may contribute to the problems as described above:

- The effect of water depth variation on the measured hydraulic forces is often difficult to identify due to the small difference between the two water depths analysed ($\Delta h = 0.05m$).
- Within this small water depth difference ($\Delta h = 0.05m$), there is only a single trunk (a cylinder) that affects the measured forces (see Fig. 4.19). These conditions lead to the small difference of the measured forces as shown in Fig. 4.20. However, for the calculation of the hydraulic resistance, there are other parameters that may affect the general behaviour of the curves.
- The location of the ADV sensor (in vertical direction) is always at similar point (about 5 cm from the bottom) regardless the variation of employed water depths. This may lead to a confusion of the measured current velocity because the magnitude of water particles velocity is related to the water depth. For example, for h = 0.565 m, the ratio of ADV measurement point to the water depth (h_a/h) is 0.089 while for h = 0.615 m is h_a/h = 0.081. This means for shallower water depth, the measurement is closer to the water surface which has a larger current velocity compared to the one closer to the bottom.
- The three ADVs used in the current experimental setup have different accuracies. Particularly after the tests with forest width B = 0.75 m, the ADV in front of the forest was altered. This problem may also lead to a confusion in determining the effect of changing forest widths to the measured hydraulic forces as shown in Fig. 4.19 where the measured hydraulic forces for the widest and the narrowest forest widths (B = 3.0 m and 0.75 m, respectively) are almost identical.

These problems definitely will affect the analysis of the hydraulic resistance. The analysis of the hydraulic resistance and its relationship to the variations of water depths and forest widths will face similar inconsistency. Though this problem does not affect the range of overall hydraulic resistance, this inconsistency exists as described in the following sections for the analysis of C_D and C_M. Keulegan-Carpenter number (KC) is often used instead of the Re-number for oscillatory flow -as induced for instance by waves - to describe the effect of the flow regime on drag coefficient and inertia coefficient (Keulegan and Carpenter, 1958).

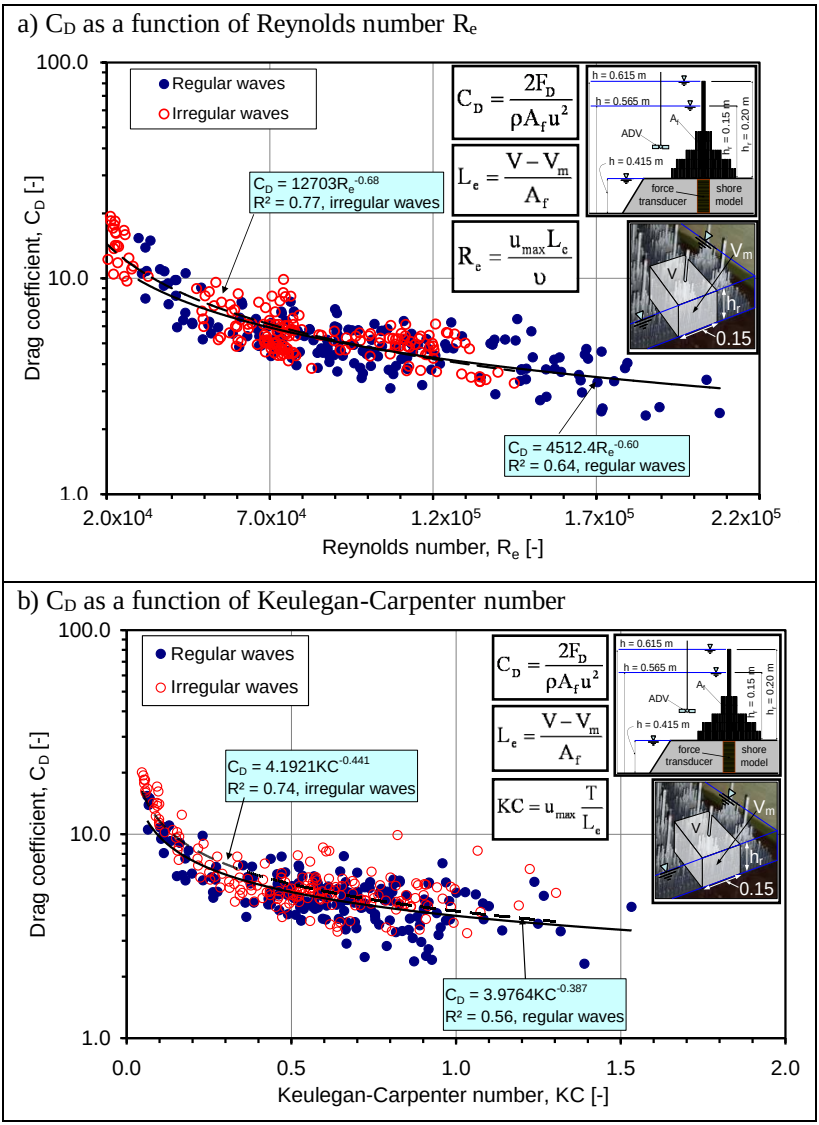

Fig. 4.21: Drag coefficient C_D as a function of R_e and KC numbers for all analysed data

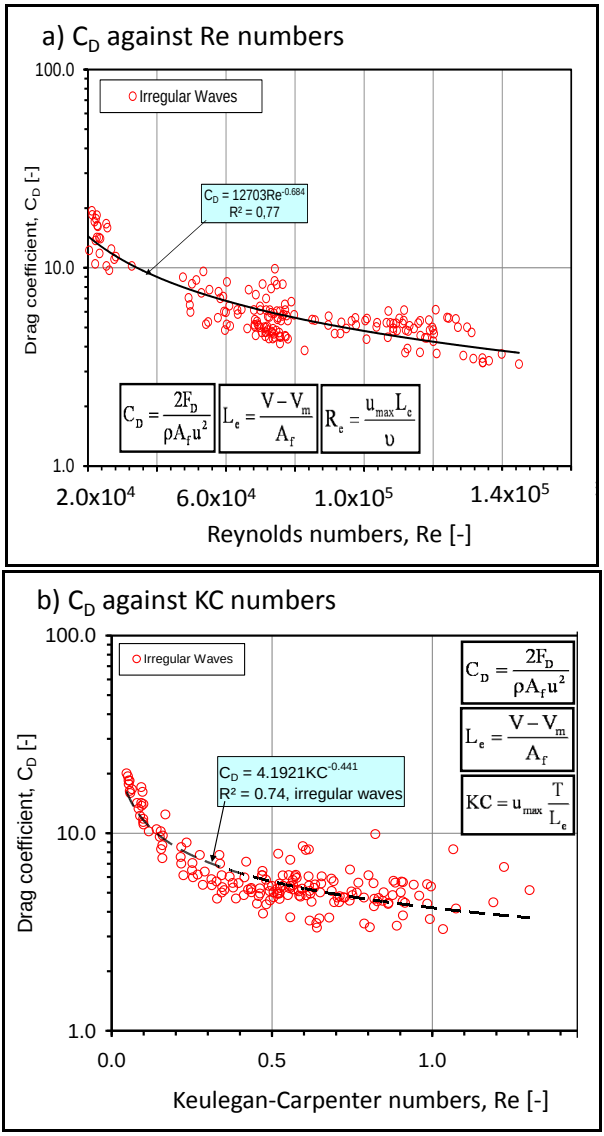

Fig. 4.22: Drag coefficient as a function of the flow regime described by Re and KC

Fig. 4.21 shows the relationship between drag coefficient C_D and R_e number and between C_D and KC number for B = 0.75 m. Similar plots for other forest widths B can be found in Husrin and Oumeraci, 2012i. The derived C_D from all analysed data (including regular and irregular waves) range from 2 – 20 for R_e numbers between 2.10^4 – 3.10^5 and KC numbers range from 0.05 – 1.6 .C_D decreases as R_e and KC increases (Fig. 4.21).

The comparison of these figures shows that the relationship between C_D and KC number is physically more consistent because KC number is a function of both wave period and current velocity which is more applicable for the case of waves compared to R_e numbers. Fig. 4.22 shows the relationship between C_D and KC provide continues data clouds while the relationship of C_D and R_e provide gapped data clouds.

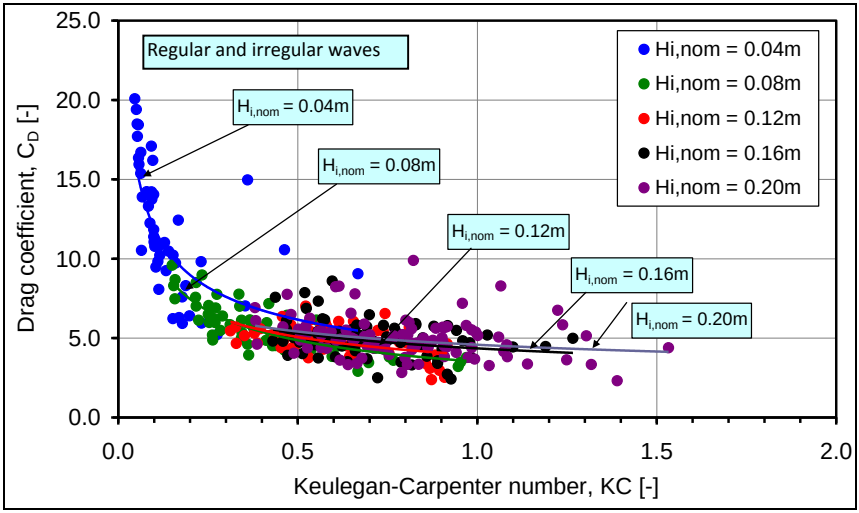

Fig. 4.23: C_D for different wave height as a function of KC (regular and irregular waves)

The drag coefficient C_D is also plotted for different wave heights. The nominal incident $H_{i,nom}$ waves are plotted to describe the influence of different wave height on the C_D values (Fig. 4.23). It clearly shows that for smaller wave heights, the drag coefficient C_D is larger compared to those obtained for higher

waves. Larger C_D for smaller wave heights mostly belongs to non-breaking wave conditions (also associated with shorter wave length) in which wave energy is much less dissipated. For larger wave heights (longer wave periods), most of the waves are broken by the foreshore topography, so that the associated C_D tends to be smaller compared to the non-breaking conditions. This is in line with the analysis from global process in term of dissipation coefficient K_D where shorter waves provide larger K_D contributed by the forest compared to the K_D of longer wave periods where much of the wave energy dissipation is contributed by the foreshore topography (Fig. 4.15). Moreover, the C_D is plotted as a function of relative water depth, h/L, the relationship $C_D = f(K_D)$ becomes much clearer (Fig. 4.24). Though, the effect of changing forest width is very difficult to recognize, there is a distinct general behaviour of C_D as a function of relative water depth h/L . The C_D increases as the h/L increases. This pattern is in agreement with Fig. 4.15 where dissipation of wave energy by forest model decreases for larger h/L (increase role of forest model).

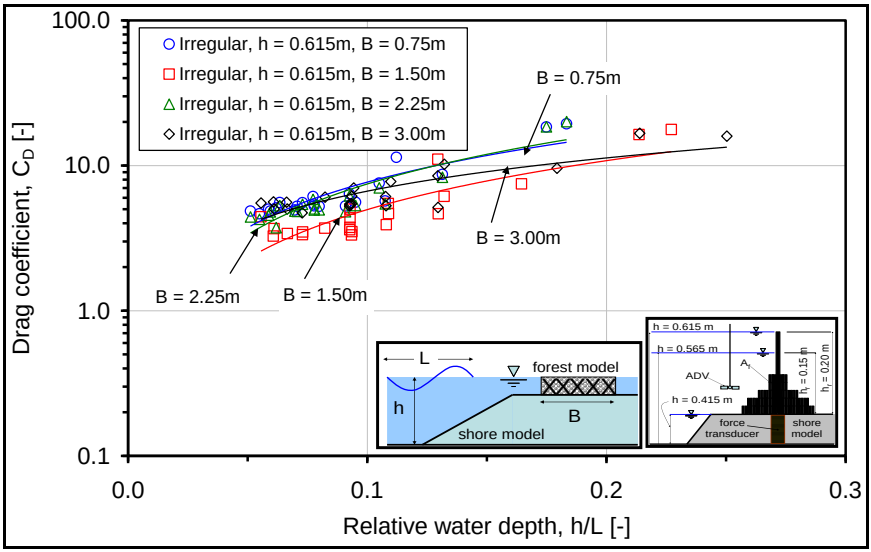

Fig. 4.24: C_D for different forest width as a function of relative water depth (h/L)

The obtained C_D values are within the data clouds of the previous C_D values obtained from the experiment in a current flume (Fig. 3.18) for the associated range of the Reynolds number (Fig. 4.25). However, the range of Reynolds number for the case of both regular and irregular waves is not wide enough as compared to the experiments in the current flume due to the following aspects:

- The generated flow velocities are wave-induced flows which are much smaller compared to the experiments in the current flume. The range of flow velocities in the current flume is between 0.1 – 1.0 m/s while the measured velocity range for experiment with regular and regular waves is between 0.05 – 0.36 m/s.
- There are only two water depths considered in the analyses with regular and irregular waves. Limited capabilities of the ADV current meter to measure flow velocity at lower water depths (h = 0.456 m and h = 0.515 m) lead to less data to be analysed.
- Larger C_D values from the analyses of regular and regular waves are associated with at least two aspects: small measured current velocities (u) and large frontal areas (A_f) or smaller submerged volume ratio. From the experiments in the current flume, this behaviour is also observed where small current velocities for larger water depth also provide larger C_D values (Fig. 3.18).

The derived C_D values found in the current analyses show that water depth significantly influences the correlation of determination of C_D as a function of KC number (Fig. 4.26). For the case of emergent conditions (h = 0.565 m), the correlation of determinations are smaller compared to those for submerged conditions (h = 0.615 m). This finding is related to the characteristics of flow passing through the objects in which for emergent conditions, the flow experiences more blockades from the tree model while for submerged conditions the flow more freely passes through the forest. Thus, turbulence is more prominent for shallower water depth (emergent conditions) compared to larger water depth (submerged conditions). Similarly, this phenomenon is also found for the cases of Kelp plants subjected to waves where emergent heights of the plants influence the C_D relationship to the KC number (Mendez and Losada, 2004). Moreover, Augustin *et al.* (2008) also observed significant effects of emergent and fully submerged

conditions of cylindrical dowels subjected to random waves to the correlation of determinations of C_D as a function of KC number. All have a similar conclusion that emergent conditions provide smaller correlation of determinations compared to submerged conditions for C_D as a function of KC number.

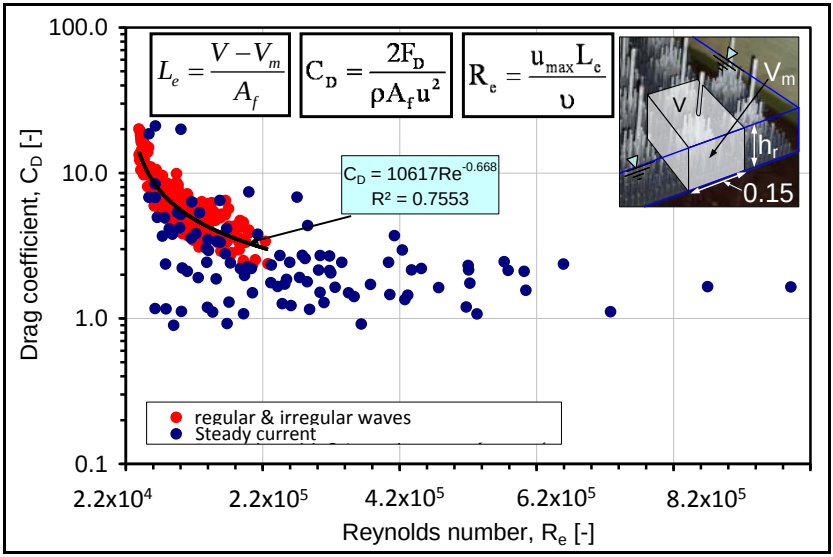

Fig. 4.25: C_D values comparison obtained from regular & irregular waves and current flume experiments

The derived C_D from the current study ranges from 2 – 20 for R_e numbers between $2x10^4$ – $3.0x10^5$ and KC numbers range from 0.05 – 1.6. As already discussed previously, KC number provide meaningful interpretation to explain the C_D of tree models subject to regular and irregular waves. By combining all the data, irrespective of the wave types, water depths and forest width, the new relationship of C_D as a function of Keulegan-Carpenter number KC can be derived (Fig. 4.27) with a coefficient of determination, $R^2 = 0.67$.

$$C_D = \frac{4.05}{KC^{0.43}}; \quad R^2 = 0.67 \tag{4.19}$$

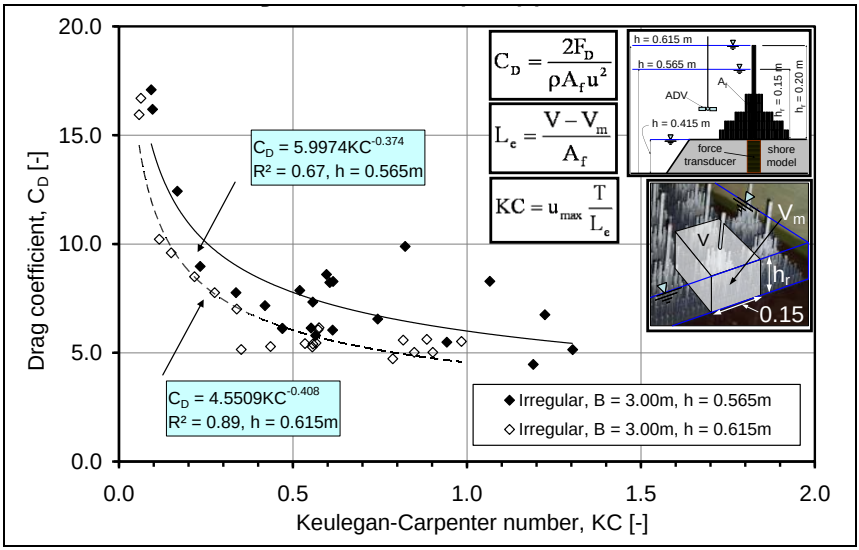

Fig. 4.26: Drag coefficient C_D as a function of KC number for forest width B = 3.0 m

Though the contribution of the foreshore topography is still dominant to the total dissipation of wave energy (Fig. 4.15 and Table 4.2), larger C_D values for the forest model subject to regular and irregular waves explain that mangrove forest may provide sufficient hydraulic resistance against storm waves. As shown in the discussion above, larger relative water depth h/L proved to have significant dissipation in terms of both K_D and C_D (Fig. 4.15 and Fig. 4.24). Many studies have shown that indeed a mangrove forest may behave as a natural barrier against storm waves (Mazda *et al.*, 1997b; Fritz, 2006).

The results of the current study are compared to the results presented by Mazda *et al.* (1997a) for different types of mangrove based on field data in Japan and Australia. Mazda *et al.* (1997a) derived C_D values based on field measurement in tidal-dominated flow area. They found the values of C_D decrease from C_D=10 (R_e=5.10^3) and converge towards C_D=0.45 (Re=10^5) as the Reynolds 'number increases. The field study from Mazda *et al.* (1997a) considered not only the density of roots but also the density of mangrove forest, including the space between individual trees. Therefore, when the measurement took place in the area

where the mangrove trees are highly sparse (this means (V-V_m) is very large), they found very large L_e values and smaller C_D values leading to C_D = 0.4 which is not observed in the present study. Moreover, in the field, there are more aspects that may influence the measurements, such as the bed roughness due to the presence of undergrowth.

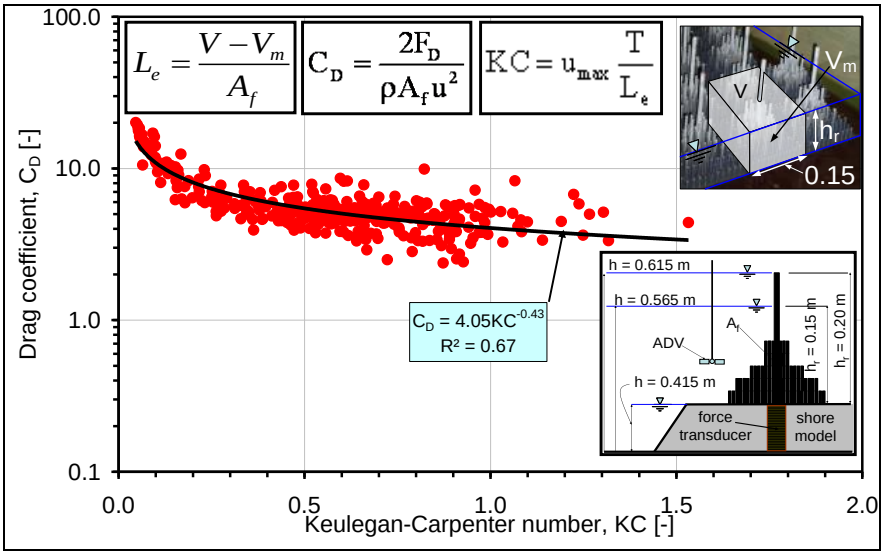

Fig. 4.27: Drag coefficient C_D as a function of KC number for both regular and irregular waves

In the current study, the control volume V was kept constant and the root density varied. The total force was measured directly on each model so that the derivation of the flow resistance is more straightforward. This controlled environment allows higher C_D values compared to the work of Mazda *et al.* (1997a). Moreover, the current study provides not only relationship of C_D against R_e numbers but also against KC numbers which is physically more consistent for oscillatory flows. The work of Imai and Matsutomi (2005) for coastal pine model showed C_D fluctuation in the range of 0.9 – 1.5. However, the study did not reveal any conclusive dependency of C_D from the associated flow regimes. The benefit of the current study is not only the inclusion of frontal area A_f and submerged vol-

ume ratio V_m/V, but also the consideration of the flow regime in terms of both Reynolds and Keulegan-Carpenter numbers.

4.2.6 Inertia coefficients of mangrove under regular/irregular waves

Unlike the drag coefficient C_D, the variation of inertia coefficient C_M over many parameters such as water depth, forest width, wave height and wave period, is not clearly observed. The values of C_M tend to be constant over the entire tested range of both Reynolds and Keulegan-Carpenter numbers. Fig. 4.28 and Fig. 4.29 show the relationship of C_M as a function of the Reynolds R_e and the Keulegan-Carpenter KC numbers, respectively.

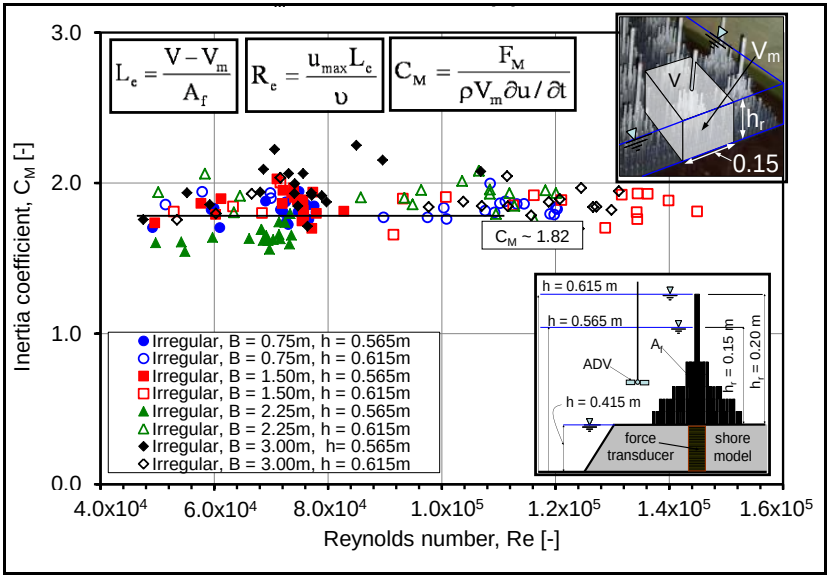

Fig. 4.28: Inertia coefficient C_M as a function of R_e number for irregular waves

The behaviour of C_M for regular and irregular waves as a function of both R_e and KC numbers is slightly different. The data clouds of C_M for regular waves tend to exhibit more scatter compared to those for irregular waves. This phenomenon is also observed as for the cases of C_D (Husrin *et al.*, 2010).

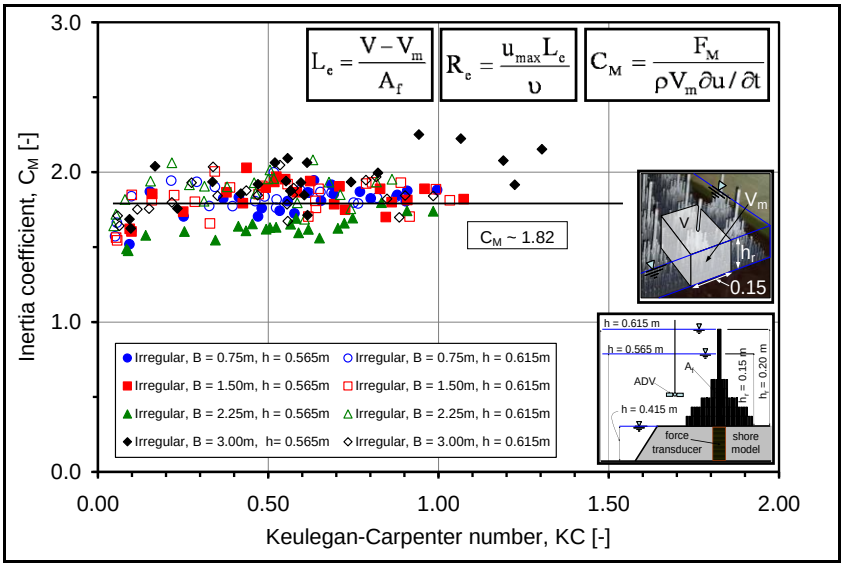

Fig. 4.29: Inertia coefficient C_M as a function of KC number for irregular waves

Table 4.4: The averaged inertia coefficient C_M for all data

water depth, h	**h=0.565 m**								**Averaged**
wave type	regular waves				irregular waves				**for h =**
Forest width, B	0.75	1.5	2.25	3	0.75	1.5	2.25	3	**0.565 m**
C_M	1.84	1.72	1.60	1.87	1.80	1.84	1.63	1.95	**1.78**
water depth, h	**h=0.615 m**								**Averaged**
wave type	regular waves				irregular waves				**for h =**
Forest width, B	0.75	1.5	2.25	3	0.75	1.5	2.25	3	**0.615 m**
C_M	1.94	1.95	1.63	1.99	1.83	1.82	1.88	1.84	**1.86**
Average	1.89	1.84	1.61	1.93	1.81	1.83	1.76	1.89	

The obtained inertia coefficient C_M values as a function of both the Reynolds and Keulegan-Carpenter numbers are entirely new for the current study. From the experiment with steady current, C_M cannot be derived because flow acceleration was negligible. The values of C_M range from 1.22 – 2.54 for the range of R_e between 1.9×10^4 – 2.1×10^5 or KC between 0.05 – 1.53. From all data, the aver-

age C_M value is 1.8. Though it is not very significant, the effect of wider forest width to the C_M is observed. C_M for the widest forest width (B = 3.0 m) is slightly larger compared to C_M for shorter forest widths (Table 4.4).

The range of C_M values obtained from this experiment is in a similar range with that obtained by Harada & Imamura (2000). The averaged C_M for their experiment using porous media subject to bores is C_M = 1.7. However, their work did not attempt to address C_M in relation to the flow regime as in the current study. We found also that C_M is slightly larger for wider forest width (Fig. 4.30 and Fig. 4.31) which is in agreement with the work of Harada and Imamura (2000) as clearly shown in Fig. 4.28 and Fig. 4.29.

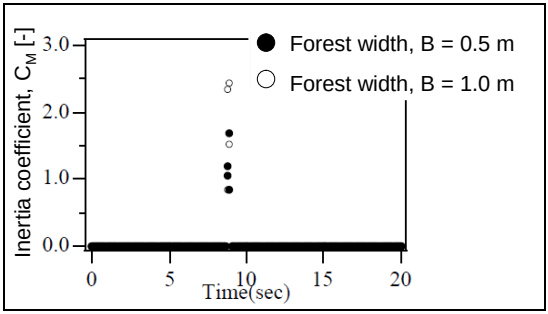

Fig. 4.30: Inertia coefficient C_M values as obtained by Harada and Imamura (2000)

Latief and Hadi (2006) proposed the values of C_M as a function of submerged volume ratio (V_m/V) for the case of mangrove model with porous media subject to bores.

$$C_M = 0.67 + 6.65(V_m / V); \quad for: V_m / V > 0.06$$
$$C_M = 1; \qquad\qquad for: V_m / V < 0.06 \qquad (4.20)$$

The first relationship provide C_M values which are generally lower than those obtained in this study for the range of tested V_m/V = 0.02- 0.10. With these V_m/V values, Eq. 4.20 would provide C_M values from 0.80 to 1.34 which are indeed smaller than the value in Table 4.4 with C_M = 1.6 to 1.95.

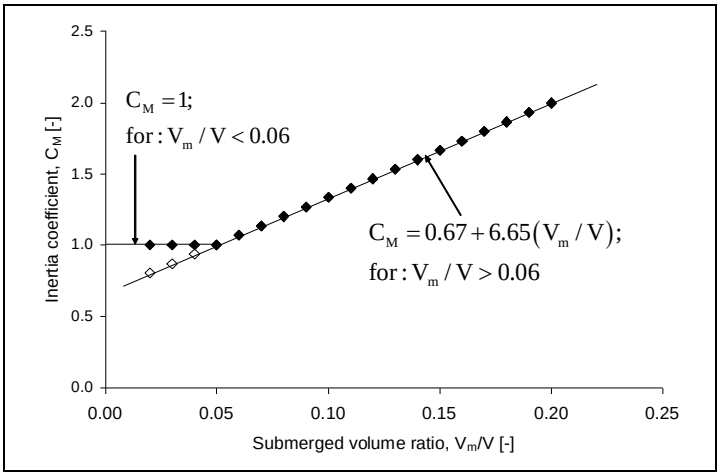

Fig. 4.31: Inertia coefficient C_M values as a function of submerged volume ratio (after Latief and Hadi, 2006)

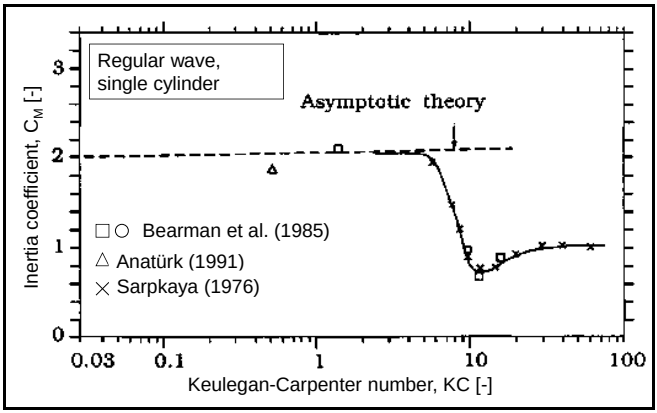

Fig. 4.32: Inertia coefficient C_M values as a function of KC for a single cylinder subject to regular waves (Sumer and Fredsoe, 2006

More crucial is that Eq. 4.20 lacks physical meaning on the limit of $V_m/V = 0.06$ and it is unable to predict the values of C_M for smaller V_m/V while in the current study C_M can be still predicted up to $V_m/V = 0.02$. Moreover, in Eq. 4.20, $C_M = 0.67$ for $V_m/V=0$ (no forest or h= 0) is also difficult to physically interpret as

there is no component due to the added mass and no components due to displaced water mass when there is no body in the flow. In the current study both V_m/V parameter and flow regime in terms of R_e and KC numbers are included.

The C_M values as a function of Keulegan-Carpenter number from the current study are smaller compared to the experimental results with a single cylinder subject to regular waves in Sumer and Fredsoe (2006) (Fig. 4.32). These results may come from the fact that for the case of forest model, group of cylinders that make up the roots block the flow and create higher water level in front of the forest model. This higher water level combined with larger object volume reduces the flow acceleration in front of the forest as well where velocity measurement is taking place.

From the discussion above, the relationship of C_M can be derived as a function of KC number. The data clouds of C_M generally have narrower margin compared to the data of C_D. Therefore, the C_M values for the parameterized tree model are determined by averaging the obtained C_M values for all experiments. By averaging the entire C_M data, it is found that C_M of the tree model for both regular and irregular waves is 1.82.

4.2.7 Remarks on regular/irregular wave attenuation by mangrove forests

The hydraulic performance of mangrove forest of different widths (B) has been systematically tested with both regular and irregular wave trains for different water depths h and breaking locations and analysed in terms of wave reflection, wave transmission and energy dissipation. The effect of single parameters such as incident wave height (H_i), wave period (T), water depth (h) and forest width (B) has first been examined in a preliminary analysis, thus illustrating the related importance of each parameter. Moreover, the results have allowed one to identify the two most relevant non-dimensional parameters which affect reflection coefficient (K_r), dissipation coefficient (K_d) and transmission coefficient (K_t); namely relative water depth (h/L) and relative forest width (B/L). Using these two non-dimensional parameters, a more detailed analysis has led to the following key results:

- **Wave reflection** is primarily caused by the shore topography and depends significantly on the wave breaking conditions and breaking locations. The contribution of the forest itself to wave reflection is almost negligible, though it slightly increases with increasing water depth (h/L).
- **Wave transmission** is determined both shore topography and forest, showing the necessity to discriminate between both effect in order to assess correctly the transmission coefficient of the forest itself. As expected, transmission coefficient (K_t) generally decreases with decreasing relative water depth (h/L) and increasing relative forest width (B/L).
- **Wave energy dissipation,** like wave transmission, is caused by both shore topography and forest. As wave reflection due to the forest is negligibly small, wave energy dissipation and wave transmission are strongly related, so that dissipation coefficient (K_d) can be directly calculated from transmission coefficient (K_t) through the approximate relationship

$$K_d = \sqrt{1 - K_t^2} \quad ; \qquad \text{valid for } K_r \sim 0 \tag{4.13}$$

Many of the results which have yet been achieved were expected from the qualitative point of view, but less from the quantitative view point. The most striking results, however, consist in the relative contributions of the forest and shore topography to reflection coefficient (K_r), transmission coefficient (K_t) and dissipation coefficient (K_d) which are largely affected by relative water depth (h/L) and relative forest width (B/L).

Overall, the wave damping performance due to both forest and shore topography increases with decreasing water depth (h/L) and increasing forest width (B/L). For smaller water depth (h/L) the contribution of the forest to wave damping is negligibly small, but becomes increasingly large with increasing water depth (h/L) and increasing forest width (B/L). The results have revealed that the combined effect of relative water depth (h/L) and relative forest width (B/L) on the relative contribution of forest and shore to topography on wave reflection, transmission and dissipation (K_r, K_d, K_t) is even more complex (e.g. Fig. 4.14 and Fig. 4.15) and needs a more detailed analysis.

Moreover, current studies have shown functional relationships of both global and local processes on the attenuation of storm waves by mangrove forest in terms of wave dissipation and hydraulic resistance (C_D and C_M). The hydraulic resistance in terms of C_D and C_M of the parameterised tree model with stiff structure assumption has been successfully derived by considering the most relevant influencing parameters such as root density, wave conditions (H, T, h), wave types (regular and irregular waves), water depths and forest widths. Drag coefficient C_D is better represented by the R_e-number while inertia coefficient C_M tends to remain nearly constant over a large range of Reynolds numbers (R_e =1.9 x 10^4 – 2.1 x 10^5). The obtained C_D well correlates with dissipation coefficient K_D of mangrove forests as obtained from the global process analysis. This relationship is observed by plotting both C_D and K_D as a function of relative forest width h/L where C_D and K_D both increase as h/L increases.

The derived drag and inertia coefficients C_D and C_M show basic similarities with the previously reported C_D and C_M with some differences exist due to different experimental setups and parameterised models. The experimental approach and the analysis applied in this study are more physically based as compared to those in the previous studies.

Nevertheless, the results achieved so far clearly reveals novel and equally vital aspects in the sense that the modelling and arrangement of the wave attenuation performance of coastal forest have to be reconsidered by taking into account properly the relative effect of the cross-shore topography, the wave evolution modes on the foreshore and inside the forest, and the combined effect of both relative water depth (h/L) and relative forest width (B/L).

4.3 Analysis of solitary wave tests

The simultaneous laboratory experiments using solitary waves to represent tsunami in different water depths are intended to better assess the incident wave conditions (non-breaking or breaking waves generating a bore) and the wave attenuation performance of mangrove forest (stiff structure assumption) as compared to the conditions without the forest. In total, there are 100 model tests involving four different forest widths B, five different water depths h and five

wave heights $H_{i,nom}$. A more complete description of the results for mangroves subject to solitary waves can be found in Strusińska and Oumeraci (2009).

4.3.1 Analysis of wave evolution modes

As the solitary waves propagate over an abrupt bathymetry or submerged structures, the shape and their physical characteristics will evolve. Thus, the determination of solitary wave evolution modes which is a part of the global processes analysis is necessary as the first step of more detailed analysis. Based on the measurements of free surface elevations and video recordings, five different evolution modes (EM) of solitary waves propagating through the foreshore topography and the mangrove forest were successfully identified. The criteria employed to characterize the modes of wave behaviour are based on the wave breaking inception, the location of the incipient wave breaking occurring in four regions along the shore profile as shown in Fig. 4.33, and the generation of wave fission resulting in a train of solitary waves (consisting of at least two solitons). The five evolution modes propagating over the foreshore and mangrove forest models are:

- EM1: non-breaking wave disintegrating into solitons. In this case, wave breaking is not observed but the wave splits into a number of solitons.
- EM2: breaking of incident wave over the foreshore slope (i.e. in region 1) with wave disintegration into solitons.
- EM3: breaking of incident wave in the region between the end of the foreshore slope and the beginning of the forest model (i.e. in region 2) with wave disintegration into solitons.
- EM4: breaking of incident wave in the forest model (i.e. in region 3) with wave disintegration into solitons.
- EM5; breaking of incident wave behind the forest model (i.e. in region 4) with wave disintegration into solitons.

These evolution modes are very important to identify the characteristics of solitary wave attenuation (i.e. wave transmission and dissipation) by either the foreshore topography, mangrove forest or a combination of both. A more detailed discussion of the observed evolution modes and their physical characteristics

related to the attenuation performance of forest models subject to solitary wave impact can be found in Strusińska and Oumeraci (2009).

a) Nonbreaking ("EM1")

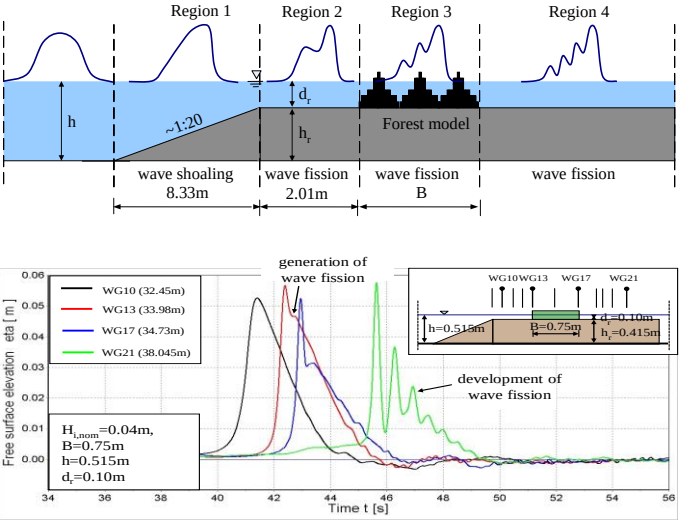

b) Breaking over slope ("EM2")

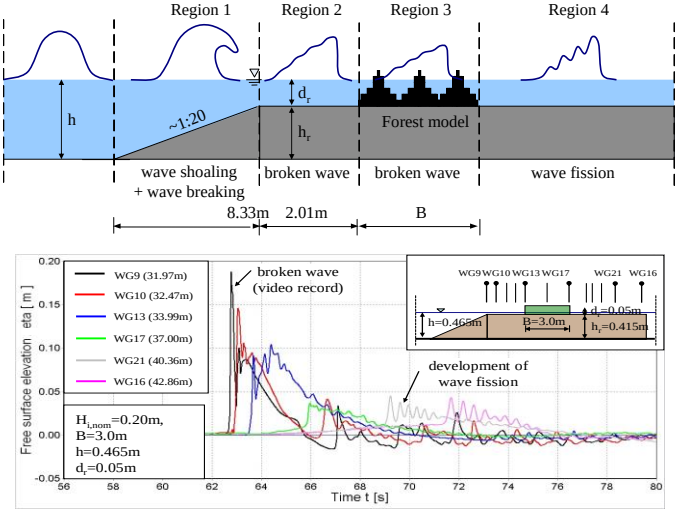

c) Breaking in front of forest (“EM3“)

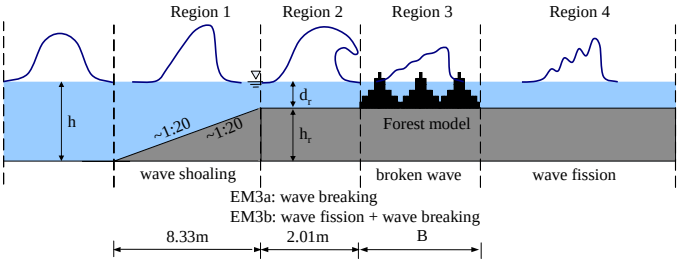

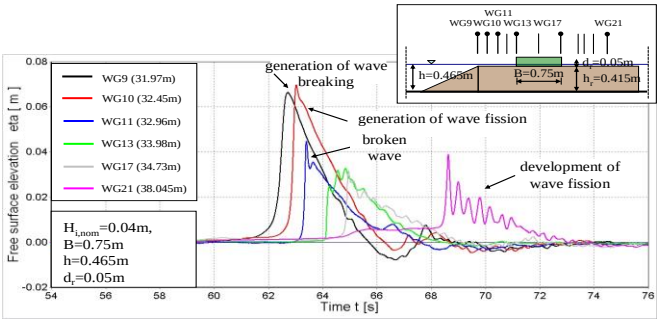

d) Breaking in forest (“EM4“)

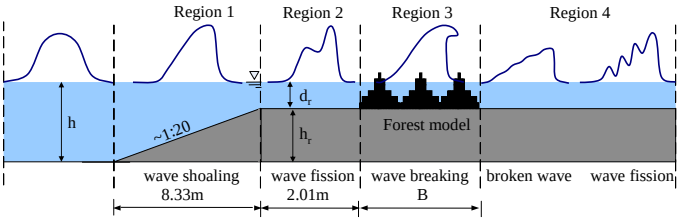

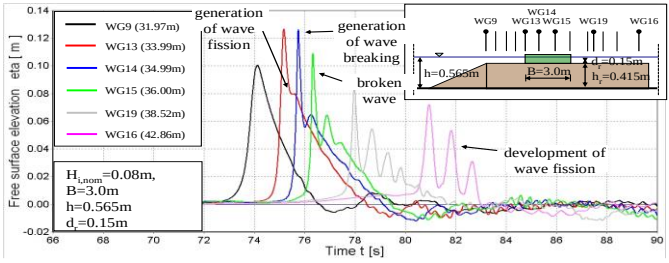

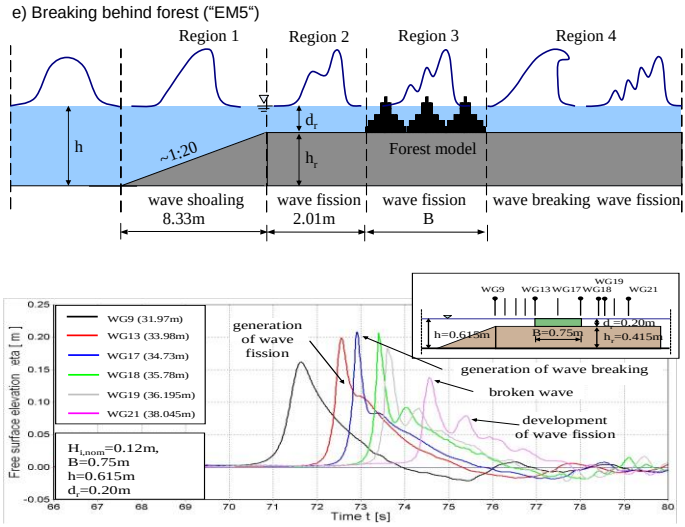

Fig. 4.33: Classification of evolution modes for solitary waves propagating in 2 m - wide flume containing the forest model (Strusińska *et al.*, 2010)

4.3.2 Analysis of wave reduction patterns

Envelopes of maximum wave height and maximum wave forces exerted on the single tree models are very important for the determination of the wave reduction pattern in the forest model (local processes). Relative force reduction R_F is used to describe the reduction of the wave forces along the forest:

$$R_F = \left(1 - \frac{F_{\max,b} - F_{\max,e}}{F_{\max,b}}\right) \times 100\% \qquad (4.21)$$

where $F_{max,b}$ represents the force measured by the force transducer FTS1 installed at the beginning of the forest model [N] and $F_{max,e}$ the force measured by the force transducer FTS10 installed at the end of the forest model [N].

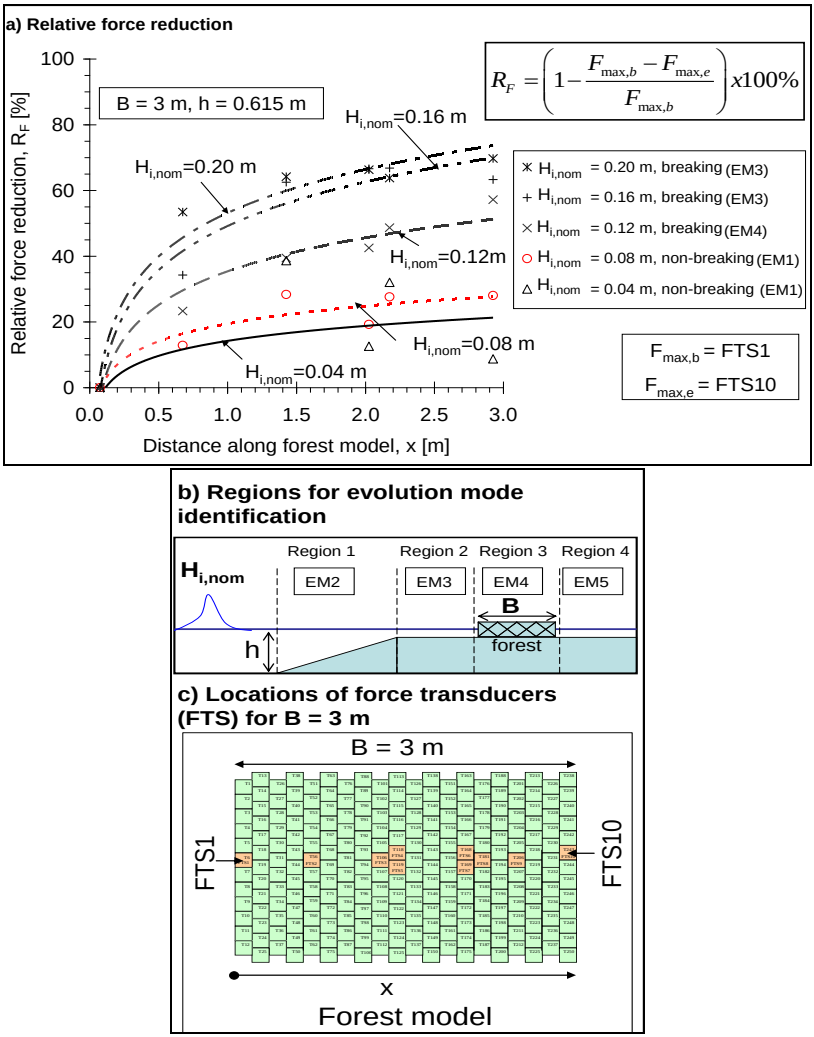

Fig. 4.34: Relative reduction of forces induced on single tree models along the forest by solitary wave of nominal height of $H_{i,nom}$=0.04-0.20 m propagating in a water depth of h=0.615 m (Husrin *et. al.*, 2012a)

Considering the observed wave evolution modes, the wave reduction pattern of non-breaking wave conditions (EM1) shows less significant reduction (R_F in the order of 10-30%), while for breaking wave conditions (EM2 – EM5) a greater substantial reduction of the forces exerted on single trees can be observed within the forest model (R_F even up to 80%) as shown in Fig. 4.34 for the case of forest width B = 3 m. Similar behaviour is also observed for the other forest widths where incident wave heights and the evolution modes significantly influence the wave reduction pattern (Strusińska and Oumeraci, 2009). In conclusion, the wave reduction patterns depend on the incident wave conditions (e.g. wave height and the wave breaking inception), local water depth (i.e. shore topography) and forest characteristics (i.e. forest width). Moreover, this also indicates the importance of foreshore topography in reducing much of the incoming wave energy compared to the mangrove forest models. More detailed discussion regarding this topic can be found in Strusińska and Oumeraci (2009) Strusińska *et al.* (2010) and Oumeraci *et al.* (2011).

4.3.3 Analysis of wave transmission

The commonly used approach of calculating wave transmission coefficients K_t in terms of wave height is hardly applicable in case of generation of wave fission, which very often leads to an increase of wave height in or behind the forest model ($K_t > 1.0$). To determine the K_t, two approaches have been adopted. The first approach, the wave transmission coefficient was expressed as the ratio of the maximum forces exerted on single trees located at the end ($F_{max,e}$) and at the beginning ($F_{max,b}$) of the forest (Oumeraci *et al.*, 2011):

$$K_t = F_{max,e} / F_{max,b} \tag{4.22}$$

Where:

$F_{max,e}$: the maximum forces exerted on single trees located at the end of the forest [N]

$F_{max,b}$: the maximum forces exerted on single trees located at the beginning of the forest [N]

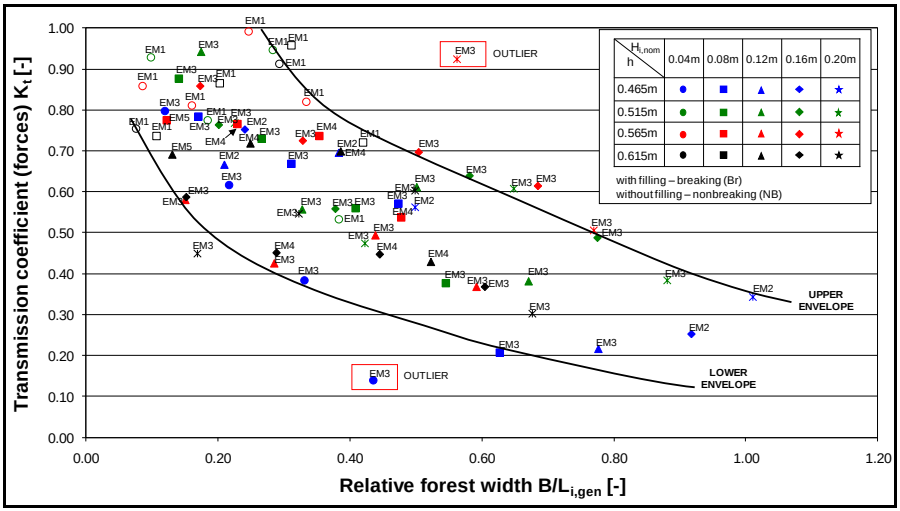

Fig. 4.35: Wave transmission coefficient for solitary waves expressed as ratio of forces exerted on single mangrove trees at the end and the front of the forest (Strusińska and Oumeraci, 2009)

By employing Eq. 4.22 for all wave conditions, forest widths and water depths, the transmission coefficients of solitary waves propagating through the foreshore topography and mangrove forest models can be obtained as shown in Fig. 4.35 as a function relative forest width $B/L_{i,gen}$ ($L_{i,gen}$ is the measured wave length by wave gauges in front of the slope) where the K_t ranges from 0.20- 0.99. It shows that most of EM1 (non-breaking wave conditions) have higher transmission coefficients (K_t = 0.534 – 0.70) while the rests show highly random behaviours. The highest damping performance (K_t = 0.2 for $B/L_{i,gen}$ > 0.5) is obtained for waves breaking in front of the forest model (EM3). There is however no clear relationship between the rate of wave transmission, K_t and the water depth, h. In order to see more precise contribution of other parameters such as water depths and forest width to the transmission coefficients, another approach based on wave energy calculation is needed.

The analysis of wave transmission employing the concept of wave energy is discussed in more details by Daenecke, (2010). The transmission coefficient is

determined as a ratio of total transmitted $E_{T,t}$ and the total incident wave energy $E_{T,i}$:

$$K_t = \sqrt{E_{T,t} / E_{T,i}} \tag{4.23}$$

The total transmitted wave energy $E_{T,t}$ is a combination of potential energy $E_{P,t}$ and kinetic energy $E_{K,t}$ of a transmitted wave (similar procedure and calculations are also applied for the total incident wave energy, $E_{T,i}$):

$$E_{T,t} = E_{P,t} + E_{K,t} \tag{4.24}$$

Where:

$$E_{P,t} = 0.5\rho g C \int_{t_1}^{t_2} \eta^2 dt \tag{4.25}$$

$$E_{T,K} = \int_{-\infty}^{\infty} \int_{-h}^{\eta} 0.5\rho C^2 \frac{\eta}{h+\eta} dz dt \tag{4.26}$$

g : gravitational acceleration [m/s²],
h : water depth [m],
C : wave celerity [m/s],
η : water free surface elevation [m]
ρ : water density [kg/m³].

The K_t in terms of forces and energy as a function of the relative forest width $B/L_{i,gen}$ has at least two similarities with the K_t in term of wave energy (Fig. 4.36). Firstly, the K_T decreases as the relative forest width $B/L_{i,gen}$ increases. Secondly, the highest wave reduction for both approaches can be observed for the shallowest water depth h = 0.465 m, at which the minimum wave transmission rate is similar (K_t = 0.2). Moreover, the K_t in terms of energy shows more pronounce effects of the water depth where the most effective wave attenuation is achieved for the lowest water level (most waves break over the foreshore model) and decreases with increasing water depth (Fig. 4.36). While the minimum K_t from both approaches is similar, the maximum K_T in term of wave energy is much lower compared to K_t in term of forces (K_t= 0.76 in term of energy as compared to K_t= 0.99 in term of forces) and is clearly attributed to waves breaking behind the forest model (EM5). The differences between the results can be explained by the fact of applying the wave particle velocity c to both non-

breaking and breaking waves may be too simple (Eqs. 4.25 and 4.26) because the wave particle velocity is actually valid only for non-breaking wave conditions.

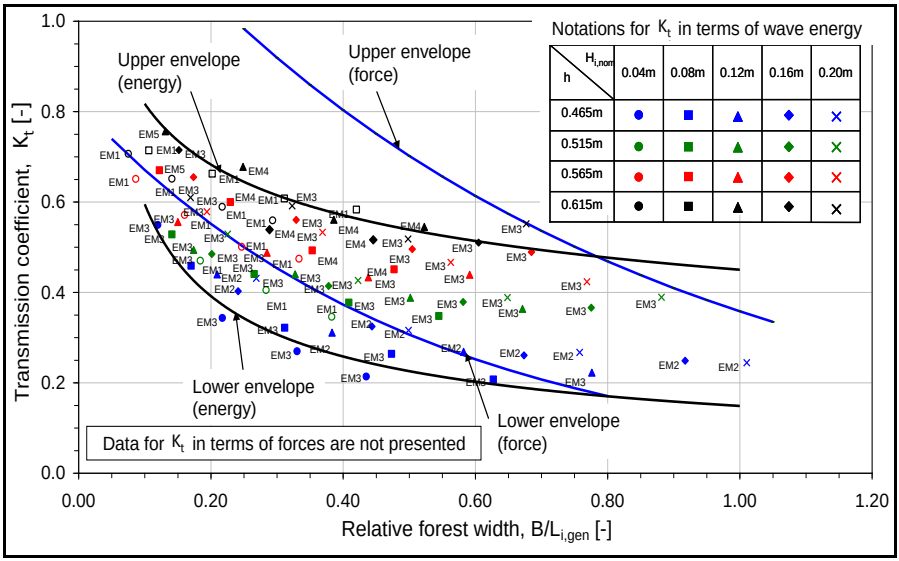

Fig. 4.36: Wave transmission coefficient for solitary waves in terms of wave-induced forces and wave energy (after Daenecke, 2010).

In order to see the effect of foreshore topography to the total wave attenuation, and by considering all forest widths, water depths h, and solitary wave heights $H_{i,nom}$, the transmission coefficient K_t in the 1 m- wide flume (without the forest) is also plotted as a function of relative forest width $B/L_{i,gen}$ (Fig. 4.37). Since there is no forest model in the 1 m- wide flume, forest width B is based on the forest width in the 2 m- wide flume for comparable results.

Fig. 4.37 indicates that the foreshore model may dissipate much of the wave energy, particularly for larger $B/L_{i,gen}$ values and this may confirm the role of topography and bathymetry in reducing the impact tsunami as mentioned by Chatenoux and Peduzzi (2005). The role of the forest model in tsunami damping increases as relative forest width $B/L_{i,gen}$ increases (Fig. 4.38). The highest K_t values for the upper and the lower envelopes of both results are almost similar

because at these points, the waves are in non-breaking conditions (EM1) in which the equations used also valid solely for non-breaking wave conditions. Moreover, the transmission coefficients as shown in Fig. 4.38 are comparable to the previously reported values from laboratory experiments, particularly for the range of K_t values. Harada *et al*. (2000) reported K_t values for porous media ranges from 1.0 – 0.5, while Kongko (2004) obtained the K_t in the range between 0.95 and 0.65 for mangrove models made of a group of cylinders. Using wires-made mangrove models, Istiyanto *et al*. (2003) obtained a wider range of K_t values (0.95 – 0.20). It should be noted here that those K_t values were derived based on different parameterized tree models as well as different foreshore models. Moreover, their models also did not take into account the influence of breaking wave conditions. For breaking and non-breaking wave conditions, however, Augustin *et al*. (2008) reported K_t values for a group of dowels subject to irregular waves in the range of 0.99 – 0.65. Additionally, the highest transmission coefficient was determined for non-breaking wave conditions, which is consistent with the results of the present study. The analysis indicates a great contribution of the foreshore topography to the wave damping in comparison to that of the mangrove forest.

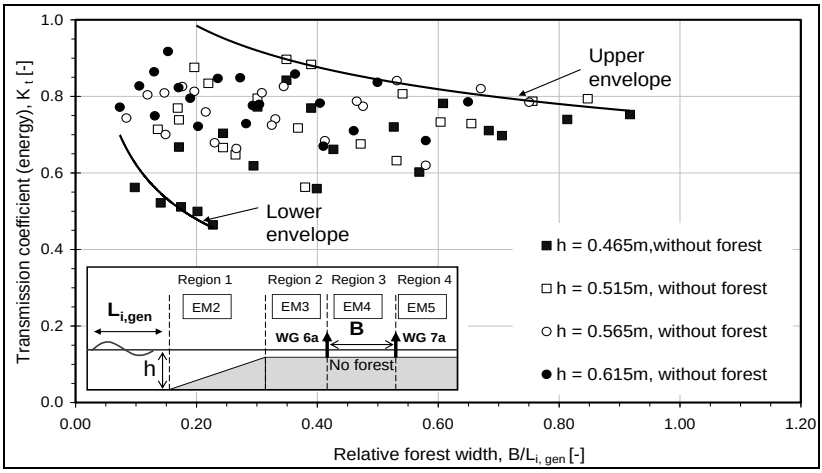

Fig. 4.37: Transmission coefficient in the 1 m- wide flume without the forest models (Husrin *et al.*, 2012b)

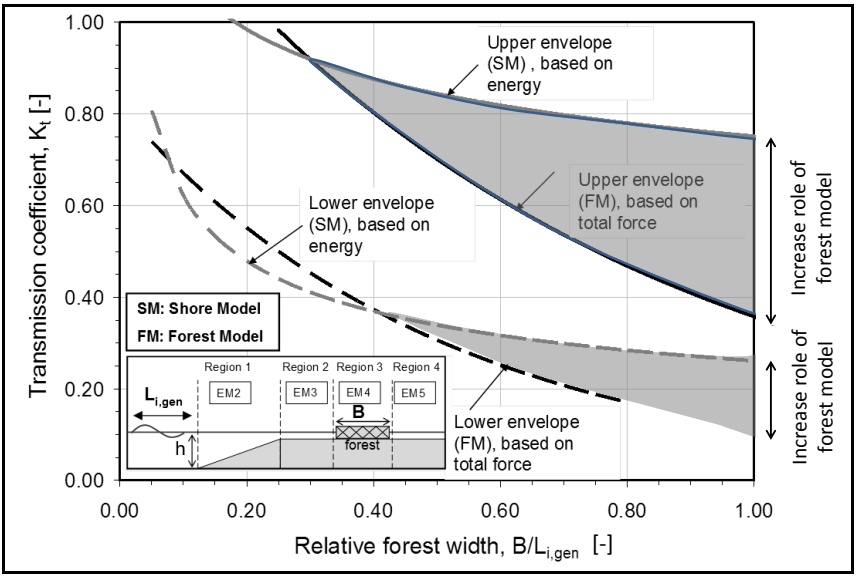

Fig. 4.38: Comparison of transmission coefficient based on force measurements (only forest model in the 2 m- wide flume) and wave gauge measurement (only (fore)shore model in 1 m- wide flume) (Husrin *et al.*, 2012a)

4.3.4 Drag coefficients of mangrove under solitary waves

The Morisson method has been implemented to derive the hydraulic resistance of mangrove forest subject to regular and irregular waves. For the solitary waves, however, this method cannot be used because of different data characteristics. Therefore, the analysis of the hydraulic resistance due to solitary waves, the least square method is used to derive C_D and C_M exerted by the mangrove forest model (see report Nr.10, Husrin and Oumeraci, 2012i).

The least square method to derive the hydraulic resistance was first used by Sarpkaya and Isaacson (1981) for the case of sinusoidal waves and the results are identical for the calculation of C_M and slightly different for C_D (Sumer and Fredsoe, 2006). Considering signal characteristics as shown exemplary in Fig. 4.33, methodologies other than the least squared method such as the Morison and

Fourier series methods are hardly able to be implemented for this type of signal (Husrin and Oumeraci, 2012i). Since simultaneous measurements of free surface elevation, current velocity, and hydraulic force at similar points (in front of and behind the forest model) are available, the least square method can be used to calculate the drag and inertia coefficients.

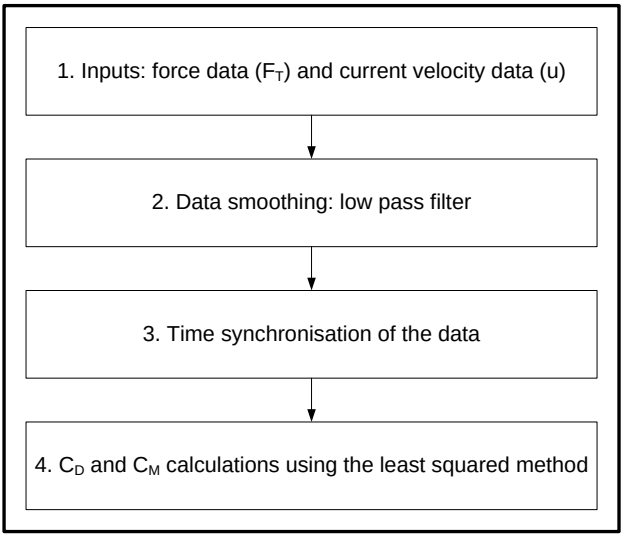

Fig. 4.39: Flow chart for the determination of drag and inertia coefficients using the Morison approach.

The collected data of the experiment with solitary waves provides horizontal total force F_T and horizontal flow velocity u. Therefore, the hydraulic resistance coefficients (C_D and C_M) can be directly derived using the least squared method. Fig. 4.39 shows the steps of the methodology to determine the hydraulic resistance of mangrove forest subject to solitary waves based on the least square method. The calculation of C_D and C_M with least squared method is carried out by means of MATLAB routines (Husrin and Oumeraci, 2012i).The derived C_D from all analyzed data ranges from 0.8 – 1.9 for R_e numbers between 1.24×10^5 – 1.2×10^6 (Fig. 4.40). C_D tends to be constant as R_e increases. The effects of different flow regimes, water depths, forest width, and wave conditions are less significant to the variation of C_D. This could be related to the following aspects:

- The characteristics of a solitary wave which is a transient wave where the flow velocities are relatively faster compared to the current velocity generated under regular and irregular waves. The current velocities by generated regular and irregular waves range between 0.05 – 0.36 m/s while for the solitary wave, the current velocities range between 0.25 m/s – 0.95 m/s.
- The fact that the submerged volume ratio V_m/V of the tree model is relatively much smaller compared to the V_m/V for the cases of regular and irregular waves.
- Larger current velocities and smaller V_m/V also lead to larger R_e ($1.24x10^5$ – $9.85x10^5$) compared to the cases of regular and irregular waves ($2x10^4$ - $3x10^5$).

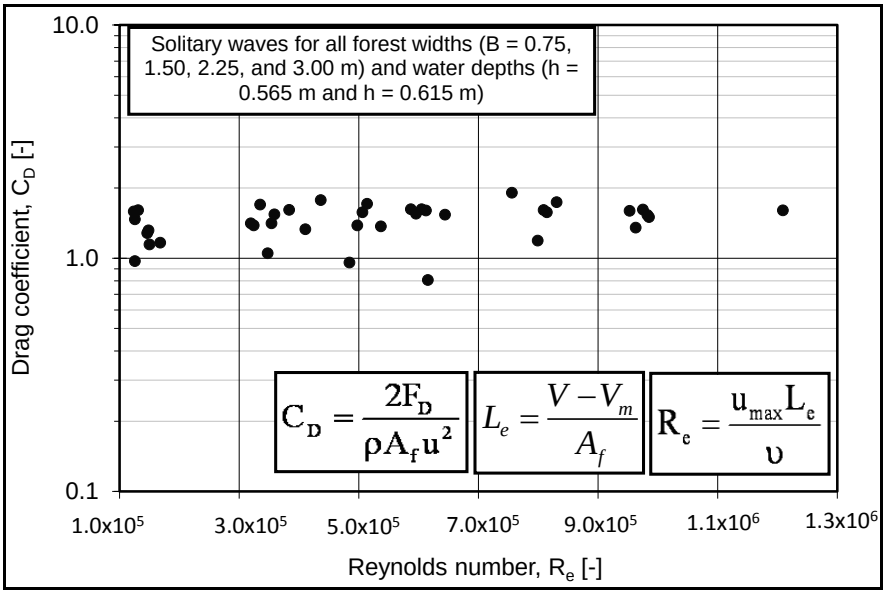

Fig. 4.40: Drag coefficient C_D as a function of R_e for all analysed data

The derived C_D as shown in Fig. 4.40 is in agreement with the previous results from the experiment in the current flume where the values of C_D for larger R_e and smaller V_m/V tends to be around C_D~1.0. By combining all the derived C_D from the experiments with steady current, regular/irregular waves and solitary

waves, the applicability of C_D for the whole range of R_e is complete and consistent. Moreover, smaller values of C_D for mangrove forest subject to solitary waves may explain the high transmission coefficients K_t as shown in Fig. 4.41 which mostly belong to the analysed data in the current study (all forest widths with water depths h = 0.565 m and 0.615 m).

The obtained C_D from solitary waves provide complete expression of C_D as a function of R_e. The results from current analysis also support the assumption that for tsunami-like waves such as the solitary wave, the C_D is no longer dependent on the Reynolds number R_e (Imai and Matsutomi, 2005; Yanagisawa *et al.*, 2009; and Huang *et al*., 2011). The selection of $C_D \sim 1$ or converged to the C_D value for a single cylinder by many authors for vegetation subject to tsunami wave has found its physical bases (Imai and Matsutomi (2005), USACE (1984), Yanagisawa *et al.* (2009), Huang *et a*l. (2011), Dekker (2006), Thuy *et al*. (2009) and Teo (2008)). The following are some physical aspects that influence the value of C_D exerted by mangrove forest with stiff structure assumption based on the analysis of both regular/irregular and solitary waves as shown in Fig. 4.41:

i. *Wave types*: Mangrove forest subject to regular/irregular waves tends to have larger C_D compared to the one subject to solitary waves
ii. *Wave conditions*: The generated wave heights and periods are associated with specific breaking wave locations. Mangrove subject to non-breaking wave conditions shows higher C_D compared to the one subject to breaking wave conditions.
iii. *Water depth:* The submerged volume ratio is a function of water depth. Because the roots are denser at the bottom, the C_D is also larger for the root subject to waves with smaller water depths/wave heights. As the water depth or wave height increases, the submerged volume ratio decreases or the effective length L_e increases (Mazda *et al*., 1997; Husrin and Oumeraci, 2009). The increase of effective length means the mangrove models turn to be highly sparse and consequently, the hydraulic resistance decreases.

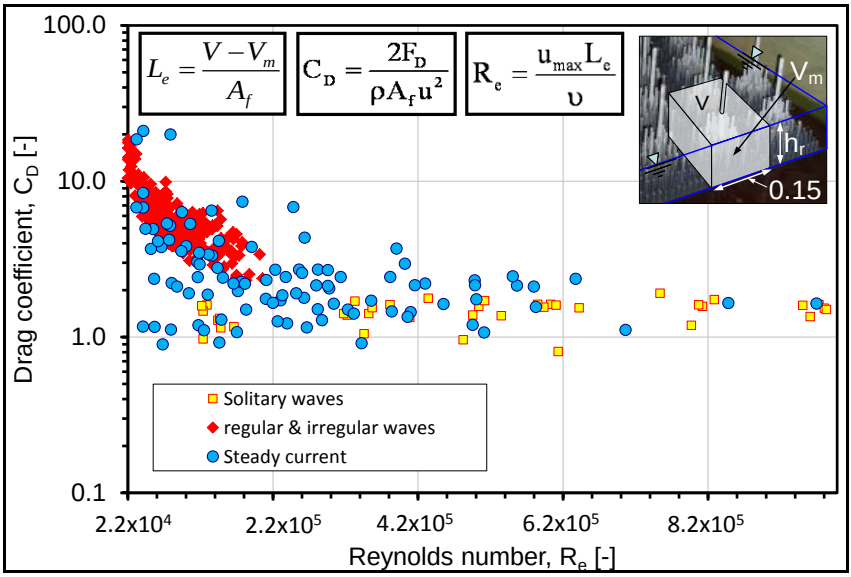

Fig. 4.41: Drag coefficient C_D as a function of R_e from the experiments with steady current, regular/irregular waves and solitary waves

4.3.5 Inertia coefficients of mangrove under solitary waves

The inertia coefficient C_M for solitary wave has been considered as less important compared to the drag coefficient C_D (e.g. Huang *et al.*, 2011) which is true for the case of purely non-breaking solitary wave. However, the measurements from the current study which include shoaling processes over the foreshore and breaking wave conditions show that significant flow acceleration exists for almost all cases, particularly at the very first impact as shown in Fig. 4.42 (Husrin and Oumeraci, 2012i). Moreover, the first impact of a solitary wave with any objects results in significant inertial forces as described by Imai and Matsutomi (2005) for the case of tsunami against coastal pine trees. Therefore, the resulted inertia coefficients in this study will explain the C_M exerted by the mangrove tree model subject to solitary waves.

The inertia coefficient C_M as a function of Reynolds number follows a similar pattern as the derived C_M from regular and irregular waves (Fig. 4.28 and Fig.

4.29). C_M variation over the range of R_e tends to be constant. As shown in Fig. 4.43, though the data cloud is more spreading, the averaged C_M is 1.81 which is almost identical to the averaged C_M from regular and irregular waves (C_M = 1.82). Two points of the data are considered as outliers due to unexplained small values of C_M. By putting the derived C_M from solitary waves and regular/irregular waves into one plot, Fig. 4.44 shows clearly that C_M from solitary wave belongs to larger R_e numbers.

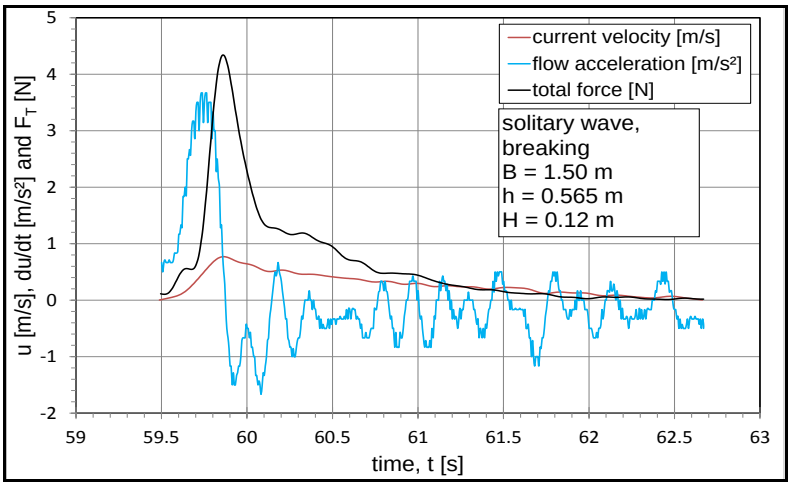

Fig. 4.42: Flow acceleration induced by solitary waves

As already discussed in the previous section, the derived C_M in the current analysis is in agreement with the work from Harada and Imamura (2000) in which they proposed a value of $C_M \sim 1.7$. Latief and Hadi (2006) also proposed a value of $C_M > 1$ for forest models with V_m/V larger than 0.06. In the recent study, the range of V_m/V is larger, between 0.02 – 0.20, so that the suggested averaged value $C_M \sim 1.81$ is consistent with the results of the previous studies. Identical C_M - values for mangrove forest subject to both regular/irregular waves and solitary waves indicate that the C_M is more deterministic to the total hydraulic resistance of the forest where influencing parameters such as water depth, wave conditions, breaking wave locations, and submerged volume ratio/frontal area are very significant.

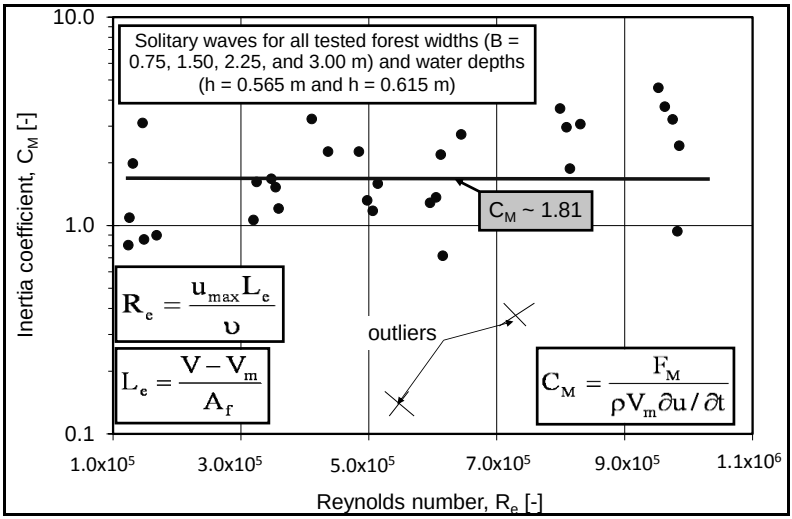

Fig. 4.43: Inertia coefficient C_M as a function of R_e number for irregular waves

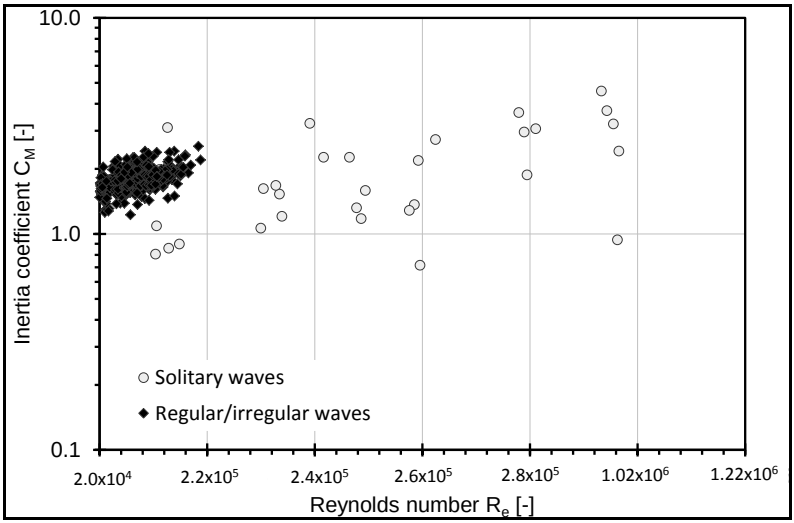

Fig. 4.44: Inertia coefficient C_M as a function of R_e number for regular/irregular waves and solitary waves

4.3.6 Remarks on solitary wave attenuation by mangrove forests

The following are key findings from the analysis of solitary wave attenuation by mangrove forest:

- The evolution mode of solitary wave has proved to be a powerful bases for the analysis of solitary wave attenuation either in terms of transmission coefficient (global process) or hydraulic resistance (local process). Determination of evolution mode in a very first stage also provides meaningful information to distinguish the contribution of foreshore topography and forest model to the total wave attenuation.

- The analysis of transmission coefficient of solitary wave propagation over the shore and mangrove forest models should consider wave energy approach because highly nonlinear characteristics of solitons. Combined with the analysis of force transducers and the knowledge on the evolution modes, both approaches have been successfully distinguished the contribution of forest and shore models to the total solitary wave attenuation.

- The derived hydraulic resistance in terms of C_D and C_M are consistent with previous model tests employing steady current and regular/irregular waves as wells as previous reported studies. Moreover, current studies provide more physical evidence showing that the hydraulic resistance is highly dependent on submerged body characteristics (i.e. frontal area and submerged volume ratio), wave types, wave conditions and water depths. In another word, the hydraulic resistance coefficient should be described as a function of flow regimes. The obtained hydraulic resistance coefficients of mangrove forest in current studies are $C_D \sim 1$ and $C_M \sim 1.81$ with R_e ranges from $1.0 \times 10^5 – 1.3 \times 10^6$. These results provide important guidance for the selection of proper hydraulic resistance coefficients used in numerical simulations as a practical tool for the assessment of tsunami attenuation by coastal forest as will be discussed in more details in the following chapter.

5 Numerical simulation

The shallow water equation (SWE) based model, COMCOT Version 1.7, was used for the simulation of solitary wave propagation in the wave flume. The objective of the numerical simulation is to investigate the performance of mangrove forest against the impact of tsunami by reproducing the simulation of laboratory experiment in the twin wave flume (TWF) and to confirm the obtained hydraulic resistance of the coastal forest models tested.

The fundamental governing equations in COMCOT consist of conservation of mass and momentum equations in term of fluxes. As the tsunami propagates in deep water, the linear terms from the governing equations are sufficient. For a small area where earth rotation is negligible and the governing equations in 2D can be written as follows:

$$\frac{\partial \eta}{\partial t} + \left\{ \frac{\partial P}{\partial x} + \frac{\partial Q}{\partial y} \right\} = -\frac{dh}{dt} \tag{5.1}$$

$$\frac{\partial P}{\partial t} + gh\frac{\partial \eta}{\partial x} - fQ = 0 \tag{5.2}$$

$$\frac{\partial Q}{\partial t} + gh\frac{\partial \eta}{\partial y} + fP = 0 \tag{5.3}$$

When tsunami reaches shallower water, the nonlinear terms should also be included. Equations 5.1, 5.2 and 5.3 can also be rewritten with the inclusion of nonlinear terms and bottom frictions providing a nonlinear shallow water equation (NLSWE) based model as follows:

$$\frac{\partial \eta}{\partial t} + \left\{ \frac{\partial P}{\partial x} + \frac{\partial Q}{\partial y} \right\} = -\frac{dh}{dt} \tag{5.4}$$

$$\frac{\partial P}{\partial t}+\frac{\partial}{\partial x}\left(\frac{P^2}{H}\right)+\frac{\partial}{\partial y}\left(\frac{PQ}{H}\right)+gH\frac{\partial \eta}{\partial x}+F_x=0 \tag{5.5}$$

$$\frac{\partial Q}{\partial t}+\frac{\partial}{\partial x}\left(\frac{PQ}{H}\right)+\frac{\partial}{\partial y}\left(\frac{Q^2}{H}\right)+gH\frac{\partial \eta}{\partial y}+F_y=0 \tag{5.6}$$

In which:

$$H=\eta+h \tag{5.7}$$

$$F_x=\frac{gn^2}{H^{7/3}}P\sqrt{P^2+Q^2} \tag{5.8}$$

$$F_y=\frac{gn^2}{H^{7/3}}Q\sqrt{P^2+Q^2} \tag{5.9}$$

$$P=\int_{-h}^{\eta} u\,dz=u(h+\eta)=uH \tag{5.10}$$

$$Q=\int_{-h}^{\eta} v\,dz=v(h+\eta)=vH \tag{5.11}$$

Where:

g	: gravity acceleration [m/s^2]
P	: volumetric flux in x- direction (West-East) [m^3/s.m]
Q	: volumetric flux in y- direction (South-North) [m^3/s.m]
h	: water depth [m]
η	: water surface elevation [m]
H	: total water depth [m]
F_x, F_y	: bottom friction in x and y direction
n	: Manning roughness coefficient [s/m$^{1/3}$]
u	: flow velocity in x direction [m/s]
v	: flow velocity in y direction [m/s]

Numerical methodology solving equations 5.1- 5.6 in COMCOT is explicit leap-frog finite difference method. This numerical scheme discretizes time and space by second order central difference formulas. The accuracy of this scheme is in the order of $O(\Delta x^2, \Delta y^2, \Delta t^2)$. For the nonlinear governing equations, the linear terms are treated similarly using leap-frog central finite difference and the nonlinear terms in momentum equation, however, are evaluated using upwind numerical scheme. This scheme is selected because the nonlinear terms (which are advection terms) are computationally preferable as long as the velocity gradient is not exaggerated and satisfy the stability condition: $\sqrt{gh}\frac{\Delta t}{\Delta x} < 1$. More detailed discussions on this topic can be found in Husrin and Oumeraci (2012g).

5.1 Testing programme and experimental setup

Based on the results of the experiments and the observation of wave evolution modes (Strusińska and Oumeraci, 2009), some experimental setups belong to water depth h = 0.415 m, 0.456 m and 0.515 m, will not be considered for further numerical investigations because those experimental setup are dominated by breaking wave conditions in front of the forest model and in the foreshore slopes. These conditions result from highly nonlinear conditions as described by the values of local wave nonlinearity ($\varepsilon=H_{i,max}/d_r$) larger than 0.3 which is beyond the capability of the COMCOT model (Wang and Liu, 2010). Therefore, the performance of the model is tested by implementing only the two deepest water depths, h = 0.565 m and 0.615 m. Table 5.1 shows the experimental setup for all forest widths with variation of wave heights. High values of nonlinearity $\varepsilon > 0.3$ are still observed. These will allow us to test the capability of COMCOT model for high nonlinearity.

In general, the setup consists of two conditions, namely: with and without the forest model. For the setup without the forest model, uniform Manning roughness coefficient, *n* is applied for the surface model domain. The example of model setup with uniform Manning roughness coefficient is shown in Fig. 5.1. For the setup with the presence of forest model, an approach of equivalent Manning

roughness coefficient, n_e is applied. The value of equivalent Manning roughness coefficient is a function of hydraulic resistance, i.e. drag coefficient, C_D. The equivalent Manning roughness coefficient has been used by many modellers due to its practical implementation and has been validated by the Morison equations (resulting in similar results) (Teh *et al.* (2009), Yanagisawa *et al*. (2009), Kongko (2012)). The equivalent Manning roughness coefficients as a function of C_D is formulated as follows (Yanagisawa *et al.*, 2009):

$$n_e = \sqrt{\frac{H_r^{4/3}}{2gV}(C_D A_f) + n_b^2} \tag{5.12}$$

Where:

C_D : drag coefficient [-]
g : gravitational acceleration [m/s^2]
A_f : frontal area of forest model [m^2]
n_b : Manning roughness for the bed surface [s/m$^{1/3}$]
V : control volume as a function of water depth [m^3]
H_r : total water depth (h+η) [m]

By implementing equation 5.12, the equivalent Manning roughness coefficients, n_e for the simulation of mangrove forest subject to solitary waves are shown in Table 5.2. The value of C_D = 1.5 is taken from the averaged C_D from laboratory experiment of mangrove forest models subject to solitary waves[10]. Fig. 5.2 shows the model setup by implementing the equivalent Manning roughness coefficients, n_e = 0.13 (with forest model).

[10] More detailed information in Report Nr.10 (Husrin and Oumeraci, 2012i)

Table 5.1: Experimental setup (h=0.565m & 0.615m) for different wave heights

Forest width, B [m]	Water depth, h [m]	Wave height, $H_{i,nom}$ [m]	File name	Evolution Modes (EM)	Wave non-linearity $H_{i,max}/d_r$ [-]	Notes
0.75	0.615	0.04	200905151	EM1	0.27	
		0.08	200905151	EM1	0.63	
		0.12	200905151	EM5	1.04	
		0.16	200905180	EM3	1.39	
		0.20	200905180	EM3	1.53	
	0.565	0.04	200905111	EM1	0.37	
		0.08	200905111	EM4	0.89	
		0.12	200905111	EM3	1.39	
		0.16	200905180	EM3	1.73	
		0.20	200905180	EM3	2.13	
1.5	0.615	0.04	200910230	EM1	0.21	
		0.08	200910210	EM1	0.50	
		0.12	200910230	EM4	0.88	
		0.16	200910230	EM4	1.50	
		0.20	200910230	EM3	1.30	
	0.565	0.04	200910130	EM1	0.29	
		0.08	200910140	EM4	0.77	
		0.12	200910140	EM3	1.19	
		0.16	200910140	EM3	1.46	
		0.20	200910140	EM3	1.79	
2.25	0.615	0.04	200909100	EM1	0.24	
		0.08	200909101	EM1	0.54	
		0.12	200909101	EM4	0.95	
		0.16	200909101	EM4	1.23	2009111112
		0.20	200909101	EM3	1.39	2009111113
	0.565	0.04	200909040	EM1	0.32	
		0.08	200909040	EM4	0.87	
		0.12	200909040	EM3	1.28	
		0.16	200909040	EM3	1.57	
		0.20	200909070	EM3	1.91	
3	0.615	0.04	200907211	EM1	0.25	
		0.08	200907211	EM1	0.56	
		0.12	200907211	EM4	0.98	
		0.16	200907211	EM3	1.29	
		0.20	200907220	EM3	1.42	
	0.565	0.04	200907030	EM1	0.34	
		0.08	200907031	EM4	0.84	
		0.12	200907060	EM3	1.35	
		0.16	200907060	EM3	1.65	
		0.20	200907060	EM3	1.92	

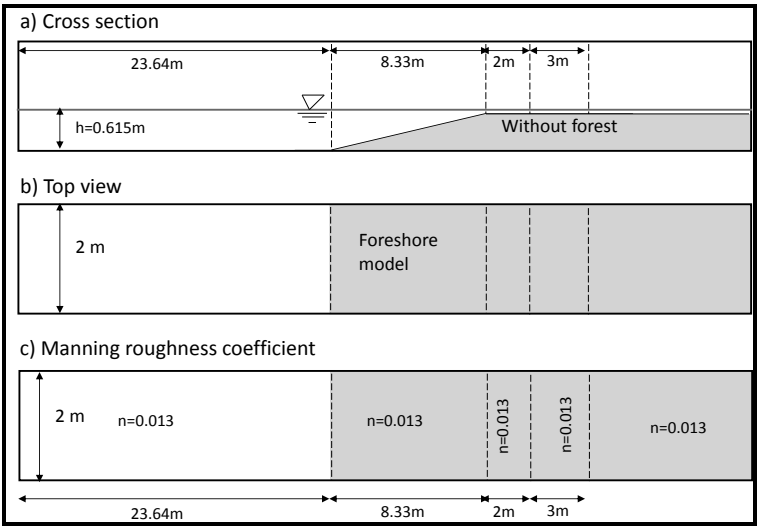

Fig. 5.1: Model set up with B = 3.0 m, h = 0.615 m without forest model

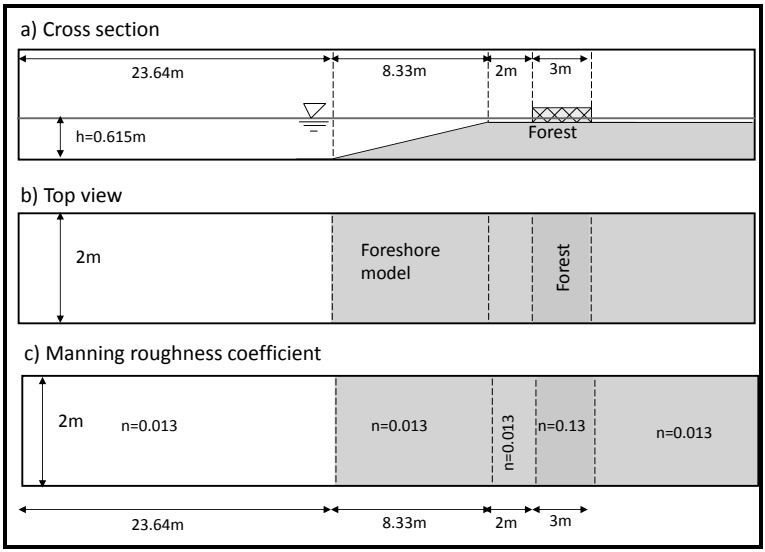

Fig. 5.2: Example of model set up with B = 3.0 m, h = 0.615 m with forest model

Table 5.2: Calculation of equivalent Manning roughness coefficient, n_e as a function of C_D

water depth, h [m]	local water depth, d_r [m]	$H_{i,max}$ [m]	total depth, H_r [m]	control volume, V [m^3]	frontal area, A_f [m^2]	drag coefficient, C_D [-]	bottom roughness,n_b [$sm^{-1/3}$]	equivalent Manning roughness, n_e [$sm^{-1/3}$]
0.615	0.20	0.04	0.24	0.0054	0.007	1.5	0.013	0.128
0.615	0.20	0.08	0.28	0.0063	0.007	1.5	0.013	0.131
0.615	0.20	0.12	0.32	0.0072	0.007	1.5	0.013	0.134
0.615	0.20	0.16	0.36	0.0081	0.007	1.5	0.013	0.136
0.615	0.20	0.20	0.40	0.0090	0.007	1.5	0.013	0.139
0.565	0.15	0.04	0.19	0.0042	0.007	1.5	0.013	0.123
0.565	0.15	0.08	0.23	0.0051	0.007	1.5	0.013	0.127
0.565	0.15	0.12	0.27	0.0060	0.007	1.5	0.013	0.130
0.565	0.15	0.16	0.31	0.0069	0.007	1.5	0.013	0.133
0.565	0.15	0.20	0.35	0.0078	0.007	1.5	0.013	0.136
Averaged value of equivalent Manning roughness coefficients								0.123

5.2 Numerical simulation without forest model

Numerical simulation using COMCOT model for the propagation of solitary waves on foreshore model without forest model are carried out for the smallest and the widest forest width (B = 0.75 m and 3.00 m). The purpose of simulating this model setup is to check the use of selected Manning roughness coefficients for the bed surface of the flume. The selected value of Manning roughness coefficient, n_b is 0.013. Models scenarios are presented in Table 5.2 and the results of simulation are presented in table 5.3, table 5.4, fig. 5.3 and fig. 5.4. The complete tables and plots of the simulation results are in Husrin and Oumeraci, (2012k).

Table 5.3: Numerical simulation scenarios for B = 0.75 m with constant Manning roughness n_b = 0.013 (solitary waves)

No	Bath-file	Input wave	Forest width	Wave height, $H_{i,nom}$	Manning roughness, n_b		
					Bed	Forest	Platform
4	layer01.dep	2009051110.dat	0.75	0.04	0.013	0.013	0.013
5	layer01.dep	2009051111.dat	0.75	0.08	0.013	0.013	0.013
6	layer01.dep	2009051112.dat	0.75	0.12	0.013	0.013	0.013
7	layer01.dep	2009051803.dat	0.75	0.16	0.013	0.013	0.013
8	layer01.dep	2009051804.dat	0.75	0.20	0.013	0.013	0.013
9	layer01.dep	2009051510.dat	0.75	0.04	0.013	0.013	0.013
10	layer01.dep	2009051511.dat	0.75	0.08	0.013	0.013	0.013
11	layer01.dep	2009051512.dat	0.75	0.12	0.013	0.013	0.013
12	layer01.dep	2009051801.dat	0.75	0.16	0.013	0.013	0.013
13	layer01.dep	2009051802.dat	0.75	0.20	0.013	0.013	0.013
14	layer01.dep	2009101309.dat	1.50	0.04	0.013	0.013	0.013
15	layer01.dep	2009070309.dat	3.00	0.04	0.013	0.013	0.013
16	layer01.dep	2009070310.dat	3.00	0.08	0.013	0.013	0.013
17	layer01.dep	2009070601.dat	3.00	0.12	0.013	0.013	0.013
18	layer01.dep	2009070602.dat	3.00	0.16	0.013	0.013	0.013
19	layer01.dep	2009070603.dat	3.00	0.20	0.013	0.013	0.013
20	layer01.dep	2009072110.dat	3.00	0.04	0.013	0.013	0.013
21	layer01.dep	2009072111.dat	3.00	0.08	0.013	0.013	0.013
22	layer01.dep	2009072112.dat	3.00	0.12	0.013	0.013	0.013
23	layer01.dep	2009072113.dat	3.00	0.16	0.013	0.013	0.013
24	layer01.dep	2009072202.dat	3.00	0.20	0.013	0.013	0.013

Before analysing the simulation results, two indicators are introduced to measure the performance of the numerical simulations for the height and arrival time of the wave. They are defined as follows:

$$\varepsilon_H = \frac{H_{gen,\max}(simulation) - H_{gen,\max}(measurment)}{H_{gen,\max}(measurment)} x100\% \tag{5.13}$$

$$\varepsilon_{times} = t_{model} - t_{measurment} \tag{5.14}$$

where:

ε_H : error indicator for wave heights [%]
ε_{time} : error indicator for arrival time of wave [s]
$H_{gen,max}$: maximum generated wave height [m]
t_{model} : arrival time in simulation [s]
$t_{measured}$: arrival time in measurement [s]

Table 5.4: Computation vs. measurement for B=0.75m, $H_{i,nom}$ = 0.04 m, h = 0.615m (solitary waves)

2009051510.dat, B=0.75m, $H_{i,nom}$ = 0.04 m, h = 0.615m, ε = 0.27						Deviation of computation from measurement		Wave conditions
WG	$H_{gen,max}$ [m]	time [s]	SWG	$H_{gen,max}$ [m]	time [s]	Elevation [%]	time [s]	
1a	0.0399	13.72	1a	0.041	13.3	3.56%	-0.321	Non-breaking
5a	0.0483	18.45	5a	0.049	17.9	0.91%	-0.548	Non-breaking
6a	0.0467	19.43	6a	0.048	18.9	2.94%	-0.455	Non-breaking
7a	0.0464	19.83	7a	0.048	19.3	3.02%	-0.451	Non-breaking
8a	0.0469	20.45	8a	0.047	19.9	1.17%	-0.51	Non-breaking
11a	0.0442	21.85	11a	0.049	21.0	10.01%	-0.754	Near- breaking

Notes:

WG, wave gauge data from measurement

SWG, wave gauge data from model simulation

Table 5.4 and Table 5.5 as well as Fig. 5.3 and Fig. 5.4 show examples of two different simulation results with solitary waves from two different model setups (namely, non-breaking and breaking wave conditions). Table 5.4 and Fig. 5.3

show the performance of COMCOT model for non-breaking wave conditions with B = 0.75 m, h = 0.615 m, and $H_{i,nom}$ = 0.04 m (nonlinearity, ε = 0.27). The simulation almost reproduces wave propagation characteristics as observed in the wave flume. This is indicated by very small differences between the numerical simulation and the measurement for both wave heights and arrival times. The errors for wave heights are less than 4% for all validation points (from deeper water depth to shallower and further water depths). The error is less than 5% and satisfies the benchmarking requirement of a numerical simulation with non-breaking wave conditions (Synolakis, *et al.*, 2007). Moreover, the timing errors for wave arrival are less than 1 s for all conditions. This result shows that the selection of n_b = 0.013 is justified. This result is also in agreement with other simulation with, i.e. for B = 3.0 m with ε < 0.3.

Table 5.5: Computation vs. measurement for B =3.00m, $H_{i,nom}$ = 0.2 m, h = 0.565 m (solitary waves)

2009070603.dat, B=0.30m, $H_{i,nom}$ = 0.20m, h = 0.565m. ε= 1.92						Deviation of computation from measurement		Wave conditions
WG	$H_{gen,max}$ [m]	time [s]	SWG	$H_{gen,max}$ [m]	time [s]	Elevation [%]	time [s]	
1a	0.1978	17.06	1a	0.1907	16.4	-3.58%	-0.62	nearly breaking
5a	0.2749	21.07	5a	0.1348	20.6	-50.96%	-0.447	Breaking
6a	0.1886	21.86	6a	0.1229	21.6	-34.86%	-0.222	Broken
7a	0.1216	23.31	7a	0.1090	23.2	-10.36%	-0.082	Broken
8a	0.1129	23.89	8a	0.1039	23.8	-7.98%	-0.068	Broken
11a	0.0911	25.06	11a	0.0954	25.0	4.76%	0.026	Broken

Notes

WG: wave gauge data from measurement

SWG: wave gauge data from model simulation

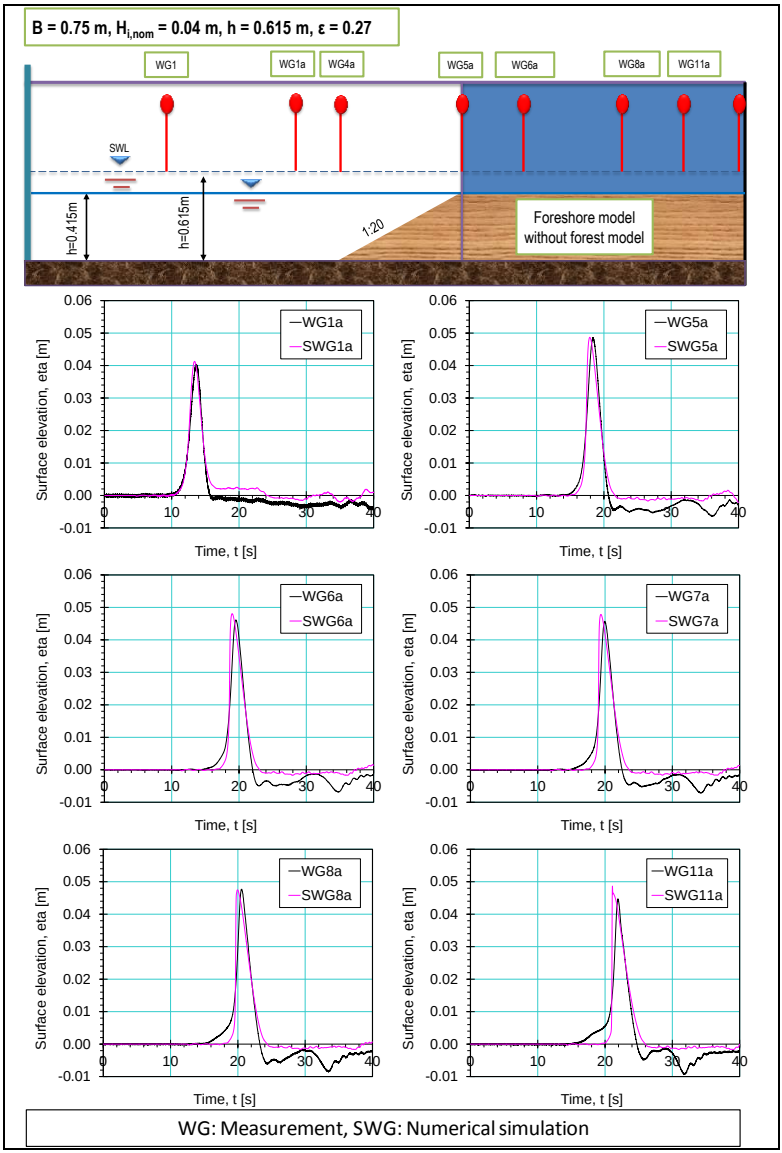

Fig. 5.3: Numerical simulation vs. measurement for B=0.75m, $H_{i,nom}$ = 0.04 m, h = 0.615m (solitary waves)

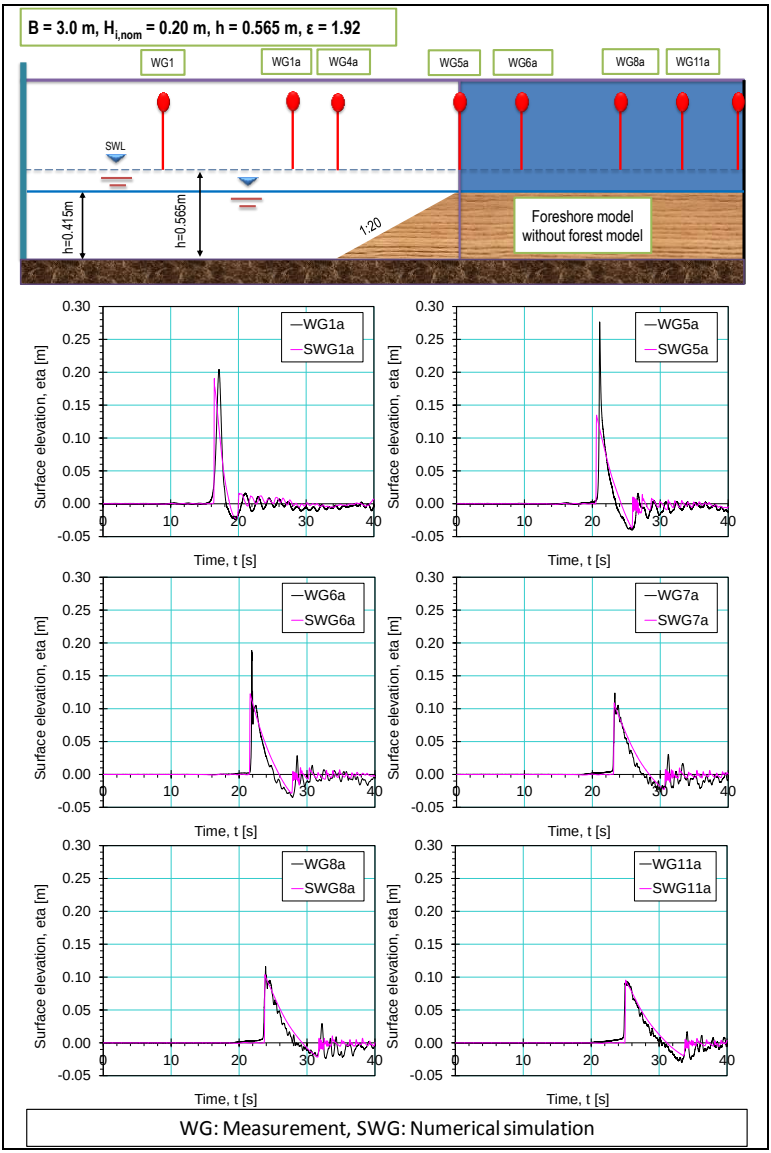

Fig. 5.4: Numerical simulation vs. measurement for B=3.00m, $H_{i,nom}$ = 0.2 m, h = 0.565 m (solitary waves)

For the case of numerical simulations with breaking wave conditions, the model performance has serious limitations, due to the nature of COMCOT as an SWE based model. Thus, breaking wave conditions will never exactly be reproduced in the simulations. However, the following patterns can be concluded from the simulation with higher nonlinearity:

- *For non-breaking wave conditions* in deeper water, the wave height obtained from the simulation are still in good agreement indicated by small error (<10%). *For non-breaking wave conditions*, errors of the SWE based model less than 20% are acceptable as described by Synolakis *et al.*, (2007) for the cases of tsunami runup in a conical island and Okushiri island (laboratory tests).
- Time arrival performs well for all conditions with $\varepsilon_{time} < 1$ s
- *For near-breaking or in breaking wave conditions*, error indicator for wave heights ε_H is very large. This is due to the fact that COMCOT is unable to produce narrow wave peaks generated by breaking wave conditions.
- For fully broken wave conditions, error indicator ε_H turns smaller and reaches its minimum at the last of the validation points or WG11a (Fig. 5.3 and Fig.5.4).

The simulation with B = 3.0 m, h = 0.565 m and $H_{i,nom}$ = 0.20 m represents the most extreme conditions reproduced in the wave flume as indicated by the highest nonlinearity parameter $\varepsilon > 1.92$. Table 5.5 and Fig. 5.4 show the pattern of wave propagation as mentioned above.

From the discussion with the numerical simulations of the model set up in the wave flume without the forest model, the following conclusions are drawn:

- The selected Manning roughness coefficient, n_b, for the flume bed is 0.013. This value is equivalent with the value of Manning roughness coefficient of smooth concrete surface proposed by Chow (1959).
- The limitations of the COMCOT model for high nonlinearity parameter values ($\varepsilon > 0.3$) should be taken into consideration when performing simulations with the presence of mangrove model. It is therefore more appropriate to perform the analysis for high nonlinearity parameters by comparing only the first and the last validation points (i.e. WG5,

WG13, WG17 and WG21 (Fig. 5.5). Moreover, the model setup with $H_{i,nom} > 0.08$m will not be considered due to the associated high values of nonlinearity parameter ε.

- The selected Manning roughness coefficient provides satisfactory agreement (for both wave height and arrival time) between the numerical simulation and the measurement in the wave flume without the presence of mangrove model for non-breaking conditions. For wave breaking conditions, however, only the results related to the arrival time are still in an acceptable range while those related to the wave heights are difficult to assess due to the inherent limitations of the SWE based models.

Table 5.6: Numerical simulation vs. measurement for all tested forest widths B with $\varepsilon < 0.3$

Forest width, B [m]	Evolution mode	Water depth, h [m]	Wave height, $H_{i,nom}$ [m]	Measurement		Simulation		Elevation error [%]	Notes
				WG	$H_{gen,max}$ [m]	SWG	$H_{gen,max}$ [m]		
0.75	EM1	0.615	0.04	5	0.0419	5	0.041	-1.51	Non-breaking
				13	0.0520	13	0.049	-4.81	Non-breaking
				17	0.0467	17	0.046	-2.59	Non-breaking
				21	0.0474	21	0.045	-5.94	Near-breaking
1.50	EM1	0.615	0.04	5	0.0371	5	0.037	-1.18	Non-breaking
				13	0.0425	13	0.044	3.97	Non-breaking
				17	0.0362	17	0.039	6.69	Near-breaking
				21	0.0349	21	0.038	9.28	Breaking
2.25	EM1	0.615	0.04	5	0.0396	5	0.039	-0.37	Non-breaking
				13	0.0470	13	0.047	0.98	Non-breaking
				17	0.0373	17	0.038	2.07	Non-breaking
				21	0.0352	21	0.039	10.15	Breaking
3.00	EM1	0.615	0.04	5	0.0404	5	0.041	0.46	Non-breaking
				13	0.0464	13	0.049	4.64	Non-breaking
				17	0.0335	17	0.037	9.72	Near-breaking
				21	0.0344	21	0.038	9.10	Breaking

5.3 Numerical simulation with forest models

The simulation is carried out for all forest widths B investigated in the laboratory, two water depths (h = 0.565 m and 0.615 m) and two wave heights, $H_{i,nom}$ = 0.04 m and 0.08 m or belongs to Evolution Mode EM1 (non-breaking), EM4 (breaking inside the forest) and EM5 (breaking behind the forest) (Strusinska and Oumeraci, 2009). For the cases with nonlinear parameter $\varepsilon < 0.3$ (EM1 with h = 0.615 m and $H_{i,nom}$ = 0.04 m), the numerical simulations reproduced the measured results accurately. This is indicated by errors less than 5% for the first two validation points (WG5 and WG13). As the forest width is getting wider, the error for the last two validation points (WG17 and WG21) is also getting larger. This also shows the influence of forest width B on wave attenuation (Table 5.6). Moreover, large error appears because COMCOT is unable to simulate detailed breaking processes (i.e. the reproduction of solitons). Fig. 5.5 shows the examples of numerical simulation results with $\varepsilon < 0.3$. The results also show that the introduced hydraulic resistance (C_D = 1.5) for the forest model in the form of equivalent Manning roughness coefficient work sufficiently.

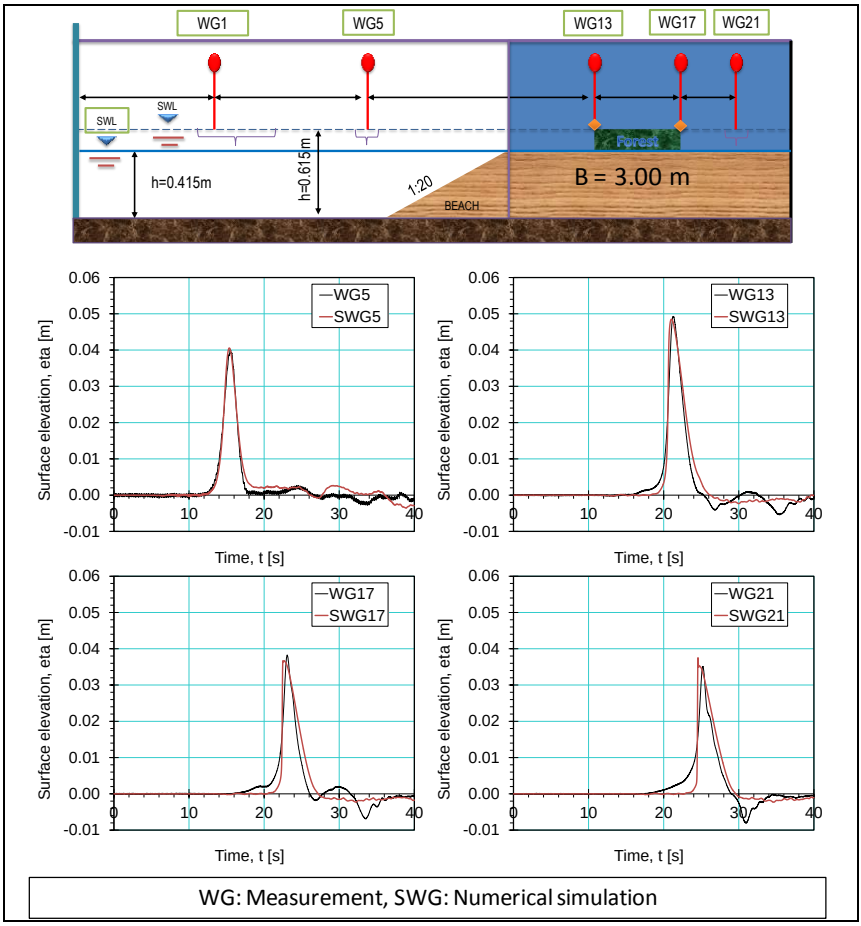

Fig. 5.5: Numerical simulation results for B = 3.00 m, $H_{i,nom}$ = 0.04 m, h = 0.615 m (EM1) with $\varepsilon < 0.3$

Table 5.7: Numerical simulation vs. measurement for all tested forest widths B with $\varepsilon > 0.3$

Forest width	Evolution mode	Water depth, h [m]	Wave height, $H_{i,nom}$ [m]	Measurement		Simulation		Elevation error [%]	Notes
				WG	$H_{gen,max}$ [m]	SWG	$H_{gen,max}$ [m]		
0.75	EM4	0.565	0.08	5	0.0863	5	0.083	-3.37	Non-breaking
				13	0.1339	13	0.082	-39.03	Breaking
				17	0.1379	17	0.072	-48.07	Breaking
				21	0.1048	21	0.065	-38.44	Breaking
1.50	EM4	0.565	0.08	5	0.0765	5	0.075	-1.71	Non-breaking
				13	0.1081	13	0.081	-25.13	Breaking
				17	0.1146	17	0.067	-41.65	Breaking
				21	0.0827	21	0.060	-27.03	Breaking
2.25	EM4	0.565	0.08	5	0.0807	5	0.079	-1.97	Non-breaking
				13	0.1226	13	0.078	-36.02	Breaking
				17	0.0938	17	0.053	-43.83	Breaking
				21	0.0824	21	0.047	-42.50	Breaking
3.00	EM4	0.565	0.08	5	0.0827	5	0.082	-1.17	Non-breaking
				13	0.1266	13	0.081	-36.28	Breaking
				17	0.0824	17	0.048	-41.99	Breaking
				21	0.0761	21	0.044	-42.79	Breaking

For the cases with nonlinear parameter $\varepsilon > 0.3$ (EM4 with h = 0.565 m and $H_{i,nom}$ = 0.08 m), the numerical simulation results actually reproduce the decay of the wave height associated with breaking waves. However, due to the inability of COMCOT to simulate detailed breaking wave processes, large deviations from the measured results occur at locations WG 13, WG 17 and WG 21(Fig. 5.6). These large errors are definitely related to the breaking wave associated processes as depicted in the measurement signals which cannot be simulated by the NLSWE model. However, large parts of wave forms and the arrival times are still maintained as shown in Fig. 5.6 and Table 5.7.

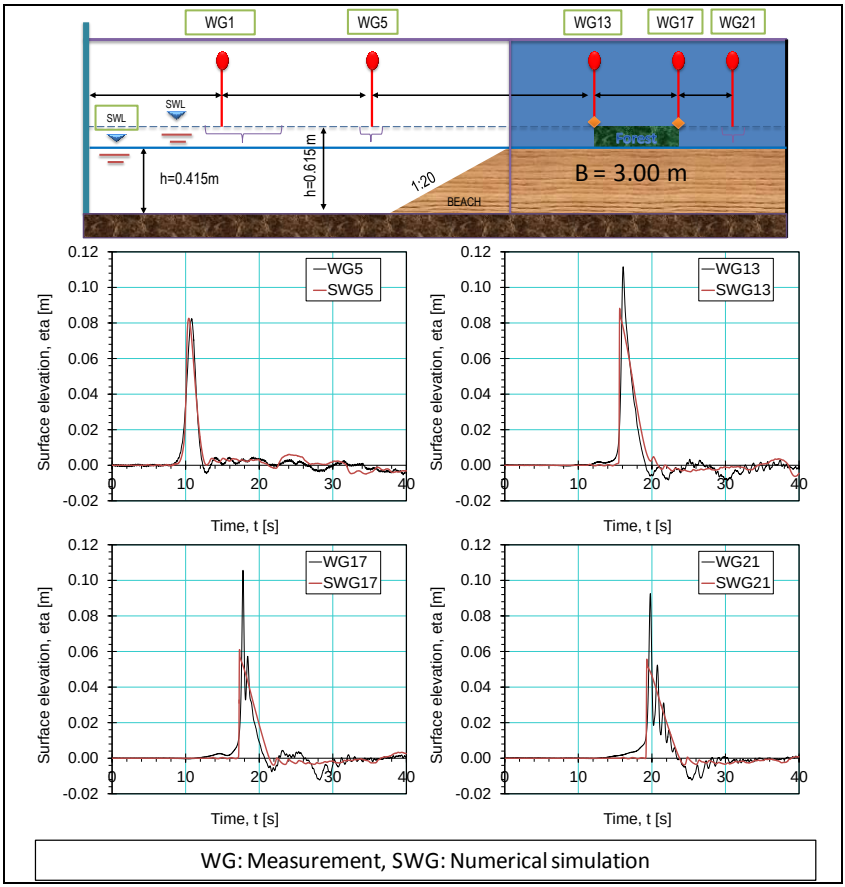

Fig. 5.6: Numerical simulation results for B = 3.00 m, $H_{i,nom}$ = 0.08 m, h = 0.565 m (EM4) with ε > 0.3

5.4 Effects of forest width

The effect of forest width B on the wave attenuation performance of the forest in the physical model is limited until B = 3 m (or 75 m in the prototype). Therefore,

based on the relatively good performance of COMCOT simulation results in the case of non-breaking wave conditions, wider forest widths can also be investigated numerically. The additional forest widths considered in the numerical simulation are B = 5 m and 7 m (125 m and 175 m at prototype scale, respectively). The numerical setup follows those related to the other forest widths. Only two water depths (h = 0.615 m and h = 0.565 m) and two solitary wave heights ($H_{i,nom}$ = 0.04 and $H_{i,nom}$ = 0.08 m) are considered in the simulation.

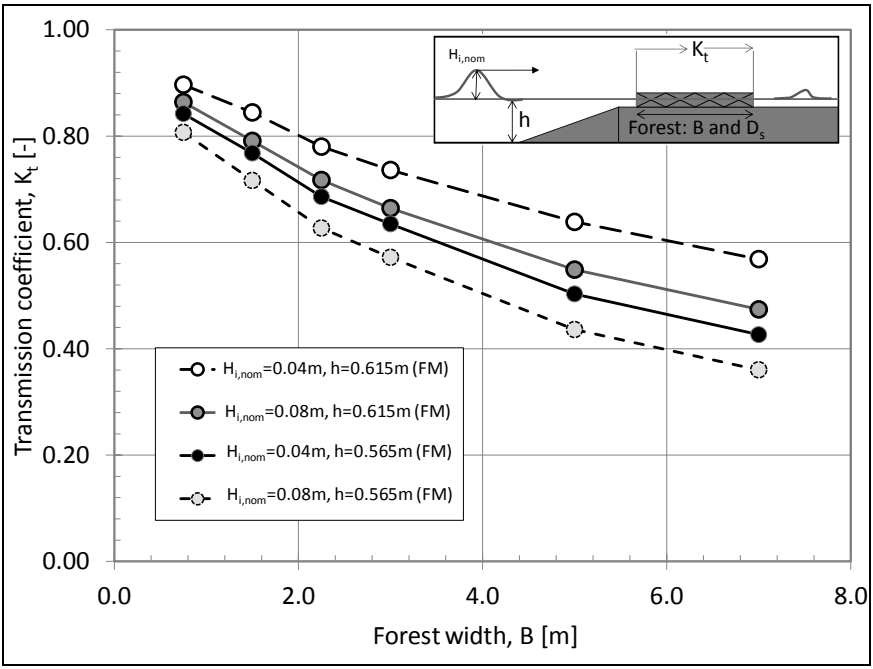

Fig. 5.7: Transmission coefficients K_t as a function of forest width B

The wave attenuation is described by transmission coefficient K_t. The calculation of K_t follows the concept of wave energy as described in section 4.3.3, equations 4.23 – 4.26. Only the wave transmission due to the forest model itself (FM) is considered in the numerical simulation. Therefore, coefficient K_t is based on the ratio of the wave height prevailing just in front of the forest to that just at the end of the forest. The relationship between K_t and forest width B for B = 0.75- 7.00

m is illustrated in Fig. 5.7. It shows clearly that an increase of forest width B results in a significant decrease of K_t. Moreover, the effects of the water depth and wave height also contribute to the evolution of K_t. The increase of water depth clearly increases the K_t while the increase of wave height reduces the K_t. The reduction of K_t as the wave height increases are related to the early breaking wave conditions in front of the forest models or on the slope of the foreshore topography as clearly observed during the tests.

5.5 Effects of forest density

Due to technical difficulties and the limited time frame of the study, the effect of forest density was not investigated in the physical model tests. The distance between tree models D_s (distance between individual trunk) in the physical model test is 15 cm or 3.75 m in the prototype (tree density, $N_s = 0.06$ tree/m^2) (Fig. 5.8). According to Mulia (2004), feasible forest density in mangrove forests planted for a commercial purpose to obtain optimum woods production may be classified in three categories characterised by the following distances between the tree trunks at prototype scale: 2x1m, 2x2m and 3x2m. Therefore, by considering the forest densities corresponding to these different distances and drag coefficient $C_D = 1.5$ (see Section 3.3.8) the equivalent Manning roughness coefficients should be recalculated using eq. 5.1. as shown in Table 5.8.

Table 5.8: Equivalent Manning roughness n_e for different forest density

No.	Distance in prototype [m]	Density in prototype, N_s [tree/m^2]	Averaged distance between tree, D_s [m]	Equivalent Manning roughness, n_e [sm$^{-1/3}$]
1	2.00x1.00	0.500	1.50 (0.06)	0.32
2	2.00x2.00	0.250	2.00 (0.08)	0.23
3	3.00x2.00	0.167	2.50 (0.10)	0.19
4	3.75x3.75	0.066	3.75 (0.15)	0.13

*) values in brackets are model values

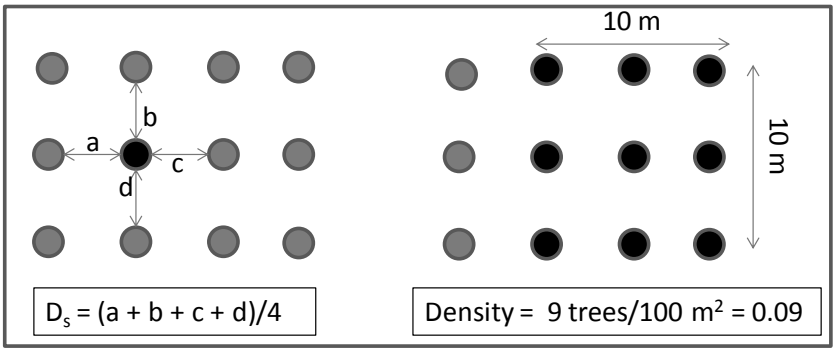

Fig. 5.8: Definitions of averaged distance D_s and forest density

The simulation results of K_t due to the forest model (FM) for different forest densities and different forest widths are given in Fig. 5.9, showing that the effect of forest density is significantly large. For B = 0.75 m, $H_{i,nom}$ = 0.04 m and h = 0.615 m, the maximum K_t due to n_e = 0.13 (D_s = 3.75 m) is 0.89 while for n_e = 0.32 (D_s =1.5 m) it decreases by 27% (K_t = 0.65). For higher nonlinearity of the waves (this means shallower water depth and higher wave height) the reduction of K_t is even higher. For example, for the simulation with B = 0.75 m, H = 0.08 m and h = 0.565 m, the K_t decreases by 35% from K_t = 0.81 (n_e = 0.13 or D_s =3 .75) to K_t =0.52 (n_e = 0.32 or D_s = 1.5) (see Fig. 5.9a and Table 5.9).

Table 5.9: Wave transmission coefficient K_t for forest widths B = 0.75 m and B = 7.00 m and different forest densities characterised by average distance D_s between the trees (see also Fig. 5.9)

B [m]	h [m]	D_s [-] (Prototype)	D_s [-] (Model)	n_e [$sm^{-1/3}$]	$H_{i,nom}$ [m]	K_t [-]		K_t reduction [%]
0.75	0.615	3.75	0.15	0.13	0.04	0.8967	Max	27%
0.75	0.615	2.50	0.10	0.19	0.04	0.8140		
0.75	0.615	2.00	0.08	0.23	0.04	0.7593		
0.75	0.615	1.50	0.06	0.32	0.04	0.6502	Min	
0.75	0.615	3.75	0.15	0.13	0.08	0.8640	Max	30%

0.75	0.615	2.50	0.10	0.19	0.08	0.7719		
0.75	0.615	2.00	0.08	0.23	0.08	0.7143		
0.75	0.615	1.50	0.06	0.32	0.08	0.6007	Min	
0.75	0.565	3.75	0.15	0.13	0.04	0.8421	Max	34%
0.75	0.565	2.50	0.10	0.19	0.04	0.7342		
0.75	0.565	2.00	0.08	0.23	0.04	0.6703		
0.75	0.565	1.50	0.06	0.32	0.04	0.5558	Min	
0.75	0.565	3.75	0.15	0.13	0.08	0.8070	Max	35%
0.75	0.565	2.50	0.10	0.19	0.08	0.6978		
0.75	0.565	2.00	0.08	0.23	0.08	0.6320		
0.75	0.565	1.50	0.06	0.32	0.08	0.5217	Min	
7.00	0.615	3.75	0.15	0.13	0.04	0.5686	Max	65%
7.00	0.615	2.50	0.10	0.19	0.04	0.3913		
7.00	0.615	2.00	0.08	0.23	0.04	0.3106		
7.00	0.615	1.50	0.06	0.32	0.04	0.1980	Min	
7.00	0.615	3.75	0.15	0.13	0.08	0.4741	Max	69%
7.00	0.615	2.50	0.10	0.19	0.08	0.3111		
7.00	0.615	2.00	0.08	0.23	0.08	0.2409		
7.00	0.615	1.50	0.06	0.32	0.08	0.1470	Min	
7.00	0.565	3.75	0.15	0.13	0.04	0.4265	Max	71%
7.00	0.565	2.50	0.10	0.19	0.04	0.2669		
7.00	0.565	2.00	0.08	0.23	0.04	0.2031		
7.00	0.565	1.50	0.06	0.32	0.04	0.122	Min	
7.00	0.565	3.75	0.15	0.13	0.08	0.3603	Max	74%
7.00	0.565	2.50	0.10	0.19	0.08	0.2172		
7.00	0.565	2.00	0.08	0.23	0.08	0.1620		
7.00	0.565	1.50	0.06	0.32	0.08	0.0944	Min	

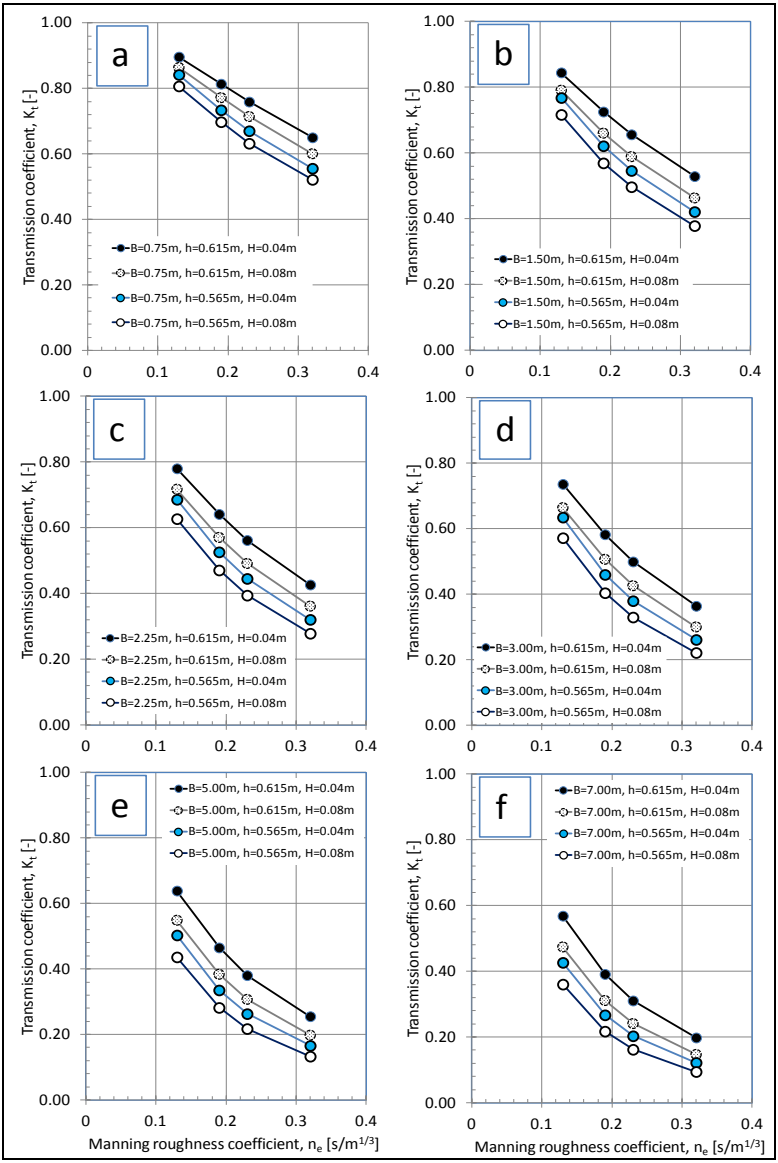

Fig. 5.9: Effect of forest density on the transmission coefficients K_t for different forest width B

For the case of wider forests, the wave reduction is even more significant. For example, for the case of B = 7 m, $H_{i,nom}$ = 0.08 m and h = 0.565 m, maximum K_t reduction reaches 74% from K_t= 0.36 to K_t =0.09. Therefore, forest width, wave height, water depth and forest densities are important parameters determining the transmission coefficients induced by the forest model (Fig. 5.9 and Table 5.9).

5.6 Formulation of wave attenuation induced by coastal forest

Forest width B and forest density described by D_s as well as local water depth h and wave height H are found to be important parameters determining the attenuation of solitary waves through the forest (wave transmission coefficient K_t).Therefore, a non-dimensional forest width factor involving all these parameters is introduced (ξ_{ff}):

$$\xi_{ff} = \frac{B}{D_s}\frac{H_f}{h_f} \tag{5.15}$$

Where:

ξ_{ff} : forest width factor [-]
B : forest width [m]
D_s : averaged distance between individual trees [m]
H_f : wave height in water depth h_f at the toe of foreshore slope [m]
h_f : local water depth at the toe of foreshore slope [m]

By using the new parameter ξ_{ff} in equation 5.15, transmission coefficient K_t is plotted as a function of forest width factor ξ_{ff} in Fig. 5.10 based on the simulations using the validated numerical model for B= 0.75 - 7.00 m, D_s = 1.5 – 3.75 m , H = 0.04 – 0.08 m and h = 0.565 – 0.615 m. The K_t is found to be not satisfactorily correlated to ξ_{ff} as shown in Fig. 5.10. Considering the high scatter of

the data and for safety reason, the upper envelope of the relationship between K_t and ξ_{ff} is selected for practical relationship of tsunami attenuation by mangrove forest:

$$K_t = e^{-0.13\xi_{ff}} \tag{5.16}$$

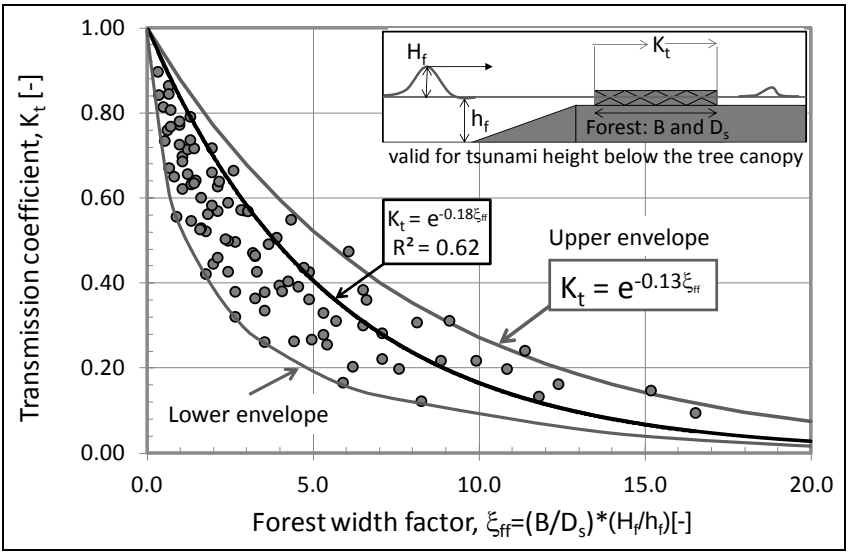

Fig. 5.10: Relationship of forest width factor ξ_{ff} to the transmission coefficients K_t

The expression shows that for the condition where the forest width B approaching zero (without forest) the transmission coefficient $K_t \sim 1.0$ while for the extremely wide forest, K_t approaches zero. It has to be underlined that the relationship shown in equation 5.16 is valid only for the case of tsunami height below the mangrove canopy and for a given foreshore topography. Therefore, for other cases, ones always have to consider the four important parameters composing the new non-dimensional forest width factor ξ_{ff} as defined in equation 5.16 as well as the foreshore topography to determine the wave transmission behind the forest.

This means for real prototype conditions, if we know that the expected tsunami height (from numerical simulation) in front of the coastal forest will be below the canopy (some authors mentioned explicitly < 5 m, e.g. Tanaka *et al.* (2006)), the attenuation performance of coastal forest due to tsunami for every location can be estimated by considering the forest width factor $\xi_{ff.}$ This means mangrove forests may still play important role in attenuating the impact of moderately high tsunami. This finding supports previous field reports mentioning that tsunami heights below the canopy may provide sufficient tsunami reduction (Table 5.10). Moreover, a closer look to Table 5.10 and considering typical geometry of mature mangroves and mature coastal pines as illustrated in Fig. 2.6, the observed tsunami heights which were effectively reduced the impact of tsunami are below the canopy.

For the cases where tsunami height reach the canopy or beyond, many additional effects may be important such as the wave attenuation performance of the canopy and the structural integrity of the trees. Such scenarios are associated with highly complex processes and interactions which depend on diverse factors (e-g. threshold for tree breakage and uprooting, debris flow, scour and sediment transport, detailed wave-tree and tree-tree interactions) that need much more investigations. Moreover, from the investigation of tree parameterisation with flexible structure assumption, the hydraulic resistance in term of C_D converges towards C_D~1.0. This means smaller C_D for water level beyond the canopy is expected or in another word the trees will hydraulically behave like a single stiff cylinder where the attenuation performance strongly depends on the geometry, density and structural integrity. Most trees, however, can not withstand tsunami height at or above canopy levels as they suffered from heavy scouring, uprooting, tilting or broken trunk. This is also confirmed by many results of field surveys from recent tsunami events showing that coastal forests do not provide sufficient protection for the cases of large tsunami heights as mentioned by Yanagisawa *et al*. (2009), Fritz *et al.* (2012), and Kongko (2012).

Table 5.10: Observed damping performance of coastal forests from past tsunami events (see Fig. 2.5 for tree dimensions at different ages)

No.	Tsunami height [m]	Forest characteristics					Tsunami height is above or below the canopy (est.)	Structural integrity	Tsunami attenuation	Field data locations	References *)
		Types	Age	Forest width	Trunk diameter	Tree density					
1	3	Mangroves	10 year old	500 m	no information	no information	Below the canopy	no information	70% hydraulic force	Banda Aceh, Indonesia	1
	> 4	Mangroves	10 year old	500 m	no information	no information	Reached the canopy	no information	None	Banda Aceh, Indonesia	1
	5	Mangroves	30 year old	500 m	no information	no information	Reached the canopy	no information	50% hydraulic force	Banda Aceh, Indonesia	1
2	3	Mangroves	no information	400 m	0.15 m	0.2 tree/m^2	Below the canopy	no information	26% inundation depth	Thailand	1
	3	Mangroves	no information	1000 m	0.15 m	0.2 tree/m^2	Below the canopy	no information	45% inundation depth	Thailand	1
	4.5	Mangroves	no information	400 m	0.15 m	0.2 tree/m^2	Below the canopy	50% survive	no information	Thailand	1
	> 6	Mangroves	no information	400 m	0.15 m	0.2 tree/m^2	Above the canopy	100% destroyed	None	Thailand	1
3	3	Many species	no information	no information	no information	30 cm/m^2	Below the canopy	Firmly standing	Observed	Srilanka & Thailand	2

	5	Mangroves and Pandanus	no information	no information	no information	80 cm/m^2	Reached the canopy	Damaged at the fringe	Observed	Srilanka & Thailand	2
	> 8	Mangroves and Pandanus	no information	no information	no information	80 cm/m^2	Above the canopy	destroyed	None	Srilanka & Thailand	2
4	15	Black pine	no information	200 m	no information	no information	Above the canopy	100% destroyed	None	Rikuzentakata, Japan	3
5	6	Black pine	no information	no information	no information	no information	Reached the canopy	Destroyed at the fringe	50% inundation depth	Hachinohe, Japan	4
6	8.5	Black pine	no information	200 m	no information	no information	Reached the canopy	80% Destroyed	Varied due to the presence of other barriers	Natori city, Japan	5

*)Notes for references: 1= Yanagisawa *et al.* (2010), 2 = Tanaka *et al.* (2006), 3 = Fritz *et al.* (2012), 4 = Cyranoski (2012), and 5 = World Bank (2012)

For practical consideration, the following stages can be used to estimate tsunami attenuation in terms of transmission coefficients by coastal forest vegetation (i.e. mangroves) at any locations assuming that the ages of the trees are in mid-age or mature stages (Fig. 5.11).

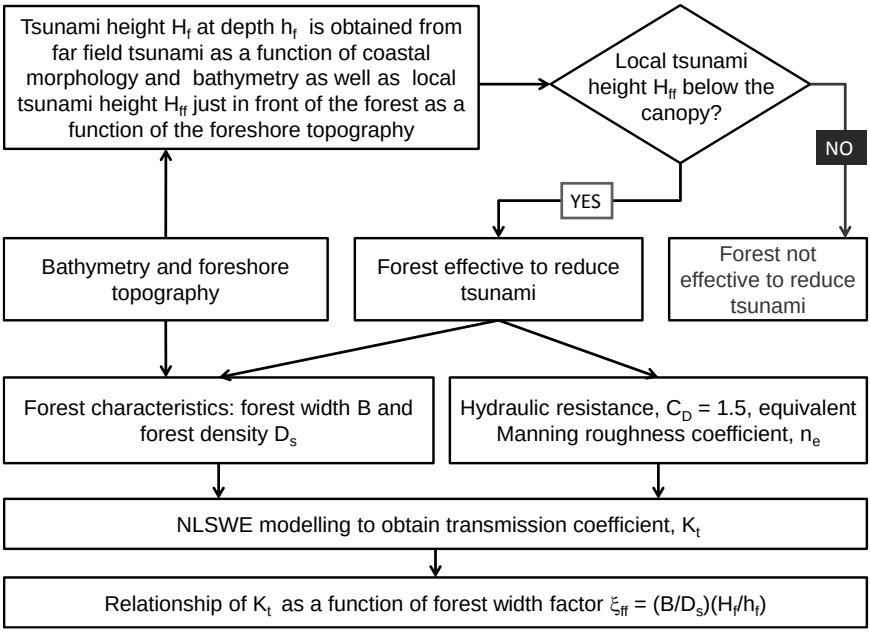

Fig. 5.11: Flow chart to assess tsunami attenuation by coastal forests such as mangroves

The flow chart shown in Fig. 5.11 is a practical methodology to assess tsunami attenuation by coastal forests in terms of transmission coefficient K_t. The first stage is to estimate the tsunami height in coastal waters (in front of the coastal forest). If the tsunami height is larger than the estimated canopy height of the trees, this means the coastal forest will not effectively reduce the tsunami considering that most trees will be destroyed (uprooted, broken trunk, tilted, laid down, etc). If the tsunami height is still below the canopy, the effectiveness of coastal forest to reduce incident tsunami height can be estimated by considering the effects of shore topography, bathymetry, forest characteristics (forest width and density) and the hydraulic resistance in terms of drag coefficient or equivalent Manning roughness. The bathymetry and topography data in large scale can be

obtained from freely accessible data (e.g. GEBCO[11] for bathymetry data, http://www.gebco.net or SRTM[12] for topography data, http://earthexplorer.usgs.gov/). Detailed bathymetry and topography data in the interest area are obtained through either hydrographical or aerial measurements (Multibeam echosounder survey, land survey, photogrammetry, LiDAR[13] or IfSAR[14]) to produce high quality Digital Elevation Model (DEM). There are two types of DEM namely Digital Terrain Model (DTM) and Digital Surface Model (DSM). For the purpose of tsunami propagation simulation through coastal forests, instead of DSM, high quality DTM data is preferable because the forest resistance can be implemented directly using the equivalent Manning roughness. Another advantage of using DTM is that it allows us to determine tsunami attenuation solely induced by shore topography by choosing the Manning roughness coefficients only for bare lands. In order to obtain a representative equivalent Manning roughness coefficient for a coastal forest, the forest characteristics should be carefully measured such as forest types (e.g: mangroves, coastal pine, etc), forest width (B), forest density (e.g. submerged volume ratio, V_m/V and averaged distance among individual tree, D_s), tree geometry (e.g: trunk diameter, tree height, etc) (see Section 3.1). The propagation of tsunami through the forest can be simulated by means of numerical model (i.e. NLSWE based model such as COMCOT) to estimate the transmission coefficient K_t. Several scenarios are worth to be implemented in order to increase the reliability of the obtained damping performance (tsunami attenuation). The transmission coefficients are calculated based on an energy approach to obtain the total energy at the beginning and at the end of the forest (see Section 4.3). The obtained K_t can be plotted against the forest width factor ξ_{ff}.

[11] **GE**neral **B**athymetric **C**harts of the **O**ceans
[12] **S**huttle **R**adar **T**opography **M**ission
[13] LiDAR: **Li**ght **D**etection **A**nd **R**anging
[14] IfSAR: **I**nter**f**erometric **S**ynthetic **A**perture **R**adar

5.7 Conclusion and remarks from the numerical simulation

The NLSWE based model, COMCOT (Version 1.7) was able to successfully simulate the solitary wave propagation in the wave flume for the cases of wave heights below the canopy. In extreme conditions, i.e. tsunami height reaches the canopy or beyond, the damping performance of coastal forests will no be longer effective and the formulae (equation 5.16) can no longer be implemented because under such extreme conditions most trees will be uprooted or broken. The obtained hydraulic resistance from physical model tests in term of drag coefficient have also been implemented to reproduce wave attenuation by mangrove forests. The hydraulic resistance in the form of equivalent Manning roughness coefficient for C_D =1.5 has successfully simulated the solitary wave propagation in the wave flume with and without the forest model particularly for the cases of non-breaking waves (errors < 5%). For the cases of dominant wave breaking conditions or high nonlinearity, only the arrival time of the wave is well simulated while the other associated processes cannot be represented due to the inherent limitations of NLSW models.

The effect of larger forest widths and other forest densities than those tested in the wave flume on the wave attenuation have also successfully been carried out numerically. The results have enabled to identify the four most important parameters affecting the tsunami attenuation namely forest width B, forest density characterised by D_s, local water depth h_f and wave height H_f. These parameters have been combined into a new single non-dimensional parameter called *forest width factor* which is well correlated with the transmission coefficient. The forest width factor ξ_{ff} represents the most appropriate and practical measure to estimate the wave attenuation performance of coastal forest vegetation.

For negligibly small forest width B (or B nearly zero), this means for smaller ξ_{ff}, transmission coefficient K_t will be maximum. For large water depth h_f, this means for small ξ_{ff}, K_t will also be large. The effects of forest density and wave height also influence the K_t to fluctuate along the forest width factor. As D_s increases or H decreases, the K_t will decrease as well.

A systematic procedure to assess the wave attenuation induced by coastal forests such as mangrove has been developed. This procedure is necessary since the estimation of wave attenuation by coastal forest cannot be done by considering only forest characteristics. Other local environment aspects such as the topography and bathymetry as well as hydrodynamic aspects such as the incident wave height should also be considered. However, it has to be noted that this procedure is valid only for the cases when tsunami height is still below the canopy and the forest are in mid-age or mature age stages. For the cases of large tsunami reaching the canopy or beyond, estimation of wave attenuation is more complicated and most likely the coastal forest will not effectively reduce the impact of tsunami due to the poor structural integrity as observed in many latest tsunami events.

6 Summary and concluding remarks

The following conclusions are drawn as the answers to the research objectives as described in Chapter 1 and in the specification of objective and methodology (Chapter 2). Some remarks to the drawn conclusions are also mentioned for further discussion and future investigations of tsunami and storm wave attenuation by coastal forests.

6.1 New physically-based methodology for the parameterisation of tree models

Typical coastal forest vegetation i.e. mangrove and coastal pine trees have been successfully parameterised based on physical parameters using a physically sound concept (see Sections 3.2 and 3.3) based on stiff and flexible structure assumptions. The parameterised tree models in previous studies were found to be too simplistic and sometimes not representing physical aspects of real conditions. The physical parameters that have been considered in the parameterisation process are the geometry, submerged control volume and the frontal area. Though, those parameters are not new, the key aspect in the parameterisation process is the reproduction of "real" tree model. The construction of "real" tree model is the combination of detailed calculation and observation. The approach making use of a real tree model turned to be powerful in solving parameterisation problems for a complex 3D structure of tree models (e.g. mangrove root system).

6.2 "Bridging the gap" from previous studies on hydraulic resistance coefficients

A wide range of hydraulic resistance coefficients for the application of tsunami/storm wave attenuation, either in terms of drag or inertia coefficients (C_D and C_M, respectively), have been observed. The implemented hydraulic resistance coefficients were often determined based on the characteristics of typical trees

regardless the role of tree components such as roots, trunk and the canopy. This resulted in heavy reliance on trial-and-error efforts in selecting appropiate hydraulic resistance coefficients. The results from this study provide a clear guidance where these hydraulic resistance coefficients should be implemented for each tree components filling the unknown information among the previously reported wide range of hydraulic resistance coefficients. This unknown information which is contributed to the role of each tree component (morphological characteristic) as a function of inundation depth might result from different approaches used for parameterisation. In this study, C_D and C_M have been derived as a function of the flow regime described by a Reynolds number in which the characteristic length is defined as a function of the most important vegetation parameter (submerged volume and frontal area). While the obtained C_M relationship confirms many previous studies, the obtained C_D provides new significant information. The C_D relationship determined in this study bridges the gaps of C_D coefficients proposed in previous studies. For example, for the case of mangroves, large values of C_D mostly belong to the situations when the inundation depth are at the bottom part of the tree (dense root system) while smaller values are for the conditions where the inundation depth at or above the canopy level. This information has never been reported due to the fact that the tree components have never been investigated separately and systematically (see **Sections 3.38** and **3.39**).

Large values of C_D ($C_D > 2$) are possible for large values of the influencing parameters, namely frontal area A_f and submerged volume ratio V_m/V. These conditions can mostly be achieved when the water level is very low. For the case of mangrove forests, the water level is still within the root system. Meanwhile, small range values of C_D ($C_D \sim 1.0 - 1.5$ or even less) are applicable for the conditions where the trees are fully submerged. This is the case when the water level is above the root system (mangroves) or at/beyond the canopy (for all types of coastal trees).

6.3 Selection of proper hydraulic resistance coefficients for numerical simulation

For the purpose of numerical simulation, inertia coefficient C_M is often omitted due to its negligible contribution to the energy dissipation of tsunami/storm waves as compared to drag coefficient C_D. This is confirmed by the results of this study where C_M tends to be constant for almost all wave conditions and for different tree characteristics (see **Sections 4.2.6** and **4.3.5**). The obtained C_M is dominant during the first rows of trees of the forest and is therefore important for the investigation of structural integrity of the trees. In such conditions, the contribution of inertia losses may reach a half of the drag losses.The later is however beyond the framework of this study.

The selection of C_D has often been carried out iteratively due to the lack of knowledge on the role of each tree component to the characteristics of incident waves. In this study, the selection of C_D for numerical simulation has been predetermined based on the characteristics of forests, incident waves and water depth as mentioned in **Section 6.2**. The selection of $C_D \sim 1.5$ has been tested and validated by numerical simulation using the Shallow Water Equation (SWE) based model, COMCOT (see **Sections 5.2** and **5.3**):

- *For non-breaking wave conditions* the simulation shows satisfactory results indicated by a relatively good reproduction of wave heights and arrival time tested in the wave flume.
- *For breaking wave conditions*, due to its inherent limitations the NLSWE based model COMCOT is unable to reproduce exactly the shape of highly nonlinear waves, the breaking process and the fission process of the solitary wave (solitons). Advanced detailed flow models such as RANS or DANS models may be appropriate. However, the arrival time and large parts of the wave forms are still relatively well reproduced. For the purpose of tsunami simulation in the common engineering practice, these limitations are still acceptable because detailed breaking wave processes are less important compared to inundation depth, run-up distance and arrival time.

6.4 Efficiency of coastal forests as a tsunami/storm wave barriers

With a proper parameterisation methodology for a typical coastal forest vegetation (i.e. mangroves), the maximum contribution of the forest to the total attenuation against storm waves may reach ~15% - 20 % for B/L > 1 (see **Section 4.2.4**). In the case of tsunami, a forest width B in the range of the tsunami wave length L (B/L ~ 1) would be required for this contribution to reach ~ 20% - 40% (see **Section 4.3.3**). This means extremely wide coastal forests similar to the length of tsunami wave are needed to achieve such damping performance. Large parts of the wave reduction, which were often attributed to forests, are contributed by the foreshore topography. This finding confirms the fact that mangrove live in sheltered areas or in a low energy environment (mostly in shallow waters of estuaries). This means much of the energy entering mangrove environment has been reduced by the foreshore bathymetry/topography. As mangrove forests and the foreshore topography constitute one system, both should always be considered as a whole in any tsunami/storm wave modelling efforts. It should be noted that geotechnical aspects (e.g. uprooted trees) and structural integrity (e.g. broken trees) are not considered in this study. Many cases where coastal forests failed to reduce effectively the impact of extreme tsunami or storm waves are related to both problems such as uprooting, breaking, tilting and laid down. Therefore, in reality, the attenuation of tsunami/storm waves by **only** coastal forest vegetation (mangroves) may even be below the aforementioned range of values.

However, for the cases of tsunami height below the canopy or within the root system and the trunk for mangroves, the impact of tsunami might be effectively reduced depending on the following four important parameters: forest width B, local water depth h, forest density characterised by distance between trees D_s and wave height H. These parameters are brought together into a new single non-dimensional parameter called *forest width factor* ξ_{ff} which well correlates with wave transmission coefficient K_t. A procedure to develop a relationship K_t vs. ξ_{ff} has been introduced in order to assess wave attenuation by coastal forests (see **Section 5.6**).

6.5 Limitations of the new results and future research needs

The results of this study provide a new insight and information for the implementation of coastal forests as a natural barrier against tsunami and storm waves. Besides, the structural integrity and geotechnical aspects which have not been considered in this study and which necessarily need to be addressed in future studies, the following limitations and future research needs are noteworthy:

– Damping performance of mangrove/coastal pines against tsunami/storm waves with stiff structure assumptions that has been implemented for the bottom part of mangroves will be valid when the roots firmly attached to the soils. In reality, this condition often cannot be achieved because mangroves (i.e. *Rhizophora* sp.) grow in muddy soils in which the top soils are easily eroded (scoured). Moreover, increasing flow velocities among individual roots will also add further scouring to the top soils around the roots. In this situation, the trees are vulnerable to uprooting that definitely influences the overall damping performance. For the case of coastal pine, this issue is even more challenging because this species has been considered by some engineers/scientists to have poor resistance against scouring. An improved knowledge on the physical processes of scouring around the roots systems will provide a more reliable assessment of tsunami/storm wave attenuation by coastal forest vegetations.

– Damping performance of mangrove against tsunami/storm waves with flexible structure assumptions has also been partially investigated. All parts of the tree (roots, trunk and canopy) have been considered to evaluate tsunami attenuation by coastal forest vegetations when tsunami reaches the canopy. In order to simplify the problems at first stage, the investigation has been dedicated on finding the most suitable materials based on trunk elasticity (Young's modulus, E). However, the breakage limit of the trunk was not part of this study whereas broken trunk cases are common when tsunami reaches the top of the canopy. The effect of broken trunk on the to-

tal tsunami attenuation has never been investigated. Among all numerical simulations, the only tools that have been used for the assessment of tsunami attenuation due to coastal forest have considered that the trees are firmly fixed. Complex interactions between fluids and the trees as well as the assessment of interaction among (broken) individual trees within the forests until they turn to be floating debris are some of challenging issues to be addressed. Moreover, the limits of coastal forests subject to extreme tsunami that may turn to be lethal floating debris also need to be investigated for a better design of green belt barriers.

– The hydraulic resistance coefficients implemented in the numerical simulation have been systematically validated by laboratory data. In order to improve the reliability of the model, validation by field data is still required. For this purpose, the following field data are required: detailed bathymetry and topography data, characteristics of coastal forest vegetations (B, D_s, V_m/V, A_f, etc), and other existing infrastructures around or within the forest. Considering some historical tsunami events, for smaller tsunami (below the canopy of the tree), the data can possibly be obtained by field surveys because the forests are still there. For the case where tsunami is extremely large or when most forests have been destroyed, the estimation of the forest characteristics still can be obtained from secondary sources (e.g. literatures).

– For the purpose of mitigation measures, multi defence strategies might help in reducing the impact of extreme tsunamis. The relatively large contribution of foreshore topography to the total tsunami attenuation as found in this study is an indicator to investigate hybrid protection systems (e.g. forests on higher grounds or combined with other natural or artificial structural means). Though such a system has been implemented in some areas in Japan, the failure of some of this system from tsunami GEJET 2011 have revealed that many “unknown” aspects still need further investigations.

References

ADRC/IRP (2011): 'Great east japan earthquake – preliminary observation--', (GLIDE: EQ-2011-000028-JPN), May 2011.

Asano, T (2008): 'Time varying tsunami attenuation ability of coastal forests bascd on forest growth models',Coastal Engineering Joumal,Vol.50, No.3, pp. 325-348.

Augustin, L.N., Irish, J.L., Balsmeier, G., & Kaihatu, J., (2008): 'Laboratory measurements of wave attenuation and wave setup by vegetation', Proceeding of 2008 ICCE Hamburg-Germany: pp. 324-330.

Ayarkwa, J., Hirashima, Y., & Sasaki, Y. (1999): 'Predicting static bending modulus of elasticity of tropical African hardwoods from density using a model based on longitudinal vibration', Ghana Journal of Forestry, (8) pp: 1-8.

BAPPENAS, (2005): 'Rencana Induk Rehabilitasi dan Rekonstruksi Wilayah Aceh dan Nias, Sumatera Utara: Buku 1 Rencana Bidang Tata Ruang dan Pertanahan', Jakarta, Indonesia (in Indonesian), 170p.

Boon, J., (2009): 'Ernesto: Anatomy of a Storm Tide' Virginia Institute of Marine Science, Prof. J. Boon: http://web.vims.edu/physical/research/ernesto.pdf?svr=www (accessed date: April 2009)

Burger, B., (2005): 'Wave Attenuation in Mangrove Forests Numerical; modelling of wave attenuation by implementation of a physical description of vegetation in SWAN', MSc Thesis, Faculty of Civil Engineering and Geosciences, TU Delft – the Netherlands. 106p.

Carrier, G.F., Wu, T.T., and Yeh, H. (2003): 'Tsunami ru-nup and drawdown on a sloping beach', J. Fluid Mech. 475, pp. 79–99.

Chatenoux, B., and Peduzzi, P., (2005): 'Analysis of the role of bathymetry and other environmental parameters in the impacts from the 2004 Indian Ocean tsunami', Report for the UNEP Asian Tsunami Disaster Task Force.,UNEP/DEWA/GRID-Europe, Switzerland. 25p.

Chow, V. T. (1959): 'Open channel hydraulics', McGraw-Hill Publishing Company, New York (http://www.fsl.orst.edu/geowater/FX3/help/8_Hydraulic_Reference/Mannings_n_Tables.htm, accessed on November 2012)

Clough, B.F., Ong, J.E. and Gong, W.K. (1997): 'Estimating leaf area index and photosynthetic production in canopies of the mangrove Rhizophora apiculata', Marine ecology progress series, vol. 159, pp: 285-292.

Clough, BF., Tan, DT., Phuong, D.X., and Buu, D.C., (2000): 'Canopy leaf area index and litter fall in stands of the mangrove Rhizophora apiculata of different age in the Mekong Delta, Vietnam', Aquat. Bot. **66** (4) (2000), pp. 311–320

Cyranoski, D (2012): 'Rebuilding Japan: After the deluge', Nature 483, 141–143 (08 March 2012) doi:10.1038/483141a

Daenecke K. (2010b): Solitary wave attenuation analyses by mangrove forest using energy dissipation approach. Master thesis D-1/10, LWI, TU Braunschweig, Germany, pp. 110.

Dahdouh-Guebas, F., L.P. Jayatissa, D. Di Nitto, J.O. Bosire, D. Lo Seen & N. Koedam, (2005): 'How effective were mangroves as a defence against the recent tsunami ?' Current Biology 15(12): pp. 443-447

Danielsen, M.K., Sorensen, M.F. Olwig, V. Selvam, F. Parish, N.D. Burgess, T. Hiralshi, V.M. Karunagaran, M.S. Rasmussen, L.B. Hansen, A. Quarto And N. Suryadiputra, (2005): 'The Asian tsunami: a protective role for coastal vegetation', Science 310 p. 643

Dao M.H. and Tkalich P. (2007): 'Tsunami Propagation Modeling - A Sensitivity Study', Natural Hazards and Earth System Sciences, Vol. 7, pp. 741–754

De Lange W.P., Prasetya G.S., Healy T.R., (2001): Modelling of Tsunamis Generated by Pyroclastic Flows (Ignimbrites) DOI: 10.1023/A:1012056920155, (24) 3, pp. 251-266.

Dean, R.G., & Bender, C.J., (2006): 'Static wave setup with emphasis on damping effects by vegetation and bottom friction', Coastal Engineering Journal. 53, pp. 149–156

Dekker, F. (2006): 'Hydrodynamics and morphodynamics in and around mangrove forests', Master thesis, University of Twente. 195p.

Duke, N.C. (1992). In: Robertson, A.I. and Alongi, D.M. (Eds). Coastal and Estuarine studies: Tropical Mangrove Ecosystems, American Geophysical Union, Washington DC., USA, pp. 63-100.

ECOS (2010): 'Coastal 'bioshields' no defence against tsunamis', ECOS, CSIRO Publishing, http://www.ecosmagazine.com/?paper=EC153p7a

EJF, (2006): 'Mangroves: Nature's defence against Tsunamis - A report on the impact of mangrove loss and shrimp farm development on coastal defences'. Environmental Justice Foundation, London, UK, 30p.

Ellis, WL, and Bell, S.S., (2004): 'Canopy gaps formed by mangrove trimming: an experimental test of impact on litter fall and standing litter stock in Southwest Florida (USA)'. Journal Experimental Marine Biology and Ecology 311: pp.201–222

FAO, (2005): 'Coastal Protection and Spatial Planning in Indonesia', Mission Report Murugesu Pushparajah FAO Consultant, Food and Agriculture Organization of the United Nations (FAO) May 2005.

FAO/MOAC, (2005): 'Report of Joint FAO/MOAC Detailed Technical Damages and Needs Assessment Mission in Fisheries and Agriculture Sectors in Tsunami Affected Six Provinces in Thailand 11-24 January 2005', Food and Agriculture Organization of the United Nations (FAO) in cooperation with Ministry of Agriculture and Cooperatives (MOAC) Thailand.

Farnsworth, E.J., and Ellison, A.M., (1996): 'Sun-shade adaptability of the red mangrove, Rhizophora mangle (Rhizoporaceae): Changes trhoug ontogeny at several levels of biological organisation', American journal of botany 83 (9), pp. 1131-1143.

Fathi-Maghadam, M., & Kouwen, N., (1997): 'Nonrigid, nonsubmerged, vegetative roughness on floodplains'. Journal of Hydraulic Engineering ASCE 123 (1997), pp. 51–57

Finnigan, J.J., & Shaw, S., (2008):'Double-averaging methodology and its application to turbulent flow in and above vegetation canovies', Acta Geophysica vol 56, no.3. pp. 534-561.

Forbes, K., Broadhead, J., (2007): 'The role of coastal forests in the mitigation of tsunami impacts', Food and Agriculture Organization of the United Nations (FAO), FAO, Bangkok. 20 p.

Fritz H.M., Borrero J.C, Synolakis C.E., Yoo J. (2006): '2004 Indian Ocean tsunami flow velocity measurements from survivor videos', Geophys. Res. Lett., Vol. 33, No. 24, L24605, doi:10.1029/2006GL026784.

Fritz, H. M., Phillips, D. A., Okayasu, A., Shimozono, T., Liu, H., Mohammed, F., Skanavis, V., Synolakis, C. E. *and* Takahashi, T. *(*2012*):* 'The 2011 Japan tsunami current velocity measurements from survivor videos at Kesennuma Bay using LiDAR', Geophys. Res. Lett., 39, *L00G23*, *doi:*10.1029/2011GL050686.

Gale, NH., and Power, WL., (2010): 'Tsunami forecasting and monitoring in New Zealand', Proceedings of the Indian Ocean Tsunami Modelling Symposium, Fremantle, Western Australia, 12-15 October 2010, pp. 26-29.

GFDRR & world bank (2012):'Green belt and coastal risk management – knowledge note 2 - 8', Report on Urban planning, land use regulation and relocations, world bank 2012. Link: http://wbi.worldbank.org/wbi/Data/wbi/wbicms/files/drupal-acquia/wbi/drm_kn2-8.pdf

Goda. Y., (2000): 'Random Seas and Design of Maritime Structures', World Scientific Publishing Co., 2000), 443p.

Gonzalez, F.I., E. Bernard, P. Dunbar, E. Geist, B. Jaffe, U. Kˆanoˇglu, J. Locat, H. Mofjeld, A. Moore, C. Synolakis, V. Titov, and R. Weiss (Science Review Working Group) (2007): 'Scientific & technical issues in tsunami hazard assessment of nuclear power plant sites'. NOAA Tech. Memo. OAR PMEL-136, Pacific Marine Environmental Laboratory, Seattle, WA, 125 pp. + appendices on CD.

Grant, P. F. and W.G. Nicking, (1998): 'Direct field measurement of wind drag on vegetation for application to windbreak design and modelling', Land Degradation and Development, **9**, pp. 57-66.

Green, E., and Clark, C. (2000): 'Assessing Mangrove Leaf Area Index and Canopy Closure' in Alasdair J. Edwards (Ed.), Remote Sensing Handbook for Tropical Coastal Management, UNESCO-CSI, http://www.unesco.org/csi/pub/source/rs.htm

Grilli, S. T., Ioualalen, M., Asavanant, J., Shi, F., Kirby, T. J., & Watts, P., (2007): 'Source Constraints and Model Simulation of the December 26, 2004 Indian Ocean Tsunami, Journal of Waterways, Port, Ocean and Coastal Engineering, -ASCE 133(6), pp.414–428

Hadi, S., Latief, H., Muliddin, (2003): 'Analysis of Surface Wave Attenuation in Mangrove Forests', PROC. ITB Eng. Science Vol. 35 B, No. 2, 2003, pp.89-108

Harada, K., and Imamura, F., (2000): 'Experimental study on the resistance by mangrove under the unsteady flow', In: Proceedings of the 1st congress of the Asian and Pacific Coastal Engineering, Dalian, pp 975–984

Harada, K., and Imamura, F., (2003): 'Experimental Study on the Effect in Reducing Tsunami by the Coastal Permeable Structures', Proceeding of the 12th International Offshore and Polar Engineering Conference, 26-31 May 2002, Kitakyushu, Japan.

Harada, K., and Imamura, F., (2006): 'Effects of coastal forest on tsunami hazard mitigation—a preliminary investigation', Tsunamis: case studies and recent developments. Advances in Natural and Technological Hazards Research, pp. 279–292

Harada, K., and Kawata, Y., (2004): 'Study on Tsunami Reduction Effect of Coastal Forests due to Forest Growth', Annuals of Disaster Prevention Research Institute, Tokyo Universty - Japan.

Harada, K., Latief, H., & Imamura,. F. (2000): 'Study on the mangrove control forest to reduce tsunami impact', In: Proceedings of 12th congress of the IAHR-APD. Bangkok.

Hawa, S., (2005): 'The use of bakau as a piling material in Malaysia ', Bachelor thesis – Universiti Teknologi Malaysia, 166p.

Hills, JG., Goda, MP., (1998): Tsunami From Asteroid and Comet Impacts: The Vulnerability of Europe, Science of Tsunami Hazards, (16) pp. 3-10.

Hiraishi, T., & Harada, K., (2003): 'Greenbelt Tsunami Prevention in South-Pacific Region'. Report of the Port and Airport Research Institute, (42) pp. 1–23

Holthuijsen L., (2007):'Waves in oceanic and coastal waters', Cambridge University press, ISBN 978-0521860284. 387p.

Horrillo, J. & Kowalik, Z.(2006): 'Wave dispersion study in the Indian ocean tsunami of December 26, 2004', Science of Tsunami Hazards, 25(1), 42p.

Huang, B.S., Huang, Y.L. , Lee, S.J., Chen, Y.G., and Jiang, J.S. (2008):'Initial rupture processes of the 2006 Pingtung earthquake from near source strong-motion records, TAO **19** (2008), pp. 547–554.

Huang, Z., Yao, Y., Sim, SY.,Yao, Y., (2011): 'Interaction of solitary waves with emergent, rigid vegetation', Ocean Engineering, (38:10) pp. 1080-1088.
Hughes, S. A. (1993): 'Physical models and laboratory techniques in coastal engineering'. Advanced Series on Ocean Engineering-Volume 7, World Scientific, Singapore.
Husrin S., and Oumeraci H. (2012a): 'Modelling of tsunami and storm wave attenuation by coastal forest, State of the art report', Internal Report Nr. 1, LWI, TU Braunschweig, Germany, 126p.
Husrin S., and Oumeraci H. (2012b): 'Parameterisation concept of coastal pine tree', Internal Report Nr. 2, LWI, TU Braunschweig, Germany, 30p.
Husrin S., and Oumeraci H. (2012c): 'Preliminary Experiments on Mangrove Model Parameterisation', Internal Report Nr. 3, LWI, TU Braunschweig, Germany, 31p.
Husrin S., and Oumeraci H. (2012d): 'Analyses of Mangrove Parameterisation with Stiff Structure Assumption', Internal Report Nr. 4, LWI, TU Braunschweig, Germany, 83p.
Husrin S., and Oumeraci H. (2012e): 'Mangrove and coastal pine parameterisation with flexible structure assumption - Part 1', Internal Report, LWI, TU Braunschweig, Germany, 79p.
Husrin S., and Oumeraci H. (2012f): 'Field survey on mangrove and coastal pine trees', Internal Report Nr. 6, LWI, TU Braunschweig, Germany, 37p.
Husrin S., and Oumeraci H. (2012g): Simulation of tsunami propagation through mangrove forests using shallow wave equations (SWE) model - preliminary investigations. Internal Report, LWI, TU Braunschweig, Germany, 169p.
Husrin S., and Oumeraci H. (2012h): 'Mangrove and coastal pine parameterisation with flexible structure assumption – review', Internal Report, LWI, TU Braunschweig, Germany, 30p.
Husrin S., and Oumeraci H. (2012i): 'Hydraulic Resistance of Mangrove Models Subjected by Solitary Waves', Internal Report, LWI, TU Braunschweig, Germany, 53p.
Husrin S., and Oumeraci H. (2012j): 'Mangrove and coastal pine parameterisation with flexible structure assumption – fibrous material-', Internal Report, LWI, TU Braunschweig, Germany, 82p.
Husrin S., and Oumeraci H. (2012k): Simulation of tsunami propagation through mangrove forests using shallow wave equations (SWE) model - detailed investigations. Internal Report, LWI, TU Braunschweig, Germany, 83p.
Husrin S., Hoque A., Oumeraci H. (2010): 'Hydrodynamic performance of mangrove forest under regular and irregular waves', Internal Report, LWI, TU Braunschweig, Germany, 76p.
Husrin S., Widiaratih R., Omeraci H. (2011): 'Hydraulic resistance of mangrove models subjected to regular and irregular waves', Internal Report, LWI, TU Braunschweig, Germany, 169p.
Husrin, S. Strusinska, A., Oumeraci, H.(2012b): 'Global and local processes of tsunami attenuation by mangrove forest', Proc. Of The VIII PIANC-COPEDEC 2012, Chennai, India. pp. 1154-1165
Husrin, S., and Oumeraci, H. (2009): 'Parameterization of coastal forest vegetation & hydraulic resistance coefficients for tsunami modelling'. Proc. of the 4th Annual International Workshop and Expo on Sumatra Tsunami Disaster and Recovery, 78-86p.
Husrin, S., Strusinska, A., Oumeraci, H., (2012a): 'Experimental study on tsunami attenuation by mangrove forest' Special Issue of Earth, Planets and Space (EPS) "Tsunami: Science, Technology, and Disaster Mitigation"(in press)
Imai, K.; Matsutomi, H., (2005): 'Fluid force on vegetation due to the tsunami flow on sand spit'. K. Satake (ed.), Tsunamis: Case Studies & Recent Developments, pp. 293-304.
Imamura F., Yalciner A.C., Ozyurt G. (2006): 'Tsunami modeling manual' (Tunami model), accessed from: www.tsunami.civil.tohoku.ac.jp/hokusai3/E/.../manual-ver-3.1.pdf, 72p.

Imamura, F., Shuto, N., Goto, C., (1988): 'Numerical simulations of the transoceanic propagation of tsunamis' In: Proceedings of the Sixth Congress Asian and Pacific Regional Division, IAHR, Japan, pp. 265–272.

International Team of Tsunami Field Survey (2010): Field Survey of the Southern Mentawai Islands following the 25 October, 2010 Earthquake and Tsunami, Rapid assessment report, 77p.

Irtem, E.,Gedik, N.,Kabdasli, M.S.,& YaSA, N.E., (2009):' Coastal forest effects on tsunami run-up heights', Ocean Engineering 36 (2009) pp.313–320.

Ishi, T., Tateda, Y., (2004): 'Leaf area index and biomass estimation for mangrove plantation in Thailand'. Central Research Institute of Electric Power Industry, pp. 2323-2326

Ishikawa, Y., T. Sakamoto, & K. Mizuhara, (2003): 'Effect of density of riparian vegetation on effective tractive force', Journal of Forest Research 8 (2003), pp. 235–246

Istiyanto, D.C., Utomo K.S., & Suranto, (2003): 'Pengaruh Rumpun Bakau Terhadap Perambatan Tsunami di Pantai'(The effect of mangrove forest to the attenuation of tsunami in coastal area), Seminar Mengurangi Dampak Tsunami: Kemungkinan Penerapan Hasil Riset, BPPT – JICA, 11 March 2003, Yogyakarta (Indonesian)

Järvelä, J., (2004): 'Determination of flow resistance caused by non-submerged woody vegetation', International Journal of River Basin Management, 2(1) pp: 61-70

Jordan II, MR. (2008):'Development of a New Storm Surge Index for Global Prediction of Tropical Cyclone Generated Storm Surge', Thesis report, Florida State University – USA

Journée, J.M.J. and Massie, W.W., (2001):'Chapter 12: Introduction in offshore hydromechanics', lecture notes, Delft Technical University, Delft, the Netherlands

Kabir, M., B. Saha, J. Hye, (2005): 'Cyclonic Storm Surge Modelling for Design of Coastal Polder', Institute of Water Modelling – Bangladesh

Kathiresan & Rajendran, (2005): 'Coastal mangrove forests mitigated tsunami', Estuarine, Coastal and Shelf Science 65 (2005), pp. 601–606.

Kerr, AM., Baird, AH., Campbell, SJ. (2006): 'Comments on ''Coastal mangrove forests mitigated tsunami'' by K. Kathiresan and N. Rajendran [Estuar. Coast. Shelf Sci. 65 (2005) 601e606], Estuarine', Coastal and Shelf Science 67 (2006) pp. 539-541

Keulegan, G. H., and Carpenter, L. H. (1958): 'Forces on cylinders and plates in an oscillating fluid', Journal of Research of the Nationl Bureau of Standards 60 (5): pp. 423–440

Kobashi, D., And Mazda, Y. (2005): 'Tidal flow in riverine-type mangroves', Wetlands Ecology and Management, (13) pp: 615–619

Kobayashi, N. & Karjadi, E. A., (1994): 'Surf-similarity parameter for breaking solitary wave runup', J. Waterw. Port C-ASCE, 120, pp. 645–650

Kongko, W. (2012): 'South Java Tsunami Model Using Highly Resolved Data and Probable Tsunamigenic Sources', PhD-Dissertation, Leibniz Universität Hannover, Franzius-Institut für Wasserbau und Küsteningenieurwesen

Kongko, W., (2004): 'Study On Tsunami Energy Dissipation In Mangrove Forest', Master Thesis Report, Iwate University, Japan.

Kudella M., (2009): 'LWI DAta and VISualisation (L~DAVIS): User's manual'. Leichtweiss Institute – TU Braunschweig, Braunschweig, Germany

Latief, H., & Hadi, S., (2006): 'Protection from Tsunamis, Coastal Protection in the Aftermath of the Indian Ocean Tsunami': What role for forests and trees?; proceedings of the regional technical workshop, FAO, Khao Lak, Thailand.

Latief, H., Harada, K., & F. Imamura. F., (1998): 'Hydraulic experiment for the effect of mangrove forest to reduce tsunami force'. Seminar of the 1998 Natural Disaster in Tohoku Area, Akita

Lin, I.-I., C.-H. Chen, I.-F. Pun, W. T. Liu, and C.-C.Wu (2009): Warm ocean anomaly, air sea fluxes, and the rapid intensification of tropical cyclone Nargis (2008), Geophys. Res. Lett., 36, L03817, doi:10.1029/2008GL035815.

Liu, P.L.-F and Wang, X. (2005): 'The Sumatera earthquake and the indian ocean tsunami, March 28, 2005', NSF report, Cornell University. Web: http://ceeserver.cee.cornell. edu/pll-group/doc/March_28_2005_Tsunami.pdf

Liu, P.L.-F., Cho, Y.B., Yoon, S.B. & Seo, S.N., (1995): 'Numerical simulation of the 1960 Chilean tsunami propagation and inundation at Hilo, Hawaii'. In: Y. Tsuchiya and N. Shuto, Editors, Tsunami Progress in Prediction, Disaster Prevention and Warning, Kluwer Academic Publisher, Amsterdam.

Liu, P.L.-F., Woo, S.B., & Cho, Y.-S., (1998): 'Computer programs for tsunami propagation and inundation', School of Civil and Environmental Engineering, Cornell University, USA. Available at: http://ceeserver.cee.cornell.edu/pll-group/doc/cocmot-technical-manual.pdf

Liu, W.C., Hsu, M.H., & Wang, C.F., (2002): 'Modeling of flow resistance in mangrove swamp at mouth of tidal Keelung River, Taiwan', Journal of Waterway, Port, Coastal and Ocean Engineering, Vol. 129, No. 2, March/April 2003, pp. 86-92

Lockridge, PA., (1998): 'Potential for Landslide-Generated Tsunamis in Hawaii', Science of Tsunami Hazards, (16) pp. 31-38.

Lowe, R.J., J.R. Koseff, And S.G. Monismith (2005): 'Oscillatory flow through submerged canopies': 1. Velocity structure, J. Geophys. Res. 110, C10016, 17 p.

Madsen P.A., Fuhrman D.R., & Schäffer H.A. (2008): 'A critical discussion of the solitary wave paradigm for tsunamis', Proc. Coastal engineering 2008, pp. 1262-1274.

Mansard E.P.D., Funke E.R., (1980): 'The measurement of incident and reflected spectra using a least squares method'. Proceedings of the 17th International Conference on Coastal Engineering, Sidney, Australia, pp. 154–172.

Massel, S.R., Furukawa, K. & Brinkman, R.M., (1999): 'Surface waves propagation in mangrove forests', Fluid Dynamics Research, (24) pp: 219-249.

Matsutomi, H., Ohnuma, K., Suzuki, A., Imai, K., (2006): 'Governing equations for inundated flow in vegetated area and similarity laws for trunk', Proceeding of the 30th ICCE 2006 conference, San Diego, Vol 2, pp: 1638-1650

Mazda ,Y., Wolanski, E.J., King, B.A., Sase, A., Ohtsuka, D., and Magi, M. (1997a): 'Drag force due to vegetation in mangrove swamps', Mangroves and Salt Marshes 1(3): pp.193-199.

Mazda, Y., Magi, M., Ikeda, Y., Kurokawa, T., & Asano, T., (2006): 'Wave reduction in a mangrove forest dominated by Sonneratia sp. Wetlands Ecology and Management 14: pp.365–78.

Mazda, Y., Magi, M., Kogo, M., & Hong, P., (1997b): 'Mangroves as a coastal protection from waves in the Tong King delta, Vietnam, Mangroves and Salt Marshes 1 (1997), pp. 127–135

Mc. Creery, C., (2007): 'Introduction to Using DARTs in Tsunami Warning Center Operations', Training Seminar on Introduction to the Deep-ocean Assessment and Reporting of Tsunamis (DART) Tsunameter 2007, Jakarta, Indonesia

Melito I., & Melby J. A. (2002): 'Wave runup, transmission and reflection for structures armored with CORE-LOC', Coastal Engineering, Vol. 45, pp. 33-52.

Mendez, F.J. & Losada, I.J. (2004): 'An empirical model to estimate the propagation of random breaking and non-breaking waves over vegetation fields, Coast. Eng. 51 (2) (2004), pp. 103–118

Mimura, N., Yasuhara, K., Kawagoe, S., Yokoki, H., & Kazama, S. (2011): 'Damage from the Great East Japan Earthquake and Tsunami - A quick report', Journal of Mitig Adapt Strateg Glob Change, DOI 10.1007/s11027-011-9297-7, Springer Verlag.

Morison, J.R. , O'brien, M.P., Johnson, J.W. & Shaaf, S.A. (1950): 'The force exerted by surface waves on piles', AIME Petroleum Transactions 189 (1950), pp. 149–154.

Morton, R.A., Gelfenbaum, Guy, & Jaffe, B.E., (2007): 'Physical criteria for distinguishing sandy tsunami and storm deposits using modern examples', in Tappin, D.R., ed., Sedimentary features of tsunami deposits—their origin, recognition, and discrimination: Sedimentary Geology, v. 200, no. 3-4 (special issue), pp. 184-207

Morton, RA., Buckley, ML., Gelfenbaum, G., Richmond, BM., Cecioni, A., Artal, O., Hoffmann, C., and Perez, F., (2010): 'Geological Impacts and Sedimentary Record of the February 27, 2010, Chile Tsunami—La Trinchera to Concepcion', USGS and Chile International Tsunami Survey Team (ITST)

Mulia, F., (2001): 'Pertumbuhan tegakan dan teknik pengusahaan hutan mangrove berkelanjutan', Accessed from: www.rimbawan.com (Indonesian)

Muttray M., Oumeraci H., Oever E. (2006): 'Wave reflection and wave runup at rubble mound breakwaters', ICCE 2006 proceeding San Diego, USA, pp. 4314-4324

Myers, E.P. & Baptista, A.M. (1995): 'Finite element modeling of the July 12, 1993 Hokkaido Nansei-Oki tsunami', Pure Appl. Geophys. 144(3/4), 769–801.

Myers, E.P. and Baptista, A.M. (2001): 'Analysis of factors influencing simulations of the 1993 Hokkaido Nansei-Oki and 1964 Alaska tsunamis', Natural Hazards 23(1), 1–28.

Olabarrieta M, Medina, R., Gonzalez, M., and Otero, L., (2010): 'C3: a finite vlume-finite difference hybrid model for tsunami propagation and run up', Computer and geosciences, doi:10.1016/j.cageo.2010.09.016 (in press)

Omira, R., Baptista, MA., Matias, L., Miranda, JM., Catita, C., Carrilho, F., Toto, E., (2009): 'Design of a Sea-level Tsunami Detection Network for the Gulf of Cadiz', Nat. Hazards Earth Syst. Sci., 9, pp.1327-1338.

Onrizal, Rugayah, Suhardjono, (2004): 'Floristics of mangrove tree species in Angke-Kapuk Protected Forest', Biodiversitas, 6(1), pp: 35-39, ISSN: 1412-033X (In Indonesian)

Oumeraci, H (2006): ' Near- and Onshore Tsunami Effects - Knowledge Base Generation and Model Development –' Background paper, prepared for the DFG-Round Table Discussion, Hannover 2006, http://www.fzk.uni-hannover.de/fileadmin/institut/Veranstaltungen/DFG-RT/DFG-pdf/Background.pdf

Oumeraci, H. & Koether, G., (2009): 'Hydraulic performance of submerged wave absorber for coastal protection', Nonlinear Wave Dynamics: ed: Patrick Lynett, World scientific.

Oumeraci, H., Strusinska, A.; Husrin, S. (2011): 'Tsunami Attenuation Performance of Coastal Forest TAPFOR', Final report, LWI, TU-Braunschweig.

Papesch, AJG., (1977):'A field study to determine the drag coefficient and the associated centre of pressure of a forest front', proceeding of the 6th Australasian hydraulic and fluid mechanics conference, Adelaide-Australia, December 1977. pp. 451-454.

Parrotta, JA., (1995):'Influence of overstory composition on understory colonisation by native species in plantations on a degraded tropical site', Journal of vegetation science, (6) pp: 627-636.

Pathirana, KPP., Raveenthiran, K., Galappatti, R., Wootton, D., Mendis, MS., (2008): 'Model investigatins on wave disturbance and ship movement in Colombo Port South Harbour, Sri lanka', Presented paper No. P-05, COPEDEC VIII, Dubai, UAE.

Peltola, H., Kellomäki, S., Hassinen, A., Granander, M., (2000): 'Mechanical stability of Scots pine, Norway spruce and birch: an analysis of tree-pulling experiments in Finland', Forest Ecology and Management 135 (2000), Elsevier, Amsterdam, 143-153 pp.

Petryk, S. & G. Bosmaijan., G. (1975): 'Analysis of flow through vegetation', Journal of Hydraulics Div., ASCE: pp:871–884.

Prasetya, G. (2007): 'Thematic Paper, in: the aftermath of the Indian Ocean tsunami: The role of coastal forests and trees in combating coastal erosion', FAO Regional Office for Asia and the Pacific

Rae, P.J., and Dattelbaum, D.M. (2004): 'The properties of poly(tetrafluoroethylene) (PTFE) in compression', Polymer 45 (2004), pp. 7615–7625.

Rathbun J.R., Cox D.T., Edge B.L. (1998): 'Wave run-up and reflection on coastal structures in depth-limited conditions', Proc. 26th Coast. Eng. Conf., Vol. 1, pp. 1050-1067.

Righetti, M., (2008):'Flow analyses in a channel with flexible vegetation using double averaging method', Acta geophysica, vol 56, no.3. pp. 801-823.

Roberts, S., Nielsen, O., Gray, D., and Sexton, J., (2009):'ANUGA user manual, Release 1.0 beta 7167 ', Geoscience Australia and the Australian National University, https://datamining.anu.edu.au/anuga

Rossetto, T., Peiris, N., Pomonis, A., Wilkinson,S.M., Del Re, D., Koo, R., Gallocher, S., (2007): 'The Indian Ocean Tsunami of December 26, 2004: Observations in Sri Lanka and Thailand', Natural Hazards. 42 (1). Pp. 105-124

Sarpkaya, T.; Isaacson, M. (1981): 'Mechanics of wave forces on offshore structures', New York: Van Nostrand Reinhold, ISBN 0442254024

Satriono (2007): 'Praktikum bilogi laut: profil mangrove taman nasional baluran (Mangrove profile in Baluran National Park)', Fakultas matematika dan ilmu pengetahuan alam, Institut Teknology Sepuluh-november (ITS), Surabaya, 26 p (In Indonesian).

Shuto, N (1991):' Numerical simulation of tsunamis — Its present and near future', Natural Hazards , 4(2-3) pp. 171-191, DOI: 10.1007/BF00162786

Shuto, N., (1987): 'The effectiveness and limit of tsunami control forests', Coastal Engineering in Japan 30: pp.143-153.

Steen, S (2009): 'Experimental method in marine hydrodynamics', lecture notes, NTNU Norway, available online : http://www.ivt.ntnu.no/imt/courses/tmr7/index.htm

Stive, M.J.F., and Wind, H.G., (1982): 'A Study of Radiation Stress and Set-up in the Nearshore Zone', Publication No. 267, Waterlopkundig Laboratorium, Delft Hydraulics Laboratory. 25p

Stockdon, H.F., Holman, R.A., Howd, P.A., & Sallenger, JR, A.H., (2006): 'Empirical parameterization of setup, swash, and runup', Coastal Engineering 53 (7), pp. 573–588

Strusińska A., Oumeraci H. (2009): Hydrodynamic performance of mangrove forest under solitary waves. Internal Report, LWI, TU Braunschweig, Germany, 145p.

Strusińska, A**.;** Husrin, S**.;** Oumeraci, H. (2010): Laboratory experiments on hydrodynamic performances of mangrove forest against tsunami impact. Proc. 4th International Tsunami Symposium, Toronto, Canada

Struve, J., Falconer, R.A., Wu, Y., (2003): 'Influence of model mangrove trees on the hydrodynamics in a flume', Estuarine, Coastal and Shelf Science 58, pp.163-171

Sumer, B.M., Fredsoe, J., (2006): 'Hydrodynamic around cylindrical structures', Advance series of coastal and ocean engineering, world scientific.

Synolakis, C.E., Bernard, E.N., Titov, V.V., Kânoğlu,, U., and Gonza´ Lez, F. (2007): 'Standards, criteria, and procedures for NOAA evaluation of tsunami numerical models', NOAA OAR Special Report, Contribution No 3053, NOAA/OAR/PMEL, Seattle, Washington, 55 p.

Synolakis, C.E., E.N. Bernard, V.V. Titov, U. Kânoğlu, & F.I. González (2008): 'Validation & Verification of Tsunami Numerical Models', Pure & Applied Geophysics Volume 165, Numbers 11-12, pp. 2197-2228, DOI: 10.1007/s00024-004-0427-y

Tahvanainen, T. & Forss, E. (2006): 'Individual tree models for the estimation of vertical branch and needle biomass distribution of Scots pine, Norway spruce, and birch and Finland', Forest ecology and management 255, pp. 455-467

Tanaka, N.; Sasaki, Y.; Mowjood, M.I.M.; Jinadasa, K.B.S.N.; & Homchuen, S., (2007): 'Coastal vegetation structures and their functions in tsunami protection: experience of the recent Indian Ocean tsunami'. Landscape and Ecological Engineering, (3) pp. 33-45.

Teh, S.Y., Koh, HL., Liu P.L-F., Ismail, A.I.M., Lee, H.L. (2009) Analytical and numerical simulation of tsunami mitigation by mangrove in Penang, Malaysia, Journal of Asian Earth Sciences, 36(2009) pp. 38–46, doi:10.1016/j.jseaes.2008.09.007.

Teo, F.Y. (2008): 'Attenuation of tsunami currents in an estuary with mangroves', http://www.swieet2007.org.uk/files/Fang%20Yenn%20Teo%20DD2008.pdf, Last accessed on Sep. 2012

Thuy, Nb.,Tanimoto K., Tanaka N., Harada K., Iimura K. (2009): 'Effect of open gap in coastal forest on tsunami run-up—Investigations by experiment and numerical simulation', Ocean Engineering, 36(15-16) pp. 1258-1269.

Titov, V.V. & Synolakis C.E. (1998): 'Numerical modeling of tidal wave runup', Journal of Waterway, Port, Coastal and Ocean Engineering, Vol. 124, No.4, pp. 157–171.

Titov, V.V. & Synolakis, C.E. (1995): 'Modeling of breaking and non-breaking long-wave evolution and runup using VTCS-2', J. Waterway, Ports, Coastal and Ocean Engin. 121(6), pp. 308–316

Tomczak, M., (1996): 'Introduction to Oceanogrpahy', Oceanography lecture notes – lecture 9, Flinders University Australia (http://www.es.flinders.edu.au/~mattom/IntroOc/lecture09.html)

U.S.Army Corps of Engineers (USAC), SPM (1984):'Shore protection Manual', Coastal Engineering Research Center, Vicksburg, Mississippi, US.

UNEP (2005): 'After the tsunami - Rapid Environmental Assessment. Thailand', UNEP Report, pp: 301-304.

USGS (2005): 'Earthquake details: Magnitude 8.6 – 2005 Northern Sumatra earthquake, Indonesia', USGS online earthquake hazards databases, http://earthquake.usgs.gov/ earthquakes/eqinthenews/2005/usweax/#details,

Vallam, S., Kantharaj, M., and Lakshmanan, N. (2011): 'Resistance of Flexible Emergent Vegetation and Their Effects on the Forces and Runup due to Waves', on 'The Tsunami Threat - Research and Technology' Edited by Nils-Axel Mörner, Intech www.intechopen.com, pp. 129-160

Walton, T.L.Jr., & Dean, R.G., (2009): 'Landward limit of wind setup on beaches', Ocean Engineering, Volume 36, Issues 9-10, July 2009, pp. 763-766

Wang, X. (2009):' User Manual for Comcot Version 1.7 (First Draft)', http://ceeserver.cee.cornell.edu/pll-group/comcot_down.htm

Wang, X., & Liu, P.L.-F., (2006): 'An analysis of 2004 Sumatra earthquake fault plane mechanisms and Indian Ocean tsunami', Journal of Hydraulic Research 44 (2) (2006), pp. 147–154

Wang, X., and Liu, P.L.-F. (2005): 'A Preliminary Simulations of 1986 & 2002Taiwan Hua-lien Tsunami, Report of COMCOT applications, Cornell university, http://ceeserver.cee.cornell.edu/pll-group/doc/simulation_1986_2002_Hualien.pdf

Wang, X., and Liu, P.L.-F. (2010): 'An explicit finite difference model for simulating weakly nonlinear and weakly dispersive waves over slowly varying water depth', Coastal Engineering, 58 (2011) pp: 173–183.

Wang, X., Liu, P.L.-F., and Orfila, A., (2008): 'Numerical simulation of tsunami run-up onto a three-dimensional beach with shallow water equations', In Advances in Coastal and Ocean Engineering 10 (World Scientific, Singapore 2008).

Wijetunge, J.J., (2009):'Numerical simulation and field survey inundation due to 2004 Indian Ocean tsunami in Trincomalee Sri-Lanka', Pure appl. geophys. 166 (2009) pp. 593–622.

Wilson, CAME., Xavier, P., Schoneboom, T., Aberle, J., Rauch, HP., Lammeraner, W., Weissteiner, C., Thomas, H., (2010):'The hydrodynamic drag of full sclae trees', proceeding of Riverflow 2010 Braunschweig, pp. 453 – 460

Wolanski, E., Jones, M. and Bunt, J.S. (1980): 'Hydrodynamics of a tidal creek mangrove swamp system', Australian Journal of Marine and Freshwater Research (31) pp. 431–450.

Wolanski, E., Mazda, Y., Ridd, P., (1992): 'Mangrove hydrodynamics', In: Robertson, A.I., Alongi, D.M. eds. , Coastal and Estuarine Studies, 41: Tropical Mangrove Ecosystems, American Geophysical Union, Washington, DC, pp. 43-62

Wolansky, E. (2006): 'Thematic paper: Synthesis of the protective functions of coastal forests and trees against natural hazards, Coastal protection in the aftermath of the Indian Ocean tsunami', FAO Regional Office for Asia and the Pacific

Yanagisawa, H., Koshimura, S., Goto, K., Miyagi,T., Imamura, F., Ruangrassamee, A. & Tanavud, C., (2009): 'The reduction effects of mangrove forest on a tsunami based on field surveys at Pakarang Cape, Thailand and numerical analysis', Estuarine, Coastal and Self Sciences 81 (2009) pp. 27–37.

Yanagisawa, H., Koshimura, S., Miyagi, T., and Imamura, F (2010): 'Tsunami damage reduction performance of a mangrove forest in Banda Aceh, Indonesia inferred from field data and a numerical model', J. Geophys.Res., 115, C06032, doi:10.1029/2009JC005587 (http://dx.doi.org/10.1029/2009JC005587).

Yeh, H. H., (1991): 'Tsunami Bore Run-up', Natural Hazards 4, Kluwer Academic Pub., pp. 209-220, the Netherlands.

Yuan, Zhi-da and Huang, Zhen-hua., (2010): 'An experimental study of inertia and drag coefficients for a truncated circular cylinder in regular waves', Journal of Hydrodynamics, Ser. B, Volume 22, Issue 5, Supplement 1, pp. 318-323.

Zhou, H., Teng, M.H., Lin, P., Gica, E., & Feng, K. (2009):' Predicting Run-Up of Breaking and Non-breaking Long Waves by Applying the Cornell COMCOT Model', Nonlinear wave dynamics, World scientific, pp. 147-164

Internet References:

General bathymetric chart of the oceans, GEBCO webpage: :http://www.gebco.net

DoITPoMS website: Department of Materials Science and Metallurgy, University of Cambridge, http://www.doitpoms.ac.uk/tlplib/wood/wood_stiffness.php, - accessed date: 20 November 2008

FAO websites: Knowledge reference for national forest assessments - observations and measurements: http://www.fao.org/forestry/8779/en/, - accessed date: April 2009

COMCOT webpage: http://ceeserver.cee.cornell.edu/pll-group/comcot.htm, latest accessed Sept, 2012

Tunami-Namidance webpage: http://namidance.ce.metu.edu.tr/, latest accessed Sept, 2012

Slideshow of tsunami aftermath in Japan, the Reuters webpage: http://www.reuters.com/news/pictures/slideshow?articleId=USRTR2JQY6#a=50, accessed date Tuesday, July 26, 2011

The Japan News webpage: http://www.yomiuri.co.jp/dy/national/T110523003977.htm , accessed date Tuesday, July 26, 2011

Plant Resources of South East Asia (PROSEA) webpage: PROSEA 11: 'Auxiliary plants', http://www.prosea.nl/prosea11.html, - accessed date: April 2009

USGS earth explorer webpage, topography data: http://earthexplorer.usgs.gov/

Virginia Institute of Marine Science, Prof. J. Boon: http://web.vims.edu/physical/research/ernesto.pdf?svr=www (accessed date: April 2009)

World Agro Forestry Centre website: 'Tree species references: Casuarina equisetifolia', http://www.worldagroforestrycentre.org/Sea/Products/AFDbases/AF/asp/SpeciesInfo.asp?SpID=477, - accessed date: April 2009